Volume 73A
Number 2
Mar.–Apr. 1969
J. Res. Nat. Bur. Stand. (U.S.), A
CODEN: JNBAA 73A (2) 113–275 (1969)

Physics and Chemistry

U.S. DEPARTMENT OF COMMERCE

SECTION A

JOURNAL OF RESEARCH

NATIONAL BUREAU OF STANDARDS

Journal of Research

of the

National Bureau of Standards

A. Physics and Chemistry

Mar.–Apr. • 1969

VOLUME • 73A

NUMBER • 2

Editor: C. W. Beckett

Associate Editor: D. D. Wagman

Publication dates:
Feb. 1, Apr. 1, June 1, Aug. 1, Oct. 1, Dec. 1, 1969

JOURNAL OF RESEARCH

The National Bureau of Standards Journal of Research reports research and development in the fields of activity shown at right. Also included from time to time are survey articles on topics closely related to the Bureau's scientific and technical program.

The Journal is published in three separate sections as follows:

A. Physics and Chemistry

Contains papers of interest primarily to scientists working in these fields. Issued six times a year. Annual subscription: domestic, $9.50; foreign, $11.75. Single copies vary in price.

B. Mathematical Sciences

Presents studies and compilations designed mainly for the mathematician and the theoretical physicist. Issued quarterly. Annual subscription: domestic, $5.00; foreign, $6.25. Single copy, $1.25.

C. Engineering and Instrumentation

Reports research and development results of interest chiefly to the engineer and the applied scientist. Issued quarterly. Annual subscription: domestic, $5.00; foreign, $6.25. Single copy, $1.25.

U.S. DEPARTMENT OF COMMERCE
Maurice H. Stans, Secretary
NATIONAL BUREAU OF STANDARDS
A. V. Astin, Director

Order all publications from the Superintendent of Documents
U.S. Government Printing Office, Washington, D.C. 20402
Use of funds for printing this publication approved by the Director of the Bureau of the Budget (June 22, 1966).

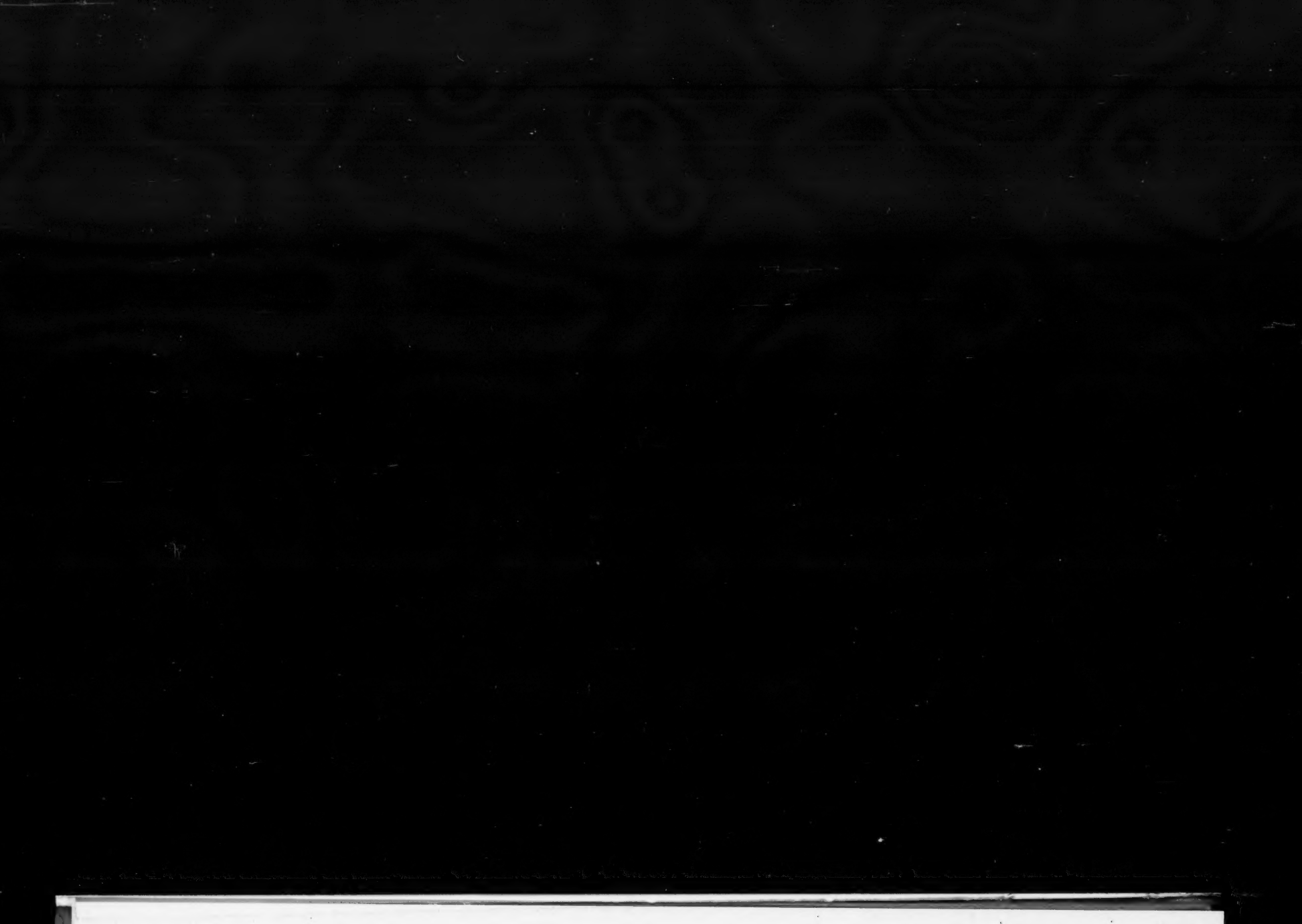

JOURNAL OF RESEARCH of the National Bureau of Standards—A. Physics and Chemistry
Vol. 73A, No. 2, March–April 1969

Color Representation of Electron Microprobe Area-Scan Images by a Color Separation Process

Harvey Yakowitz and Kurt F. J. Heinrich

Institute for Materials Research, National Bureau of Standards, Washington, D.C. 20234

(August 9, 1968)

Composite color photographs were prepared using x-ray area scanned images from the electron probe microanalyzer. Three-color composites are completely interpretable in terms of the primary color (red, green or blue) chosen to represent each element. The color pictures were obtained by preparing conventional black-and-white scanning images which were then used as color-separation-positives, with appropriate filters, to make color prints. Methods for preparing and interpreting color composites are considered. Specifically, color mixing, proper choice of filters to match film characteristics, exposure criteria, and choice for each partial image are discussed in detail. Finally, typical applications drawn from the fields of metallurgy, mineralogy, and biology are shown to illustrate the principles described. With the use of Polaroid film this procedure is quite convenient.

Key words: Color photography; metallography; petrography; photomicrography; scanning electron microprobe; x-ray microscopy.

1. Introduction

The scanning electron probe microanalyzer [1][1] can produce images of microscopic areas as a function of the emission of x-rays or of electrons. The various electron images provide mainly topographic information, while the x-ray images show the spatial distribution of the elements present in the specimen. Thus, the scanning electron probe is a microscope as well as an x-ray spectrometer [2].

Black-and-white photographs showing the topographic distribution of a single signal are widely used. It is difficult, however, to show the correlation of signals from two or more x-ray lines, or of x-ray signals, with the topography provided by the electron images, without the use of color. Therefore, several investigators have proposed color photography for this purpose and some examples have been shown [3–6].

This paper describes the results of a systematic study of color composite micrographs. In discussing the results, emphasis will be placed on the interpretation of the composite color micrograph.

2. General Methods for the Preparation of Color Composites

Color micrographs of x-ray area scans can be obtained in three ways:

1. By the use of a three-gun color cathode ray tube (CRT) and color photography of the three signals generated simultaneously [6].

2. By using a single-gun cathode ray tube with color filters interposed between the screen and the color film in the oscilloscope camera. In this case, a phosphor of broad spectral distribution is used; and the three individual signals are recorded sequentially, changing filters between exposures [5].

3. By preparing conventional black-and-white scanning images and using them as color-separation-positives, with appropriate filters, to make color prints [3, 4]. We shall call this method the color-separation method.

The first method (which we have not used) is the only one permitting immediate simultaneous viewing of the signals in their respective colors. As many as three signals can be recorded simultaneously. This method requires, however, the addition of fairly expensive and massive equipment.

The second method requires only minor modifications if the conventional equipment for area scans is available. In this method, the various signals must be sequentially recorded. Since the color composite is not visually displayed, this technique is tedious unless rapid access photography, such as the Polaroid process is used. However, with the currently available films, and the low brightness and limited spectral range of oscilloscope-tube phosphors, the recording of x-ray pulse signals is difficult. Furthermore, if any of the three exposures is incorrect, the entire procedure must be repeated.

The third method also requires that the signals be recorded sequentially (unless several oscilloscopes are provided with cameras). However, the exposures can be made by the usual technique for black-and-white scanning photographs. As shown here, readily interpretable color composites can be produced routinely, with the aid of a camera equipped with a Polaroid back. No large expenditures for equipment are necessary.

[1] Figures in brackets indicate the literature references at the end of this paper.

The second and third methods were investigated and reported upon in a paper by Jones, Gavrilovič, and Beaven [7]. These authors concluded that the method of preparing composites directly on the microprobe (second method) was more satisfactory than the color-separation method. We have investigated both methods in detail and have arrived at the conclusion that the color-separation method is the most advantageous.

The color-separation technique can be easily used on a routine basis, by unskilled personnel, with a minimum of training. Another important advantage is the possibility of deciding upon the best color combination after the individual black-and-white pictures have been taken. The yield can be 15 to 20 color composites of uniform quality per hour. In view of the advantages of this technique, the work presented in this paper was performed by means of the color-separation technique.

The color photograph is prepared as follows:

1. The appropriate x-ray and electron signal scans are prepared as positive black-and-white prints by photographing the cathode ray tube of the microprobe in the usual fashion [6].

2. The separation-positives are sequentially photographed by the copying camera (which is loaded with Polaroid color film); for each partial exposure, a different color filter is placed between the camera lens and the separation-positive.

The success of this technique depends upon: (1) the quality of the black-and-white images, (2) the characteristics of the light source, the film and color filters, (3) the exposure times, (4) the proper choice of color for each partial image, and (5) avoiding the relative displacement of the black-and-white images during the color exposure. Before discussing each of these requirements, we must consider the effect of mixing two or more colors. This consideration is of prime importance for the interpretation of the final color picture.

3. Aspects of Additive Color Mixing

In color reproduction one obtains a wide range of colors by mixing relatively few basic primary colors in varying proportions. Red, green, and blue are customarily chosen as primary colors for additive mixing because mixing them produces a wide range of colors. None of the primaries can be obtained from mixing the other two. Hence, the presence or absence of primaries can be ascertained in color mixtures if these three primaries are chosen. Almost any color can be made by a mixture of red, green, and blue light in a particular proportion which then, in principle, defines uniquely this nonprimary color. This includes white, gray or black which thus may be considered to be a mixture of red, green and blue. Due to the characteristics of the human eye, we cannot unequivocally interpret mixtures of more than three components. Therefore, we should not have more than three primary colors in one system.

Color film is based upon the same primaries—red, green, and blue. Like the eye, the color film can only resolve mixtures of three primaries. Thus, only three primaries can be used if any color produced by mixing in the composite is to be interpreted in terms of the primaries. For example, let iron on the separation-positive be made red and nickel on the second separation be made blue. If an Fe-Ni alloy is present on the composite, a red-blue mixture (magenta) occurs. All magenta regions on the composite can then be interpreted as resulting from the simultaneous presence of Fe and Ni. Using more than three primary colors [7, 8] leads to color mixtures of the *same* chromaticity (hue and saturation) for more than one combination of elements. On the other hand, if color is only being used to identify a phase, as in coloring a map, then as many colors as there are phases can be used—color mixtures will then have no clear meaning in terms of composition. If, for instance, only discrete elements (with no mixing) occur, then as many colors as there are elements can be used, in principle, to show the structural relationships in the specimen.

The process of exposing color composites consists of adding primaries since each successive filter color is stored on the color film. The three primary colors add to make white. The intermediate colors are: magenta (pinkish) which can be considered as red plus blue, or white minus green, yellow which is red plus green, or white minus blue, and cyan (sky color) which is blue plus green, or white minus red. The color resulting from omitting a single primary from white is called the complement of that primary.

The x-ray and electron micrographs used may contain all shades of gray. They are almost never pure black-and-white. For preparing composite color photographs, the ternary mixtures of the primaries resulting from such black-and-white pictures must be considered.

The ternary mixtures can be shown by the following method: A standard 16-step logarithmic gray scale is prepared and cut into an equilateral triangle having white as an apex and black along a base. The triangle is successively photographed with a red, green, and blue filter, having been rotated 120° between each exposure. The gray scale is shown in figure 1 and the color triangle is seen in figure 2 (see color plate 1).[2] The primary colors appear at the apices. The binary mixtures yellow, magenta, and cyan can be observed in the center of each corresponding side of the triangle. Ternary color mixtures (including gray) are in the interior of the triangle.

Any mixed color in the picture can always be associated with its component primaries. However, quantitative interpretation of the color picture in terms of the composition corresponding to each point on the picture is impractical. This is because of the rigid standardization and control of the pictorial process which would be required starting with the black-and-whites on through a colorimetric reduction of the color data from the picture. Quantitative raster scanning

[2] Color plates 1, 2, and 3 appear at the end of the paper.

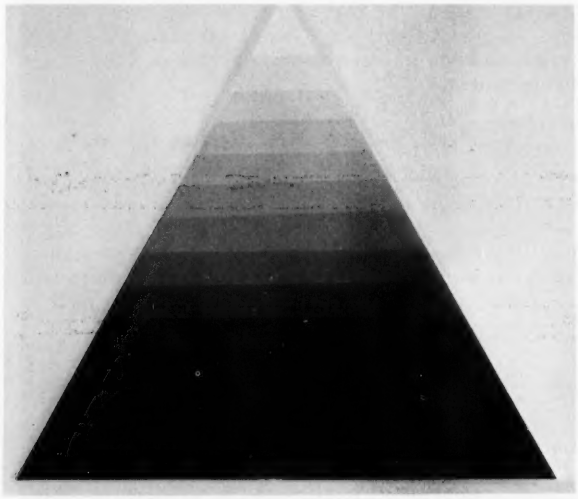

FIGURE 1. *Triangular logarithmic 16-step grey scale used for color balancing.*

[9] is a much simpler and more accurate means of obtaining quantitative information in digital form from a selected region of the specimen. For this reason, only qualitative information can be obtained from the picture, i.e., whether one, two, or three elements occur at the same physical place in the microstructure. Of the primary colors (figure 2—plate 1), red attracts the attention more so than green which in turn has a higher attention value than blue. Of the binary mixtures, yellow tends to be lighter than magenta and cyan. Hence, for pure elements which we wish to emphasize, red is a good choice while for mixtures requiring emphasis, yellow is often a good choice.

Much of the color mixing in a typical picture is binary because of the nature of most microprobe specimens. Thus, the binary color mixing occurring along the bases of the color triangle is worth a detailed examination. For this purpose, a double-length strip from the 16-step gray scale was photographed successively with each pair of primary color filters after being rotated 180° between exposures. The results show that yellow is easily distinguished from both red and green—more so than magenta and cyan from their respective primary neighbors.

The relations and contrasts of colors obtainable from three primaries can be better illustrated by the following representation. Consider the color triangle discussed previously with the pure primaries at the apices. In the center we find neutral gray. However, since we distinguish a lightness scale from white to black, a vertical lightness scale can be represented on a perpendicular to the color triangle. Connecting the extremes (black and white) to the three primaries, we obtain a triangular bipyramid, figure 3, which is similar to the Munsell color solid [10]. However, on this diagram, the horizontal plane represents the same lightness of the black-and-white pictures rather than the color picture. We have marked on this figure rela-

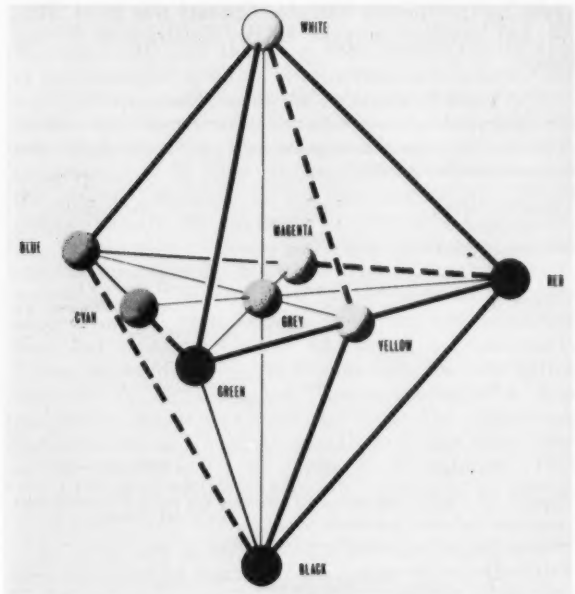

FIGURE 3. *Schematic representation of the color solid pertaining to the red, green, blue primary system.*

Highly contrasting pairs of colors are connected by bold solid lines, intermediate contrast is indicated by solid lines and poor contrast is denoted by broken line.

tions of high contrast by solid lines and poor contrast by broken lines. This graph may be helpful in color selections.

Figure 2 (plate 1) was prepared using a particular set of red, green and blue filters. Since other primary filters could have been used, the color triangle of figure 2 is a particular case among many. Choosing a particular filter set defines the gamut for a given film. The filters chosen for the color-separations should be picked so as to yield the widest gamut.

Proper balance of color on the film for a given set of filters is achieved when the addition of equal lightnesses on the black-and-white pictures yields a neutral gray on the color picture. This criterion was satisfied by obtaining a color picture of the *unrotated* gray scale, adjusting the exposure time for each filter until the photograph showed neutral gray steps. Changing the exposure time for a given filter changes the color balance. The light sources we used were incandescent photofloods. We also used cold white fluorescent tubes.

There are at least three sets of filters which can be properly balanced and which yield good color quality when using Polaroid film. These sets are standard Kodak Wratten series numbers 25, 58, 47, numbers 92, 93, 94, and numbers 33, 93, 45 for red, green and blue respectively. The first set is that used to match the dye peaks of most sheet color films, the second was recommended by the film manufaeturer and the third we found after some experimentation. The exposure times for each filter set are shown in table 1. With a variety of input subjects, the 33, 93, 45 set provided the most satisfactory results. The mixed colors could

easily be interpreted and color quality was good. This set was used to prepare all the illustrations in this paper.

TABLE 1. *Exposure times for color composites**

Kodak Wratten filter set number	Color	Time (sec.)
Light source: Four reflector flood lamps spaced 2 ft apart, 3 ft from subject. Camera 20½ in from subject. Lens setting f5.6.		
92	Red	1/4
93	Green	12
94	Blue	60 (add 1/30 white)
25	Red	1/8
58	Green	5/8
47	Blue	5
33	Red	1/5
93	Green	10
45	Blue	3 (add 1/60 white)
Light source: Two cold white fluorescent bulbs 15 in long placed 18 in from subject. Camera 3½ in from subject. Lens setting f5.6.		
33		1.5
93		40
45		7.5 (add 1/60 white)

*Included as a guide only. These values give approximately equal lightness.

Using the 33, 93, 45 set of filters, blue is sometimes difficult to distinguish from black. The lightness of blue can be increased by adding a small amount of white light to the blue subject. One exposes a subject with the aid of the blue filter and then reexposes the same subject for a much shorter time without a filter.

For dark separation-positives, the exposure time should be increased. This upgrades the dark separation-positive at the expense of the overall color balance of the composite. Exposure adjustment to minimize the effect of separation-positives of low quality is, however, a poor method which should be avoided.

4. Preparation of Black-and-White Images

In this paper we have used the conventional x-ray images, in which every detected pulse is shown as a white dot on black background. Rate-meter output images [2] can also be used in a similar fashion.

The first requirement for a satisfactory color composite is a set of x-ray black-and-white images of good quality. The main points to observe are:

1. The areas of high x-ray emission should be white, and those with no exposure, black. The effects of a gray background (e.g., through too short development time of the black-and-white picture) cannot be easily corrected in the making of the composite.

2. The interpretation of the color picture is often aided if equal lightness of the separation-positives corresponds to equal concentrations of the elements represented.

3. A sufficient amount of x-ray counts should be recorded [2].

4. Care should be taken that the specimen position with respect to the scan does not change between exposures, due to electrostatic charges or mechanical displacement.

5. Registration Device

A simple device provides entirely satisfactory alinement of the partial images. The separation-positives are located within a holder by means of several dial pins. By means of drilling the bed of the aluminum top plate with some holes, cementing the top and bottom plates and evacuating the assembly, one can hold the picture flat.

6. Choice of Color for Each Partial Image

Since the primaries and binary mixtures of the primaries differ inherently in attention-value, the choice of color for each constituent can be used to direct our attention to selected features of the composite. Thus, in figure 4a, plate 1 the yellow area stands up markedly against the dark blue background.

An extreme case occurs where small areas of an x-ray signal are superposed upon the target current, backscatter, or even an x-ray image used as topographic background. In this case, the localized x-ray signal should be shown white (or yellow). A fairly dark color, such as green or cyan makes a satisfactory background. Since the lightness range of the background should be small but distinct, it might be difficult to produce the contrast within the background necessary for orientation. From this viewpoint blue is not very useful. Small areas of high lightness in the separation-positive for the background must be avoided. If these areas are toned down to the maximum lightness tolerable in the background, the remaining background topography will be lost. It is therefore advisable to overexpose the background separation-positive so that a considerable fraction of it attains maximum lightness. On toning down the lightness level for background, this will be the only remaining background information.

Different colors—primary as well as others—possess different degrees of attention value. Hence, the viewer's attention can be directed to various features of the color picture by a careful selection of the primary color used to represent each constituent. As an example figure 5 (see plate 2 for the d, e, f, g, h, and i parts of this figure) shows three typical x-ray separation-positives and all six possible color composites obtainable from them. As the color combinations change the prominence of certain features including background changes.

7. Applications

The optical photomicrograph shown in figure 6a is a portion of a crack located near the edge of a specimen of a Ni base superalloy. The crack appeared during service at high temperature in air. The optical microscopist can distinguish two shades of gray in the crack. The microprobe identified Al and Cr in the

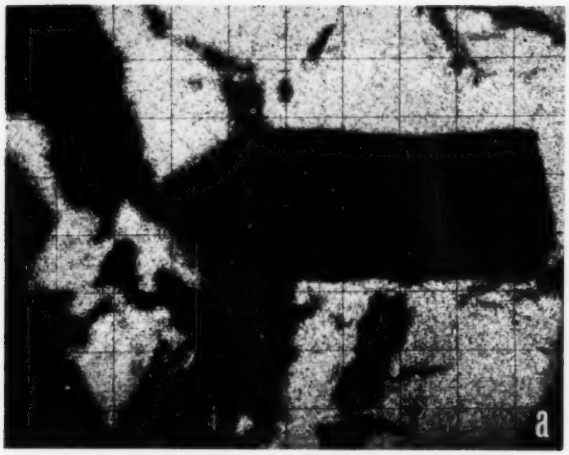

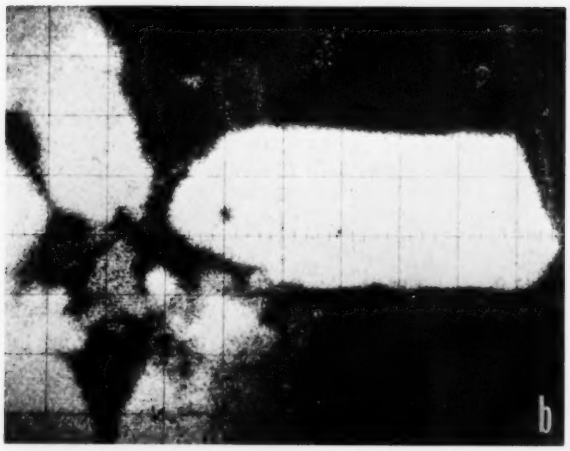

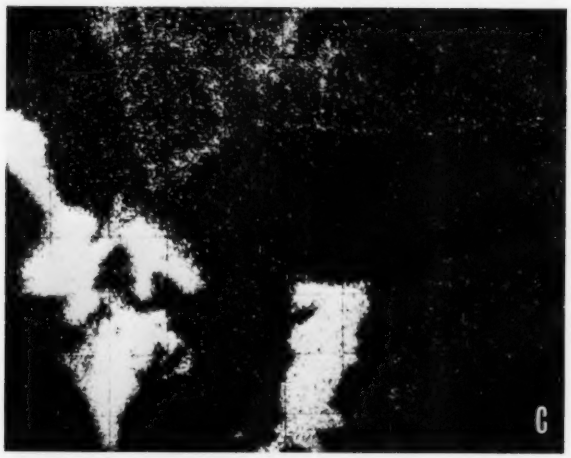

FIGURE 5. *X-ray separation-positives of the naturally occurring mineral, galena, used for illustrating effects of color choice for each partial image.*

a. S–Kα. b. Si–Kα. c. Ag–Lα.

crack, and the locations of these elements as well as Ni are shown by the x-ray area scans (figs. 6b, c, d). Working with only the x-ray area scans, a good deal of patience and intuition is required to reconstruct the exact phase positions in the microstructure. Furthermore, the locations of superposed elements are difficult to discern. The color composite with Al red, Cr green, and Ni blue (fig. 6e, plate 3) shows exactly the phase positions in the microstructure. Mixed colors indicate the presence of superposed elements. The composite is topographically analogous to the optical micrograph, but the major constituents responsible for the structure are identified. The conclusion of the metallurgists regarding the specimen was that oxides of Cr and Al formed during service. These oxides are larger in volume than the host lattice and the Ni lattice failed. Crack propagation then proceeded as more oxide formed. The composite indicates that Cr oxidizes rapidly and that after most of the available Cr is oxidized, Al oxidizes. This mechanism is illustrated by the presence of the Al shell around the Cr.

A typical set of input area scans of a heated dental alloy is shown in figure 7. Exact element superposition is difficult to ascertain without carefully measuring each picture—a tedious, time-consuming task. The composite figure 7d, plate 3 shows Ag-Sn signal superposition yellow. In addition, there are a few particles containing Ag, Hg, and Sn which appear white. The presence of dendrites rich in tin is shown in red and the matrix is cyan which is a Hg-Ag combination. All three phases are immediately apparent. This amalgam also contains Cu which occurs in the same places as does the Hg.

The crystals in this amalgam stand so far above the rest of the surface that optical microscopy is unsatisfactory [2]. No specimen preparation was performed prior to microanalysis. The great depth of focus of the x-ray signal enabled the black-and-whites of figure 7 (See plate d) to be prepared. The color picture serves as a satisfactory "micrograph" of the structure in addition to showing composition effects.

The Tazewell meteorite (Fe-16.7% Ni) is interesting because the iron distribution in the structure constrains the microprobe operator to prepare the Fe input subject in a special fashion. The meteorite was at one time a single-phase alloy of γ-Fe-Ni called taenite. As cooling (at a rate of about 2 °C per million years) proceeded, α-Fe called kamacite, was rejected. Finally, at a low enough temperature two-phase $\alpha+\gamma$, called plessite, formed. In addition a number of phosphides of the type (Fe-Ni P)—called schreibersite—precipitated out.

The iron weight fraction in kamacite is not much greater than in taenite. Similarly, the Ni level in taenite is not much higher than in plessite; Ni is absent from kamacite. Thus, the x-ray area for Fe must be taken with the sharpest focus of oscilloscope dot possible (and at low brightness) in order to preserve the structural identity of kamacite. Exposure times are long in this case and the final image is usually gray rather than

white. Figure 8 shows the results for Fe and Ni; schreibersite inclusions occur in the kamacite (and probably serve as nucleation sites of kamacite [11]).

The composite must show the kamacite to be nearly pure Fe, the Ni gradient from taenite into plessite, and the schreibersite. These features can be seen in figure 8d, plate 1. Kamacite is pure red, the Ni + Fe of taenite is bright yellow near the kamacite and the yellow intensity decreases going further away from the kamacite and into plessite. Schreibersite is nearly white. The exposure time for red was increased to compensate for the grayness of figure 8a.

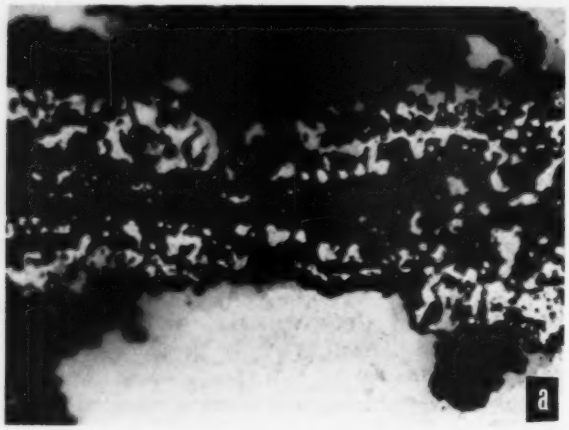

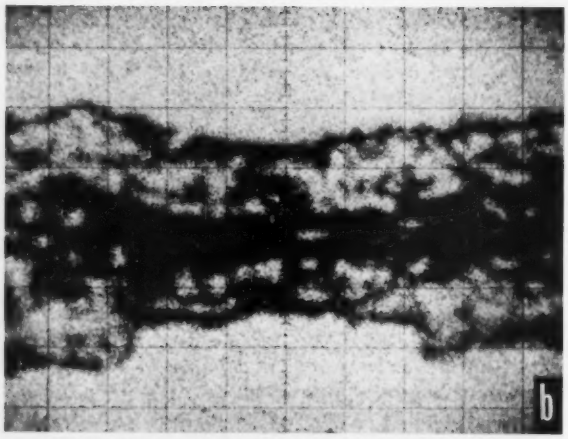

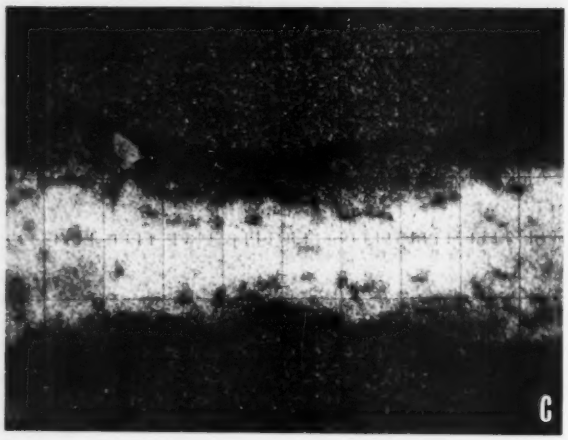

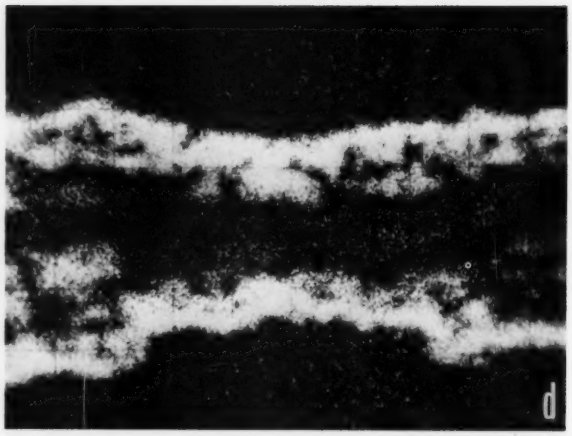

FIGURE 6. *Study of a cracked nickel-base superalloy.*
a. Optical image (unetched). b. X-ray area scan for Ni, (Kα line).
c. X-ray area scan for Cr, (Kα line). d. X-ray area scan for Al, (Kα line).

A two-color application is shown in figure 9, plate 1. The specimen is an Amphiuma red blood cell [12]. Phosphorus (red) occurs mainly in the nucleus while sulfur (cyan) is found primarily outside the nucleus. However, regions containing phosphorus are apparent in the periphery (red and white) and, in turn, some sulfur is present in the nucleus as shown by the white regions. White here indicates the superposition of the phosphorus and sulfur signals. The red dots interspersed in the periphery indicate that some phosphorus occurs where there is no sulfur. This tendency is not readily apparent when examining the original black-and-white area scans.

A gold ore serves as a mineralogical application (fig. 10). Several elements are present in the structure. The composite showing Au, Si, and Ti is shown in figure 10d, plate 3. The ring around the Si is due to diffusion of x-ray signals and not to Au-Si interaction. The input subject for Si was overexposed. The Ti, Si, and Au superpose at many places; these positions can be easily seen on the composite. The Ti rich region seems to be a vein in the ore.

Figure 11 (See plate 3 for fig. 11c) shows Cu located in the Ti rich vein but more finely dispersed than Ti. Backscattered electron signals were used to mark the background.

8. Conclusion

Composite color photographs of microprobe scans can be prepared by color-separation methods in a

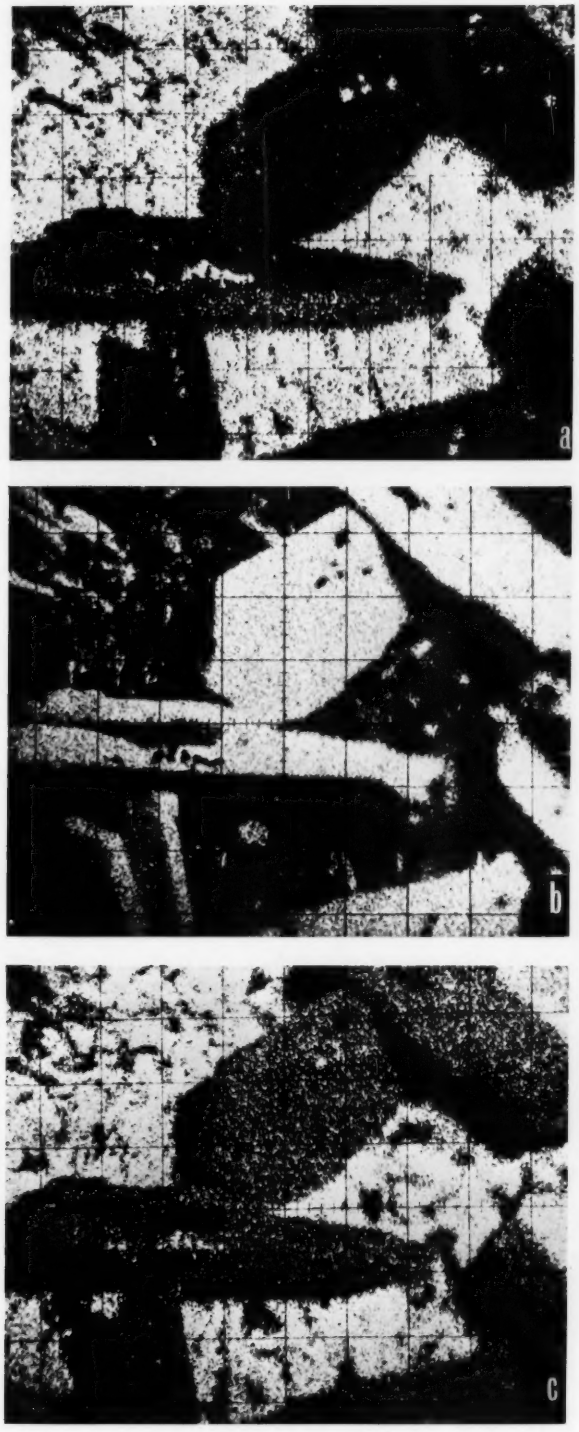

FIGURE 7. *Study of a dental amalgam.*
a. Area scan for Ag, (Lα line). b. Area scan for Sn, (Lα line).
c. Area scan for Hg, (Mα line).

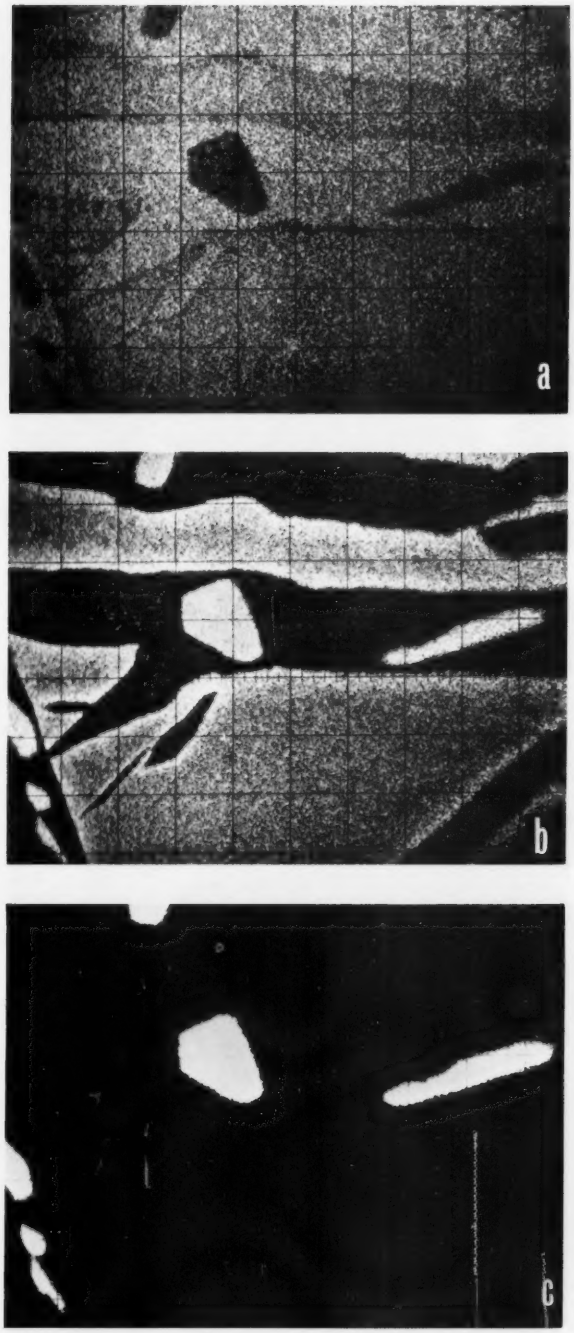

FIGURE 8. *Study of Tazewell meteorite.*
a. Area scan for Fe (Kα line). b. Area scan for Ni (Kα line). c. Area scan for P (Kα line).

routine fashion. The composites can be readily interpreted in terms of the primary colors representing each element and may be aesthetically pleasing as well.

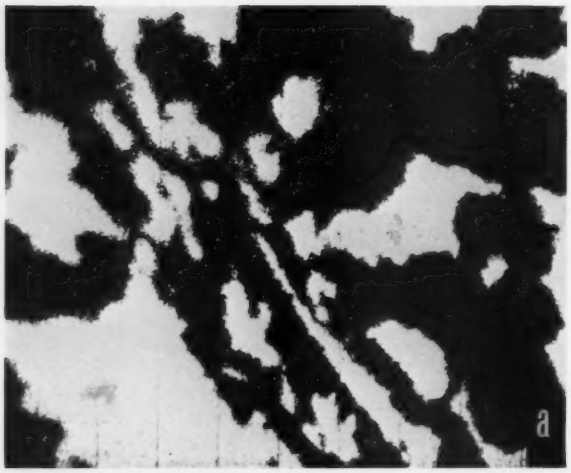

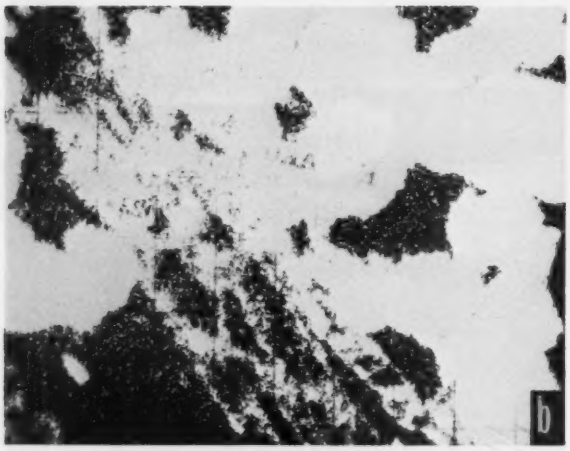

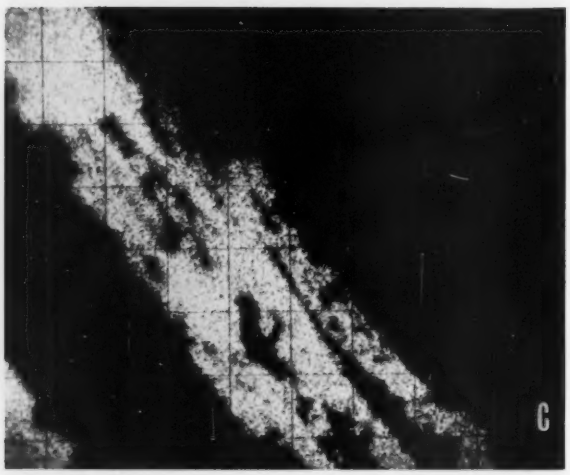

FIGURE 10. *Study of gold ore.*

a. Area scan for Au (Kα line). b. Area scan for Si (Kα line). c. Area scan for Ti (Kα line).

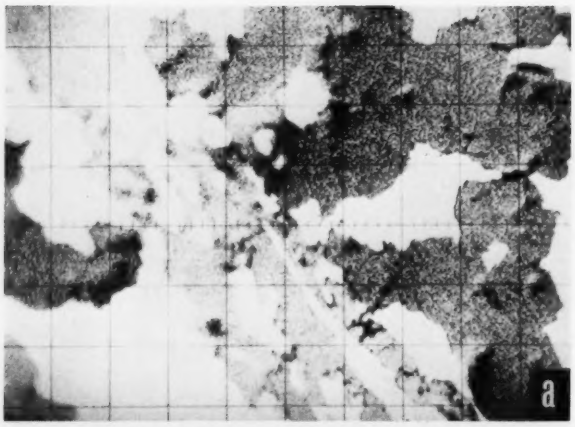

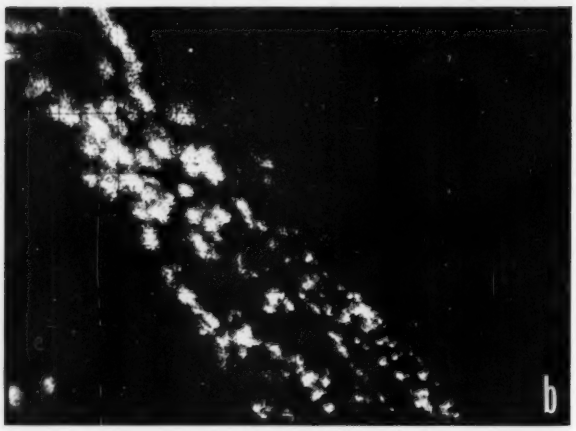

FIGURE 11. *Location of Cu in gold ore.*

a. Backscattered electron photograph. b. Area scan for Cu (Kα line).

Since the cost of preparing color composites is not prohibitive in time, effort or money, we believe that this method will be accepted as a common means of microprobe data presentation.

9. References

[1] Duncumb, P., and Cosslett, V. E., in X-ray Microscopy and Microradiography, p. 347 (V. E. Cosslett, A. Engström and H. H. Pattee, Jr., eds.) (Academic Press, New York (1957)).
[2] Heinrich, K. F. J., ASTM Spec. Tech. Publ. **430,** 315 (1968).
[3] Duncumb, P., Op. Cit. p. 617.
[4] Theisen, R., Mem. Sci. Rev. Met. **60,** 189 (1963).
[5] Heinrich, K. F. J., Adv. X-ray Anal. **7,** 382 (1963).
[6] Ficca, J., private communication (1967).
[7] Jones, M. P., J. Gavrilovič, and Beaven, C. H. J., Trans. Inst. Mining and Met. (Sec. B) **75,** B274 (1966).
[8] Lennartz, G., and Laffolie, H., Mikrochimica Acta **1967** (Suppl. II) p. 279.
[9] Yakowitz, H., and Heinrich, K. F. J., Metallography **1,** No. 1, 55 (1968).
[10] "Color" in Life Magazine for July 3, 1944.
[11] Goldstein, J. I., private communication (1967).
[12] Andersen, C. A., in Methods of Biochemical Analysis **15,** 147, D. Glick, editor (John Wiley & Sons, New York, N.Y., 1967).

(Paper 73A2–539)

Plate 1

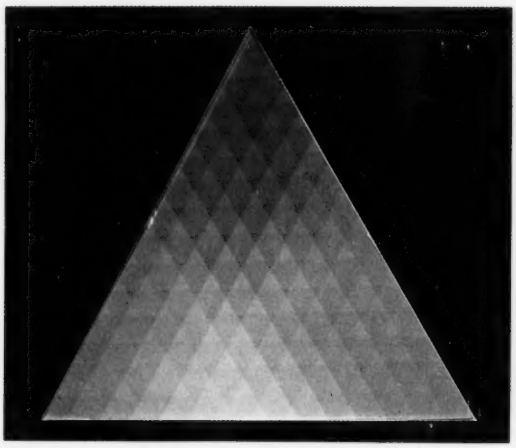

FIGURE 2. *Ternary color mixtures available using rapid development film.*
Note grey central region and cyan, magenta, and yellow fields.

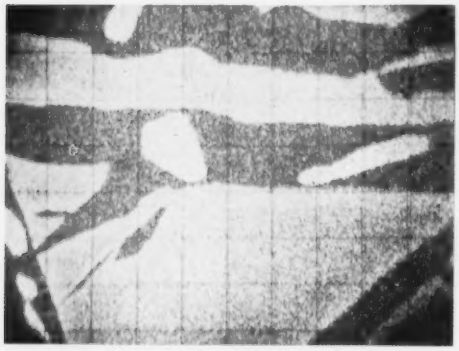

FIGURE 8d. *Composite* Fe *red,* Ni *green,* P *blue.*

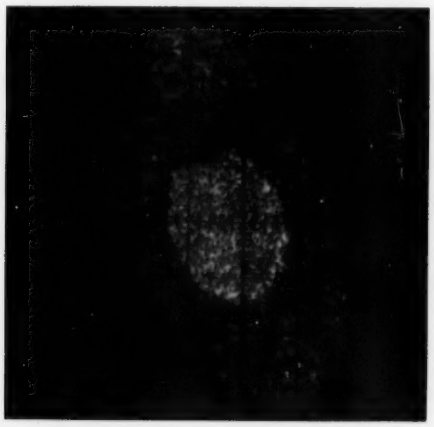

FIGURE 9. *Amphiuma red blood cell.*
Phosphorus red, sulfur cyan. (Original separation-positives made available through the courtesy of C. A. Andersen, Applied Research Laboratories, Inc., Goleta, Calif.)

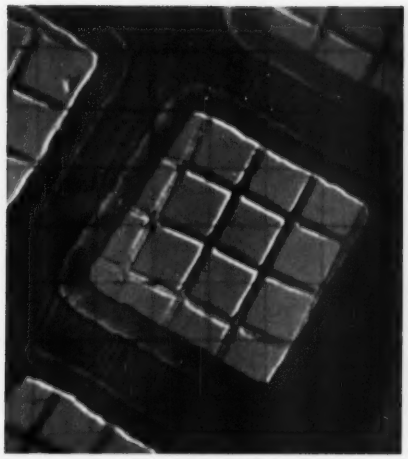

FIGURE 4. *Contrast of each primary and its complement.*
a. *Magenta versus green.*

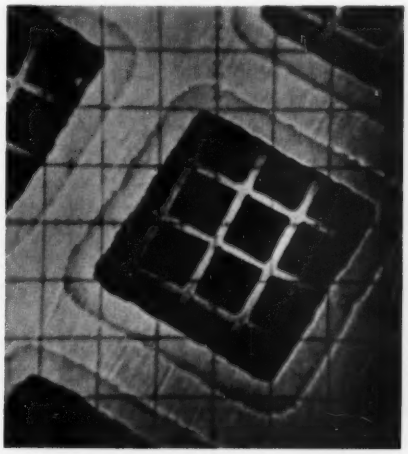

FIGURE 4b. *Yellow versus blue. Note poor yellow-white contrast.*

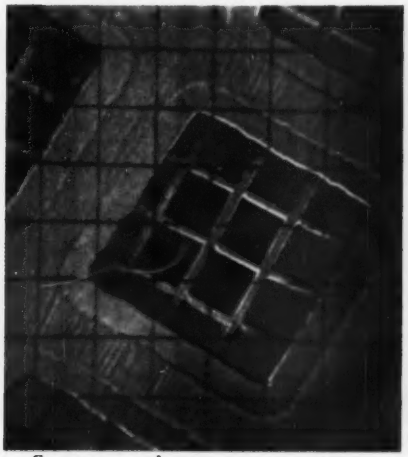

FIGURE 4c. *Cyan versus red.*

Plate 2

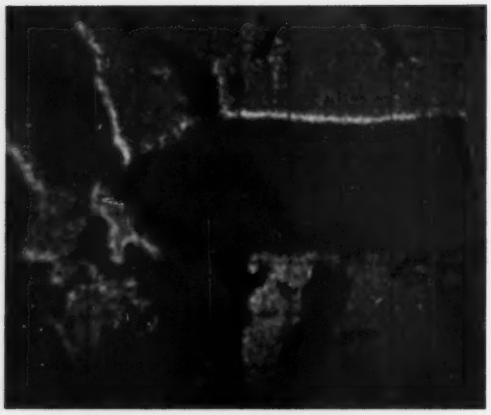

FIGURE 5d. Si *green*, Ag *blue*, S *red*—Si-S *contrast good*; Ag-S *superposition has fair contrast against* S; *background suppressed.*

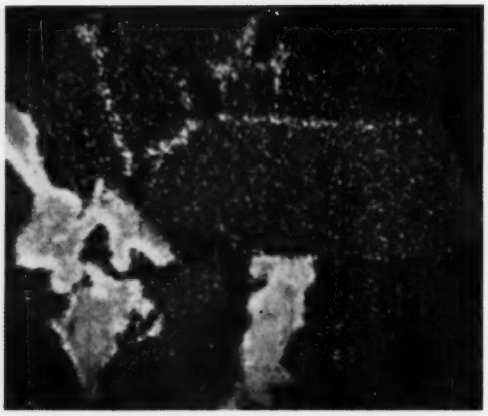

FIGURE 5e. Si *green*, Ag *red*, S *blue*—Si-S *combination poorly contrasted*; Ag-S *juxtaposition stands out; background prominent.*

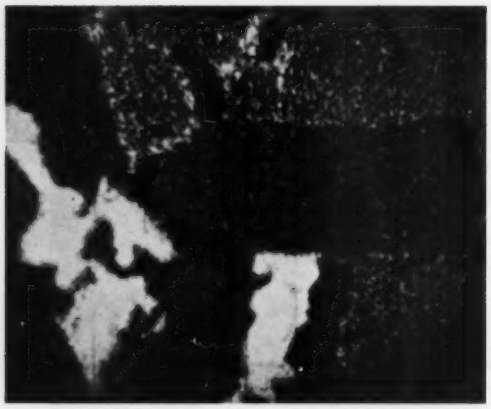

FIGURE 5f. Si *blue*, Ag *red*, S *green*—Si-S *contrast poor*; Ag-S *superposition stands out; background visible.*

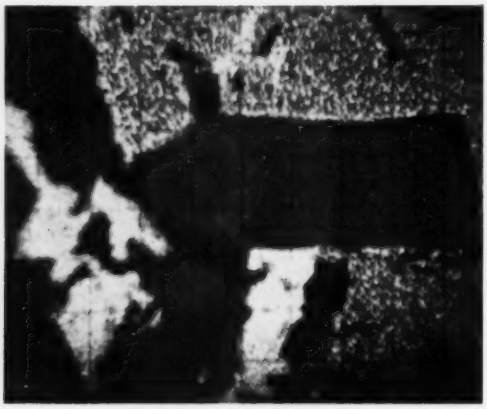

FIGURE 5g. Si *Blue*, Ag *green*, S *red*—Si-S *contrast good*; Ag-S *superposition stands out; background prominent.*

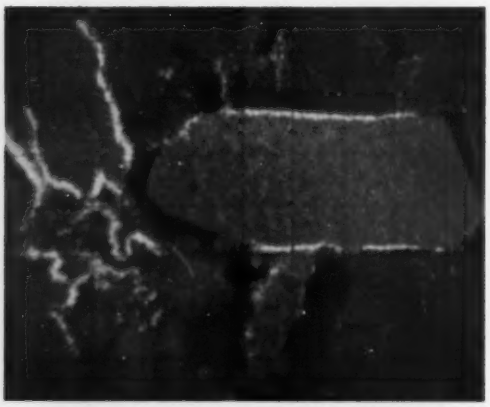

FIGURE 5h. Si *red*, Ag *blue*, S *green*—Si *stands out*; Ag-S *superposition poorly contrasted with* S; *background suppressed.*

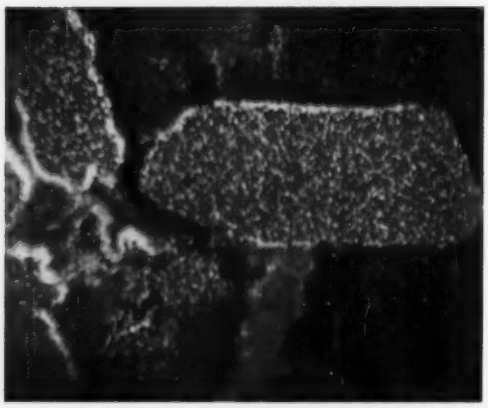

FIGURE 5i. Si *red*, Ag *green*, S *blue*—Si *stands out*; Ag-S *superposition poorly contrasted with* S; *background prominent.*

Plate 3

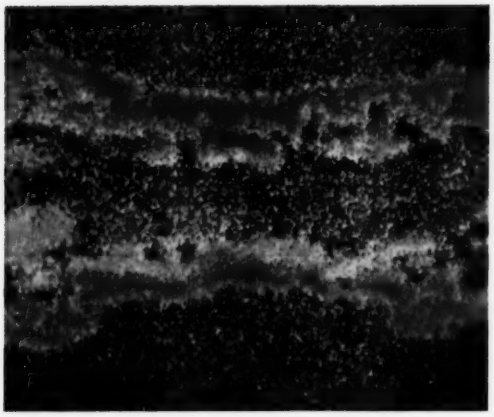

FIGURE 6e. *Composite* Ni *blue*, Cr *green, and* Al *red.*

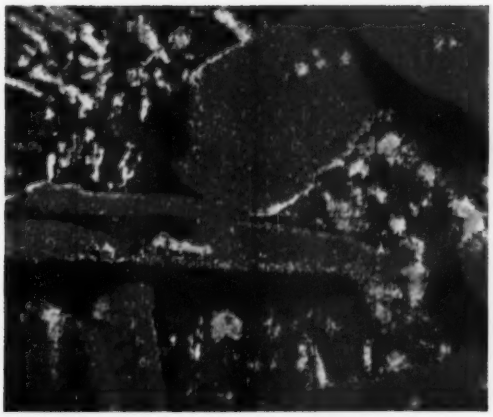

FIGURE 7d. *Composite* Ag *green*, Sn *red*, Hg *blue.*

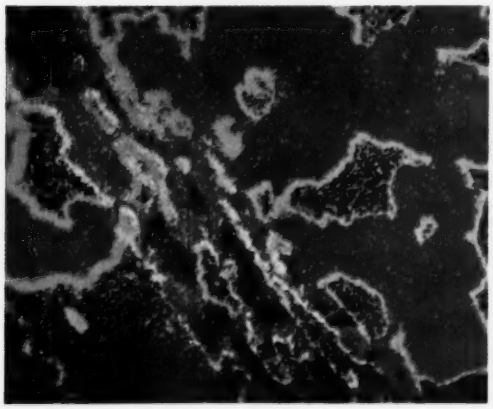

FIGURE 10d. *Composite* Au *green*, Si *red*, Ti *blue.*

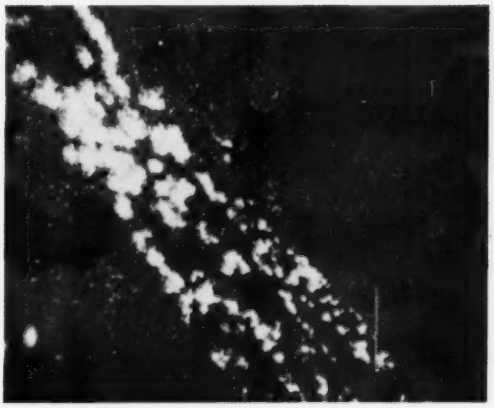

FIGURE 11c. Cu-K *x-ray signal white, backscattered electron picture showing the structure is cyan.*

JOURNAL OF RESEARCH of the National Bureau of Standards—A. Physics and Chemistry
Vol. 73A, No. 2, March–April 1969

Configurations $3d^n4p$ in Singly Ionized Atoms of the Iron Group*

C. Roth[1]

Experimental levels of the configuration $3d^n4p$ in the second spectra of the iron group were compared with corresponding calculated values. Besides the electrostatic and spin-orbit interactions the α, β and T corrections were considered in the individual and general treatments. The insertion of the parameters β and T improved the results by about 21 percent. The rms error on fitting 703 levels by means of 21 free interaction parameters was 231 cm^{-1}. Altogether 912 energy levels were predicted.

Key words: Configurations $3d^n4p$; β and T corrections; energy levels; interaction parameters; iron group; second spectra.

1. Introduction

The configurations $3d^n+3d^{n-1}4s$ in the second spectra of the iron group were considered by Racah and Shadmi [1].[2] Individual and general treatments including the α, β and T corrections were performed for the configurations $3d^n4p$ of the third spectra of the iron group by the author [2]. The configurations $3d^n4p$ in the second spectra of the iron group were considered by Racah and Spector [3], but only in the Russell-Saunders approximation. In the present investigation the spin-orbit interaction was inserted and, in addition, the effects of β and T were considered.

Racah and Trees [4–6] have shown that second order effects caused by perturbations on the configuration l^n by configurations differing from l^n by two electrons can be described by a model interaction of the form

$$\sum_{i<j} 2\alpha(\bar{l}_i \cdot \bar{l}_j)+\beta q_{ij},$$

where q_{ij} is the seniority operator [7]. For the configuration d^n this becomes

$$\alpha[L(L+1)-6n]+\beta Q,$$

where Q is the total seniority operator [7]. If the constant $-6n\alpha$ is incorporated into the height of the configuration the above correction reduces to

$$\alpha L(L+1)+\beta Q.$$

The $\alpha L(L+1)$ correction was first introduced by Trees [4]. The effect of the βQ correction was studied by Racah and Shadmi [8] in the even configurations $(3d+4s)^n$ of the second spectra of V, Cr, and Fe.

Trees and Jorgensen [9] have shown that the main perturbing configuration on $3s^23p^63d^n$ is the configuration $3s^23p^43d^{n+2}$. Trees [10] also remarked that the configuration $3s3p^63d^{n+1}$ should give a perturbation of the same magnitude as $3s^23p^43d^{n+2}$. This perturbation is not included in $\sum_{i<j} 2\alpha(\bar{l}_i \cdot \bar{l}_j)+\beta q_{ij}$, since now the configurations differ by only one electron. By second-order perturbation theory this effect depends upon the ratio $H^2/\Delta E$, where H is the interaction parameter that appears in the nondiagonal term,

$$H=\frac{R^2(3d\ 3d,\ 3d\ 3s)}{35},$$

and ΔE is the energy difference between the two configurations. The parameter $H^2/\Delta E$ is denoted by T. When calculating the model interaction one uses second-order perturbation theory of degenerate configurations which permits the introduction of these interactions before diagonalizing the energy matrices of the separate configurations. Hence the algebraic matrices of T are not diagonal. It should be noted that T represents a three-body interaction whereas α and β represent two-body interactions.

Rajnak and Wybourne [11], by using second-order perturbation theory obtained expressions for the matrix elements of the electrostatic interaction between the l^n configuration and the different species of perturbing configurations differing from l^n by one or two electrons or electron-holes. Effective three-body interactions were considered to account for the perturbation due to one-electron excitations. Racah and Stein [12] developed an elegant method which considerably simplified the calculations of Rajnak and Wybourne.

The electrostatic and spin-orbit interaction matrices for the configurations d^np were available from the

*An invited paper.
[1] Present address: McGill University, Montreal, Canada.
[2] Figures in brackets indicate the literature references at the end of this paper.

matrix library at the Hebrew University. To these matrices the author added the algebraic matrices of the parameters β and T using the program ADDCONF of Racah.

In the first part (the individual treatment, ILS), the algebraic matrices multiplied by radial parameters are diagonalized using the program of Racah [13]. Besides the eigenvalues, the diagonalization routine also yields the derivatives of the eigenvalues with respect to the parameters, the squares of the eigenvectors (percentage compositions) and the calculated Lande g values. The appropriate experimental levels are then fitted to the eigenvalues and using the derivatives obtained in the diagonalization, least squares are performed. In these calculations the improved values of the theoretical energy levels, the corrected values of the parameters including their statistical deviations and the sum of the squares of the differences between the observed and calculated levels are obtained. Then the rms error is defined as

$$\Delta = \sqrt{\frac{\sum_{i=1}^{n} \Delta_i^2}{n-m}}$$

where the Δ_i are the differences between the observed and calculated levels, n is the number of known levels and m is the number of free parameters. The value of Δ is also given by the least squares routine. The same derivatives can be used for several variations in the least squares either imposing different conditions on the parameters or inserting the experimental levels with different assignments. These latter variations are particularly important since they help to determine whether certain experimental levels may be inserted with changed assignments, or in some cases even rejected. The parameters of that variation which yields the best results are used to perform a new diagonalization. This iterative process is continued until mathematical convergence is attained.

If the parameters obtained from the individual treatments can be expressed in terms of simple interpolation formulas a general diagonalization is performed. Then in the general least squares (GLS) all the configurations $3d^n4p$ are considered as one problem by forcing the interaction parameters to vary linearly, or perhaps linearly with small quadratic corrections.

2. Parameters

For the d–d interaction the Slater parameters F^2 and F^4 were replaced by

$$B = \frac{1}{441}\,[9F^2(dd) - 5F^4(dd)] = F_2(dd) - 5F_4(dd)$$

$$C = \frac{5}{63}\,F^4(dd) = 35F_4(dd).$$

For the d-p interaction the parameters F_2, G_1, and G_3 are given by

$$F_2 = \frac{1}{35}\,F^2(dp),\ G_1 = \frac{1}{15}\,G^1(dp) \text{ and } G_3 = \frac{3}{245}\,G^3(dp).$$

The parameters of the spin-orbit interactions for the electrons d and the electron p are denoted by ζ_d and ζ_p, respectively. The three correction parameters mentioned previously are denoted by α, β, and T. Finally, the additive parameter chosen to normalize to zero the lowest energy value for a particular configuration, is denoted by A.

3. Discussion and Results

The electrostatic parameters for the initial diagonalization were taken from Racah and Spector [3]. Since d^n is the core of the configuration d^np, approximate values for the parameters B, C, α, and ζ_d could be obtained from Shadmi [16] in the treatment of the configurations $3d^n + 3d^{n-1}4s$ in the third spectra of the iron group. As B, C, and α are already given [3], we only need to take the values of ζ_d from Shadmi. We then obtain [16]

$$\zeta_d(d^np) = 387 + 95(n-5) + 9[(n-5)^2 - 10].$$

The initial values of ζ_p were obtained by using the experimental levels of Ca II-$4p$ and Zn II-$3d^{10}4p$ for $\zeta_p(p)$ and $\zeta_p(d^{10}p)$, and then interpolating.

Thus, initially,

$$\zeta_p(d^np) = 43n + 149.$$

Using interpolative values for the interaction parameters, the energy matrices for the configurations d^np were diagonalized. Individual least squares were then performed for the configurations Sc II-d^1p, Ti II-d^2p, V II-d^3p, Cr II-d^4p, Mn II-d^5p, Fe II-d^6p, Co II-d^7_p, Ni II-d^8p and Cu II-d^9p, by means of which we determined how to fit the experimental levels.

General least squares were then considered in which 372 theoretical terms splitting into 912 levels were taken into account. Initially, 224 experimental terms splitting into 599 levels were fitted. As the matrices in the initial diagonalization did not include the matrices of β and T, we only considered one variation in the GLS. With 28 free parameters, the rms error was 295.

The parameters obtained from the GLS were used in the diagonalizations of the second iteration. There the matrices of β and T were already included, but the initial values of the parameters β and T were zero. However, derivatives with respect to these two parameters were obtained enabling the study of the effects of β and T on a particular configuration and in the general problem. With β and T eliminated in the GLS the rms error in the second iteration was 293. When β and T were allowed to vary linearly from configuration to configuration the rms error was reduced to 233. In that variation the values of β and T were

$$\beta(d^np) = -465 \pm 32 - (9 \pm 22)(n-5)$$

$$T(d^np) = -3.4 \pm 0.2 + (0 \pm 0.2)(n-5).$$

As in the configurations $d^n p$ of the third spectra, the insertion of β and T caused the value of α to drop. With β and T eliminated α had the values

$$\alpha_1(d^n p) = (75.1 \pm 1.4) + (6.1 \pm 1.1)(n-5).$$

When β and T were allowed to vary linearly we obtained

$$\alpha_2(d^n p) = (41.3 \pm 2.0) + (5.9 \pm 1.7)(n-5).$$

As for the configurations $d^n p$ in the third spectra the values of C increased notably when β and T were permitted to vary linearly. With β and T eliminated we had

$$C_1(d^n p) = (3216.0 \pm 8.3) + (293.2 \pm 6.5)(n-5)$$

whereas for β and T changing linearly, we obtained

$$C_2(d^n p) = (3413.2 \pm 15.1) + (320 \pm 10.2)(n-5).$$

This result is as expected since if we consider the basis configuration d^2 the only term affected by β is ^1S which contains 7C.

The above values of 233 and 293 for the rms errors in the GLS with and without β and T respectively, should be compared with the value of 361 obtained by Racah and Spector [3].

From the results of Iglesias and Velasco [14], we inserted an additional 49 terms splitting into 104 levels in the spectrum of Mn II $-3d^5 4p$. In the GLS with β and T allowed to vary linearly the rms error on fitting 273 terms splitting into 703 levels by means of 32 free parameters was 231. The fact that the rms error dropped in the GLS seems to indicate that the levels of Iglesias and Velasco are indeed valid levels.

In the plots of the parameters versus atomic number in figures 1–8, the values given are from the individual least squares (the vertical lines indicate the rms errors in the values of the parameters). The straight lines (for ζ_d the parabola) give the values of the parameters from the corresponding general least squares. From the graphs it is apparent that the assumption of linearity (for ζ_d with a small quadratic correction) is valid here.

Unless specified otherwise the source of the experimental data is "Atomic Energy Levels," Vols. **I** and **II** by C. E. Moore [15], henceforth referred to as AEL.

The numerical values of all levels and parameters are in cm^{-1}.

We now wish to discuss briefly the results for each configuration.

Ca II-$4p$

This configuration consists of only one term splitting into two levels. It is useful in providing a value for ζ_p.

Sc II-$3d4p$

In Sc II-dp, all the predicted levels are given in AEL. In the individual least squares we initially fitted the 6 terms splitting into 12 levels by using the 4 electrostatic parameters A, F_2, G_1 and G_3, and the spin-orbit parameters ζ_d and ζ_p. The rms error was 478. This very high value can be attributed to the fact that there is a strong interaction between the configurations dp and sp. The 4 levels of the terms ^1P and ^3P were thus not considered in the GLS.

The 8 levels of the terms ^1D, ^3D, ^1F, and ^3F fitted well in the GLS. The experimental g values also fitted nicely to the calculated values.

Ti II-$3d^2 4p$

In the configuration $d^2 p$ there are 19 theoretical terms splitting into 45 levels. The only experimental term missing for Ti II is $(^1S)^2P$.

In the individual least squares a rms error of 319 was obtained, which seems to indicate that this configuration is strongly perturbed by the configuration $3d4s4p$. There were no changes in assignment.

Since there are no observed levels based on the term $3d^2\,^1S$, we can have only 4 electrostatic parameters of the core, i.e., A, B, C and α to determine the parents ^3P, ^1D, ^3F, and ^1G of d^2. If we give either β or T freedom, then the problem is overdefined.

The above value of 319 for the rms error should be compared with the value of 421 obtained by Racah and Spector [3].

V II $-3d^3 4p$

In the configuration $d^3 p$ there are 48 predicted terms splitting into 110 levels. The experimental data for V II $-3d^3 4p$ is almost complete. There are only 5 terms missing, all based on the parent term $3d^3 B^2 D$. In addition to the 43 terms splitting into 101 levels, which are assigned to $d^3 p$, there are 7 additional odd levels whose configuration assignments are not given.

The level 1°_4 at 62761.9 definitely does not belong to the configuration $d^3 p$ as there is no calculated level in that vicinity to which it could be assigned.

In the individual least squares several attempts were made to fit the nine high levels (above 75,000) given in AEL. However, we could not come to a definite conclusion whether any or all of these levels belong to $d^3 p$. Thus, it was decided not to insert any of these high levels in the individual least squares, which were then performed with 42 terms splitting into 98 levels. Since no levels based upon the term $d^3 B^2 D$ (the only term having a nonvanishing value of Q) were inserted into the individual least squares, the only meaningful variation was to let both β and T to equal zero. The rms error in the second iteration was then 269, which should be compared with Racah and Spector's value of 390 [3].

The high levels were again considered in the GLS. When these experimental levels were compared with the calculated levels in the GLS closest to them, the deviations in each case were greater in magnitude than 600. When the levels were actually inserted into the GLS, the values of β were

$$\beta(d^n p) = -495 \pm 32 + (92 \pm 21)(n-5).$$

Thus for V II $-d^3 p$, this would cause β to have a value of -679, which is not reasonable. It is probable that most or all of these high levels belong to the configuration $d^2 sp$.

The following changes in assignment were performed:

1. $(a\ ^4F)z\ ^5D_3 \leftrightarrow (a\ ^4F)z\ ^3D_3$
2. $(a\ ^4P)z\ ^3P_{0,1,2} \leftrightarrow (a\ ^4P)y\ ^5D_{0,1,2}$
3. $(a\ ^2G)z\ ^1G_4 \leftrightarrow (a\ ^2G)y\ ^3F_4$
4. $(a\ ^2P)z\ ^1P_1 \leftrightarrow (a\ ^2D)y\ ^1P$

In all four exchanges there was strong mixing between the eigenfunctions of the levels involved.

The agreement between the experimental and calculated g values is quite good except for the case of $(^4P)y\ ^5D_4$. This level is 98 percent $(^4P)\ ^5D$, and the remaining 2 percent are also ^5D. Thus, the calculated g value exactly equals the theoretical g value of 1.500 for pure LS compling. The value of 2.28 given in AEL for this level seems definitely wrong, as 1.5 is the highest theoretical g value for any level of J equal to 4 in the configuration d^3p.

Cr II-$3d^44p$

The configuration d^4p comprises 68 theoretical terms splitting into 180 levels; in AEL, 51 experimental terms splitting into 139 levels are given. We included all the experimental levels, but performed the following changes in assignment:

1. $(a\ ^5D)z\ ^4P_{5/2} \leftrightarrow (a\ ^5D)z\ ^6D_{5/2}$
2. $(a\ ^3H)z\ ^4G_{5/2,\ 7/2,\ 9/2,\ 11/2} \leftrightarrow (a\ ^3F)y\ ^4G_{5/2,\ 7/2,\ 9/2,\ 11/2}$
3. AEL $(a\ ^3P)z\ ^2D_{3/2} \rightarrow (A^3P)z\ ^2P_{3/2}$
4. AEL $(a\ ^3P)z\ ^2P_{3/2} \rightarrow (A^3F)y\ ^4F_{3/2}$
5. AEL $(a\ ^3P)z\ ^2D_{5/2} \rightarrow (A^3F)y\ ^4F_{5/2}$
6. AEL $(a\ ^3F)y\ ^4F_{3/2,\ 5/2} \rightarrow (A^3F)z\ ^2D_{3/2,\ 5/2}$
7. AEL $(a\ ^3G)x\ ^4F_{3/2} \rightarrow (A^3P)\ ^2D_{3/2}$
8. AEL $(a\ ^3F)y\ ^2D_{5/2} \rightarrow (A^3P)\ ^2D_{5/2}$
9. AEL $(a\ ^3F)y\ ^2D_{3/2} \rightarrow (^3G)x\ ^4F_{3/2}$
10. $(a\ ^1I)y^2I_{13/2} \leftrightarrow (^1I)z\ ^2K_{13/2}$
11. $(a\ ^1G)w\ ^2H_{9/2,\ 11/2} \leftrightarrow (^1I)x\ ^2H_{9/2,\ 11/2}$
12. AEL $(a\ ^3D)x\ ^2F_{5/2,\ 7/2} \rightarrow (A^1G)x\ ^2F_{5/2,\ 7/2}$
13. AEL $(a\ ^1G)w\ ^2F_{5/2,\ 7/2} \rightarrow (^3D)w\ ^2F_{5/2,\ 7/2}$
14. AEL $(b\ ^3F)u\ ^2G_{7/2,\ 9/2} \rightarrow (B^3F)\ ^4G_{7/2,\ 9/2}$

In the first instance, the eigenfunctions of the levels $z\ ^4P_{5/2}$ and $z\ ^6D_{5/2}$ were mixed considerably. Without the exchange the splittings of the two terms $z\ ^4P$ and $z\ ^6D$ were very bad, whereas after the exchange they were excellent.

Although the eigenfunctions of the levels of the terms $z\ ^4G$ and $y\ ^4G$ are mixed slightly, it is apparent that the parents of these two terms are not correct in AEL and thus should be exchanged as indicated in 2.

In the first diagonalization the term $(A^3F)^2D$ was at 67,000 and the term $(A^3P)^2D$ at around 69,500. Thus, the parents of $z\ ^2D$ and $y\ ^2D$ do not seem to be correct as given in AEL and so we made the exchange $(a\ ^3P)z\ ^2D \leftrightarrow (a\ ^3F)y\ ^2D$. Some high deviations of around 600–700 still appeared in the individual least squares for the terms $(A^3P)^2P$, $(A^3F)^2D$, $(A^3F)^4F$, $(A^3P)^2D$ and $(^3G)^4F$. However, by making the changes 3, 4, 5, 6, 7, 8, and 9 the agreement of all the levels involved was improved considerably. Although these changes are quite numerous, it should be emphasized that in most cases the eigenfunctions of the levels involved were strongly mixed.

The eigenfunctions of the levels $(^1I)z\ ^2K_{13/2}$ and $(^1I)y\ ^2I_{13/2}$ are mixed considerably. The exchange 10 improved the agreement of these 2 levels as well as the splittings of the terms $z\ ^2K$ and $y\ ^2I$.

Theoretically, the term $(A^1G)^2H$ is predicted at around 74,500, whereas the term $(^1I)^2H$ is predicted at around 77,500. Thus, it is necessary to exchange $x\ ^2H$ and $w\ ^2H$ as indicated in 11. Changes 12 and 13 are similar to 11.

The term $(B^3F)^2G$ is predicted at around 94,000. Thus, if the experimental levels of $u\ ^2G$ are fitted to the theoretical levels of the same term designation, then the resulting deviations are about -3000. However, the term $(B^3F)^4G$ is predicted at 91,000. Therefore, if the levels of $u\ ^2G$ are fitted to $(B^3F)^4G_{7/2,\ 9/2}$, the agreement is excellent as the deviations in the general least squares are then only 194 and 223 (in the individual least squares they are 141 and 160).

Most of the changes in this investigation, and especially the change in assignment 14, indicate that poor agreement can be obtained by using the Russell-Saunders approximation. In the L–S approximation [3] the rms error was 550, which was partly attributed to the fact that the term $(B^3F)\ u\ ^2G$ had a very large deviation. This term was then neglected altogether and subsequently the rms error was reduced to 384. Actually, the levels $u\ ^2G$ can be fitted very nicely if assigned to $(B^3F)^4G$.

In the GLS of Racah and Spector [3], deviations of 735 and 1117 were obtained for the terms $(a\ ^1D)w\ ^2D$ and $(a\ ^1D)v\ ^2F$, respectively. The deviations we obtained were much lower. In the GLS, the deviations for $w\ ^2D$ were 348 and 307, whereas for $v\ ^2F$ they were 461 and 451. In these two cases the deviations were reduced because of β and T, since in the GLS with β and T eliminated the deviations for these two terms were of about the same magnitude as those obtained by Racah and Spector [3].

In the individual least squares of the first iteration the rms error was 292. In the second iteration, with β and T eliminated, the rms error was reduced to 287. When β and T were allowed to change freely, the rms error dropped to 200. In that variation the values of β and T were

$$\beta = -495 \pm 64$$

$$T = -4.1 \pm 0.4.$$

The agreement between the experimental and calculated g values is very good.

Mn II – $3d^54p$

From 88 theoretical terms splitting into 214 levels, only 20 experimental terms splitting into 66 levels are given in AEL. In the individual least squares, the following change in assignment was performed

1. $(a\ ^4G)z\ ^5F_{1,2} \leftrightarrow (a\ ^4P)z\ ^5D_{1,2}$

There was some mixing between the eigenfunctions of the levels involved and the deviations as well as the

splittings of the terms $z\ ^5D$ and $z\ ^5F$ were improved considerably after the exchange.

The two Lande g values for the levels $(a\ ^4G)z\ ^5G_2$ and $(a\ ^4G)z\ ^5H_3$, given in AEL, seem to be misprints. The calculated g value for the level $z\ ^5G_2$ is 0.338, whereas the theoretical g value for $^5G_2$ is 0.333. Thus, the experimental value of 1.31 does not fit for this level. Similarly the calculated g value for $z\ ^5H_3$ is 0.519, and the theoretical g value for $^5H_3$ is 0.500. Again, the experimental value of 1.30 cannot be accepted for this level. We tried to refer to the original work on the measurements of the g-values, but this work was performed by Catalan and the results were not published.

In the first iteration, the rms error in the individual least squares was 180. In the second iteration with β and T eliminated, the rms error was reduced to 172. As explained by Racah [17], the parameter T has very little significance in the configuration d^5p. Thus, we only considered the variation with β free and T eliminated. Then, the rms error was reduced to 167, with β having a value of -410 ± 97.

We tried to fit the levels of Iglesias and Velasco [14] in the individual as well as the general least squares. Iglesias and Velasco assign 50 new terms splitting into 108 levels to the configuration $3d^54p$. Of these, the three levels of the term w^5P should be assigned to $3d^5(a\ ^6S)5p\ ^5P$. This follows simply from the fact that these three levels are not new and were already given in AEL with that assignment. They definitely do not belong to the configuration $3d^54p$. In addition, the level x^5F_1 at 81237 was rejected as it would fit only with a deviation of -1300 in the GLS. Then, by inserting 104 new levels in the individual least squares of the second iteration with T eliminated and β free, the rms error increased from 167 to 226. In that variation, the value of β was -356 ± 37. In the GLS the 104 new levels fitted very well and the rms error did not rise by the insertion of these levels. Also, the experimental g values of Iglesias and Velasco fitted well to the calculated g values.

The following changes in assignment were made for the 104 new levels:

1. $(^4F)x\ ^5F_2 \leftrightarrow (^4F)y\ ^5G_2$
2. $(^4F)x\ ^5F_3 \leftrightarrow (A^2D)x\ ^3D_3$
3. $(^4F)x\ ^5F_4 \leftrightarrow (A^2F)y\ ^3G_4$
4. $(A^2G)y\ ^1G_4 \leftrightarrow (^4F)v\ ^3F_4$
5. $(A^2G)v\ ^3G_5 \leftrightarrow (A^2G)y\ ^1H_5$

When the levels of the term x^5F were assigned to the theoretical levels of $(^4F)x\ ^5F$ the deviations were around -1000 for the levels of J equal 2–5, and almost -1500 for $x\ ^5F_1$. Several variations were attempted to reduce these deviations. However, in all cases the magnitude of the deviation for $x\ ^5F_1$ was always greater than 1000. Thus, we rejected this level. After the exchanges 1, 2, and 3 the agreement between the observed and calculated values of the levels and g factors of the terms $y\ ^5G$, $x\ ^3D$ and $y\ ^3G$ is very good. The agreement of the four remaining levels of x^5F is also quite good. However, here the experimental and calculated splittings of $(^4F)x\ ^5F$ do not correspond as closely as for the other three terms, $y\ ^3G$, $x\ ^3D$ and $y\ ^5G$.

The changes 4 and 5 were accepted because of the subsequent improvements in the fitting of all the levels involved. The calculated intervals between the levels of the terms $v\ ^3F$ and $v\ ^3G$ also corresponded more closely to the experimental intervals after the changes.

All the new levels of Iglesias and Velasco [14] are of unspecified parentage. In table 16 the calculated percentage composition of each level is indicated.

Fe II – $3d^64p$

In the configuration d^6p there are 68 theoretical terms splitting into 180 levels. In AEL, 54 experimental terms splitting into 149 levels are given. All the experimental levels were inserted, with the following changes in assignment:

1. $(a\ ^3H)z\ ^4H_{9/2,\ 11/2,\ 13/2} \longleftrightarrow (a\ ^3H)z\ ^4I_{9/2,\ 11/2,\ 13/2}$
2. $(a\ ^3D)x\ ^2F_{5/2,\ 7/2} \longrightarrow (A^1G)^2F_{5/2,\ 7/2}$

As in most instances of changes in assignment, here also the eigenfunctions of the levels involved in both changes are mixed considerably.

The term whose experimental assignment is $(a\ ^3D)x\ ^2F$, is fitted to $(A^1G)^2F$, whereas the levels of $w\ ^2F$ are fitted to $(A^3D)^2F$. The other terms, with no specified parentage in AEL, i.e., $x\ ^2H$ and $w\ ^2H$, are assigned to $(A^1G)x\ ^2H$ and $(^1I)w\ ^2H$, respectively.

In the first iteration the rms error in the individual least squares was 277. In the second iteration with β and T allowed to change freely the rms error was reduced to 176. In that variation the values of β and T were

$$\beta = -525 \pm 39$$

$$T = -3.5 \pm 0.3.$$

The value of 176 should be compared with the rms error of 366 in the $L-S$ approximation [3].

In AEL, 29 very high odd levels are given without any configuration assignment. It is possible to assign several of these levels to the configuration $3d^64p$. However, it is quite likely that most or all of these levels actually belong to the configurations $3d^54s4p$ and/or $3d^65p$. Thus, we did not insert any of them in the least squares calculations.

At this opportunity we wish to point out a misprint in AEL. The term $y\ ^6P$ should be labeled as $3d^54s(a\ ^7S)4p$, and not as $3d^6(a\ ^7S)4p$.

Co II – $3d^74p$

From 48 theoretical terms, splitting into 110 levels, only 11 experimental terms splitting into 37 levels are given in AEL. All known terms are based on ^4P and ^4F of $3d^7$. Thus, the parameters C and α must be kept fixed in the least squares calculations in order to obtain meaningful results. The 37 experimental levels fitted without changes in assignment. The agreement between the experimental and calculated g values was very good. In the individual least squares, the rms error was 148. As expected, this is only a small improvement from the value of 158 obtained by Racah and Spector [3]. The level $3d^7(a\ ^4P)4p\ ^5D_1$, which is given with a question mark in AEL, fits nicely to the calculated level with the same assignment.

Ni II $-3d^84p$

As in Ti II $-3d^24p$, the only term missing in this configuration is $3d^8(^1S)4p\,^2P$. The 18 experimental terms split into 43 levels. There were no changes in assignment, and the rms error in the individual least squares was 158 for both iterations. As in Ti II, since there are no levels based on $d^8\,^1S$, the parameters β and T must be eliminated in the individual least squares. The two levels of the term $(^1G)x\,^2F$, which are given as uncertain in AEL, fit quite well, although in the last GLS the deviation for the level $(^1G)x\,^2F_{5/2}$ was -526.

There is considerable sharing in g values between the experimental levels $(^3P)y\,^2P_{1/2}$ and $(^3P)z\,^2S_{1/2}$. This is evident from the fact that the experimental g value of $y\,^2P_{1/2}$ is given as 1.039, whereas the theoretical g value for $^2P_{1/2}$ is 0.667 and the theoretical g value for $^2S_{1/2}$ is 2.000. However, the calculated eigenfunction of $(^3P)^2P$ has only 5 percent of $(^3P)^2S$ and so the experimental g value of 1.039 fits poorly to the calculated value of 0.730. Although the experimental values of the two levels $y\,^2P_{1/2}$ and $z\,^2S_{1/2}$ differ by 380, the calculated levels in the GLS differ by 923.

The agreement between the experimental and calculated g values of the other levels is very good.

Cu II $-3d^9\,4p$

In this configuration all the 6 theoretical terms splitting into 12 levels are known experimentally. The following changes in assignment were performed:

1. $^3D_2 \leftrightarrow {}^1D_2$

2. $^3D_3 \leftrightarrow {}^1F_3$

The above changes are analogous to those of Zn III $-3d^94p$ [2], and again the eigenfunctions of the levels involved are mixed. In the individual least squares the rms error was 119.

The agreement between the observed and calculated g-factors of the $^3D_1$ and $^1P_1$ levels in the general treatment is poor. However, in the individual treatment of the configuration Cu II $-3d^9\,4p$ the agreement for all the g-factors is excellent.[3] Thus, since the parameters were forced to be linear in the general treatment the theoretical levels $^3D_1$ and $^1P_1$ were not mixed properly.

Zn II $-3d^{10}\,4p$

This configuration consists of only 1 term splitting into 2 levels and is useful in obtaining a value for ζ_p.

4. Table Entries

4.1. Parameters: Tables 1–10

In the general diagonalization all the parameters with the exception of ζ_d had approximate expressions of the form

$$P(d^np) = P + (n-5)\Delta P.$$

In the general least squares then only P and ΔP were the independent parameters.

For ζ_d we had

$$\zeta_d(d^np) = \zeta_d + (n-5)\Delta_1\zeta_d + [(n-5)^2 - 10]\Delta_2\zeta_d.$$

Here ζ_d, $\Delta_1\zeta_d$ and $\Delta_2\zeta_d$ were the independent parameters in the general least squares.

The numerical values of the parameters for the initial general diagonalization are given in the column GDIAG 1.

The columns ILS1 and GLS1 give the values of the parameters of the initial iteration with β and T eliminated, in the individual and general least squares, respectively. The columns ILS2 and GLS2 give the values of the parameters of the second iteration with β and T eliminated, in the individual and general least squares, respectively. The columns ILS'2 and GLS'2 give the values of the parameters of the second iteration with β and T free to change in the individual and general least squares, respectively.

[3] Results to be published soon in a paper dealing specifically with the odd configurations of Cu II.

TABLE 1. *Parameters of* Sc II $-$ 3d4p

Parameters	GDIAG 1	ILS 1 (All levels)	GLS 1	GLS 2	GLS' 2
A	29588	28972 ± 154	28926	28948	29071
F_2	287	244 ± 27	285	293	285
G_1	354	345 ± 39	330	334	335
G_3	21	14 ± 13	26	26	26
α	55	Fix 55	51	49	25
ζ_d	61	160 ± 194	54	51	55
ζ_p	192	-56 ± 490	191	192	197
Δ	.....	478	.....	.....	.....

TABLE 2. *Parameters of* Ti II – $3d^24p$

Parameter	GDIAG 1	ILS 1	GLS 1	ILS 2	GLS 2	GLS′ 2
A	37585	37568 ± 94	37596	37569 ± 94	37608	38241
B	685	694 ± 9	701	697 ± 9	692	718
C	2291	2358 ± 69	2336	2349 ± 69	2327	2420
F_2	299	288 ± 9	295	286 ± 9	302	295
G_1	348	329 ± 12	326	328 ± 12	331	330
G_3	24	26 ± 4	28	25 ± 4	28	28
α	60	57 ± 10	57	57 ± 10	56	30
β	.....	.....	.....	Fix 0	Fix 0	−426
T	.....	.....	.....	Fix 0	Fix 0	−3.2
ζ_d	93	132 ± 55	116	134 ± 55	118	123
ζ_p	235	209 ± 137	229	216 ± 138	230	226
Δ	.....	320	.....	319	.....	.....

TABLE 3. *Parameters of* V II – $3d^34p$

Parameter	GDIAG 1	ILS 1	GLS 1	ILS 2	GLS 2	GLS′ 2
A	49601	49698 ± 90	49661	49750 ± 79	49628	50344
B	750	755 ± 5	763	764 ± 5	756	773
C	2605	2602 ± 26	2630	2629 ± 24	2625	2749
F_2	311	319 ± 8	306	306 ± 7	312	306
G_1	342	325 ± 8	323	326 ± 7	327	325
G_3	27	34 ± 3	30	34 ± 3	30	30
α	65	63 ± 4	63	60 ± 4	62	34
β	.....	.....	.....	Fix 0	Fix 0	−436
T	.....	.....	.....	Fix 0	Fix 0	−3.2
ζ_d	143	199 ± 44	185	183 ± 39	191	197
ζ_p	278	209 ± 99	267	196 ± 89	268	255
Δ	.....	284	.....	269	.....	.....

TABLE 4. *Parameters of* Cr II – $3d^4 4p$

Parameter	GDIAG 1	ILS 1	GLS 1	ILS 2	ILS′ 2	GLS 2	GLS′ 2
A	68645	68493 ± 125	68679	68502 ± 123	69338 ± 116	68673	69142
B	815	818 ± 5	825	816 ± 5	833 ± 4	820	828
C	2919	2959 ± 17	2923	2961 ± 16	3092 ± 19	2922	3078
F_2	323	314 ± 7	316	316 ± 6	310 ± 5	321	316
G_1	336	321 ± 7	320	324 ± 7	321 ± 5	323	320
G_3	30	31 ± 2	32	30 ± 2	32 ± 2	31	32
α	70	66 ± 3	69	64 ± 3	34 ± 4	68	38
β	.....	.....	.....	.....	−495 ± 64	.....	−445
T	.....	.....	.....	.....	−4.1 ± 0.4	.....	−3.2
ζ_d	211	208 ± 46	262	230 ± 38	283 ± 31	270	277
ζ_p	321	378 ± 81	305	362 ± 74	309 ± 55	306	283
Δ	.....	292	.....	287	200	.....	.....

TABLE 5. *Parameters of* Mn II – $3d^5 4p$ [a]

Parameter	GDIAG 1	ILS 1 (66 levels)	GLS 1	ILS 2	ILS′ 2	GLS 2	GLS′ 2
A	73570	74544 ± 229	73829	73790 ± 151	73244 ± 133	73774	73586
B	880	904 ± 7	887	886 ± 4	874 ± 4	884	884
C	3233	3151 ± 17	3216	3220 ± 13	3334 ± 16	3220	3407
F_2	335	318 ± 9	327	313 ± 7	320 ± 6	331	326
G_1	330	302 ± 7	317	311 ± 6	300 ± 5	320	315
G_3	33	36 ± 2	33	37 ± 2	38 ± 2	33	34
α	75	74 ± 3	75	73 ± 2	59 ± 2	75	43
β	.....	.....	.....	Fix 0	−356 ± 37	Fix 0	−456
T	.....	.....	.....	Fix 0	Fix 0	Fix 0	−3.3
ζ_d	297	452 ± 78	347	394 ± 48	412 ± 38	354	364
ζ_p	364	446 ± 85	343	311 ± 78	361 ± 62	344	312
Δ	.....	180	.....	285	226	.....	.....

[a] The parameters in ILS 1 and GLS 1 were obtained by not considering the levels of Iglesias and Velasco [14].

The parameters in ILS 2 and ILS′ 2 for Mn II as well as GLS 2 and GLS′ 2 were obtained by using the new levels of Iglesias and Velasco.

TABLE 6. *Parameters of* Fe II—$3d^64p$

Parameter	GDIAG 1	ILS 1	GLS 1	ILS 2	ILS′ 2	GLS 2	GLS′ 2
A	64940	65176 ± 112	65089	65086 ± 112	65040 ± 73	65056	64998
B	945	954 ± 4	950	951 ± 4	942 ± 3	949	939
C	3547	3506 ± 16	3509	3511 ± 16	3745 ± 20	3518	3736
F_2	347	353 ± 6	338	351 ± 6	344 ± 4	340	336
G_1	324	326 ± 7	314	321 ± 7	309 ± 4	316	310
G_3	36	34 ± 2	35	34 ± 2	36 ± 1	35	36
α	80	84 ± 3	81	83 ± 3	45 ± 3	81	47
β	.....	.....	.....	Fix 0	−525 ± 39	Fix 0	−465
T	.....	.....	.....	Fix 0	−3.5 ± 0.3	Fix 0	−3.3
ζ_d	401	462 ± 39	439	463 ± 39	451 ± 25	446	457
ζ_p	407	374 ± 71	381	377 ± 70	377 ± 44	382	340
Δ	.....	277	.....	270	176	.....	.....

TABLE 7. *Parameters of* Co II—$3d^74p$

Parameter	GDIAG 1	ILS 1	GLS 1	ILS 2	GLS 2	GLS′ 2
A	60888	60900 ± 51	61060	60919 ± 61	61069	61176
B	1010	992 ± 4	1012	996 ± 5	1013	994
C	3861	Fix 3861	3802	Fix 3802	3815	4064
F_2	359	364 ± 7	348	363 ± 8	350	347
G_1	318	304 ± 8	311	305 ± 8	313	305
G_3	39	36 ± 2	37	37 ± 3	37	38
α	85	Fix 85	87	Fix 88	87	51
β	.....	.....	.....	Fix 0	Fix 0	−475
T	.....	.....	.....	Fix 0	Fix 0	−3.3
ζ_d	523	502 ± 28	539	502 ± 28	542	557
ζ_p	450	277 ± 75	419	262 ± 78	420	369
Δ	.....	149	.....	148	.....	.....

331-607- O - 69 - 2

TABLE 8. *Parameters of* Ni II – $3d^84p$

Parameter	GDIAG 1	ILS 1	GLS 1	ILS 2	GLS 2	GLS′ 2
A	61720	61922 ± 55	61789	61921 ± 54	61786	62007
B	1075	1058 ± 6	1074	1057 ± 6	1077	1049
C	4175	4207 ± 44	4096	4208 ± 45	4113	4393
F_2	371	346 ± 6	359	346 ± 6	359	357
G_1	312	300 ± 6	308	300 ± 6	309	300
G_3	42	45 ± 3	39	45 ± 3	38	40
α	90	68 ± 6	93	68 ± 6	94	56
β	.....	.....	.....	Fix 0	Fix 0	−485
T	.....	.....	.....	Fix 0	Fix 0	−3.3
ζ_d	663	638 ± 30	646	638 ± 30	646	663
ζ_p	493	344 ± 62	457	343 ± 62	458	398
Δ	.....	158	.....	158	.....	.....

TABLE 9. *Parameters of* Cu II – $3d^94p$

Parameter	GDIAG 1	ILS 1	GLS 1	ILS 2	GLS 2	GLS′ 2
A	70281	69798 ± 56	69225	69802 ± 42	69226	69465
F_2	383	341 ± 9	370	344 ± 7	369	367
G_1	306	313 ± 11	304	305 ± 7	305	295
G_3	45	38 ± 8	41	38 ± 6	40	42
α	95	Fix 95	100	Fix 100	100	61
ζ_d	821	766 ± 52	761	802 ± 43	756	727
ζ_p	536	589 ± 93	495	502 ± 82	496	426
Δ	.....	154	.....	119	.....	.....

TABLE 10. *General parameters of the second spectra of the iron group*

Parameter	GDIAG 1	GLS 1	GLS 2	GLS'2
B	880	887.4 ± 1.9	884.5 ± 2.1	883.6 ± 1.9
ΔB	65	62.1 ± 1.2	64.1 ± 1.3	55.2 ± 1.2
C	3233	3216.0 ± 8.3	3220.1 ± 8.9	3406.7 ± 12.8
ΔC	314	293.2 ± 6.5	297.6 ± 6.3	328.8 ± 9.7
F_2	335	327.1 ± 2.7	330.6 ± 2.6	326.2 ± 2.3
ΔF_2	12	10.6 ± 1.3	9.5 ± 1.4	10.3 ± 1.2
G_1	330	317.2 ± 2.8	319.8 ± 3.0	314.8 ± 2.3
ΔG_1	−6	−3.1 ± 1.5	−3.6 ± 1.4	−5.3 ± 1.3
G_3	33	33.4 ± 1.0	33.1 ± 1.0	34.1 ± 0.8
ΔG_3	3	1.8 ± 0.6	1.8 ± 0.5	2.1 ± 0.6
α	75	75.1 ± 1.4	74.6 ± 1.3	42.6 ± 2.1
$\Delta \alpha$	5	6.1 ± 1.1	6.3 ± 1.1	4.3 ± 1.7
β	.....	.....	Fix 0	−455.5 ± 29.0
$\Delta \beta$	.....	.....	Fix 0	−9.9 ± 29.7
T	.....	.....	Fix 0	−3.3 ± 0.2
ΔT	.....	.....	Fix 0	0.0 ± 0.2
ζ_d	387	384.8 ± 26.5	385.4 ± 28.6	396.1 ± 24.0
$\Delta_1 \zeta_d$	95	88.4 ± 7.6	87.9 ± 8.1	89.9 ± 6.8
$\Delta_2 \zeta_d$	9	3.8 ± 3.8	3.1 ± 3.6	3.2 ± 3.3
ζ_p	364	343.1 ± 31.6	344.1 ± 30.9	311.8 ± 26.7
$\Delta \zeta_p$	43	38.0 ± 14.7	38.1 ± 14.1	28.6 ± 13.2
Δ	.....	295.2	294.3	231.4

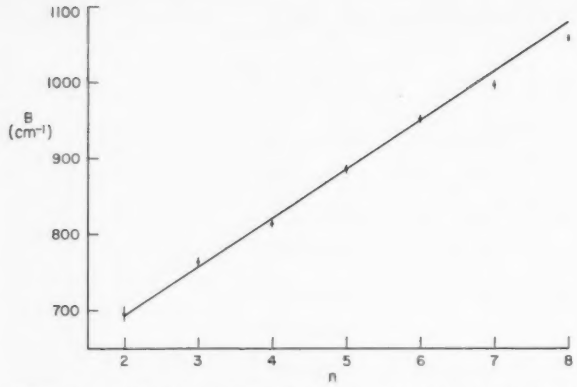

FIGURE 1. *Initial interpolation of parameter* B *with values obtained from individual diagonalizations of* $3d^n4p$ *configurations.*

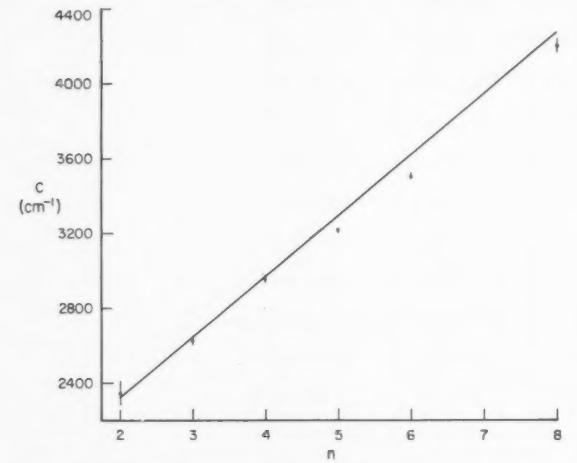

FIGURE 2. *Initial interpolation of parameter* C *with values obtained from individual diagonalizations of* $3d^n4p$ *configurations.*

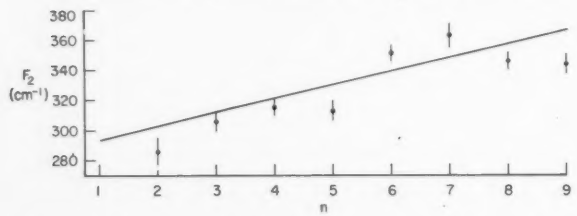

FIGURE 3. *Initial interpolation of parameter* F_2 *with values obtained from individual diagonalizations of* $3d^n4p$ *configurations.*

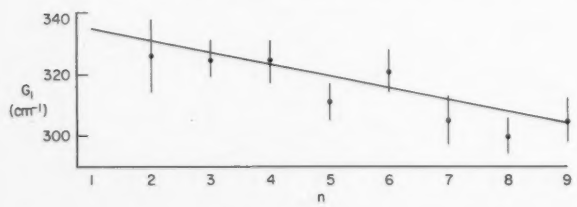

FIGURE 4. *Initial interpolation of parameter* G_1 *with values obtained from individual diagonalizations of* $3d^n4p$ *configurations.*

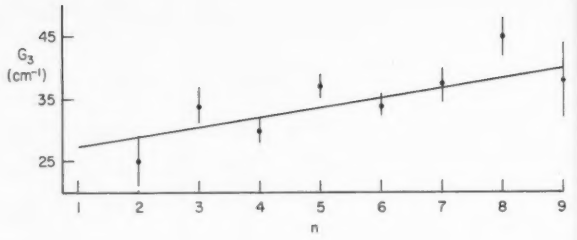

FIGURE 5. *Initial interpolation of parameter* G_3 *with values obtained from individual diagonalizations of* $3d^n4p$ *configurations.*

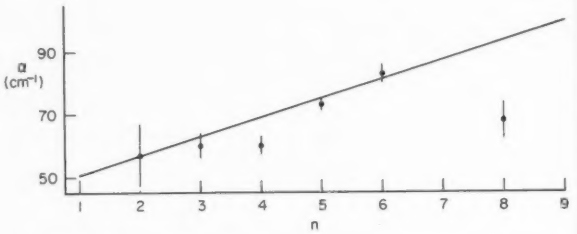

FIGURE 6. *Initial interpolation of parameter* α *with values obtained from individual diagonalizations of* $3d^n4p$ *configurations.*

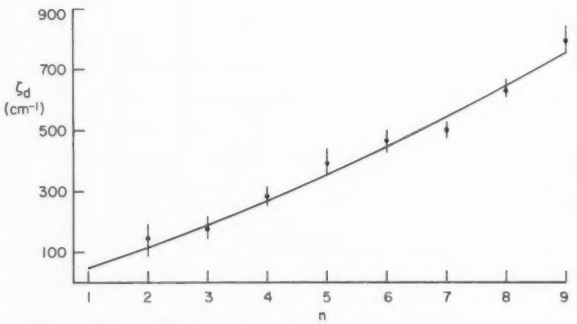

FIGURE 7. *Initial interpolation of parameter* ζ_d *with values obtained from individual diagonalizations of* $3d^n4p$ *configurations.*

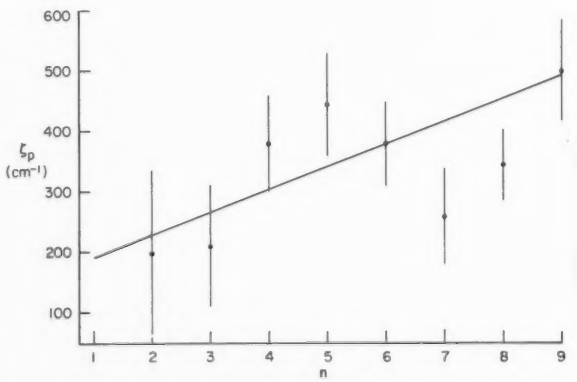

FIGURE 8. *Initial interpolation of parameter* ζ_p *with values obtained from individual diagonalizations of* $3d^n4p$ *configurations.*

4.2. Levels: Tables 11–21

In the column "NAME" the calculated designation of the term is given. Whenever terms of the parent d^n have different seniorities these are denoted by the letters A and B (for $d^5\ ^2D$ by A, B and C), the lower calculated term being designated by A. Whenever a calculated term has a corresponding experimental term, the small letters z, y, x . . . are used as in AEL [15].

The entries in the columns "J", "OBS LEVEL (cm^{-1})" and "CALC. LEVEL (cm^{-1})" are self-evident. In the column "PERCENTAGE", for each calculated level either the three highest contributions or all those contributions exceeding 5 percent are given.

Whenever the experimental and calculated term designations differ, the experimental designation is entered in the column "AEL" using the notation of C. Moore [15]. In many instances the exchanges involve complete terms rather than isolated levels. Unless specified otherwise the entries in the column "AEL" pertain to exchanges in terms. The column "O–C" gives the difference between the observed and calculated values of the levels. The columns "OBS. g-FACTOR" and "CALC. g-FACTOR" give the values of the observed and calculated Lande g-factors, respectively.

The entries are in ascending order of magnitude of the calculated terms. The values of the levels and parameters are in cm^{-1}.

TABLE 11. *Observed and calculated levels of* Ca II 4p

NAME	J	PERCENTAGE	AEL	OBS. LEVEL (cm^{-1})	CALC. LEVEL (cm^{-1})	O–C	OBS. g-FACTOR	CALC. g-FACTOR
$(^1S)z\ ^2P$	1/2	100		25192	25196	−4		0.667
	3/2	100		25414	25410	4		1.333

TABLE 12. *Observed and calculated levels of* Sc II 3d4p

NAME	J	PERCENTAGE	AEL	OBS. LEVEL (cm^{-1})	CALC. LEVEL (cm^{-1})	O–C	OBS. g-FACTOR	CALC. g-FACTOR
$(^2D)z\ ^1D$	2	99		26081	26371	−290	1.00	0.997
$(^2D)z\ ^3F$	2	97		27444	27553	−109	0.65	0.678
	3	97		27602	27690	−88	1.10	1.093
	4	100		27841	27908	−67	1.25	1.250
$(^2D)z\ ^3D$	1	100		27918	27916	2	0.51	0.501
	2	98		28021	28009	12	1.16	1.158
	3	97		28161	28131	30	1.33	1.325
$(^2D)z\ ^3P$	0	100			30366			
	1	99			30351			1.498
	2	100			30348			1.499
$(^2D)z\ ^1F$	3	100		32350	31839	511	1.00	1.000
$(^2D)z\ ^1P$	1	99			32118			1.003

TABLE 13. *Observed and calculated levels of* Ti II-$3d^24p$

NAME	J	PERCENTAGE	AEL	OBS. LEVEL (cm^{-1})	CALC. LEVEL (cm^{-1})	O–C	OBS. g-FACTOR	CALC. g-FACTOR
$(^3F)z\ ^4G$	5/2	99		29544	29482	62	0.57:	0.576
	7/2	99		29734	29670	64	0.98:	0.984
	9/2	100		29968	29901	67		1.172
	11/2	100		30241	30174	67		1.273
$(^3F)z\ ^4F$	3/2	99		30837	30714	123	0.40:	0.405
	5/2	99		30959	30834	125	1.03:	1.028
	7/2	99		31114	30996	118	1.24:	1.238
	9/2	100		31301	31188	113		1.332
$(^3F)z\ ^2F$	5/2	$86+8(^1D)^2F$		31207	31406	−199	0.86:	0.861
	7/2	$90+8(^1D)^2F$		31491	31676	−185	1.14:	1.143
$(^3F)z\ ^2D$	3/2	$76+10(^3F)^4D+9(^3P)^2D$		31756	32141	−385	0.92	0.841
	5/2	$64+23(^3F)^4D+8(^3P)^2D$		32026	32393	−367	1.20	1.231
$(^3F)z\ ^4D$	1/2	98		32532	32598	−66	0.00	0.002
	3/2	$89+9(^3F)^2D$		32603	32665	−62	1.20	1.163
	5/2	$71+23(^3F)^2D$		32698	32781	−83	1.37	1.357
	7/2	95		32767	32848	−81	1.43:	1.425
$(^3F)z\ ^2G$	7/2	96		34543	34215	328	0.89:	0.887
	9/2	95		34748	34422	326	1.11:	1.114
$(^3P)z\ ^2S$	1/2	99		37431	37589	−158	2.09	1.996
$(^1D)z\ ^2P$	1/2	98		39675	39524	151	0.67:	0.673
	3/2	92		39603	39328	275	1.21	1.322
$(^1D)y\ ^2F$	5/2	$88+8(^3F)^2F$		39927	39479	448	0.86:	0.866
	7/2	90		40075	39596	479	1.14:	1.145
$(^3P)z\ ^4S$	3/2	$83+13(^1D)^2D$		40027	40058	−31		1.814
$(^1D)y\ ^2D$	3/2	$63+14(^3P)^4S+7(^1D)^2D$		39233	39878	−645	0.80:	1.019
	5/2	$74+12(^3P)^4D+7(^3P)^2D$		39477	40082	−605	1.20:	1.208
$(^3P)y\ ^4D$	1/2	97		40330	40165	165		0.008
	3/2	$90+7(^1D)^2D$		40426	40262	164		1.166
	5/2	$88+9(^1D)^2D$		40582	40410	172		1.348
	7/2	95		40798	40623	175		1.426
$(^3P)z\ ^4P$	1/2	100		41997	41964	33		2.663
	3/2	99		42069	42023	46		1.730
	5/2	99		42209	41172	37		1.596
$(^1G)y\ ^2G$	7/2	96		43741	43660	81	0.89:	0.886
	9/2	96		43781	43689	92	1.11:	1.108
$(^3P)x\ ^2D$	3/2	$80+12(^1D)^2D+6(^3F)^2D$		44915	44780	135	0.80:	0.803
	5/2	$81+11(^1D)^2D+6(^3F)^2D$		44902	44759	143	1.20:	1.201
$(^1G)z\ ^2H$	9/2	99		45674	45231	443		0.909
	11/2	100		45905	45463	442		1.091
$(^3P)y\ ^2P$	1/2	99		45473	45851	−378	0.66:	0.666
	3/2	98		45549	45932	−383	1.33:	1.329
$(^1G)x\ ^2F$	5/2	98		47625	48254	−629	0.86:	0.858
	7/2	98		47467	48075	−608	1.14:	1.142
$(^1S)^2P$	3/2	98			62345			0.666
	5/2	99			62639			1.332

TABLE 14. *Observed and calculated levels of* V II—$3d^34p$

NAME	J	PERCENTAGE	AEL	OBS. LEVEL (cm^{-1})	CALC. LEVEL (cm^{-1})	O–C	OBS. g-FACTOR	CALC. g-FACTOR
$(^4F)z\ ^5G$	2	100		34593	34569	24	0.31	0.334
	3	100		34746	34735	11	0.93	0.917
	4	100		34947	34952	−5	1.14	1.150
	5	100		35193	35218	−25	1.16	1.267
	6	100		35483	35532	−49		1.333
$(^4F)z\ ^5F$	1	$71+26(^4F)^3D$		36489	36610	−121	0.35	0.166
	2	$79+16(^4F)^3D$		36674	36769	−95	1.08	1.046
	3	$92+5(^4F)^3D$		36919	36973	−54	1.24	1.262
	4	99		37151	37194	−43		1.349
	5	99		37352	37430	−78	1.40:	1.398
$(^4F)z\ ^3D$	1	$46+27(^4F)^5F+23(^4F)^5D$		36955	37081	−126	0.24	0.596
	2	$35+43(^4F)^5D+18(^4F)^5F$		37041	37174	−133	1.08	1.280
	3	$65+27(^4F)^5D$	$(a\ ^4F)z\ ^5D$	37521	37774	−253	1.47	1.379
$(^4F)z\ ^5D$	0	98		37201	37187	14		
	1	$74+20(^4F)^3D$		37259	37299	−40	1.39	1.239
	2	$52+41(^4F)^3D$		37369	37494	−125	1.39	1.338
	3	$69+22(^4F)^3D+7(^4F)^5F$	$(a\ ^4F)z\ ^3D$	37205	37356	−151	1.32	1.444
	4	97		37531	37630	−99	1.44	1.496
$(^4F)z\ ^3G$	3	$94+5(^2G)^3G$		39234	39002	232	0.84	0.753
	4	$93+5(^2G)^3G$		39404	39208	196	1.03	1.054
	5	$93+5(^2G)^3G$		39613	39467	146	1.19	1.203
$(^4F)z\ ^3F$	2	96		40002	40140	−138	0.65	0.667
	3	96		40196	40365	−169	1.02	1.081
	4	96		40430	40638	−208	1.22	1.252
$(^4P)z\ ^5P$	1	99		46755	46401	354	2.28	2.490
	2	98		46880	46526	354	1.65	1.820
	3	99		47052	46701	351	1.58	1.661
$(^4P)y\ ^5D$	0	$62+30(^4P)^3P$	$(a\ ^4P)z\ ^3P$	46586	46567	19		
	1	$69+27(^4P)^3P$		46690	46646	44	1.44	1.496
	2	$52+40(^4P)^3P$		46740	46750	−10	1.48	1.501
	3	98	$(a\ ^4P)y\ ^5D$	47181	47040	141	1.48:	1.498
	4	98		47420	47282	138	(2.28)	1.500
$(^4P)z\ ^3P$	0	$51+36(^4P)^5D+6(^2P)^1S$	$(a\ ^4P)y\ ^5D$	47028	47011	17		
	1	$62+29(^4P)^5D+6(A^2D)^3P$		47108	47079	29	1.43	1.507
	2	$45+46(^4P)^5D$		47102	47040	62	1.47	1.506
$(^2G)z\ ^3H$	4	$89+11(^2H)^3H$		47056	46979	77	0.78	0.801
	5	$88+11(^2H)^3H$		47297	47228	69	1.01	1.032
	6	$89+11(^2H)^3H$		47608	47543	65	1.13	1.167
$(^2G)y\ ^3G$	3	$89+6(^4F)^3G$		48580	48644	−64	0.67	0.761
	4	$91+6(^4F)^3G$		48731	48792	−61	1.02	1.052
	5	$86+6(^4F)^3G+5(^2G)^1H$		48853	48920	−67	1.22	1.186
$(^2P)z\ ^1S$	0	$92+8(^4P)^3P$		48258	49030	−772		
$(^2G)z\ ^1G$	4	$55+38(^2G)^3F$	$(a^2G)y\ ^3F$	49269	49384	−115	1.18:	1.106
$(^2G)y\ ^3F$	2	$71+19(A^2D)^3F+6(^2P)^1D$		49202	49410	−208	0.63	0.692
	3	$69+12(^2G)^1F+12(A^2D)^3F$		49211	49435	−224	0.99	1.061
	4	$47+42(^2G)^1G+\ (A^2D)^3F$	$(a^2G)z^1G$	49724	49768	−44	0.96	1.132
$(^2G)z\ ^1H$	5	$75+17(^2H)^1H+6(^2G)^3G$		49593	49547	46	0.95	1.011
$(^4P)z\ ^5S$	2	97		49731	49690	41		1.986
$(^2G)z\ ^1F$	3	$70+12(^2G)^3F+11(A^2D)^1F$		49568	49920	−352	0.97	1.012
$(^2P)z\ ^1D$	2	$50+28(A^2D)^1D+10(^2G)^3F$		49898	50249	−351	0.93	0.996

TABLE 14. *Observed and calculated levels of* V II – $3d^3 4p$ – Continued

NAME	J	PERCENTAGE	AEL	OBS. LEVEL (cm^{-1})	CALC. LEVEL (cm^{-1})	O–C	OBS. g-FACTOR	CALC. g-FACTOR
$(^2P)y\ ^3P$	0	$71+28(A^2D)^3P$		50662	50412	250		
	1	$66+29(A^2D)^3P$		50739	50504	235	1.39	1.492
	2	$57+25(A^2D)^3P+8(^2P)^3D$		51123	50942	181	1.51	1.447
$(^2P)y\ ^3D$	1	$72+21(^4P)^3D+6(^4F)^3D$		50474	50818	−344	0.49	0.511
	2	$59+14(^4P)^3D+7(^2P)^3P$		50775	51136	−361	1.11	1.186
	3	$67+23(^4P)^3D+6(^4F)^3D$		51086	51394	−308	1.27	1.324
$(^2H)y\ ^3H$	4	$87+10(^2G)^3H$		52083	51838	245	0.70	0.802
	5	$88+11(^2G)^3H$		52154	51914	240	0.98	1.032
	6	$88+11(^2G)^3H$		52253	52022	231	1.04:	1.164
$(^4P)x\ ^3D$	1	$64+19(^2P)^3D+7(A^2D)^3D$		52604	52244	360	0.63	0.558
	2	$62+18(^2P)^3D+9(A^2D)^3F$		52700	52200	500	1.10	1.110
	3	$65+24(^2P)^3D$		52767	52228	539	1.26	1.320
$(^2P)z\ ^3S$	1	$89+7(^4P)^3S$		52181	52417	−236	1.85	1.972
$(A^2D)x\ ^3F$	2	$69+15(^2G)^3F+7(^4P)^3D$		52246	52279	−33	0.68	0.735
	3	$77+15(^2G)^3F$		52392	52428	−36	1.07	1.101
	4	$85+14(^2G)^3F$		52658	52577	81	1.18:	1.230
$(A^2D)z\ ^1P$	1	$67+22(^2P)^1P+6(^4P)^3D$	$(a^2P)z\ ^1P$	52804	52564	240	0.92	0.974
$(^2H)z\ ^3I$	5	99		52878	52524	354	0.84:	0.836
	6	99		53077	52726	351	0.98:	1.025
	7	100		53320	52976	344	1.11:	1.143
$(A^2D)w\ ^3D$	1	90		53751	53433	318	0.49:	0.522
	2	93		53869	53597	272	1.10	1.172
	3	93		53927	53726	201	1.37	1.326
$(^2H)y\ ^1G$	4	$84+13(^2F)^1G$		54144	54564	−420	1.00	1.002
$(A^2D)x\ ^3P$	0	$63+26(^2P)^3P+11(^4P)^3P$		54813	54737	79		
	1	$59+24(^2P)^3P+12(^4P)^3P$		54718	54634	84		1.504
	2	$60+26(^2P)^3P+12(^4P)^3P$		54716	54598	118		1.498
$(A^2D)y\ ^1F$	3	$82+11(^2G)^1F$		55142	54752	390	0.94	1.006
$(^2H)z\ ^1I$	6	99		55403	54902	501	1.01:	1.001
$(^2H)y\ ^1H$	5	$78+19(^2G)^1H$		55499	55204	295	1.03:	1.005
$(^2H)x\ ^3G$	3	93		55350	55756	−406	0.82	0.765
	4	93		55304	55779	−475	1.02	1.042
	5	92		55207	55702	−495	1.15	1.196
$(^4P)y\ ^3S$	1	$56+23(^2P)^1P+7(^2P)^3S$		55663	55860	−197	1.92	1.646
$(^2P)y\ ^1P$	1	$48+33(^4P)^3S+16(A^2D)^1P$	$(a\ ^2D)y\ ^1P$	56171	56180	−9	1.05:	1.329
$(A^2D)y\ ^1D$	2	$61+37(^2P)^1D$		57343	57107	236	0.98	1.002
$(^2F)w\ ^3F$	2	97		62085	62485	−400	0.58:	0.670
	3	96		62133	62495	−362	1.00	1.076
	4	96		62176	62520	−344	1.36:	1.248
$(^2F)w\ ^3G$	3	95		64057	63669	388	0.72:	0.751
	4	94		64131	63737	394	1.02	1.053
	5	97		64229	63820	409		1.200
$(^2F)x\ ^1D$	2	$84+14(B^2D)^1D$		64586	64881	−295	1.03:	0.999
$(^2F)v\ ^3D$	1	96		64931	65315	−384	0.46:	0.501
	2	95		64804	65181	−377	1.02:	1.162
	3	95		64604	64972	−368	1.22:	1.330
$(^2F)x\ ^1G$	4	$86+13(^2H)^1G$		65790	65568	222	0.94	1.002

TABLE 14. *Observed and calculated levels of* V II-$3d^3$4p—Continued

NAME	J	PERCENTAGE	AEL	OBS. LEVEL (cm^{-1})	CALC. LEVEL (cm^{-1})	O–C	OBS. g-FACTOR	CALC. g-FACTOR
$(^2F)x\ ^1F$	3	96		66304	66922	−618	0.95	1.001
$(B^2D)^3D$	1	97			76394			0.503
	2	96			76395			1.166
	3	97			76426			1.331
$(B^2D)^1D$	2	$66+27(B^2D)^3F$			77554			0.916
$(B^2D)^3F$	2	$72+24(B^2D)^1D$			77776			0.755
	3	97			77732			1.085
	4	99			77815			1.250
$(B^2D)^3P$	0	100			79552			
	1	99			79451			1.497
	2	99			79246			1.498
$(B^2D)^1F$	3	98			79612			1.001
$(B^2D)^1P$	1	100			83501			1.000

TABLE 15. *Observed and calculated levels of* Cr II—$3d^4$4p

NAME	J	PERCENTAGE	AEL	OBS. LEVEL (cm^{-1})	CALC. LEVEL (cm^{-1})	O–C	OBS. g-FACTOR	CALC. g-FACTOR
$(^5D)z\ ^6F$	1/2	100		46824	46697	127	−0.689	−0.665
	3/2	100		46906	46785	121	1.124	1.067
	5/2	100		47041	46930	111	1.314	1.314
	7/2	100		47228	47131	97	1.378	1.397
	9/2	100		47465	47384	81	1.416	1.434
	11/2	100		47752	47688	64		1.454
$(^5D)z\ ^6P$	3/2	38		48399	48190	209	2.382	2.388
	5/2	98		48491	48328	163	1.875	1.881
	7/2	100		48632	48529	103	1.710	1.714
$(^5D)z\ ^4P$	1/2	$67+31(^5D)^6D$		48750	48782	−32	2.844	2.874
	3/2	$55+42(^5D)^6D$		49006	49038	−32	1.802	1.799
	5/2	$71+27(^5D)^6D$	$(a\ ^5D)z\ ^6D$	49706	49798	−92	1.624	1.617
$(^5D)z\ ^6D$	1/2	$69+31(^5D)^4P$		49493	49470	23	3.155	3.124
	3/2	$58+41(^5D)^4P$		49565	49574	−9	1.824	1.811
	5/2	$73+26(^5D)^4P$	$(a\ ^5D)z\ ^4P$	49352	49371	−19	1.628	1.643
	7/2	99		49646	49649	−3	1.577	1.585
	9/2	98		49838	49881	−43	1.570	1.552
$(^5D)z\ ^4F$	3/2	97		51584	51365	219	0.406	0.402
	5/2	97		51670	51473	197	1.025	1.031
	7/2	96		51789	51627	162	1.248	1.241
	9/2	96		51943	51828	115	1.338	1.337
$(^5D)z\ ^4D$	1/2	98		54418	54541	−123	0.007	0.001
	3/2	98		54500	54641	−141	1.178	1.200
	5/2	98		54626	54796	−170	1.376	1.371
	7/2	98		54785	54991	−206	1.430	1.428
$(^3H)z\ ^4H$	7/2	$82+16(^3G)^4H$		63601	63787	−186	0.680	0.671
	9/2	$80+16(^3G)^4H$		63707	63900	−193	1.030	0.966
	11/2	$80+15(^3G)^4H$		63849	64062	−213	1.138	1.127
	13/2	$83+13(^3G)^4H$		64031	64277	−246	1.234	1.226
$(A^3P)y\ ^4D$	1/2	$87+7(A^3F)^4D$		63802	63692	110	0.000	0.022
	3/2	$86+8(A^3F)^4D$		64062	63970	92	1.199	1.202
	5/2	$85+10(A^3F)^4D$		64449	64390	59	1.380	1.371
	7/2	$80+14(A^3F)^4D$		64924	64920	4	1.411	1.427

TABLE 15. *Observed and calculated levels of* Cr II – $3d^4 4p$ – Continued

NAME	J	PERCENTAGE	AEL	OBS. LEVEL (cm^{-1})	CALC. LEVEL (cm^{-1})	O–C	OBS. g-FACTOR	CALC. g-FACTOR
$(^3H)z\ ^4I$	9/2	96		65218	64938	280		0.738
	11/2	95		65420	65151	269		0.973
	13/2	96		65618	65363	255		1.112
	15/2	100		65813	65566	247		1.200
$(A^3P)z\ ^2S$	1/2	$73 + 7(A^3P)^4P$		65030	65316	−286		2.010
$(A^3F)z\ ^4G$	5/2	$79 + 14(^3G)^4G$	$(a\ ^3H)z^4G$	66157	65233	−76	0.593	0.574
	7/2	$70 + 12(^3G)^4G + 9(A^3F)^2G$		65257	65371	−114	0.920	0.975
	9/2	$59 + 10(^3G)^4G + 8(A^3F)^2G$		65384	65534	−150	1.120	1.157
	11/2	$73 + 13(^3G)^4G$		65710	65814	−104	1.265	1.269
$(^3H)z\ ^2G$	7/2	$49 + 33(A^3F)^2G + 7(^3G)^2G$		65543	65804	−261		0.898
	9/2	$41 + 31(A^3F)^2G + 17(A^3F)^4G$		65680	65922	−242		1.121
$(A^3P)y\ ^4P$	1/2	$76 + 13(A^3P)^2S$		66257	66208	49	2.545	2.413
	3/2	90		66355	66255	100	1.671	1.723
	5/2	92		66727	66746	−19	1.502	1.582
$(A^3P)z\ ^2P$	1/2	$79 + 14(A^3P)^2S$		66872	67104	−232		0.880
	3/2	$53 + 15(A^3F)^2D + 10(A^3P)^2D$	$(a\ ^3P)z\ ^2D$	66650	66988	−338		1.158
$(A^3F)y\ ^4F$	3/2	$51 + 21(A^3P)^2P + 14(A^3F)^2D$	$(a\ ^3P)z\ ^2P$	67070	67130	−60		0.783
	5/2	$71 + 13(A^3F)^2D$	$(a\ ^3P)z\ ^2D$	67012	67170	−158		1.036
	7/2	$76 + 10(^3H)^4G$		67394	67272	122		1.188
	9/2	$63 + 18(^3H)^4G$		67449	67329	120		1.277
$(^3H)z\ ^2I$	11/2	93		67506	67303	203		0.933
	13/2	95		67589	67443	146		1.079
$(A^3F)z\ ^2D$	3/2	$28 + 32(A^3F)^4F + 16(A^3P)^2D$	$(a^3F)y\ ^4F$	67380	67483	−103		0.848
	5/2	$50 + 18(A^3F)^4F + 13(A^3F)^2D$		67387	67399	−12		1.171
$(^3H)y\ ^4G$	5/2	$66 + 13(A^3F)^4G + 12(^3G)^4G$	$(a\ ^3F)y\ ^4G$	67344	67572	−228		0.609
	7/2	$60 + 18(A^3F)^4F + 11(A^3F)^4G$		67334	67445	−111		1.033
	9/2	$51 + 32(A^3F)^4F + 9(A^3F)^4G$		67354	67483	−129		1.223
	11/2	$65 + 22(A^3F)^4G + 10(^3G)^4G$		67369	67442	−73		1.264
$(A^3P)z\ ^4S$	3/2	$70 + 17(A^3P)^2P$		68306	67813	493	1.978	1.748
$(A^3F)x\ ^4D$	1/2	$88 + 11(A^3P)^4D$		67860	68104	−244		0.007
	3/2	$84 + 12(A^3P)^4D$		67870	68124	−254		1.190
	5/2	$77 + 13(A^3P)^4D$		67868	68125	−257		1.339
	7/2	$69 + 19(A^3P)^4D$		67876	68142	−266		1.397
$(^3H)z\ ^2H$	9/2	$81 + 12(A^1G)^2H$		68477	68547	−70		0.913
	11/2	$84 + 10(A^1G)^2H$		68738	68856	−118		1.094
$(^3G)y\ ^4H$	7/2	$83 + 16(^3H)^4H$		68844	68712	132		0.671
	9/2	$82 + 14(^3H)^4H$		68993	68886	107		0.971
	11/2	$82 + 13(^3H)^4H$		69171	69077	94		1.131
	13/2	$85 + 13(^3H)^4H$		69388	69296	92		1.228
$(A^3F)z\ ^2F$	5/2	$50 + 21(^3G)^2F + 13(^3D)^2F$		68583	68751	−168		0.898
	7/2	$59 + 18(^3G)^2F + 11(^3D)^2F$		68760	68932	−172		1.155
$(A^3P)y\ ^2D$	3/2	$65 + 28(A^3F)^2D$	$(a\ ^3G)x\ ^4F$	69348	68940	408		0.795
	5/2	$66 + 20(A^3F)^2D$	$(a\ ^3F)y\ ^2D$	69954	69484	470		1.170
$(^3G)x\ ^4F$	3/2	$81 + 13(^3D)^4F$	$(a\ ^3F)y\ ^2D$	69639	69892	−253		0.418
	5/2	$71 + 11(^3D)^4F$	$(a\ ^3G)x\ ^4F$	69478	69885	−407		0.998
	7/2	$60 + 11(A^3F)^2G + 9(^3D)^4F$		69506	69854	−348		1.157
	9/2	$60 + 13(A^3F)^2G + 9(^3D)^4F$		69498	69837	−339		1.266
$(A^3F)y\ ^2G$	7/2	$42 + 25(^3H)^2G + 11(^3G)4F$		69903	70044	−141		0.951
	9/2	$37 + 25(^3H)^2G + 15(^3G)^4F$		70108	70277	−169		1.148
$(^3G)y\ ^2H$	9/2	$57 + 19(^3G)^4G + 7(^3H)^4G$		70394	70436	−42		1.000
	11/2	$47 + 34(^3G)^4G + 10(^3H)^4G$		70399	70483	−84		1.171

TABLE 15. *Observed and calculated levels of* Cr II – $3d^4 4p$ – Continued

NAME	J	PERCENTAGE	AEL	OBS. LEVEL (cm^{-1})	CALC. LEVEL (cm^{-1})	O–C	OBS. g-FACTOR	CALC. g-FACTOR
$(^3G)x\ ^4G$	5/2	$60+17(^3H)^4G+11(^3G)^2F$		70317	70396	−79		0.636
	7/2	$61+19(^3H)^4G+10(^3G)^4F$		70427	70540	−113		1.016
	9/2	$44+22(^3G)^2H+13(^3H)^4G$		70679	70753	−74		1.109
	11/2	$41+38(^3G)^2H+11(^3H)^4G$		70880	70949	−69		1.191
$(^3G)y\ ^2F$	5/2	$45+32(A^3F)^2F+5(^3G)^4G$		70585	70605	−20		0.844
	7/2	$59+20(A^3F)^2F$		70852	70932	−80		1.140
$(^3G)x\ ^2G$	7/2	$79+11(^3H)^2G$		72649	72768	−119		0.894
	9/2	$75+13(^3H)^2G+9(A^1G)^2G$		72717	72862	−145		1.111
$(^3D)w\ ^4D$	1/2	96		73407	73701	−294		0.023
	3/2	91		73412	73697	−285		1.173
	5/2	87		73436	73711	−275		1.352
	7/2	89		73486	73760	−274		1.412
$(A^1G)x\ ^2H$	9/2	$82+11(^3H)^2H$	$(a\ ^1I)x\ ^2H$	74456	74094	362		0.912
	11/2	$72+11(^1I)^2I+10(^3H)^2H$		74707	74342	365		1.071
$(^1I)y\ ^2I$	11/2	$85+12(A^1G)^2H$		74422	74206	216		0.945
	13/2	$64+35(^1I)^2K$	$(a\ ^1I)z\ ^2K$	74743	74438	305		1.027
$(^3D)w\ ^4F$	3/2	$82+13(^3G)^4F$		74273	74244	29		0.442
	5/2	$48+40(^3D)^4P$		74319	74281	38		1.271
	7/2	$89+6(^3D)^4F$		74424	74341	83		1.412
	9/2	$86+13(^3G)^4F$		74505	74428	77		1.333
$(^1I)z\ ^2K$	13/2	$65+33(^1I)^2I$	$(a\ ^1I)y\ ^2I$	74424	74156	268		0.983
	15/2	100		74959	74556	403		1.067
$(A^1G)x\ ^2F$	5/2	$77+7(^3D)^2F$	$(a^3D)x\ ^2F$	74436	74594	−158		0.859
	7/2	$64+19(^3D)^4F$		74114	74322	−208		1.162
$(^3D)x\ ^4P$	1/2	96		74921	74725	196		2.644
	3/2	93		74718	74571	147		1.716
	5/2	$53+30(^3D)^4F+9(^3D)^4D$		74484	74338	146		1.373
$(^3D)y\ ^2P$	1/2	$55+40(A^1S)^2P$		74854	74881	−27		0.667
	3/2	$61+33(A^1S)^2P$		74985	74983	2		1.335
$(A^1G)w\ ^2G$	7/2	$82+8(^3G)^2G$		75717	75768	−51		0.893
	9/2	$80+12(^3G)^2G$		75810	75889	−79		1.111
$(^3D)w\ ^2F$	5/2	$72+13(A^1G)^2F+8(^3G)^2F$						
			$(a\ ^1G)w\ ^2F$	76988	77136	−148		0.858
	7/2	$73+12(A^1G)^2F+7(^3G)^2F$		76879	77009	−130		1.142
$(^1I)w\ ^2H$	9/2	$90+8(^3G)^2H$	$(a\ ^1G)w\ ^2H$	77270	77490	−220		0.910
	11/2	$88+8(^3G)^2H$		77079	77281	−202		1.090
$(A^1S)x\ ^2P$	1/2	$48+32(^3D)^2P+15(A^1D)^2P$		77778	77769	9		0.667
	3/2	$31+26(^3D)^2D+12(^3D)^2P$		77714	77732	−18		1.111
$(^3D)x\ ^2D$	3/2	$48+22(A^1S)^2P+10(^3D)^2P$		78110	78094	16		1.013
	5/2	$65+26(A^1D)^2D$		77935	77972	−37		1.200
$(A^1D)w\ ^2D$	3/2	$74+13(^3D)^2D$		80288	79940	348		0.813
	5/2	$65+21(^3D)^2D$		80420	80113	307		1.189
$(A^1D)w\ ^2F$	5/2	86		81233	80772	461		0.869
	7/2	89		81432	80981	451		1.143
$(A^1D)w\ ^2P$	1/2	$89+9(^3D)^2P$		82854	82749	105		0.668
	3/2	$78+11(^3D)^2P$		82920	82838	82		1.332
$(^1F)u\ ^2F$	5/2	89		84605	84264	341		0.859
	7/2	87		84677	84332	345		1.139
$(^1F)v\ ^2G$	7/2	95		85573	85372	201		0.893
	9/2	97		85940	85702	238		1.112

TABLE 15. *Observed and calculated levels of* Cr II – $3d^4 4p$ – Continued

NAME	J	PERCENTAGE	AEL	OBS. LEVEL (cm^{-1})	CALC. LEVEL (cm^{-1})	O–C	OBS. g-FACTOR	CALC. g-FACTOR
$(^1F)w\ ^2D$	3/2	$79 + 12(B^3P)^2D$		86511	87233	−722		0.800
	5/2	$75 + 13(B^3P)^2D + 9(B^3F)^2D$		86507	86774	−267		1.189
$(B^3F)^4F$	3/2	97			89391			0.419
	5/2	93			89405			1.054
	7/2	95			89422			1.243
	9/2	98			89456			1.331
$(B^3P)^4P$	1/2	95			89869			2.594
	3/2	$88 + 6(B^3P)^4D$			89725			1.688
	5/2	$82 + 7(B^3P)^4D$			89706			1.547
$(B^3P)^4D$	1/2	$70 + 26(B^3F)^4D$			90491			0.070
	3/2	$61 + 24(B^3F)^4D$			90408			1.204
	5/2	$51 + 20(B^3F)^4D$			90288			1.368
	7/2	$69 + 26(B^3F)^4D$			90160			1.419
$(B^3F)^4G$	5/2	94			90702			0.591
	7/2	95	$(b\ ^3F)u\ ^2G$	90986	90792	194		0.991
	9/2	98	$(b\ ^3F)u\ ^2G$	91103	90880	223		1.172
	11/2	99			90950			1.273
$(B^3P)^2D$	3/2	$53 + 21(B^3F)^2D + 17(^1F)^2D$		91557	91280	277		0.829
	5/2	$50 + 18(^1F)^2D + 15(B^3F)^2D$		91426	91119	307		1.220
$(B^3F)^2F$	5/2	$85 + 5(B^3F)^4G$			91473			0.847
	7/2	$87 + 5(B^1G)^2F$			91395			1.141
$(B^3P)^4S$	3/2	97			92759			1.993
$(B^3F)^2G$	7/2	98			93805			0.989
	9/2	98			93611			1.111
$(B^3F)^4D$	1/2	$72 + 27(B^3P)^4D$			93975			0.004
	3/2	$72 + 27(B^3P)^4D$			93929			1.200
	5/2	$72 + 27(B^3P)^4D$			93828			1.370
	7/2	$73 + 27(B^3P)^4D$			93650			1.427
$(B^3P)^2P$	1/2	92			94788			0.696
	3/2	94			94530			1.333
$(B^3P)^2S$	1/2	98			96187			1.969
$(B^1G)^2H$	9/2	$86 + 12(B^1G)^2G$			97179			0.935
	11/2	98			97523			1.091
$(B^1G)^2G$	7/2	97			97589			0.892
	9/2	$86 + 12(B^1G)^2H$			97744			1.086
$(B^3F)^2D$	3/2	$70 + 29(B^3P)^2D$			98249			0.801
	5/2	$71 + 29(B^3P)^2D$			98110			1.192
$(B^1G)^2F$	5/2	$86 + 6(B^3F)^2F$			99314			0.865
	7/2	$87 + 8(B^3F)^2F$			99110			1.141
$(B^1D)^2P$	1/2	96			111658			0.667
	3/2	95			111442			1.332
$(B^1D)^2F$	5/2	95			112845			0.859
	7/2	96			113144			1.143
$(B^1D)^2D$	3/2	99			115404			0.802
	5/2	99			115535			1.199
$(B^1S)^2P$	1/2	97			131229			0.667
	3/2	97			131613			1.333

TABLE 16. *Observed and calculated levels of* Mn II – $3d^54p$

NAME	J	PERCENTAGE	AEL	OBS. LEVEL (cm^{-1})	CALC. LEVEL (cm^{-1})	O–C	OBS. g-FACTOR	CALC. g-FACTOR
$(^6S)z\ ^7P$	2	100		38366	38071	295	2.32	2.332
	3	100		38543	38221	322	1.94?	1.916
	4	100		38807	38443	364	1.76	1.750
$(^6S)z\ ^5P$	1	99		43557	43340	217	2.49	2.499
	2	98		43484	43262	222	1.83	1.834
	3	98		43370	43143	227	1.67	1.667
$(^4G)z\ ^5G$	2	97		64456	64579	−123	1.31	0.338
	3	93		64473	64598	−125	1.26	0.900
	4	$91 + 7(^4G)^5H$		64494	64620	−126		1.133
	5	$90 + 8(^4G)^5H$		64519	64657	−138		1.253
	6	$92 + 6(^4G)^5H$		64550	64699	−149		1.325
$(^4G)z\ ^5H$	3	95		65483	65163	320	1.30	0.519
	4	$92 + 7(^4G)^5G$		65566	65254	312	1.21	0.918
	5	$92 + 8(^4G)^5G$		65658	65351	307		1.113
	6	$94 + 6(^4G)^5G$		65754	65444	310		1.221
	7	100		65847	65522	325		1.286
$(^4P)z\ ^5D$	0	$83 + 16(^4D)^5D$		66625	66666	−41		
	1	$73 + 14(^4D)^5D + 9(^4G)^5F$	$(a\ ^4G)z\ ^5F$	66645	66671	−26		1.335
	2	$54 + 26(^4G)^5F + 10(^4D)^5D$		66677	66692	−15		1.336
	3	$52 + 35(^4G)^5F + 9(^4D)^5D$	$(a\ ^4P)z\ ^5D$	67089	67080	−71	1.45	1.414
	4	$78 + 11(^4D)^5D + 9(^4G)^5F$		67295	67305	−10	1.49	1.485
$(^4G)z\ ^5F$	1	$82 + 9(^4P)^5D + 5(^4D)^5F$	$(a\ ^4P)z\ ^5D$	65894	66989	−95		0.164
	2	$64 + 26(^4P)^5D$		66901	67013	−112		1.168
	3	$56 + 27(^4P)^5D + 7(^4D)^5F$	$(a\ ^4G)z\ ^5F$	66686	66733	−47		1.333
	4	$83 + 6(^4D)^5F + 6(^4P)^5D$		66643	66755	−112		1.358
	5	93		66542	66702	−160	1.40	1.399
$(^4P)z\ ^5S$	2	95		66929	67048	−119		1.974
$(^4G)z\ ^3H$	4	98		67910	67778	132	0.78	0.801
	5	98		67846	67739	107	1.03	1.034
	6	97		67744	67662	82	1.16	1.168
$(^4G)z\ ^3F$	2	92		67767	67960	−193	0.66	0.670
	3	92		67812	68014	−202	1.08	1.086
	4	93		67866	68079	−213	1.25	1.251
$(^4P)y\ ^5P$	1	$83 + 8(^4D)^5P + 5(^4P)^3P$		68496	68521	−25		2.422
	2	$74 + 12(^4D)^5P + 7(^4P)^3P$		68417	68402	15		1.792
	3	$74 + 20(^4D)^5P$		68284	68233	51	1.65	1.656
$(^4P)z\ ^3P$	0	$80 + 15(^4D)^3P$		69319	69396	−77		
	1	$74 + 15(^4D)^3P + 6(^4P)^5P$		69216	69269	−53	1.49	1.554
	2	$68 + 16(^4D)^3P + 9(^4P)^5P$		69045	69061	−16	1.49	1.536
$(^4D)y\ ^5F$	1	$86 + 8(^4G)^5F$		70150	70143	7		0.029
	2	$85 + 7(^4G)^5F$		70231	70224	7		1.014
	3	$84 + 6(^4G)^5F$		70343	70334	9		1.258
	4	$90 + 6(^4G)^5F$		70497	70480	17	1.39?	1.352
	5	$91 + 5(^4G)^5F$		70657	70565	92	1.40	1.396
$(^4G)z\ ^3G$	3	96		70518	70531	−13	0.75	0.751
	4	96		70546	70571	−25	1.15?	1.051
	5	95		70527	70608	−81	1.20	1.204
$(^4P)z\ ^3D$	1	89		71078	71142	−64	0.50	0.513
	2	$83 + 5(^4D)^5D$		70940	71006	−66	1.16	1.169
	3	$79 + 5(^4D)^5F$		70745	70818	−73	1.33	1.332
$(^4D)x\ ^5P$	1	$60 + 26(^4D)^5D + 6(^4P)^5D$		71264	71695	−431		2.146
	2	$46 + 33(^4D)^5D + 11(^4P)^5P$		71323	71649	−326		1.686
	3	$52 + 21(^4D)^5D + 18(^4P)^5P$		71390	71566	−176		1.608

TABLE 16. *Observed and calculated levels of* Mn II—$3d^54p$—Continued

NAME	J	PERCENTAGE	AEL	OBS. LEVEL (cm^{-1})	CALC. LEVEL (cm^{-1})	O–C	OBS. g-FACTOR	CALC. g-FACTOR
$(^4D)y\ ^5D$	0	$81+16(^4P)^5D$		72322	71915	407		
	1	$52+29(^4D)^5P+10(^4P)^5D$		72321	71984	337		1.821
	2	$44+37(^4D)^5P+9(^4P)^5D$		72307	72106	201		1.624
	3	$57+23(^4D)^5P+11(^4P)^5D$		72247	72194	53		1.532
	4	$84+13(^4P)^5D$		72011	71530	481	1.48	1.496
$(^4D)y\ ^3D$	1	$89+5(^4F)^3D$		73385	73219	166		0.511
	2	$87+5(^4F)^3D$		73396	73206	190		1.174
	3	$31+5(^4F)^3D$		73395	73165	230		1.340
$(^4D)y\ ^3F$	2	91		73785	73789	−4	0.75	0.681
	3	88		73781	73793	−12	1.09	1.099
	4	92		73683	73687	−4	1.24	1.253
$(^4P)z\ ^3S$	1	96		73911	73842	69		1.985
$(^4D)y\ ^3P$	0	$81+16(^4P)^3P$		75563	75865	−302		
	1	$78+16(^4P)^3P$		75720	76039	−319		1.512
	2	$77+19(^4P)^3P$		75919	76256	−337		1.499
$(^2I)z\ ^3K$	6	$91+8(^2I)^3I$	$z\ ^3K$	77842	77627	215	0.909	0.872
	7	$91+5(^2I)^3I$		77946	77837	109	1.050	1.024
	8	100		77820	78083	−263	1.14	1.125
$(^2I)z\ ^3I$	5	$90+5(^2I)^1H$	$z\ ^3I$	78085	78182	−97	0.83	0.846
	6	$88+8(^2I)^3K$		78341	78369	−28	1.014	1.012
	7	$81+8(^2I)^1K+7(^2I)^3K$		78475	78323	152	1.13	1.122
$(^2I)z\ ^1K$	7	$88+11(^2I)^3I$	$z\ ^1K$	79147	79029	118	1.003	1.015
$(^2I)z\ ^1H$	5	$78+6(^2I)^3I+6(A^2G)^1H$	$z\ ^1H$	79113	79452	−339	1.011	0.992
$(A^2D)z\ ^1D$	2	$44+24(A^2F)^1D+18(A^2D)^3F$	$z\ ^1D$	78913	79541	−628	0.938	0.923
$(A^2D)x\ ^3F$	2	$14+29(A^2F)^3F+14(A^2D)^1D$	$x\ ^3F$	79458	79207	251	0.734	0.760
	3	$60+34(A^2F)^3F$		79513	79573	−60	1.075	1.067
	4	$66+30(A^2F)^3F$		79913	79925	−12	1.24	1.230
$(^2I)y\ ^3H$	4	92	$y\ ^3H$	79801	80080	−279	0.81	0.809
	5	90		79740	80048	−308	1.03	1.032
	6	94		79592	79920	−328	1.16	1.164
$(A^2F)z\ ^1G$	4	$53+24(A^2F)^3G+8(^2H)^1G$	$z\ ^1G$	81280	81144	136	1.010	1.027
$(A^2D)z\ ^1F$	3	$45+35(A^2F)^3G+10(A^2F)^3F$	$z\ ^1F$	81221	81239	−18	0.92	0.919
$(A^2D)x\ ^3P$	0	$92+4(^4F)^5D$	$x\ ^3P$	81713	81549	164		
	1	$74+12(A^2D)^3D+6(A^2F)^3D$		81322	81252	70		1.291
	2	$77+12(A^2F)^3D$		81148	81039	109	1.372	1.422
$(A^2D)x\ ^3D$	1	$69+15(A^2D)^3P+8(^4F)^5F$		81732	81706	26	0.44	0.619
	2	$45+44(^4F)^5G$		81813	81746	67	0.90	0.781
	3	$58+11(^4F)^5G+6(A^2D)^3F$	$x\ ^5F$	81052	81032	20	1.24	1.208
$(^4F)y\ ^5G$	2	$43+33(A^2D)^3D+11(A^2F)^3F$	$x\ ^5F$	81054	81030	23		0.728
	3	$73+13(A^2F)^3G+11(A^2D)^3D$	$y\ ^5G$	81781	81607	174	0.92	0.945
	4	$55+19(A^2F)^3G+11(A^2F)^1G$		81863	81703	160	1.20	1.116
	5	$71+26(A^2F)^3G$		82117	81896	221	1.28	1.248
	6	96		82142	81846	296	1.36	1.328
$(^2I)z\ ^1I$	6	94	$z\ ^1I$	81803	81877	−74	1.00	1.005
$(A^2F)y\ ^3G$	3	$48+25(A\ ^2D)^1F+6(^4F)^5G$	$y\ ^3G$	82388	82416	−28	0.906	0.923
	4	$36+34(^4F)^5G+28(A^2F)^3F$	$x\ ^5F$	81994	81909	85	1.25	1.145
	5	$68+24(^4F)^5G$	$y\ ^3G$	81886	81652	234		1.218
$(^4F)x\ ^5F$	1	$82+8(A^2D)^3D$			82501			0.111
	2	$77+7(^4F)^5D+6(A^2F)^3F$	$y\ ^5G$	82193	82432	−239		1.008
	3	$74+10(^4F)^5D+8(A^2F)^3D$	$x\ ^3D$	81660	82002	−342	1.32	1.264
	4	$83+9(^4F)^5D$	$y\ ^3G$	82100	82353	−253		1.351
	5	91	$x\ ^5F$	82232	82402	−170	1.296	1.389

TABLE 16. *Observed and calculated levels of* Mn II – $3d^54p$ – Continued

NAME	J	PERCENTAGE	AEL	OBS. LEVEL (cm^{-1})	CALC. LEVEL (cm^{-1})	O–C	OBS. g-FACTOR	CALC. g-FACTOR
$(A^2F)w\,^3D$	1	$56+35(A^2D)^1P$	$w\,^3D$	82939	82655	284	0.51	0.698
	2	$80+6(^4F)^5D+6(A^2D)^3P$		83071	82813	258	1.21	1.203
	3	$57+21(A^2F)^3F+9(^4F)^5F$		82419	82417	2	1.336	1.237
$(A^2F)w\,^3F$	2	$46+16(A^2D)^3F+8(^4F)^5G$	$w\,^3F$	82918	82974	−56	0.70	0.726
	3	$36+35(A^2F)^3D+14(A^2D)^3D$		82936	82759	177	1.12	1.203
	4	$33+23(A^2D)^3F+11(A^2F)^3G$		82831	82730	101	1.22	1.185
$(^4F)x\,^5D$	0	$94+4(A^2D)^3P$	$x\,^5D$	82839	83408	−568		
	1	$91+4(A^2D)^3P$		82775	83395	−620		1.447
	2	$82+5(A^2F)^3D+5(^4F)^5F$		82735	83400	−665		1.448
	3	$85+8(^4F)^5F$		82713	83311	−598	1.46	1.649
	4	$86+9(^4F)^5F$		82605	83196	−591	1.47	1.481
$(^4F)x\,^3G$	3	$69+17(^2H)^3G+9(A^2F)^3G$	$x\,^3G$	83934	84138	−204	0.76	0.758
	4	$46+16(^2H)^3H+16(A^2G)^3H$		83875	84225	−350	1.02	0.975
	5	$40+21(A^2G)^3H+20(^2H)^3H$		83912	84128	−216	1.20	1.122
$(A^2D)z\,^1P$	1	$58+30(A^2F)^3D$	$z\,^1P$	84268	84254	14	0.96	0.829
$(A^2G)x\,^3H$	4	$31+31(^2H)^3H+23(^4F)^3G$	$x\,^3H$	84307	84056	251	0.81	0.892
	5	$32+31(^4F)^5G+23(^2H)^3H$		84428	84311	117	1.103	1.108
	6	$46+45(^2H)^3H+7(^2H)^3I$		84644	84558	86	1.15	1.155
$(^2H)y\,^3I$	5	$89+5(^2H)^3H$	$y\,^3I$	85448	85179	269	0.82	0.851
	6	$89+5(^2H)^3H$		85636	85373	263	1.05	1.033
	7	97		85811	85564	247	1.12	1.142
$(A^2F)y\,^1D$	2	$64+32(A^2D)^1D$	$y\,^1D$	85368	85497	−129	1.03	0.994
$(^2H)w\,^3G$	3	$18+35(A^2G)^3G+22(A^2F)^1F$	$w\,^3G$	85735	85634	101	0.75	0.843
	4	$32+44(A^2G)^3G+10(^4F)^5G$		85674	85531	143	1.051	1.050
	5	$34+40(A^2G)^3G+11(^4F)^5G$		85543	85423	120	1.19	1.193
$(A^2G)y\,^1G$	4	$37+19(^2H)^1G+16(A^2F)^1G$	$v\,^3F$	85759	85744	15	1.15	1.055
$(A^2F)y\,^1F$	3	$51+14(A^2G)^3G+13(^2H)^3G$	$y\,^1F$	86062	85999	63		0.924
$(^4F)w\,^3F$	2	$43+24(A^2G)^3F+22(^4F)^3D$	$v\,^3F$	85989	86148	−159	0.77	0.801
	3	$40+24(^4F)^3D+23(A^2G)^3F$		85953	86105	−152	1.06	1.150
	4	$49+17(A^2G)^3F+12(A^2G)^1G$	$y\,^1G$	86449	86475	−26	1.092	1.186
$(^4F)w\,^3D$	1	$85+8(A^2F)^3D$	$v\,^3D$	86208	86345	−137	0.58	0.512
	2	$62+18(^4F)^3F+6(A^2G)^3F$		86190	86391	−201		1.034
	3	$57+20(^4F)^3F+10(A^2G)^3F$		86303	86448	−145	1.15	1.252
$(^2H)y\,^1I$	6	$90+5(^2H)^3H$	$y\,^1I$	86869	86658	211	1.02	1.010
$(^2H)w\,^3H$	4	$49+45(A^2G)^3H$	$w\,^3H$	87941	87745	196	0.82	0.813
	5	$44+47(A^2G)^3H$		87996	87775	221	1.03	1.042
	6	$43+49(A^2G)^3H+5(^2H)^1I$		88198	87997	201	1.16	1.157
$(A^2G)u\,^3F$	2	$51+26(^4F)^3F+17(A^2F)^3F$	$(w\,^3F)$	87859	88012	−153		0.673
	3	$51+25(^4F)^3F+16(A^2F)^3F$		87718	87876	−158	1.06	1.076
	4	$55+21(^4F)^3F+15(A^2F)^3F$		87580	87727	−147	1.23	1.240
$(A^2G)v\,^3G$	3	$43+21(A^2F)^3G+17(^4F)^3G$	$v\,^3G$	89126	88835	291	0.78	0.767
	4	$45+18(A^2F)^3G+13(^2H)^3G$		89097	88850	247	1.08	1.050
	5	$40+20(A^2F)^3G+14(^2H)^3G$	$y\,^1H$	88772	88644	128		1.174
$(A^2G)y\,^1H$	5	$66+24(^2H)^1H$	$v\,^3G$	89063	89022	41	1.14	1.009
$(^2H)x\,^1H$	5	$60+24(A^2G)^1H+11(^2I)^1H$	$x\,^1H$	89760	89366	394	1.02	1.010
$(B^2F)x\,^1G$	4	$48+19(A^2G)^1G+15(^2H)^1G$	$x\,^1G$	89465	89533	−68		1.013
$(B^2F)t\,^3F$	2	$75+13(A^2G)^3F+5(A^2F)^1D$	$t\,^3F$	89519?	89400	119		0.692
	3	$76+8(A^2G)^3F+7(A^2G)^1F$		89571	89498	73	1.14	1.072
	4	$77+8(A^2G)^3F+7(^4F)^3F$		89800	89675	125		1.234

TABLE 16. *Observed and Calculated Levels of* Mn II – $3d^54p$ – Continued

NAME	J	PERCENTAGE	AEL	OBS. LEVEL (cm^{-1})	CALC. LEVEL (cm^{-1})	O–C	OBS. g-FACTOR	CALC. g-FACTOR
$(A^2G)x\ ^1F$	3	$76+6(A^2F)^3F$	$x\ ^1F$	89950	90108	−158		1.002
$(B^2F)x\ ^1D$	2	$85+7(B^2F)^3F$	$x\ ^1D$	90597	90356	241	1.02	0.980
$(B^2F)u\ ^3G$	3	$59+33(^2H)^3G$	$u\ ^3G$	91018	90906	112	0.71	0.762
	4	$62+30(^2H)^3G$		91179	91077	102		1.055
	5	$66+29(^2H)^3G$		91302	91280	22	1.24	1.200
$(B^2F)u\ ^3D$	1	$93+4(^4F)^3D$	$u\ ^3D$	92061	92026	35		0.506
	2	$91+5(^4F)^3D$		92040	92117	−77	1.17	1.167
	3	$83+8(^4F)^3D+6(B^2F)^3D$		92083	92229	−146		1.331
$(^2H)w\ ^1G$	4	$37+41(B^2F)^1G+20(B^2G)^1G$	$w\ ^1G$	92517	92410	107	1.01	1.055
$(^2S)w\ ^3P$	0	$89+9(B^2D)^3P$	$(v\ ^3P)$	93720	93546	174		
	1	$88+9(B^2D)^3P$		93868	93676	192		1.491
	2	$88+10(B^2D)^3P$		94231	93975	256		1.498
$(B^2F)w\ ^1F$	3	95	$w\ ^1F$	94182	93907	275	1.00	1.002
$(^2S)y\ ^1P$	1	$84+13(B^2D)^1P$	$y\ ^1P$	95081	95585	−504		1.004
$(B^2D)^3F$	2	$86+10(B^2D)^3D$			100195			0.716
	3	$79+16(B^2D)^3D$			100330			1.121
	4	95			100574			1.249
$(B^2D)^3D$	1	96			100430			0.513
	2	$87+9(B^2D)^3F$			100511			1.125
	3	$81+17(B^2D)^3F$			100651			1.289
$(B^2D)x\ ^1F$	3	$88+7(B^2G)^1F$	$(u\ ^1F)$	101588	101350	238	1.04	1.005
$(B^2D)^3P$	0	$90+9(^2S)^3P$			101931			
	1	$87+10(^2S)^3P$			101927			1.477
	2	$86+10(^2S)^3P$			101934			1.490
$(B^2D)^1P$	1	$85+10(^2S)^1P$			102651			1.009
$(B^2D)w\ ^1D$	2	94	$w\ ^1D$	103600	103153	447		1.001
$(B^2G)^3H$	4	96			106755			0.803
	5	95			106873			1.038
	6	99			107058			1.167
$(B^2G)^3G$	3	$81+17(B^2G)^3F$			107675			0.811
	4	$65+32(B^2G)^3F$			107927			1.117
	5	94			107940			1.191
$(B^2G)^3F$	2	96			108080			0.667
	3	$79+18(B^2G)^3G$			107995			1.023
	4	$63+33(B^2G)^3G$			107637			1.181
$(B^2G)^1H$	5	96			108854			1.005
$(B^2G)v\ ^1G$	4	96	$v\ ^1G$	109474	109408	66		1.004
$(B^2G)^1F$	3	$90+9(C^2D)^1F$			110566			0.999
$(^2P)^3P$	0	$81+19(C^2D)^3P$			118425			
	1	$80+19(C^2D)^3P$			118522			1.502
	2	$80+19(C^2D)^3P$			118782			1.499
$(^2P)^1S$	0	100			119886			
$(^2P)^3D$	1	96			120907			0.502
	2	$73+19(^2P)^1D$			120878			1.127
	3	95			121159			1.333

TABLE 16. *Observed and calculated levels of* Mn II—$3d^5 4p$—*Continued*

NAME	J	PERCENTAGE	AEL	OBS. LEVEL (cm^{-1})	CALC. LEVEL (cm^{-1})	O–C	OBS. g-FACTOR	CALC. g-FACTOR
$(^2P)^1D$	2	$65 + 22(^2P)^3D + 10(C^2D)^1D$			121475			1.037
$(^2P)^3S$	1	99			122607			1.993
$(^2P)^1P$	1	$85 + 12(C^2D)^1P$			123766			1.002
$(C^2D)^3F$	2	95			127282			0.678
	3	93			127364			1.090
	4	97			127562			1.250
$(C^2D)^3D$	1	96			128251			0.504
	2	94			128408			1.154
	3	93			128591			1.325
$(C^2D)^1D$	2	$69 + 15(C^2D)^3P + 13(^2P)^1D$			128920			1.047
$(C^2D)^3P$	0	$81 + 19(^2P)^3P$			129837			
	1	$81 + 19(^2P)^3P$			129667			1.499
	2	$66 + 16(^2P)^3P + 14(C^2D)^1D$			129433			1.202
$(C^2D)^1F$	3	96			129762			1.002
$(C^2D)^1P$	1	$86 + 13(^2P)^1P$			132851			0.999

TABLE 17. *Observed and calculated levels of* Fe II—$3d^6 4p$

NAME	J	PERCENTAGE	AEL	OBS. LEVEL (cm^{-1})	CALC. LEVEL (cm^{-1})	O–C	OBS. g-FACTOR	CALC. g-FACTOR
$(^5D)z\,^6D$	1/2	100		39109	39219	−110	3.35	3.327
	3/2	99		39013	39106	−93	1.86	1.864
	5/2	98		38859	38924	−65	1.653	1.655
	7/2	98		38660	38686	−26	1.584	1.586
	9/2	99		38459	38431	28	1.542	1.554
$(^5D)z\,^6F$	1/2	99		42440	42165	275	−0.647	−0.667
	3/2	98		42401	42114	287	1.04	1.068
	5/2	98		42335	42026	309	1.304	1.315
	7/2	97		42237	41899	338	1.399	1.397
	9/2	97		42115	41730	385	1.43	1.433
	11/2	100		41968	41520	448		1.454
$(^5D)z\,^6P$	3/2	99		43621	44090	−469	2.398	2.395
	5/2	98		43239	43687	−448	1.869	1.878
	7/2	96		42658	43077	−419	1.702	1.706
$(^5D)z\,^4D$	1/2	96		45206	45144	62	−0.021	−0.001
	3/2	94		45044	44975	69	1.15	1.185
	5/2	91		44785	44698	87	1.35	1.361
	7/2	$89 + 6(^5D)^4F$		44447	44331	116	1.40	1.423
$(^5D)z\,^4F$	3/2	96		45290	45448	−158	0.445	0.422
	5/2	93		45080	45210	−130	1.069	1.048
	7/2	$91 + 6(^5D)^4D$		44754	44850	−96	1.29	1.253
	9/2	97		44233	44306	−73	1.32	1.335
$(^5D)z\,^4P$	1/2	99		47626	47798	−172	2.70	2.664
	3/2	99		47390	47534	−144	1.717	1.732
	5/2	98		46967	47062	−95	1.592	1.599
$(A^3P)z\,^4S$	3/2	$63 + 35(A^3P)^4P$		59663	59859	−196	1.89	1.887

TABLE 17. *Observed and calculated levels of* Fe II—$3d^64p$—*Continued*

NAME	J	PERCENTAGE	AEL	OBS. LEVEL (cm^{-1})	CALC. LEVEL (cm^{-1})	O–C	OBS. g-FACTOR	CALC. g-FACTOR
$(^3H)z\ ^4G$	5/2	$43+50(A^3F)^4G$		61042	61099	−57	0.799	0.587
	7/2	$41+44(A^3F)^4G$		60957	60984	−27	0.969	0.977
	9/2	$34+32(A^3F)^4G+15(^3H)^4I$		60807	60821	−14	1.155	1.089
	11/2	$53+33(A^3F)^4G+5(^3G)^4G$		60625	60711	−86	1.24	1.253
$(^3H)z\ ^4I$	9/2	$56+16(^3H)^4H+16(^3H)^4G$	$(a\ ^3H)z\ ^4H$	60989	61007	−18		0.887
	11/2	$60+24(^3H)^4H+6(^3H)^4G$		60888	60871	17		1.038
	13/2	$64+26(^3H)^4H+5(^3H)^2I$		60838	60830	8		1.144
	15/2	100		61347	61068	279		1.200
$(A^3P)y\ ^4P$	1/2	93		61035	61366	−331	2.613	2.522
	3/2	$38+32(A^3P)^4S+20(A^3P)^4D$		61333	61539	−206	1.74	1.632
	5/2	$76+18(A^3P)^4D$		60402	60593	−191	1.58	1.539
$(^3H)z\ ^4H$	7/2	$68+9(^3H)^2G+8(^3G)^4H$		61157	61361	−204	0.720	0.737
	9/2	$55+27(^3H)^4I+6(^3H)^2G$	$(a\ ^3H)z\ ^4I$	61513	61511	2		0.926
	11/2	$61+31(^3H)^4I+5(^3G)^4H$		61587	61579	8		1.082
	13/2	$64+29(^3H)^4I+5(^3G)^4H$		61528	61519	9		1.192
$(A^3P)z\ ^2D$	3/2	$44+17(A^3P)^4D+11(A^3P)^4P$		62126	62360	−234	1.019	1.068
	5/2	$67+12(A^3P)^4P+9(A^3P)^4D$		61093	61234	−141	1.01	1.257
$(A^3F)y\ ^4F$	3/2	$83+6(^3D)^4F$		62245	62376	−131	0.43	0.466
	5/2	$82+5(^3D)^4F$		62152	62299	−147	1.025	1.030
	7/2	$86+6(^3H)^4H$		62066	62208	−142	1.198	1.190
	9/2	$86+4(^3D)^4F$		62158	62237	−79	1.33	1.314
$(^3H)z\ ^2G$	7/2	$49+12(^3G)^2G+11(A^3F)^4F$		62322	62556	−234		0.941
	9/2	$65+16(^3G)^2G+6(^3H)^4H$		62083	62354	−271	1.097	1.096
$(^3H)z\ ^2I$	11/2	94		62662	62672	−10	0.910	0.931
	13/2	93		62293	62307	−14	1.069	1.080
$(A^3P)y\ ^4D$	1/2	92		62829	62801	28		0.122
	3/2	$57+26(A^3P)^2D$		62962	63028	−66	1.14	1.092
	5/2	$70+15(A^3P)^2D$		62690	62657	33	1.349	1.358
	7/2	96		61726	61481	245	1.411	1.421
$(A^3F)x\ ^4D$	1/2	$87+8(^3D)^4D$		63560	63831	−271	0.013	0.009
	3/2	$87+8(^3D)^4D$		63465	63724	−259	1.21	1.187
	5/2	$84+8(^3D)^4D$		63273	63516	−243	1.351	1.345
	7/2	$76+7(^3D)^4D$		62945	63193	−248	1.385	1.371
$(A^3F)y\ ^4G$	5/2	$37+36(^3H)^4G+20(A^3F)^2F$		64088	64194	−106	0.617	0.651
	7/2	$43+36(^3H)^4G+16(A^3F)^2F$		64041	64096	−55	0.975	0.998
	9/2	$48+34(^3H)^4G+12(A^3F)^2G$		63949	63940	9	1.15	1.164
	11/2	$62+32(^3H)^4G$		63876	63832	44	1.24	1.265
$(A^3F)z\ ^2F$	5/2	$52+15(^3H)^4G$		64425	64556	−131	0.82	0.782
	7/2	$53+11(^3G)^2F+5(^3H)^4G$		64286	64415	−129	1.135	1.097
$(A^3P)z\ ^2P$	1/2	$66+24(A^3P)^2S$		64807	64873	−66		1.012
	3/2	89		64834	65087	−253	1.329	1.324
$(A^3F)y\ ^2G$	7/2	$79+5(A^3F)^2F$		65110	65126	−16	0.896	0.907
	9/2	$75+6(^3G)^2H$		64832	64802	30	1.101	1.102
$(^3H)z\ ^2H$	9/2	$52+29(^3G)^2H+7(^1I)^2H$		65556	65662	−106	0.913	0.928
	11/2	$23+32(^3G)^2H+26(^3G)^4G$		65364	65567	−203	1.066	1.143
$(^3G)x\ ^4G$	5/2	$83+6(A^3F)^2F$		66078	66029	49	0.62	0.622
	7/2	$78+11(^3G)^4F$		65931	65879	52	1.00	1.021
	9/2	$61+28(^3G)^4F$		65696	65654	42		1.223
	11/2	$60+22(^3H)^2H+8(^3G)^2H$		65580	65490	90		1.214
$(A^3P)z\ ^2S$	1/2	$75+21(A^3P)^2P$		66249	65980	269		1.669

TABLE 17. *Observed and calculated levels of* Fe II – $3d^64p$ – Continued

NAME	J	PERCENTAGE	AEL	OBS. LEVEL (cm^{-1})	CALC. LEVEL (cm^{-1})	O–C	OBS. g-FACTOR	CALC. g-FACTOR
$(^3G)y\ ^4H$	7/2	$82+11(^3H)^4H$		66672	66376	296	0.69	0.690
	9/2	$79+8(^3H)^4H+4(^3H)^2H$		66589	66296	293	0.959	0.985
	11/2	$75+11(^3H)^2H+7(^3H)^4H$		66464	66176	288	1.13	1.133
	13/2	$89+9(^3H)^4H$		66412	66012	400		1.228
$(^3G)x\ ^4F$	3/2	$69+11(A^3F)^2D+10(^3D)^4F$		66613	66636	−23		0.468
	5/2	$67+11(A^3F)^2D+10(^3D)^4F$		66522	66566	−44	1.02	1.018
	7/2	$68+11(^3G)^4G+10(^3D)^4F$		66377	66437	−60	1.21	1.189
	9/2	$54+26(^3G)^4G+7(^3D)^4F$		66013	66068	−55		1.261
$(A^3F)y\ ^2D$	3/2	$69+14(A^3P)^2D+11(^3G)^4F$		67274	67422	−148	0.719	0.741
	5/2	$75+8(^3G)^4F$		67001	67128	−127	1.16	1.176
$(^3G)y\ ^2H$	9/2	$56+36(^3H)^2H$		68001	68266	−265	0.907	0.918
	11/2	$52+40(^3H)^2H$		67516	67752	−236	1.07	1.095
$(^3G)y\ ^2F$	5/2	$61+15(^3D)^2F+14(A^3F)^2F$		69651	69686	−35	0.857	0.864
	7/2	$59+13(A^3F)^2F+9(^3G)^2G$		69607	69619	−12	1.13	1.112
$(^3G)x\ ^2G$	7/2	$69+14(^3H)^2G+5(^3G)^2F$		70524	70415	109	0.87	0.924
	9/2	$77+18(^3H)^2G$		70315	70189	126	1.11	1.107
$(^1I)z\ ^2K$	13/2	99		70987	70999	−12		0.935
	15/2	100		71433	71373	60	1.05	1.067
$(A^1G)x\ ^2H$	9/2	$83+10(^1I)^2H$	$x\ ^2H^\cdot$	72130	71956	174	0.91	0.917
	11/2	$78+18(^1I)^2H$		72262	72178	84	1.08	1.091
$(^3D)w\ ^4P$	1/2	$73+17(^3D)^4D+5(^3D)^2P$		72213	72220	−7		2.049
	3/2	$78+9(^3D)^4D+4(^3D)^2P$		72043	72066	−23	1.66	1.613
	5/2	92		71965	71982	−17		1.585
$(^3D)w\ ^4F$	3/2	$77+15(^3G)^4F$		72169	72101	68		0.458
	5/2	$78+14(^3G)^4F$		72239	72184	55		1.035
	7/2	$72+12(^3G)^4F$		72352	72298	54		1.235
	9/2	$85+11(^3G)^4F$		72651	72510	141		1.329
$(^3D)w\ ^4D$	1/2	$57+23(^3D)^4P+10(^3D)^2P$		72430	72418	12		0.720
	3/2	$69+13(^3D)^4P+7(^3D)^2P$		72525	72510	15		1.272
	5/2	$82+8(A^3F)^4D$		72620	72613	7		1.353
	7/2	$50+19(A^1G)^2F+13(^3D)^2F$		72652	72628	24		1.301
$(A^1G)w\ ^2G$	7/2	$69+12(^3D)^4D$		73143	72956	187	0.91	0.992
	9/2	$87+4(^3H)^2G$		73092	72940	152		1.105
$(A^1G)x\ ^2F$	5/2	$44+32(^3D)^2F+8(A^3F)^2F$	$(a\ ^3D)x\ ^2F$	73055	73049	6		0.877
	7/2	$31+25(^3D)^4D+20(A^1G)^2G$		73016	73065	−49		1.163
$(^3D)y\ ^2P$	1/2	$63+15(^3D)^4D+15(A^1S)^2P$		73187	73150	37		0.558
	3/2	$68+15(A^1S)^2P+11(^3D)^4D$		73189	73076	113		1.319
$(^1I)w\ ^2H$	9/2	$79+12(B^1G)^2H$	$w\ ^2H$	73751	73978	−227		0.912
	11/2	$63+20(B^1G)^2H+10(^1I)^2I$		73604	73705	−101		1.075
$(^1I)y\ ^2I$	11/2	$89+9(^1I)^2H$		73970	74161	−191		0.941
	13/2	99		73967	74163	−196		1.076
$(^3D)x\ ^2D$	3/2	93		74498	74562	−64		0.807
	5/2	93		74607	74683	−76		1.202
$(^3D)w\ ^2F$	5/2	$49+40(A^1G)^2F$	$w\ ^2F$	75915	75728	187	0.844	0.861
	7/2	$55+32(A^1G)^2F$		75601	75370	231	1.125	1.143
$(A^1S)x\ ^2P$	1/2	$66+17(^3D)^2P+10(A^1D)^2P$		76578	76654	−76		0.670
	3/2	$62+23(A^1D)^2P$		76130	76258	−128	1.34	1.332
$(A^1D)w\ ^2F$	5/2	$79+6(A^1D)^2D$		77743	77892	−149		0.883
	7/2	$85+8(A^1G)^2F$		78138	78274	−136	1.13	1.144

TABLE 17. *Observed and calculated levels of* Fe II – $3d^64p$ – *Continued*

NAME	J	PERCENTAGE	AEL	OBS. LEVEL (cm^{-1})	CALC. LEVEL (cm^{-1})	O–C	OBS. g-FACTOR	CALC. g-FACTOR
$(A^1D)w\ ^2D$	3/2	$63 + 19(A^1D)^2P$		78487	78543	−56		0.956
	5/2	$80 + 11(^1F)^2D$		78691	78700	−9		1.176
$(A^1D)w\ ^2P$	1/2	$84 + 10(A^1S)^2P$		78842	78607	235		0.670
	3/2	$51 + 26(A^1D)^2D$		79244	78920	324		1.178
$(^1F)w\ ^2G$	7/2	94		83305	83154	151		0.891
	9/2	96		83871	83627	244		1.112
$(^1F)w\ ^2D$	3/2	$85 + 8(A^1D)^2D$		84360	84563	−203		0.804
	5/2	$80 + 13(A^1D)^2D$		83869	84131	−262		1.198
$(^1F)u\ ^2F$	5/2	92		86548	86346	202		0.865
	7/2	92		86483	86286	197		1.146
$(B^3P)w\ ^4D$	1/2	$56 + 43(B^3F)^4D$		86389	86642	−253		0.003
	3/2	$53 + 45(B^3F)^4D$		86544	86799	−255		1.197
	5/2	$50 + 49(B^3F)^4D$		86768	87005	−237		1.366
	7/2	$41 + 46(B^3F)^4D$		86930	87176	−246		1.424
$(B^3P)^2S$	1/2	95			89360			2.014
$(B^3F)^4G$	5/2	98			89755			0.573
	7/2	98			89891			0.984
	9/2	97			90015			1.171
	11/2	98			90116			1.272
$(B^3P)^4S$	3/2	95			90836			1.983
$(B^3P)^4P$	1/2	94			91777			2.622
	3/2	90			92046			1.710
	5/2	$81 + 8(B^3P)^2D$			92471			1.543
$(B^3F)u\ ^2G$	7/2	91		92603	92556	47		0.902
	9/2	91		92427	92273	154		1.122
$(B^3F)u\ ^2D$	3/2	$51 + 40(B^3P)^2D$		92216	92317	−101		0.813
	5/2	$56 + 30(B^3P)^2D$		92696	92781	−85		1.213
$(B^3F)^4D$	1/2	$55 + 40(B^3P)^4D$			92757			0.039
	3/2	$43 + 37(B^3P)^4D + 13(B^3F)^4F$			92914			1.107
	5/2	$31 + 40(B^3F)^4F + 23(B^3P)^4D$			93099			1.241
	7/2	$38 + 30(B^3F)^4D + 30(B^3F)^4F$			93596			1.366
$(B^3F)u\ ^4F$	3/2	$82 + 8(B^3F)^4D$		93329	93168	161		0.532
	5/2	$53 + 22(B^3F)^4D + 22(B^3P)^4D$		93396	93368	28		1.192
	7/2	$65 + 19(B^3P)^4D + 12(B^3F)^4D$		93488	93217	271		1.286
	9/2	$94 + 5(B^3F)^2G$		93485	93386	99		1.321
$(B^3P)^2D$	3/2	$37 + 38(B^3F)^2D + 17(B^3P)^2P$			94092			0.889
	5/2	$61 + 35(B^3F)^2D$			94679			1.207
$(B^3P)^2P$	1/2	93			94531			0.665
	3/2	$77 + 13(B^3P)^2D + 5(B^3F)^2D$			95112			1.232
$(B^3F)u\ ^2F$	5/2	97		96280	95406	874		0.858
	7/2	94		96357	95427	930		1.142
$(B^1G)^2H$	9/2	97			97972			0.912
	11/2	98			98338			1.091
$(B^1G)^2F$	5/2	92			99483			0.858
	7/2	$68 + 24(B^1G)^2G$			99159			1.081
$(B^1G)^2G$	7/2	$72 + 21(B^1G)^2F$			99896			0.952
	9/2	96			99796			1.110
$(B^1D)^2D$	3/2	98			115424			0.803
	5/2	98			115541			1.197

TABLE 17. *Observed and calculated levels of* Fe II – $3d^6 4p$ – Continued

NAME	J	PERCENTAGE	AEL	OBS. LEVEL (cm^{-1})	CALC. LEVEL (cm^{-1})	O–C	OBS. g-FACTOR	CALC. g-FACTOR
$(B^1D)^2F$	5/2	96			117913			0.860
	7/2	97			118266			1.143
$(B^1D)^2P$	1/2	96			119387			0.667
	3/2	95			119218			1.331
$(B^1S)^2P$	1/2	96			138558			0.667
	3/2	96			139013			1.333

TABLE 18. *Observed and calculated levels of* Co II – $3d^7 4p$

NAME	J	PERCENTAGE	AEL	OBS. LEVEL (cm^{-1})	CALC. LEVEL (cm^{-1})	O–C	OBS. g-FACTOR	CALC. g-FACTOR
z^5F	1	97		46786	46706	80	0.06	0.038
	2	$91 + 7(^4F)^5D$		46453	46383	70	1.058	1.022
	3	$83 + 13(^4F)^5D$		45972	45920	52	1.303	1.273
	4	$73 + 22(^4F)^5D$		45379	45355	24	1.407	1.377
	5	96		45198	45014	184	1.396	1.394
$(^4F)z^5G$	2	$93 + 3(^4F)^5F + 3(^4F)^5D$		48388	48012	376	0.35	0.391
	3	$90 + 5(^4F)^5F$		48151	47767	384	0.92	0.943
	4	$87 + 6(^4F)^3F + 6(^4F)^3G$		47807	47413	394	1.154	1.159
	5	$84 + 11(^4F)^3G$		47346	46947	399	1.260	1.264
	6	100		47078	46531	547	1.350	1.333
$(^4F)z^5D$	0	$94 + 6(^4P)^5D$		47995	48188	−193		
	1	$92 + 6(^4P)^5D$		47848	48022	−174	1.42	1.464
	2	$85 + 5(^4F)^5F + 5(^4P)^5D$		47537	47672	−135	1.43	1.420
	3	$80 + 11(^4F)^5F + 5(^4F)^5G$		47039	47125	−86	1.43	1.445
	4	$72 + 20(^4F)^3F + 4(^4F)^5G$		46321	46354	−33	1.442	1.455
$(^4F)z^3G$	3	$75 + 22(^4F)^3F$		50036	50105	−69	0.811	0.834
	4	$59 + 36(^4F)^3F$		49348	49343	5	1.111	1.129
	5	$88 + 12(^4F)^5G$		48556	48546	10	1.19	1.207
$(^4F)z^3F$	2	$94 + 3(^2G)^3F$		50914	50849	65	0.689	0.678
	3	$69 + 22(^4F)^3G$		50382	50335	47	1.059	1.017
	4	$60 + 34(^4F)^3G$		49698	49647	51	1.197	1.178
$(^4F)z^3D$	1	95		52684	52650	34	0.524	0.501
	2	94		52230	52170	60	1.167	1.157
	3	$92 + 4(^4F)^3F$		51512	51412	100	1.33	1.321
$(^4P)z^5S$	2	99		56011	56328	−317	2.00	1.996
$(^4P)y^5D$	0	$92 + 6(^4F)^5D$		61458	61579	−121		
	1	$87 + 6(^4F)^5D$		61348?	61461	−113		1.502
	2	$88 + 5(^4F)^5D$		61260	61347	−87	1.490	1.490
	3	$89 + 5(^4F)^5D$		61241	61281	−40	1.504	1.493
	4	$95 + 4(^4F)^5D$		61388	61331	57	1.442	1.499
$(^4P)z^3S$	1	$60 + 16(^4P)^5P + 12(^2P)^3S$		62440	62647	−207		2.020
$(^2G)^3H$	4	$83 + 8(^2G)^3G + 6(^2G)^3F$			63511			0.852
	5	$78 + 15(^2G)^1H + 5(^2G)^3G$			63103			1.033
	6	97			63234			1.164
$(^4P)z^5P$	1	$77 + 19(^4P)^3S$		63665	63865	−200	2.62	2.349
	2	$67 + 21(^4P)^3D + 4(^2P)^3P$		63367	63598	−231	1.86	1.630
	3	$82 + 13(^4P)^3D$		63344	63564	−220	1.67	1.610

TABLE 18. *Observed and Calculated Levels of* Co II – $3d^74p$ – Continued

NAME	J	PERCENTAGE	AEL	OBS. LEVEL (cm^{-1})	CALC. LEVEL (cm^{-1})	O–C	OBS. g-FACTOR	CALC. g-FACTOR
$(^4P)y\,^3D$	1	$81+7(^2P)^3D$		63865	64147	−282		0.592
	2	$57+27(^4P)^5P+4(^4P)^5D$		63616	63858	−242	1.33	1.358
	3	$77+14(^4P)^5P$		63587	63776	−189		1.381
$(^2G)^1G$	4	$46+23(^2G)^3F+19(^2G)^3G$			64511			1.064
$(^2G)^1H$	5	$48+32(^2G)^3G+20(^2G)^3H$			64849			1.070
$(^2G)^3F$	2	95			65022			0.674
	3	$83+10(^2G)^3G$			64410			1.044
	4	$66+12(^2G)^3H+9(^2G)^1G$			63684			1.153
$(^2P)^3P$	0	$57+20(A^2D)^3P+16(^4P)^3P$			64683			
	1	$59+17(A^2D)^3P+9(^4P)^3P$			65146			1.485
	2	$45+35(^4P)^3P+5(^2P)^3D$			65187			1.437
$(^2G)^3G$	3	$85+9(^2G)^3F$			65220			0.794
	4	$67+22(^2G)^1G+6(^2H)^1G$			65249			1.029
	5	$62+35(^2G)^1H$			64573			1.125
$(^4P)^3P$	0	$63+24(^2P)^3P+12(^2P)^1S$			65887			
	1	$83+8(^2P)^3P$			65947			1.469
	2	$53+23(^2P)^3P+18(A^2D)^3P$			65521			1.500
$(^2G)^1F$	3	$72+18(A^2D)^1F$			65898			0.997
$(^2P)^1D$	2	$37+19(^2P)^3D+12(^4P)^3D$			67369			1.063
$(^2P)^3D$	1	$68+18(A^2D)^3D+5(^4P)^3D$			67820			0.569
	2	$54+21(^2P)^1D+11(A^2D)^3D$			68024			1.124
	3	$81+10(A^2D)^3F$			67398			1.312
$(^2P)^1S$	0	$81+18(^4P)^3P$			68337			
$(^2H)^3I$	5	97			68759			0.839
	6	$75+24(^2H)^1I$			68281			1.019
	7	100			68413			1.143
$(A^2D)^3D$	1	$50+25(^2P)^1P+16(^2P)^3D$			69188			0.656
	2	$67+11(^2P)^3D+6(^2P)^1D$			69430			1.133
	3	$85+8(A^2D)^3F$			68860			1.314
$(^2H)^3G$	3	$85+4(A^2D)^3F$			69499			0.781
	4	92			69020			1.053
	5	95			68421			1.199
$(^2H)^1I$	6	$75+24(^2H)^3I$			69652			1.008
$(A^2D)^3F$	2	$75+9(A^2D)^3D$			70599			0.774
	3	$70+8(^2P)^3D+6(A^2D)^3D$			70262			1.095
	4	98			69898			1.248
$(^2P)^3S$	1	$53+16(^2P)^1P+10(A^2D)^3D$			70486			1.599
$(^2P)^1P$	1	$38+27(^2P)^3S+12(A^2D)^1P$			70812			1.262
$(A^2D)^1D$	2	$39+32(A^2D)^3P+13(^2P)^1D$			72351			1.225
$(^2H)^3H$	4	96			72205			0.807
	5	96			71895			1.034
	6	99			71586			1.166
$(A^2D)^1F$	3	$72+16(^2G)^1F+7(A^2D)^3F$			72609			1.014
$(A^2D)^3P$	0	$79+17(^2P)^3P$			73472			
	1	$68+12(^2P)^3P+10(^2P)^1P$			73153			1.448
	2	$46+30(A^2D)^1D+13(^2P)^1D$			72351			1.225
$(^2H)^1G$	4	$76+22(^2G)^1G$			73235			0.997

TABLE 18. *Observed and calculated levels of* Co II – $3d^74p$ – *Continued*

NAME	J	PERCENTAGE	AEL	OBS. LEVEL (cm^{-1})	CALC. LEVEL (cm^{-1})	O–C	OBS. g-FACTOR	CALC. g-FACTOR
$(A^2D)^1P$	1	$86+8(^2P)^1P$			74510			1.045
$(^2H)^1H$	5	97			74714			1.001
$(^2F)^1D$	2	$62+32(^2F)^3F$			83192			0.895
$(^2F)^3G$	3	$89+5(^2F)^3F+5(^2H)^3G$			83157			0.768
	4	$87+7(^2F)^3F$			83460			1.063
	5	96			83888			1.200
$(^2F)^3F$	2	$65+30(^2F)^1D$			83915			0.783
	3	$90+5(^2F)^3G$			83930			1.073
	4	$60+30(^2F)^1G+8(^2F)^3G$			84177			1.158
$(^2F)^3D$	1	95			84403			0.501
	2	$89+6(^2F)^1D$			84433			1.156
	3	92			84312			1.324
$(^2F)^1G$	4	$68+30(^2F)^3F$			84454			1.079
$(^2F)^1F$	3	98			87762			1.002
$(B^2D)^3P$	0	99			101199			
	1	99			101191			1.494
	2	99			101247			1.498
$(B^2D)^3F$	2	97			102024			0.669
	3	98			102357			1.083
	4	98			102770			1.250
$(B^2D)^1P$	1	96			104543			0.991
$(B^2D)^1F$	3	98			104681			1.004
$(B^2D)^3D$	1	96			106136			0.514
	2	$57+41(B^2D)^1D$			106216			1.095
	3	97			106763			1.329
$(B^2D)^1D$	2	$56+41(B^2D)^3D$			106593			1.070

TABLE 19. *Observed and calculated levels of* Ni II $3d^84p$

NAME	J	PERCENTAGE	AEL	OBS. LEVEL (cm^{-1})	CALC. LEVEL (cm^{-1})	O–C	OBS. g-FACTOR	CALC. g-FACTOR
$(^3F)z\ ^4D$	1/2	96		54176	54237	−61	−0.005	0.003
	3/2	$94+4(^3P)^4D$		53635	53717	−82	1.186	1.187
	5/2	93		52739	52860	−121	1.356	1.360
	7/2	94		51558	51742	−184	1.420	1.423
$(^3F)z\ ^4G$	5/2	$94+5(^3F)^4F$		55019	54767	252	0.616	0.601
	7/2	$81+10(^3F)^4F+8(^3F)^2G$		54263	54078	185	1.02	1.006
	9/2	$67+23(^3F)^2G+10(^3F)^4F$		53365	53274	91	1.156	1.174
	11/2	100		53497	53110	387	1.305	1.273
$(^3F)z\ ^4F$	3/2	95		56425	56417	8	0.412	0.423
	5/2	$87+6(^3F)^4G+4(^3F)^2F$		56075	56027	48	0.985	1.006
	7/2	$76+10(^3F)^2F+9(^3F)^4G$		55418	55360	58	1.184	1.203
	9/2	$80+19(^3F)^2G$		54557	54546	11	1.26	1.289
$(^3F)z\ ^2G$	7/2	$84+8(^3F)^4G+7(^3F)^2F$		56372	56481	−109	0.940	0.916
	9/2	$58+32(^3F)^4G+10(^3F)^4F$		55300	55245	55	1.152	1.153

TABLE 19. *Observed and calculated levels of* Ni II – $3d^84p$ – *Continued*

NAME	J	PERCENTAGE	AEL	OBS. LEVEL (cm^{-1})	CALC. LEVEL (cm^{-1})	O–C	OBS. g-FACTOR	CALC. g-FACTOR
$(^3F)z\ ^2F$	5/2	$74 + 20(^3F)^2D + 4(^3F)^4F$		58493	58544	−51	0.946	0.934
	7/2	$81 + 11(^3F)^4F + 6(^3F)^2G$		57080	57159	−79	1.154	1.136
$(^3F)z\ ^2D$	3/2	$89 + 7(^1D)^2D$		58706	58617	89	0.795	0.796
	5/2	$74 + 20(^3F)^2F + 4(^1D)^2D$		57420	57361	59	1.116	1.131
$(^3P)z\ ^4P$	1/2	$85 + 11(^1D)^2P + 4(^3P)^2P$		67031	66905	126	2.331	2.366
	3/2	$73 + 12(^1D)^2P + 7(^1D)^2D$		66580	66525	55	1.550	1.580
	5/2	$73 + 20(^1D)^2D$		66571	66462	109	1.48	1.484
$(^1D)y\ ^2F$	5/2	$84 + 8(^3P)^4P + 4(^3P)^2D$		67694	67591	103	0.960	0.934
	7/2	$86 + 9(^3P)^4D$		68131	67950	181	1.200	1.170
$(^1D)y\ ^2D$	3/2	$65 + 18(^3P)^4P + 7(^3F)^2D$		68154	68214	−60	1.02	1.014
	5/2	$74 + 19(^3P)^4P + 4(^1D)^2F$		68735	68695	40	1.26	1.260
$(^1D)z\ ^2P$	1/2	$61 + 23(^3P)^2P + 15(^3P)^4P$		68281	68234	47	1.008	0.971
	3/2	$64 + 15(^1D)^2D + 11(^3P)^2P$		68966	68944	22	1.305	1.282
$(^3P)y\ ^4D$	1/2	$95 + 4(^3F)^4D$		70748	70779	−31		0.012
	3/2	$91 + 4(^3F)^4D$		70707	70715	−8	1.190	1.188
	5/2	$83 + 9(^3P)^2D + 4(^1D)^2F$		70635	70645	−10	1.32	1.336
	7/2	$87 + 9(^1D)^2F$		70777	70726	51	1.38	1.399
$(^3P)x\ ^2D$	3/2	$82 + 11(^3P)^2P$		72375	72365	10	0.844	0.880
	5/2	$87 + 10(^3P)^4D$		71771	71877	−106	1.240	1.211
$(^3P)y\ ^2P$	1/2	$70 + 24(^1D)^2P + 5(^3P)^2S$		73903	73647	256	1.039	0.730
	3/2	$67 + 16(^1D)^2P + 13(^3P)^2D$		72985	72725	260	1.326	1.267
$(^3P)z\ ^2S$	1/2	$94 + 4(^1D)^2P$		74283	74570	−287		1.919
$(^3P)z\ ^4S$	3/2	97		74300	74589	−289		1.982
$(^1G)z\ ^2H$	9/2	100		75150	75088	62	0.903	0.910
	11/2	100		75722	75538	184	1.119	1.091
$(^1G)x\ ^2F$	5/2	95		75890?	76416	−526		0.858
	7/2	$94 + 4(^1D)^2F$		75917?	76047	−130	1.16	1.143
$(^1G)y\ ^2G$	7/2	99		79823	80133	−310		0.890
	9/2	100		79924	80227	−303		1.111
$(^1S)x\ ^2P$	1/2	99			105888			0.667
	3/2	99			106418			1.333

TABLE 20. *Observed and calculated levels of* Cu II $3d^94p$

NAME	J	PERCENTAGE	AEL	OBS. LEVEL (cm^{-1})	CALC. LEVEL (cm^{-1})	O–C	OBS. g-FACTOR	CALC. g-FACTOR
$(^2D)z\ ^3P$	0	100		68850	68638	212		
	1	98		67917	67812	105	1.49	1.483
	2	99		66419	66496	−77	1.49	1.495
$(^2D)z\ ^3F$	2	95		69868	69735	133	0.67	0.688
	3	$71 + 27(^2D)^1F$		68448	68528	−80	1.06	1.065
	4	100		68731	68534	197	1.23	1.250
$(^2D)z\ ^1F$	3	$66 + 20(^2D)^3F$	$(^2D)\ ^3D_3$	70842	70941	−99		1.062
$(^2D)z\ ^1D$	2	$61 + 35(^2D)^3D$	$(^2D)\ ^3D_2$	71494	71764	−270	1.08	1.047
$(^2D)z\ ^3D$	1	$75 + 23(^2D)^1P$		73102	73164	−62	0.47	0.636
	2	$61 + 38(^2D)^1D$	$(^2D)\ ^1D$	73353	73507	−154	0.99	1.103
	3	$85 + 9(^2D)^3F$	$(^2D)\ ^1F$	71920	72055	−135		1.290
$(^2D)z\ ^1P$	1	$76 + 24(^2D)^3D$		73596	73365	231	1.04	0.881

TABLE 21. *Observed and calculated levels of* Zn II $3d^{10}4p$

NAME	J	PERCENTAGE	AEL	OBS. LEVEL (cm^{-1})	CALC. LEVEL (cm^{-1})	O−C	OBS. g-FACTOR	CALC. g-FACTOR
$(^1S)_2\ ^2P$	1/2	100		48481	48485	−4		0.667
	3/2	100		49354	49350	4		1.333

This paper was supported in part by the National Bureau of Standards, Washington, D.C.

The author wishes to acknowledge with everlasting gratitude and appreciation the unremitting kind interest in this work by the late Professor Giulio Racah.

5. References

[1] Racah, G., and Shadmi, Y., Bull. Res. Counc. of Israel **8F,** No. 1, 15 (1959).
[2] Roth, C., J. Res NBS **72A** (Phys. and Chem.) No. 5, 505 (1968).
[3] Racah, G., and Spector, N., Bull. Res. Counc. of Israel **9F**, No. 2, 75 (1960).
[4] Trees, R. E., Phys. Rev. **83,** 756 (1951); ibid., **84,** 1089 (1951).
[5] Racah, G., Phys. Rev. **85,** 381 (1952).
[6] Racah, G., Rydberg Centennial Conference, Lunds Univ. Arsskr. **50,** 31 (1955).
[7] Racah, G., Phys. Rev. **63,** 367 (1943).
[8] Racah, G., and Shadmi, Y., Phys. Rev. **119,** 156 (1960).
[9] Trees, R. E., and Jorgensen, C. K., Phys. Rev. **123,** 1278 (1961).
[10] Trees, R. E., Phys. Rev. **129,** 1220 (1963).
[11] Rajnak, K., and Wybourne, B. G., Phys. Rev. **132,** 280 (1963).
[12] Racah, G., and Stein, J., Phys. Rev. **156,** 58 (1967).
[13] Racah, G., Bull. Res. Counc. of Israel **8F,** No. 1 (1953).
[14] Iglesias, L., and Velasco, R., An. Real. Soc. Espan. Fis. Quim. (Spain) **59(A),** No. 11–12, 227 (1963).
[15] Moore, C. E., Atomic Energy Levels, NBS Circ. 467, **I** (1949), ibid., **II** (1952).
[16] Shadmi, Y., Bull. Res. Counc. of Israel **10F,** No. 3, 109 (1962).
[17] Racah, G., J. Quant. Spectrosc. Radiat. Transfer **4,** 617 (1964) (Pergamon Press Ltd.).

Paper 73A2–540)

JOURNAL OF RESEARCH of the National Bureau of Standards—A. Physics and Chemistry
Vol. 73A, No. 2, March–April 1969

Configurations $3d^n4p + 3d^{n-1}4s4p$ in Sc II, Ti II, and V II*

C. Roth[1]

(November 27, 1968)

Experimental levels of the configurations $3d^n4p + 3d^{n-1}4s4p$ for Sc II, Ti II, and V II were compared with corresponding calculated values. Electrostatic, spin-orbit interactions, as well as the α, β and T corrections, whenever possible, were considered for $3d^n4p$ and $3d^{n-1}4s4p$. The electrostatic interaction between the configurations $3d^n4p$ and $3d^{n-1}4s4p$ was included explicitly. The rms errors for Sc II, Ti II and V II were 4.6, 75 and 66 cm^{-1}, respectively.

Key words: Configurations $3d^n4p + 3d^{n-1}4s4p$; energy levels; interaction between configurations; iron group; second spectra.

1. Introduction

The configurations $(3d+4s)^n$ in the second spectra of the iron group were considered by Racah and Shadmi [1].[2] Individual and general treatments including the α, β, and T corrections were performed for the configurations $3d^n4p$ of the third and second spectra of the iron group by the author [2, 3].[3]

The results for the configurations d^np in the third spectra of the iron group indicate that there the interactions with the configurations $d^{n-1}sp$ are weak [2]. Thus good agreement was obtained between the theoretically predicted levels and experimental levels without taking into consideration the configurations $d^{n-1}sp$. However, the configurations d^np in the second spectra, and especially those on the left side of the periodic table are strongly perturbed by the configurations $d^{n-1}sp$, [3].

The algebraic matrices for the configurations $(d+s)^np$ were put on tape and checked by the author. Unfortunately these matrices could not be used to study systematically the configurations $(3d+4s)^n4p$ here, since the experimental data for the configuration $3d^{n-1}4s4p$ is very scarce and nonexistent for $3d^{n-2}4s^24p$, [4]. Thus it is feasible to consider the configurations $3d^n4p + 3d^{n-1}4s4p$ and these only for Sc II, Ti II, V II, and Cu II. In the last case other interaction besides $3d^n4p - 3d^{n-1}4s4p$ must be taken into consideration. This problem will be investigated in a future paper.

The parameters A, B, C, F_2, G_1, G_3, α, β, T, ζ_d and ζ_p refer to the configurations d^np. The same parameters primed refer to the configurations $d^{n-1}sp$. The parameters G_{ds} and G_{ps} refer to the interactions d-s and p-s in the configuration $d^{n-1}sp$.

$$G_{ds} = \frac{1}{5}G^2(ds) = \frac{R^2(ds, sd)}{5}$$

$$G_{ps} = \frac{1}{3}G^1(ps) = \frac{R^1(ps, sp)}{3}.$$

The parameters of the electrostatic interaction between the configurations d^np and $d^{n-1}sp$ are denoted by H, J, and K

$$H = \frac{R^2(dd, ds)}{35}$$

$$J = \frac{R^2(dp, sp)}{5}$$

$$K = \frac{R^1(dp, ps)}{3}.$$

In Sc II $-3d4p + 4s4p$, there are eight terms determined by eight electrostatic parameters, i.e., A, F_2, G_1, G_3, A', G_{ps}, J, and K. Thus the problem is solved mathematically, but the parameters may absorb interactions with other configurations, and thus give a distorted representation of the configuration $3d4p + 4s4p$. Hence the parameters of Sc II cannot be considered as being very reliable for use as the starting parameters of Ti II. In Ti II there is an inherent instability if in the core $d^2 + ds$ the term $d^2\,{}^1S$ is missing. This is due to the fact that there are then six terms in $d^2 + ds$ with the seven electrostatic parameters A, B, C, α, A', G_{ds} and H to determine them. Even if α is held fixed at the value obtained for Ti II from the general least squares of d^np, the values of the other parameters cannot be considered as reliable enough to be used for the next spectrum, V II. On the other hand, in V II $-3d^34p + 3d^24s4p$ there are many more terms than electrostatic parameters. It is thus theo-

---

* An invited paper.

[1] Present address: McGill University, Montreal, Canada.

[2] Figures in brackets indicate the literature references at the end of this paper.

[3] The reader is referred to the above papers for an explanation of the method used, notation and significance of the various parameters pertaining to d^np.

retically most stable and for this reason it was investigated first.

2. V II $-3d^3 4p + 3d^2 4s4p$

2.1. Initial Parameters

The starting values of the parameters B, C, F_2, G_1, G_3, α, ζ_d and ζ_p were taken from the configurations $d^n p$ of the second spectra, [3]. By making the initial approximation that the values of the above parameters are the same for the configurations $d^3 p$ and $d^2 sp$ we obtain the following values from the variation of the general least squares where β and T are eliminated:

$$\begin{aligned} B &= B' = 750 \\ C &= C' = 2600 \\ F_2 &= F_2' = 310 \\ G_1 &= G_1' = 330 \\ G_3 &= G_3' = 30 \\ \alpha &= \alpha' = 64 \\ \beta &= \beta' = 0 \\ T &= T'' = 0 \\ \zeta_d &= \zeta_d' = 200 \\ \zeta_p &= \zeta_p' = 260 \end{aligned}$$

Since G_{ds} represents the interaction of the electrons d and s in the core $d^2 s$, its approximate value can be taken from V III $-d^3 + d^2 s$. From Shadmi [5], we obtain

$$G_{ds} = 1750.$$

A starting value for the parameter G_{ps} is obtained from the interpolation of $G_{ps}(sp)$ and $G_{ps}(d^{10}sp)$. From AEL, Vol. **I**, the center of gravity of $4s(^2S)4p\,y\,^3P$ in Sc II is 39230 cm^{-1} and $4s(^2S)4p\,y\,^1P$ in Sc II is 55716 cm^{-1}. Thus,

$$G_{ps}(sp) = 8243.$$

A similar calculation for Ga II $-3d^{10}4s4p$ yields

$$G_{ps}(d^{10}sp) = 11212.$$

Thus by interpolation

$$G_{ps}(d^2 sp) = 8837.$$

Shadmi [5] found that the interaction between the configurations d^n and $d^{n-1}s$ in the third spectra was too weak to determine the value of the parameter H. He thus let H equal to zero for all the spectra of the third row. Furthermore, in the configurations $d^n p$ and $d^{n-1}sp$ the relative phase of H with respect to J and K is not known. Thus as a starting point we also let H equal to zero.

The initial values for J and K are obtained from Sc II $-3d4p + 4s4p$. The electrostatic interaction matrix for ^1P is given by

$$\begin{pmatrix} X & -\sqrt{2}(K+J) \\ -\sqrt{2}(K+J) & Y \end{pmatrix}.$$

Here X is the unperturbed level $dp\ ^1P$. Its value can be taken as the calculated level of $dp\ ^1P$, Sc II, in the GLS of $d^n p$. Then from table 12, [3]

$$X = 32115.$$

From AEL, [4], the experimental value for the level $dp\ ^1P$, Sc II, is 30816. Thus the level $dp\ ^1P$ is lowered by 1299 due to the interaction with $sp\ ^1P$. Similarly the unperturbed value of the level $sp\ ^1P$ is lower by 1299 than the experimental value of $sp\ ^1P$, at 55716. Since Y represents the value of the unperturbed level $sp\ ^1P$,

$$Y = 55716 - 1299 = 54417.$$

The eigenvalues λ_1 and λ_2 of the electrostatic interaction matrix of ^1P are simply the experimental levels $dp\ ^1P$ and $sp\ ^1P$ at 30816 and 55716, respectively.

We thus obtain

$$J + K = \pm 3915.$$

For the case of ^3P the electrostatic interaction matrix is

$$\begin{pmatrix} x & \sqrt{2}(K-J) \\ \sqrt{2}(K-J) & y \end{pmatrix}.$$

Performing a similar calculation as for ^1P and using values for the center of gravity yields

$$K - J = \pm 1660.$$

From the above values for the sum and difference of K and J it is not possible to solve for these parameters uniquely. All four possibilities were considered by performing four different diagonalizations with all the parameters except J and K having the same values in all diagonalizations. From the least squares calculations it was evident that both J and K must be positive and that $K > J$. This result is in agreement with the values of J and K obtained by Z. B. Goldschmidt in the rare-earth spectra [6].

Thus the following values of J and K were taken for the first diagonalization of V II,

$$J = 1100, \qquad K = 2800.$$

In order to obtain starting values for the parameters A and A' those terms whose electrostatic interaction matrix elements are of order two, here ^5F and ^5G, are considered. Since all the levels of $3d^2 4s(b^4F)4p\,y\,^5G$ are given as uncertain in AEL, [4], ^5G is neglected.

The electrostatic interaction matrix of ^{5}F is given by

$$\begin{pmatrix} A-15B+3F_2-6G_1-26G_3+12\alpha & \frac{-3\sqrt{5}}{5}(K-J) \\ \frac{-3\sqrt{5}}{5}(K-J) & A'-8B'-2G_{ds}-3F_2'-G_1'-16G_3'-G_{ps}+12\alpha' \end{pmatrix}$$

Using the values of the parameters already found the above matrix becomes

$$\begin{pmatrix} A-12312 & \frac{-3\sqrt{5}}{5}(1700) \\ \frac{-3\sqrt{5}}{5}(1700) & A'-19309 \end{pmatrix}$$

From AEL [4], the centers of gravity of $3d^3(a^4\mathrm{F})4pz\ ^5\mathrm{F}$ and $3d^24s(b^4\mathrm{F})4py\ ^5\mathrm{F}$ are 37042 and 63972 cm^{-1} respectively. By evaluating the sum and difference of the eigenvalues of the above matrix we obtain

$$A=49550 \quad \text{and} \quad A'=83090$$

2.2. Results

The configuration d^3p comprises 48 theoretical terms splitting into 110 levels. In d^2sp there are 38 terms splitting into 90 levels. In AEL, 41 terms splitting into 101 levels are assigned to the configuration V II $-d^3p$ and 9 terms splitting into 27 levels are assigned to V II $-d^2sp$. In addition, there are 7 odd experimental levels without definite configuration assignments. Of the 135 experimental levels which may be fitted to d^3p+d^2sp the following 12 levels were neglected:

1. The level 1_4° at 62762.
2. The five levels of $3d^24s\ (b\ ^4\mathrm{F})\ 4py\ ^5\mathrm{G}$.
3. The level $3d^24s\ (b\ ^2\mathrm{G})\ 4p\ x\ ^1\mathrm{H}$.
4. The level $3d^24s\ (b\ ^2\mathrm{G})\ 4p\ w\ ^1\mathrm{G}$.
5. The level $3d^24s\ (b\ ^2\mathrm{G})\ 4p\ w\ ^1\mathrm{F}$.
6. The level $u\ ^3\mathrm{F}_4$ at 76644.
7. The level 2_3° at 76405.
8. The level $w\ ^1\mathrm{D}$ at 78791.

Of the 123 levels fitted it was necessary to make the following changes in assignment:

1. $3d^3\ (a\ ^2\mathrm{P})4px\ ^3\mathrm{D} \leftrightarrow 3d^3(a\ ^4\mathrm{P})4py\ ^3\mathrm{D}$.
2. $3d^3\ (a\ ^2\mathrm{D})4py\ ^1\mathrm{P} \leftrightarrow 3d^3\ (a\ ^2\mathrm{P})4pz\ ^1\mathrm{P}$.
3. AEL $3d^3\ (c\ ^2\mathrm{D})\ 4pt\ ^3\mathrm{D}_{1,2,3}? \rightarrow 3d^2(^1\mathrm{D})4s4p(^3\mathrm{P})^3\mathrm{D}$.
4. AEL $u\ ^3\mathrm{F}_{2,3} \rightarrow 3d^2(^3\mathrm{P})4s4p\ (^3\mathrm{P})\ ^5\mathrm{P}$.

In addition, the following pairs of terms were strongly mixed:

1. $3d^3(a\ ^4\mathrm{F})4pz\ ^5\mathrm{F}_{1,2,3}$ and $3d^3(a\ ^4\mathrm{F})4pz\ ^3\mathrm{D}_{1,2,3}$.
2. $3d^3(a\ ^4\mathrm{P})4pz\ ^3\mathrm{P}_{0,1,2}$ and $3d^3(a\ ^4\mathrm{P})4py\ ^5\mathrm{D}_{0,1,2}$.
3. $3d^3(^2\mathrm{H})4px\ ^3\mathrm{G}_3$ and $3d^3(a\ ^2\mathrm{D})4py\ ^1\mathrm{F}_3$.

The 123 levels were fitted by means of 16 free electrostatic parameters and 3 free spin-orbit parameters to yield a rms error of only 66. The following parameters were obtained in the least squares of the final iteration:

$$\begin{aligned} A &= 51096 \pm 74 \\ A' &= 82727 \pm 119 \\ B = B' &= 792 \pm 2 \\ C = C' &= 2746 \pm 12 \\ G_{ds} &= 1820 \pm 25 \\ F_2 &= 339 \pm 2 \\ F_2' &= 392 \pm 10 \\ G_1 = G_1' &= 360 \pm 2 \\ G_3 = G_3' &= 30 \pm 1 \\ G_{ps} &= 7900\ (\text{fix}) \\ \alpha &= 32 \pm 2 \\ \alpha' &= 77 \pm 10 \\ \beta = \beta' &= -179 \pm 66 \\ T = T' &= -3.8 \pm 0.3 \\ H &= 86 \pm 7 \\ J &= 1011 \pm 72 \\ K &= 3288 \pm 58 \\ \zeta_d &= 171 \pm 10 \\ \zeta_d' &= 197 \pm 15 \\ \zeta_p = \zeta_p' &= 262 \pm 20 \\ \Delta &= 66. \end{aligned}$$

As G_{ps} is much larger than G_{ds} the interaction p–s is stronger than the interaction d–s. Thus, the levels of the configuration d^2sp are coupled as $d^2\ (v_1S_1L_1)\ sp\ (^{1,3}\mathrm{P})\ SL$ and not $d^2s\ (S_2L_1)p\ SL$, as given in AEL.

In the variation of the least squares from which the above parameters were taken the sum of the squares of the deviations dropped only from 483, 520 to 454, 850. Thus, no further iteration was required.

2.3. Discussion

Of the 12 levels neglected, 3 could be fitted with deviations much larger than the rms error of 66, whereas the other 9 levels definitely have no place in the configurations d^3p+d^2sp.

All the five levels of the term $3d^24s(b\ ^4\mathrm{F})4py\ ^5\mathrm{G}$ are given as uncertain in AEL. In addition all the combinations of $y\ ^5\mathrm{G}$ with even levels are given with a question mark in the original paper of Meggers and Moore [7]. In the initial diagonalization the mean difference between the experimental and theoretical levels of $d^2s(^4\mathrm{F})y\ ^5\mathrm{G}$ was over 4000. This value is much higher than for the other levels and so immediately the levels of $y\ ^5\mathrm{G}$ were neglected.

The level 1_4° at 62762 could be fitted to $d^3(^2\mathrm{F})p\ ^3\mathrm{F}_4$ with a deviation of 310. However, as this deviation is

almost five times the rms error and there is no experimental g value, it was decided not to include this level.

The levels $3d^24s(^2G)4p$ [^1H, ^1G, and ^1F] are theoretically at 98370, 96020, and 102680, respectively. Thus, the assignments given in AEL are definitely not correct for these levels. The level $w\,^1H$ at 70936 cannot be assigned to any level of J equal to 5. The closest calculated level to $w\,^1G$ for J equal to 4 is $d^2s(^2F)p\,^1G$ at 73563. Therefore, the level $w\,^1G$ must also be neglected. The level $w\,^1F$ at 74664 could be assigned to $d^2s(^2G)p\,^3F_3$ with a deviation of around-350. For the same reasons as for the level 1^c_4, the level $w\,^1F$ was not included. These three levels could conceivably belong to $3d^35p$.

The two levels $u\,^3F_{2,3}$ at 76220 and 76386 fit with deviations of 47 and -37 to the calculated levels $d^2s(^4P)p\,^5P_{2,3}$. However, the level $u\,^3F_4$ at 76644 could not be assigned to any theoretical level of J equal to 4. The level $w\,^1D$ at 78791 would fit with a deviation of only about 210 to the level $d^3(B^2D)p\,^3P_2$. However, as $w\,^1D$ is given as uncertain in AEL, we were reluctant to insert it and make the subsequent change in assignment. If, on the other hand, the level $w\,^1D$ is assigned to $d^3(B^2D)p\,^1D$, then the deviation is 700, which is definitely too high.

The term $3d^3\ (c^2D)4pt\,^3D$, whose assignment is questioned in AEL, fits very well to the theoretical term $d^2s(^2D)p\,^3D$, both in the values and g-factors of the levels. In one variation the levels $t\,^3D$ were fitted with the same theoretical assignments. However, then the deviations were much larger and in addition, a value of β equal to -700 was obtained, which seems definitely too high when compared with the values of β in the GLS of d^np [3].

The level 3^c_3 at 79040 has a deviation of only -48 when assigned to $d^2s(^3G)p\,^3G_3$.

It is evident from the theoretical compositions that the parents of the terms $z\,^1P$ and $y\,^1P$ should be exchanged, as indicated by the second change.

The final parameters seem very reasonable. It is impossible to have both A' and G_{ps} free since all the terms of d^2sp inserted have nearly the same derivative of -1 with respect to G_{ps}. Nevertheless, it was found that with G_{ps} equal to 7900 instead of the original value of 8837, the results are improved. This is due to the fact that a few of the levels of d^2sp inserted, have corresponding eigenvalues, whose derivatives with respect to G_{ps} are positive. Thus, G_{ps} is not completely undefined, but since if it is left free the deviation in G_{ps} is greater than 1000, it is more meaningful to have this parameter fixed. Variations were performed in which all or a few of the parameters, B', C', G_1', G_3', and ζ_p' were allowed to be free. Although the values of the parameters were reasonable, they were not well defined. This follows from the fact that there are only 9 experimental terms in d^2sp which split into 28 levels and thus it is more reasonable to have

$$B'=B$$
$$C'=C$$
$$G_1'=G_1$$
$$G_3'=G_3$$
$$\zeta_p'=\zeta_p.$$

However, the parameters F_2', α', and ζ_d' should be free as not only do they have well-defined reasonable values, but they also lower the rms error. If α' is forced to equal α, and no other changes are made, the rms error rises from 66 to 74. If, in addition ζ_d' equals ζ_d, the rms error increases to 81. If, furthermore, F_2' equals F_2 the rms error rises to 98.

The parameters β and T are significant. We are not able to compare the effect of β and T in the last iteration because β and T already differed from zero in the diagonalization of that iteration. In the previous iteration, the rms error with β and T fixed at zero was 121, whereas with β and T free, the rms error dropped to 79. The values of β and T for that iteration were

$$\beta=-190\pm71$$
$$T=-3.9\pm0.4.$$

The values of the parameters J and K are also very reasonable and do not differ greatly from the initial values. As expected, H is small but well defined.

The agreement between the experimental and calculated g values is very good except for the case of $(^4P)y\,^5D_4$. The eigenfunction of this level comprises 97 per cent $(^4P)\,^5D$, and the remaining 3 per cent are also ^5D. Thus, the calculated g value exactly equals the theoretical g value of 1.500. The value of 2.28 in AEL seems definitely not correct as 1.5 is the highest theoretical g value for any level of J equal to 4 in the configurations d^3p+d^2sp.

By considering the interaction with the configuration d^2sp, not only is there a great improvement in the fitting of the experimental levels (rms error of 66 versus 269 for V II $-d^3p$), but also the g values fit much better now. As a particular example we can consider the two levels $d^3(^4F)pz\,^5F_1$ and $d^3(^4F)pz\,^3D_1$, whose experimental g factors are 0.35 and 0.24, respectively. In the treatment of V II $-d^3p$ the calculated g factors for these two levels are 0.166 and 0.596, whereas the present calculated values are 0.300 and 0.238, respectively.

3. Ti II $-3d^24p+3d4p4s$

3.1. Initial Parameters

As for V II, the initial parameters B, C, F_2, G_1, G_3, α, ζ_d, and ζ_p were taken from the GLS of the configurations d^np of the second spectra, [3]. From the variation with β and T eliminated and with the same approximation as for V II,

$$B=685$$
$$C=2290$$
$$F_2=F_2'=300$$
$$G_1=G_1'=335$$
$$G_3=G_3'=29$$
$$\alpha=58$$
$$\zeta_d=\zeta_d'=130$$
$$\zeta_p=\zeta_p'=230.$$

The initial values of G_{ds}, H, J, and K for Ti II can be taken from the final results of V II. Then

$$G_{ds} = 1820$$
$$H = 86$$
$$J = 1011$$
$$K = 3288.$$

As for V II the initial value of G_{ps} is obtained by interpolating the values of G_{ps} from Sc II and Ga II. Then,

$$G_{ps} = 8540.$$

The initial values of A and A' were obtained from the electrostatic interaction matrix of ^{4}P, which is of order 2 one term assigned to d^2p and the other to dsp. Performing a calculation similar to that of ^{5}F for V II yields

$$A = 38435$$
$$A' = 64775.$$

From the GLS of d^np [3], the value of A for Ti II $-$ d^2p equals 37607. This value is, as expected, lower than the present value since the configuration $3d^24p$ is lower than $3d4s4p$ and thus each term of $3d^24p$ which feels an interaction with $3d4s4p$ tends to be lowered by this interaction. In the diagonalization of Ti II $-$ $d^2p + dsp$, the matrices of $(d+s)^2p$ were used with all the parameters pertaining to the configuration s^2p having a value equal to zero.

3.2. Discussion and Results

The configuration d^2p comprises 19 theoretical terms splitting into 45 levels. In dsp there are 12 theoretical terms splitting into 23 levels. In AEL, 18 terms splitting into 43 levels are assigned to d^2p and 7 terms splitting into 17 levels are assigned to dsp.

As in V II, the interaction s-p is much stronger than the interaction d-s and so the levels of dsp are coupled as d(^{2}D)sp(^{1,3}P)SL.

The experimental value for the center of gravity of the term $d(^2\mathrm{D})sp\,^3\mathrm{P}x\,^2\mathrm{P}$ in AEL is 53126. Theoretically, this term was calculated initially at 59900. Thus, the experimental levels of the terms $x\,^2$P cannot be fitted to the calculated levels of this term. Now, in the region 52000–54000 there are the theoretical terms $d(^2\mathrm{D})sp(^3\mathrm{P})y\,^4\mathrm{F}$, $d(^2\mathrm{D})sp(^3\mathrm{P})x\,^4\mathrm{D}$ and $d(^2\mathrm{D})sp(^3\mathrm{P})w\,^2\mathrm{D}$. Thus, it is possible to fit only one of the two experimental levels, $x^4\mathrm{D}_{1/2}$ at 52330 and $x\,^2\mathrm{P}_{1/2}$ at 53121. On the other hand, we can attempt to fit the level $x\,^2\mathrm{P}_{3/2}$ at 53128 to the theoretical level $y\,^4\mathrm{F}_{3/2}$, as the term ^{2}D(^{3}P)^{4}F predicted in this region, is not found experimentally. With these assignments the rms error in the least squares of the first diagonalization was 162. We also considered the variation in which the following changes were made:

AEL $3d4s\ (a\,^2\mathrm{D})4px\,^2\mathrm{P}_{1/2,3/2} \rightarrow d(^2\mathrm{D})sp(^3\mathrm{P})x\,^4\mathrm{D}_{1/2,3/2}$

AEL $3d4s\ (a\,^2\mathrm{D})4px\,^4\mathrm{D}_{3/2,5/2,7/2} \rightarrow d(^2\mathrm{D})sp(^3\mathrm{P})y\,^4\mathrm{F}_{3/2,5/2,\,7/2}$

and then the level $x\,^4\mathrm{D}_{1/2}$ at 52330 was neglected. In this variation the rms error was 121. In addition, from a consideration of the combinations of $x\,^2\mathrm{P}_{3/2}$ and $x\,^4\mathrm{D}_{3/2}$, [8], it is more reasonable to fit the level $x\,^4\mathrm{D}_{3/2}$ to $y\,^4\mathrm{F}_{3/2}$ than to fit $x\,^2\mathrm{P}_{3/2}$ to $y\,^4\mathrm{F}_{3/2}$. Thus, the latter variation was considered for parameters of the next iteration and subsequently the above changes were adopted.

Since the experimental term $d^2(^1\mathrm{S})p\,^2\mathrm{P}$ is missing, it is necessary to hold α fixed at the initial value of 58.

Using the initial approximation that the parameters F_2, G_1, G_3, ζ_d, and ζ_p of d^2p and dsp are equal in the least squares, we found that H tended to change its sign from the value given in the diagonalization. This instability in H was overcome by giving the parameter F_2' freedom. It then became apparent that also G_1' and G_3' should be free in order to improve the results. However, the parameters ζ_d' and ζ_p' are not well defined by the experimental data available. Thus, we set

$$\zeta_d' = \zeta_d \qquad \text{and} \qquad \zeta_p' = \zeta_p$$

In the final variation of the least squares, 30 experimental terms splitting into 59 levels were fitted by 15 free electrostatic parameters and 2 free spin-orbit interaction parameters to yield a rms error of only 75. In the least squares of the last iteration the sum of the squares of the deviations dropped only from 237,680 to 236,621. The final values for the parameters were

$$A = 38036 \pm 23$$
$$A' = 63372 \pm 56$$
$$B = 704 \pm 2$$
$$C = 2391 \pm 11$$
$$G_{ds} = 1379 \pm 39$$
$$F_2 = 335 \pm 3$$
$$F_2' = 419 \pm 7$$
$$G_1 = 364 \pm 3$$
$$G_1' = 485 \pm 14$$
$$G_3 = 34 \pm 2$$
$$G_3' = 60 \pm 4$$
$$G_{ps} = 7326 \pm 63$$
$$\alpha = 58 \text{ (Fix)}$$
$$H = 29 \pm 16$$
$$J = 1363 \pm 102$$
$$K = 3240 \pm 56$$
$$\zeta_d = \zeta_d' = 117 \pm 9$$
$$\zeta_p = \zeta_p' = 243 \pm 24$$
$$\Delta = 75.$$

In Ti II the interaction with the configuration dsp is very important. In Ti II $-$ d^2p the rms error was 319, whereas here for $d^2p + dsp$, it is reduced to only 75.

4. Sc II — 3d4p + 4s4p

4.1. Initial Parameters

The initial values of the parameters F_2, G_1, G_3, ζ_d, and ζ_p were taken from the GLS of the configurations d^np of the second spectra with β and T eliminated [3]. For G_{ps} the approximate value of 8243 needed for inter-

polating the initial value of G_{ps} for V II, was used here. The initial values of J and K were taken from the final values of Ti II $-3d^24p+4s4p$. Thus for Sc II initially,

$$\begin{aligned} F_2 &= 290 \\ G_1 &= 340 \\ G_3 &= 27 \\ G_{ps} &= 8243 \\ J &= 1363 \\ K &= 3240 \\ \zeta_d &= 68 \\ \zeta_p = \zeta_p' &= 200. \end{aligned}$$

The initial values of A and A' were obtained by using the electrostatic matrices of ^{3}P and ^{1}P and averaging. Then,

$$\begin{aligned} A &= 29595 \\ A' &= 46148. \end{aligned}$$

4.2. Discussion and Results

The configuration dp comprises 6 terms splitting into 12 levels and the configuration sp has 2 theoretical terms splitting into 4 levels. All 16 experimental levels are given for Sc II in AEL.

The 8 terms splitting into 16 levels were determined in the least squares calculations by 8 electrostatic parameters and 3 spin-orbit interaction parameters. The rms error obtained was only 4.6. There were no changes in assignment and the 10 experimental g factors fitted very well to the calculated values. The following values for the parameters were obtained in the final least-squares:

$$\begin{aligned} A &= 29357 \pm 2 \\ A' &= 46130 \pm 7 \\ F_2 &= 325 \pm 0.4 \\ G_1 &= 386 \pm 0.4 \\ G_3 &= 25 \pm 0.4 \\ G_{ps} &= 7835 \pm 9 \\ J &= 1254 \pm 10 \\ K &= 3248 \pm 6 \\ \zeta_d &= 81 \pm 2 \\ \zeta_p &= 181 \pm 5 \\ \zeta_p' &= 251 \pm 5 \\ \Delta &= 4.6. \end{aligned}$$

Although there are 8 electrostatic parameters to determine the 8 terms, we note that the above parameters are very reasonable when compared with those of V II and Ti II. We thus conclude that there is a strong interaction between the configurations dp and sp, but neither dp nor sp feels any strong interaction(s) from other configuration(s). Otherwise, this interaction(s) would be noticed from the values of the above parameters.

5. Tables of the Observed and Calculated Levels and g-Factors

In the column "NAME" the calculated designation of the term is given. Whenever the terms of the parent d^n have different seniorities these are denoted by the letters A and B, the lower calculated term being designated by A. Whenever a calculated term has a corresponding experimental term, the small letters z, y, x, . . . are used as in AEL. The terms of $d^{n-1}sp$ are denoted by $d^{n-1}v_1S_1L_1$ $(sp\,^{1,3}\mathrm{P})SL$.

The entries in the columns "J", "OBS. LEVEL cm^{-1}" "CALC. LEVEL cm^{-1}" are self-evident. In the column "PERCENTAGE", for each calculated level either the three highest contributions or all those contributions exceeding 5 percent are given.

Whenever the experimental and calculated term designations differ, the experimental designation is entered in the column "AEL" using the notation of C. E. Moore [4]. In many instances the exchanges involve complete terms rather than isolated levels. Unless specified otherwise the entries in the column "AEL" pertain to exchanges in terms.

The column "O−C" gives the difference between the observed and calculated values of the levels.

The columns "OBS. g-FACTOR" and "CALC. g-FACTOR" give the observed and calculated values of the Lande g-factors respectively.

The entries are in ascending order of magnitude of the calculated terms.

TABLE 1. *Observed and calculated levels of* Sc II, 3d4p + 4s4p

NAME	J	PERCENTAGE	AEL	OBS. LEVEL (cm^{-1})	CALC. LEVEL (cm^{-1})	O−C	OBS. g-FACTOR	CALC. g-FACTOR
$(^2D)z\ ^1D$	2	$99 + 1(^2D)^3F$		26081.32	26081.18	0.14	1.00	0.998
$(^2D)z\ ^3F$	2	$99 + 1(^2D)^1D$		27443.65	27446.31	−2.66	0.65	0.672
	3	$99 + 1(^2D)^3D$		27602.32	27604.11	−1.79	1.10	1.085
	4	100		27841.17	27836.83	4.34	1.25	1.250
$(^2D)z\ ^3D$	1	100		27917.69	27912.04	5.65	0.51	0.502
	2	99		28021.21	28020.89	0.32	1.16	1.165
	3	99		28161.03	28167.08	−6.05	1.33	1.331
$(^2D)z\ ^3P$	0	$90 + 10(^2S)^3P$		29736.22	29736.98	−0.76		
	1	$88 + 10(^2S)^3P$		29742.12	29743.62	−1.50		1.489
	2	$90 + 10(^2S)^3P$		29823.92	29821.63	2.29	1.50	1.499
$(^2D)z\ ^1P$	1	$91 + 7(^2D)^1P$		30815.65	30815.64	0.01	1.00	1.008
$(^2D)z\ ^1F$	3	100		32349.98	32349.98	0.00	1.00	1.000
$(^2S)y\ ^3P$	0	$90 + 10(^2D)^3P$		39001.59	39001.63	−0.04		
	1	$90 + 10(^2D)^3P$		39114.44	39114.06	0.38		1.500
	2	$90 + 10(^2D)^3P$		39344.90	39345.23	−0.33		1.500
$(^2S)y\ ^1P$	1	$93 + 7(^2D)^1P$		55715.52	55715.52	0.00		1.000

TABLE 2. *Observed and calculated levels of* Ti II − $3d^24p + 3d4s4p$

NAME	J	PERCENTAGE	AEL	OBS. LEVEL (cm^{-1})	CALC. LEVEL (cm^{-1})	O−C	OBS. g-FACTOR	CALC. g-FACTOR
$(^3F)z\ ^4G$	5/2	98		29544	29592	−48	0.57:	0.577
	7/2	99		29734	29780	−46	0.98:	0.986
	9/2	100		29968	30013	−45		1.172
	11/2	100		30241	30287	−46		1.273
$(^3F)z\ ^4F$	3/2	96		30837	30760	77	0.40:	0.412
	5/2	98		30959	30886	73	1.03:	1.031
	7/2	98		31114	31045	69	1.24:	1.238
	9/2	99		31301	31234	67		1.333
$(^3F)z\ ^2F$	5/2	$85 + 7(^1D)^2F$		31207	31237	−30	0.86:	0.867
	7/2	$89 + 7(^1D)^2F$		31491	31499	−8	1.14:	1.147
$(^3F)z\ ^2D$	3/2	$83 + 9(^3P)^2D$		31756	31742	14	0.92	0.797
	5/2	$78 + 8(^3P)^2D + 5(^3F)^4D$		32026	32019	7	1.20	1.191
$(^3F)z\ ^4D$	1/2	96		32532	32577	−45	0.00	0.000
	3/2	94		32603	32643	−40	1.20	1.188
	5/2	91		32698	32733	−35	1.37	1.362
	7/2	95		32767	32793	−26	1.43:	1.426
$(^3F)z\ ^2G$	7/2	95		34543	34517	26	0.89:	0.889
	9/2	95		34748	34705	43	1.11:	1.113
$(^3P)z\ ^2S$	1/2	99		37431	37448	−17	2.09	1.997
$(^1D)z\ ^2P$	1/2	97		39675	39563	112	0.67:	0.672
	3/2	$73 + 19(^1D)^2D$		39603	39424	179	1.21	1.220
$(^1D)y\ ^2D$	3/2	$61 + 21(^1D)^2P + 8(^3P)^2D$		39233	39498	−265	0.80:	0.932
	5/2	$42 + 40(^1D)^2F + 6(^3P)^2D$		39477	39603	−126	1.20:	1.048
$(^1D)y\ ^2F$	5/2	$49 + 37(^1D)^2D + 4(^3P)^2D$		39927	39907	−20	0.86:	1.016
	7/2	$87 + 8(^3F)^2F$		40075	39988	87	1.14:	1.152

331-607 O - 69 - 4

TABLE 2. *Observed and calculated levels of* Ti II – $3d^24p + 3d4s4p$ – *Continued*

NAME	J	PERCENTAGE	AEL	OBS. LEVEL (cm^{-1})	CALC. LEVEL (cm^{-1})	O–C	OBS. g-FACTOR	CALC. g-FACTOR
$(^3P)z\ ^4S$	3/2	96		40027	40109	−82		1.972
$(^3P)y\ ^4D$	1/2	97		40330	40287	43		0.002
	3/2	96		40426	40387	39		1.197
	5/2	95		40582	40547	35		1.368
	7/2	93		40798	40767	31		1.418
$(^3P)z\ ^4P$	1/2	96		41997	41988	9		2.664
	3/2	96		42069	42070	−1		1.731
	5/2	96		42209	42255	−16		1.598
$(^1G)y\ ^2G$	7/2	95		43741	43746	−5	0.89:	0.891
	9/2	95		43781	43787	−6	1.11:	1.110
$(^3P)x\ ^2D$	3/2	$74 + 12(^1D)^2D + 5(^3P)^2P$		44915	44990	−75	0.80:	0.828
	5/2	$79 + 12(^1D)^2D$		44902	44976	−74	1.20:	1.200
$(^3P)y\ ^2P$	1/2	94		45473	45419	54	0.66:	0.667
	3/2	89		45549	45499	50	1.33:	1.304
$(^1G)z\ ^2H$	9/2	99		45674	45667	7		0.910
	11/2	100		45909	45922	−13		1.092
$(^1G)x\ ^2F$	5/2	$90 + 7^2D(^3P)^2F$		47625	47631	−6	0.86:	0.856
	7/2	$90 + 7^2D(^3P)^2F$		47467	47453	14	1.14:	1.142
$^2D(^3P)^4F$	3/2	98	$ds(a\ ^3D)px\ ^4D$	52459	52342	117		0.407
	5/2	98		52471	52478	−7		1.031
	7/2	99		52631	52672	−41		1.239
	9/2	99			52916			1.333
$^2D(^3P)^4D$	1/2	97	$ds(a\ ^3D)px\ ^2P$	53121	53088	33		0.001
	3/2	95		53128	53150	−22		1.188
	5/2	91			53257			1.361
	7/2	96			53436			1.427
$^2D(^3P)w\ ^2D$	3/2	92	$ds(a\ ^3D)pw\ ^2D$	53597	53628	−31		0.802
	5/2	89		53555	53601	−46		1.211
$^2D(^3P)y\ ^4P$	1/2	97	$ds(a\ ^3D)py\ ^4P$	56223	56241	−18		2.666
	3/2	96		56249	56267	−18		1.733
	5/2	96		56326	56329	−3		1.599
$^2D(^3P)w\ ^2F$	5/2	96	$ds(a\ ^3D)pw\ ^2F$	59322	59300	22		0.856
	7/2	96		59468	59453	15		1.144
$^2D(^3P)^2P$	1/2	$80 + 20(^1S)^2P$			60059			0.667
	3/2	$84 + 16(^1S)^2P$			59969			1.333
$(^1S)^2P$	1/2	$74 + 20^2D(^3P)^2P$			64325			0.667
	3/2	$78 + 16^2D(^3P)^2P$			64500			1.333
$^2D(^1P)w\ ^2D$	3/2	95	$ds(b\ ^1D)pv\ ^2D$	69327	69322	5		0.801
	5/2	94		69622	69573	49		1.197
$^2D(^1P)y\ ^2F$	5/2	94	$ds(b\ ^1D)pv\ ^2F$	70606	70680	−74		0.859
	7/2	95		70893	70875	18		1.143
$^2D(^1P)^2P$	1/2	92			73597			0.667
	3/2	92			73879			1.333

TABLE 3. *Observed and calculated levels of* V II $3d^34p + 3d^24s4p$

NAME	J	PERCENTAGE	AEL	OBS. LEVEL (cm^{-1})	CALC. LEVEL (cm^{-1})	O−C	OBS. g-FACTOR	CALC. g-FACTOR
$(^4F)z\,^5G$	2	100		34593	34590	3	0.31	0.334
	3	100		34746	34740	6	0.93	0.917
	4	100		34947	34939	8	1.14	1.150
	5	100		35193	35184	9	1.16	1.267
	6	100		35483	35473	10		1.333
$(^4F)z\,^3D$	1	$51 + 42(^4F)^5F$	$d^3(a\,^4F)pz\,^5F$	36489	36470	19	0.35	0.300
	2	$44 + 44(^4F)^5F$	$d^3(a\,^4F)pz\,^3D$	37041	37020	21	1.08	1.117
	3	$55 + 21(^4F)^5D + 17(^4F)^5F$		37205	37207	−2	1.32	1.354
$(^4F)z\,^5F$	1	$56 + 37(^4F)^3D$	$d^3(a\,^4F)pz\,^3D$	36955	36925	30	0.24	0.238
	2	$54 + 38(^4F)^3D$	$d^3(a\,^4F)pz\,^5F$	36674	36654	20	1.08	1.086
	3	$81 + 13(^4F)^3D$		36919	36897	22	1.24	1.269
	4	98		37151	37126	25		1.350
	5	98		37352	37338	14	1.40:	1.398
$(^4F)z\,^5D$	0	97		37201	37254	−53		
	1	94		37259	37311	−52	1.39	1.464
	2	$87 + 10(^4F)^3D$		37369	37421	−52	1.39	1.462
	3	$73 + 23(^4F)^3D$		37521	37572	−51	1.47	1.458
	4	97		37531	37603	−72	1.44	1.498
$(^4F)z\,^3G$	3	$91 + 7(^2G)^3G$		39234	39268	−34	0.84	0.752
	4	$91 + 7(^2G)^3G$		39404	39437	−33	1.03	1.052
	5	$91 + 7(^2G)^3G$		39613	39652	−39	1.19	1.202
$(^4F)z\,^3F$	2	94		40002	40007	−5	0.65	0.667
	3	94		40196	40203	−7	1.02	1.083
	4	94		40430	40444	−14	1.22	1.250
$(^4P)z\,^5P$	1	94		46755	46669	86	2.28	2.446
	2	$62 + 20(^4P)^5D + 14(^4P)^3P$		46880	46809	71	1.65	1.705
	3	98		47052	46957	95	1.58	1.663
$(^4P)z\,^3P$	0	$39 + 48(^4P)^5D$	$d^3(a\,^4P)py\,^5D$	47028	47047	−19		
	1	$48 + 41(^4P)^5D$		47108	47113	−5	1.43	1.511
	2	$44 + 34(^4P)^5P + 13(^4P)^5D$	$d^3(a\,^4P)pz\,^3P$	46740	46754	−14	1.48	1.614
$(^4P)z\,^5D$	0	$48 + 40(^4P)^3P$	$d^3(a\,^4P)pz\,^3P$	46586	46627	−41		
	1	$55 + 33(^4P)^3P$		46690	46717	−27	1.44	1.537
	2	$63 + 26(^4P)^3P$	$d^3(a\,^4P)py\,^5D$	47102	47092	10	1.47	1.511
	3	95		47181	47152	29	1.48:	1.502
	4	97		47420	47380	40	(2.28)	1.500
$(^2G)z\,^3H$	4	$88 + 12(^2H)^3H$		47056	47047	9	0.78	0.801
	5	$87 + 12(^2H)^3H$		47297	47281	16	1.01	1.034
	6	$87 + 12(^2H)^3H$		47608	47578	30	1.13	1.166
$(^2P)z\,^1S$	0	$90 + 7(^4P)^3P$		48258	48473	−215		
$(^2G)y\,^3G$	3	$80 + 7(^4F)^3G + 7(^2G)^1F$		48580	48654	−74	0.67	0.784
	4	$87 + 7(^4F)^3G$		48731	48815	−84	1.02	1.054
	5	$84 + 7(^4F)^3G$		48853	48940	−87	1.22	1.187
$(^2G)y\,^3F$	2	$78 + 15(A^2D)^3F$		49202	49254	−52	0.63	0.680
	3	$46 + 29(^2G)^1F + 10(^2G)^3G$		49211	49215	−4	0.99	1.017
	4	$60 + 28(^2G)^1G$		49269	49265	4	1.18	1.174
$(^2G)z\,^1F$	3	$49 + 34(^2G)^3G + 7(A^2D)^1F$		49568	49518	50	0.97	1.033
$(^2G)z\,^1H$	5	$72 + 21(^2H)^1H$		49593	49545	48	0.95	1.011
$(^2G)z\,^1G$	4	$69 + 23(^2G)^3F$		49724	49678	46	0.96	1.068
$(^4P)z\,^5S$	2	96		49731	49738	−7		1.992
$(^2P)z\,^1D$	2	$50 + 36(A^2D)^1D$		49898	49920	−22	0.93	0.999

TABLE 3. *Observed and calculated levels of* V II $3d^34p + 3d^24s4p$—*Continued*

NAME	J	PERCENTAGE	AEL	OBS. LEVEL (cm^{-1})	CALC. LEVEL (cm^{-1})	O–C	OBS. g-FACTOR	CALC. g-FACTOR
$(^2P)y\ ^3P$	0	$63 + 36(A^2D)^3P$		50662	50545	117		
	1	$50 + 29(A^2D)^3P + 10(^2P)^3D$		50739	50647	92	1.39	1.328
	2	$58 + 38(A^2D)^3P$		51123	51030	93	1.51	1.493
$(^2P)y\ ^3D$	1	$52 + 21(^4P)^3D + 9(^2P)^3P$	$d^3(a\ ^4P)py\ ^3D$	50474	50539	−65	0.49	0.675
	2	$58 + 27(^4P)^3D$		50775	50843	−68	1.11	1.157
	3	$55 + 32(^4P)^3D$		51086	51155	−69	1.27	1.327
$(^2P)z\ ^3S$	1	$82 + 11(^4P)^3S$		52181	52099	82	1.85	1.974
$(^2H)y\ ^3H$	4	$86 + 12(^2G)^3H$		52083	52046	37	0.70	0.804
	5	$87 + 12(^2G)^3H$		52154	52123	31	0.98	1.034
	6	$87 + 12(^2G)^3H$		52253	52229	24	1.04:	1.166
$(A^2D)x\ ^3F$	2	$74 + 12(^2G)^3F$		52246	52299	−53	0.68	0.710
	3	$58 + 22(^4P)^3D + 9(^2G)^3F$		52392	52436	−44	1.07	1.157
	4	$85 + 10(^2G)^3F$		52658	52718	−60	1.18:	1.250
$(^4P)x\ ^3D$	1	$52 + 16(^2P)^3D + 13(A^2D)^3D$	$d^3(a\ ^2P)px\ ^3D$	52604	52562	42	0.63	0.577
	2	$51 + 25(^2P)^3D + 13(A^2D)^3D$		52700	52624	76	1.10	1.137
	3	$34 + 29(^2P)^3D + 23(A^2D)^3F$		52767	52680	87	1.26	1.266
$(A^2D)z\ ^1P$	1	$73 + 11(^2P)^1P$	$d^3(a\ ^2P)pz\ ^1P$	52804	52833	−29	0.92	0.951
$(^2H)z\ ^3I$	5	99		52878	52848	30	0.84:	0.835
	6	100		53077	53047	30	0.98	1.024
	7	100		53320	53290	30	1.11:	1.143
$(A^2D)w\ ^3D$	1	$76 + 12(^2P)^3D$		53751	53722	29	0.49:	0.522
	2	$80 + 11(^2P)^3D$		53869	53852	17	1.10	1.169
	3	$84 + 7(^2P)^3D$		53927	53914	13	1.37	1.325
$(^2H)y\ ^1G$	4	$82 + 11(^2F)^1G$		54144	54131	13	1.00	1.001
$(A^2D)x\ ^3P$	0	$52 + 30(^2P)^3P + 14(^4P)^3P$		54813	54817	−4		
	1	$48 + 28(^2P)^3P + 13(^4P)^3P$		54718	54723	−5		1.499
	2	$48 + 32(^2P)^3P + 15(^4P)^3P$		54716	54696	20		1.496
$(A^2D)y\ ^1F$	3	$53 + 34(^2H)^3G$		55142	55156	−14	0.94	0.912
$(^2H)x\ ^3G$	3	$57 + 33(A^2D)^1F$		55350	55344	6	0.82	0.848
	4	$88 + 6^3F(^3P)^3G$		55304	55255	49	1.02	1.049
	5	$79 + 10(^2H)^1H$		55207	55160	47	1.15	1.174
$(^2H)z\ ^1I$	6	100		55403	55428	−25	1.01:	1.001
$(^2H)y\ ^1H$	5	$66 + 20(^2G)^1H + 12(^2H)^3G$		55499	55546	−47	1.03:	1.026
$(^4P)y\ ^3S$	1	$55 + 22(^2P)^1P + 10(^2P)^3S$		55663	55809	−146	1.92	1.708
$(^2P)y\ ^1P$	1	$60 + 25(^4P)^3S + 8(A^2D)^1P$	$d^3(a\ ^2D)y\ ^1P$	56171	55996	175	1.05:	1.273
$(A^2D)y\ ^1D$	2	$54 + 40(^2P)^1D$		57343	57292	51	0.98	1.002
$^3F(^3P)^5G$	2	96			62055			0.347
	3	$90 + 8(^2F)^3F$			62211			0.933
	4	$88 + 10(^2F)^3F$			62452			1.161
	5	100			62722			1.267
	6	100			63043			1.333
$(^2F)w\ ^3F$	2	$85 + 7^3F(^1P)^3F$		62085	62255	−170	0.58:	0.656
	3	$80 + 9^3F(^3P)^5G$		62133	62286	−153	1.00	1.067
	4	$78 + 11^3F(^3P)^5G$		62176	62299	−123	1.36:	1.237

TABLE 3. *Observed and calculated levels of* V II $3d^34p + 3d^24s4p$ – Continued

NAME	J	PERCENTAGE	AEL	OBS. LEVEL (cm^{-1})	CALC. LEVEL (cm^{-1})	O–C	OBS. g-FACTOR	CALC. g-FACTOR
$^3F(^3P)y\,^5F$	1	98	$d^2s(b\,^4F)$					
			$py\,^5F$	63548:	63472	76		0.001
	2	98		63657	63576	81		1.000
	3	98		63817	63731	86		1.249
	4	98		64027	63934	93		1.348
	5	$91 + 7(^2F)^3G$		64287	64181	106		1.385
$(^2F)w\,^3G$	3	95		64057	64037	20	0.72:	0.753
	4	94		64131	64116	15	1.02	1.052
	5	$89 + 7\,^3F(^3P)^5F$		64229	64228	1		1.215
$(^2F)x\,^1D$	2	$67 + 16(^2F)^3D + 9(B^2D)^1D$		64586	64777	−191	1.03:	1.028
$(^2F)w\,^3D$	1	$88 + 6\,^3P(^3P)^3D$		64931	64921	10	0.46:	0.500
	2	$72 + 15(^2F)^1D + 6\,^3P(^3P)^3D$		64804	64822	−18	1.02:	1.137
	3	$88 + 6\,^3P(^3P)^3D$		64604	64629	−25	1.22:	1.331
$(^2F)x\,^1G$	4	$87 + 10(^2H)^1G$		65790	65855	−65	0.94	1.001
$^3F(^3P)x\,^5D$	0	94	$d^2s(b\,^4F)$					
			$px\,^5D$	65783	65817	−34		
	1	94		65816	65857	−41		1.497
	2	93		65885	65940	−55		1.497
	3	93		65997	66071	−74		1.495
	4	94		66159	66260	−101		1.499
$(^2F)x\,^1F$	3	$74 + 22\,^3F(^3P)^1F$		66304	66122	182	0.95	1.004
$^3F(^3P)w\,^3F$	2	$77 + 11\,^1D(^3P)^3F$	$d^2s(b\,^4F)$					
			$pv\,^3F$	67738	67779	−41		0.669
	3	$77 + 11\,^1D(^3P)^3F$		67905	67938	−33		1.084
	4	$78 + 11\,^1D(^3P)^3F$		68147	68169	−22		1.250
$^3F(^3P)u\,^3D$	1	$81 + 4\,^1D(^3P)^3D$	$d^2s(b\,^4F)$					
			$pu\,^3D$	68759	68764	−5		0.502
	2	$80 + 4\,^1D(^3P)^3D$		68798	68831	−33		1.166
	3	$80 + 4\,^1D(^3P)^3D$		68945	68994	−49		1.331
$^3F(^3P)w\,^3G$	3	92	$d^2s(b\,^4F)$					
			$pv\,^3G$	69644	69649	−5		0.753
	4	92		69912	69869	43		1.051
	5	93		70228	70149	79		1.200
$^3F(^3P)^1F$	3	$73 + 19(^2F)^1F$			71348			1.000
$^3F(^3P)^1D$	2	$82 + 9\,^3P(^3P)^1D$			71376			1.001
$^3F(^3P)^1G$	4	93			73563			1.005
$^3P(^3P)^5S$	2	95			73059			1.993
$^3P(^3P)^5D$	0	96			73664			
	1	96			73721			1.499
	2	95			73830			1.495
	3	94			73986			1.490
	4	90			74181			1.483
$^3P(^3P)^3S$	1	92			74039			1.986
$^1D(^3P)^3F$	2	$80 + 12\,^3F(^1P)^3F$			74792			0.674
	3	$79 + 12\,^3F(^1P)^3F$			74912			1.095
	4	$76 + 10\,^3F(^1P)^3F$			75121			1.263
$^1D(^3P)^3P$	0	$89 + 6\,^3P(^3P)^1S$			75249			
	1	$77 + 9\,^1D(^3P)^3D$			75252			1.433
	2	$84 + 6\,^1D(^3P)^3D$			75104			1.490

TABLE 3. *Observed and calculated levels of* V II $3d^34p + 3d^24s4p$—*Continued*

NAME	J	PERCENTAGE	AEL	OBS. LEVEL (cm^{-1})	CALC. LEVEL (cm^{-1})	O–C	OBS. g-FACTOR	CALC. g-FACTOR
$^1D(^3P)\,^3D$	1	$58 + 12(B^2D)^3D + 11\,^1D(^3P)^3D$	$d^3(c\,^2D)$ pt ^3D	75715:	75695	20	0.50:	0.624
	2	$56 + 13(B^2D)^3D + 8\,^1D(^3P)^3D$		75758	75796	−38	1.14:	1.224
	3	$54 + 19\,^3P(^3P)^3P + 10(B^2D)^3D$		75848	75840	8	1.27:	1.396
$^3P(^3P)\,^1S$	0	92			75927			
$^3P(^3P)^3P$	1	94			76052			2.456
	2	92	$u\,^3F$	76220	76173	47		1.787
	3	$80 + 10\,^1D(^3P)^3D$	$u\,^3F$	76386	76422	−36		1.599
$(B^2D)^3D$	1	$73 + 18\,^1D(^3P)^3D$			77278			0.510
	2	$70 + 19\,^1D(^3P)^3D$			77277			1.172
	3	$69 + 22\,^1D(^3P)^3D$			77322			1.334
$(B^2D)^1D$	2	$74 + 14\,^3P(^3P)\,^1D$			78093			0.982
$(B^2D)^3F$	2	$66 + 12(B^2D)^3P + 6\,^1G(^3P)^3F$			78566			0.834
	3	$85 + 8\,^1G(^3P)^3F$			78594			1.084
	4	$86 + 8\,^1G(^3P)^3F$			78689			1.250
$(B^2D)^3P$	0	$66 + 33\,^3P(^3P\,^3P$			78753			
	1	$66 + 23\,^3P(^3P)^3P$			78694			1.492
	2	$55 + 24\,^3P(^3P)^3P + 15(B^2D)^3F$			78578			1.347
$^1G(^3P)^3G$	3	$77 + 21\,^3F(^1P)^3G$	3°	79040	79089	−49		0.750
	4	$79 + 19\,^3F(^1P)^3G$			79166			1.050
	5	$81 + 17\,^3F(^1P)^3G$			79259			1.200
$(B^2D)^1F$	3	93			80596			1.001
$^3P(^3P)^3D$	1	$64 + 14\,^3F(^1P)^3D + 8\,^1D(^3P)^3D$			81585			0.513
	2	$66 + 14\,^3F(^1P)^3D + 7\,^1D(^3P)^3D$			81658			1.166
	3	$67 + 15\,^3F(^1P)^3D + 7\,^1D(^3P)^3D$			81737			1.333
$^1G(^3P)^3H$	4	99			82179			0.800
	5	99			82309			1.034
	6	100			82465			1.167
$(B^2D)^1P$	1	$55 + 42\,^3P(^3P)\,^1P$			82512			0.988
$^3F(^1P)^3F$	2	91			82636			0.669
	3	$48 + 38\,^3F(^1P)^3G + 9\,^1G(^3P)^3G$			82865			0.924
	4	$72 + 17\,^3F(^1P)^3G$			83305			1.209
$^3F(^1P)^3G$	3	$42 + 43\,^3F(^1P)^3F + 8\,^1G(^3P)^3G$			83004			0.910
	4	$64 + 19\,^3F(^1P)^3F + 12\,^1G(^3P)^3G$			83152			1.091
	5	$83 + 13\,^1G(^3P)^3G$			83495			1.200
$^3P(^3P)^3P$	0	$70 + 28(B^2D)^3P$			83859			
	1	$71 + 27(B^2D)^3P$			83909			1.499
	2	$71 + 25(B^2D)^3P$			84010			1.487
$^3P(^3P)\,^1D$	2	$64 + 10\,^3F(^3P)\,^1D + 10(B^2D)\,^1D$			84561			1.017
$^3F(^1P)^3D$	1	$80 + 13\,^3P(^3P)^3D$			84591			0.502
	2	$79 + 12\,^3P(^3P)^3D$			84854			1.160
	3	$82 + 13\,^3P(^3P)^3D$			85203			1.333
$^1G(^3P)^3F$	2	$86 + 9(B^2D)^3F$			86594			0.668
	3	$86 + 10(B^2D)^3F$			86516			1.083
	4	$85 + 10(B^2D)^3F$			86414			1.250
$^3P(^3P)\,^1P$	1	$55 + 41(B^2D)\,^1P$			88072			1.000
$^1D(^1P)\,^1F$	3	93			91023			1.002
$^1D(^1P)\,^1P$	1	$67 + 27\,^3P(^1P)^3S$			91172			1.282
$^3P(^1P)^3S$	1	$69 + 26\,^1D(^1P)\,^1P$			91547			1.717

TABLE 3. *Observed and calculated levels of* V II $3d^34p + 3d^24s4p$—*Continued*

NAME	J	PERCENTAGE	AEL	OBS. LEVEL (cm^{-1})	CALC. LEVEL (cm^{-1})	O–C	OBS. g-FACTOR	CALC. g-FACTOR
$^1D(^1P)^1D$	2	$83 + 6^3P(^1P)^3D$			93563			1.014
$^3P(^1P)^3D$	1	$89 + 7^3F(^1P)^3D$			93810			0.501
	2	$83 + 6^1D(^1P)^1D$			93961			1.157
	3	$89 + 6^3F(^1P)^3D$			94104			1.331
$^3P(^1P)^3P$	0	92			94873			
	1	92			95927			1.499
	2	91			96041			1.496
$^1G(^1P)^1G$	4	96			96025			1.000
$^1G(^1P)^1H$	5	99			98373			1.000
$^1S(^3P)^3P$	0	93			102293			
	1	93			102392			1.500
	2	94			102594			1.500
$^1G(^1P)^1F$	3	94			102676			1.000
$^1S(^1P)^1P$	1	96			118520			1.000

This paper is supported in part by the National Bureau of Standards, Washington, D.C.

The author wishes to acknowledge with everlasting gratitude and appreciation the unremitting kind interest in this work by the late Professor Giulio Racah.

6. References

[1] Racah, G., and Shadmi, Y., Bull. Res. Council of Israel **8F**, No. 1, 15 (1959).

[2] C. Roth, J. Res. Nat. Bur. Stand. (U.S.), **72A** (Phys. and Chem.), No. 5, 505 (1968).

[3] C. Roth, J. Res. Nat. Bur. Stand. (U.S.), **73A** (Phys. and Chem.), No. 3, (1969).

[4] Moore, C. E., Atomic Energy Levels, NBS Circular 467, **I** (1949), referred to as AEL.

[5] Shadmi, Y., Bull. Res. Council of Israel **10F**, No. 3, 109 (1962).

[6] Goldschmidt, Z. B., Ph.D. Thesis, The Hebrew University of Jerusalem (1966).

[7] Meggers, W. F., and Moore, C. E., J. Res., Nat. Bur. Std., **25**, 83 RP1317 (1940).

[8] Russell, H. N., Astroph. J. **66**, 283 (1927); Mt. Wilson Contr. No. 344 (1927).

(Paper 73A2–541)

JOURNAL OF RESEARCH of the National Bureau of Standards—A. Physics and Chemistry
Vol. 73A, No. 2, March–April 1969

Effective Interactions in the Even Configurations of the Third Spectra of the Iron Group*

Y. Shadmi,** E. Caspi,*** and J. Oreg***

(November 19 1968)

Four hundred eighty-three levels belonging to the configurations $3d^n + 3d^{n-1}4s$ of all third spectra of the iron group were calculated, and 334 observed levels were fitted to them. In addition to the usually used approximation, we first introduced a complete set of two-body and three-body effective-interaction parameters between $3d$ electrons. Using only two-body effective interactions, we obtained a rms error of 175 cm^{-1}; while the addition of three-body effective interactions reduced the rms error to 46 cm^{-1}. When a parameter representing three-body effective interaction between $3d$ and $4s$ electrons was also introduced, the rms error was reduced to 38 cm^{-1}

Key words: Atomic theory; iron group; third spectra.

1. Introduction

In the present paper, we describe a systematic treatment of the even configurations in all third spectra of the iron group. Section 2 of the present paper is completely analogous to the treatment already performed for the second spectra [1].[1] In that treatment, a considerable improvement in our theoretical approximation was achieved by including a set of parameters which completely represent all possible effective-interactions between $3d$ electrons.

The first author of the present paper published a series of papers in which he reported on systematic theoretical investigations of various sequences of spectra of transition elements [2–5]. In all these papers, practically the same approximation was used: The Slater approximation was improved by including the interaction between the three configurations $3d^n$, $3d^{n-1}4s$, $3d^{n-2}4s^2$; the $\alpha L(L+1)$ correction; and the spin-orbit interaction.

The result of a long theoretical development to which many physicists (e.g., Bacher and Goudsmit [6], Trees [7–9], Racah [10–11], Rajnak and Wybourne [12], Stein [13], Judd [14], and Feneuille [15]) made their contributions, was that in order to completely describe the second-order perturbations of a d^n configuration by configurations lying far from it, one needs to improve the Slater approximation by adding two parameters of two-body effective-interactions (namely α and β), and two parameters of three-body interactions, T and Tx.

A more detailed description of the above mentioned development, and a detailed definition of the new above mentioned parameters, as well as of the old ones, are given in reference [1]. For that reason, in this paper, we shall only repeat briefly that the two two-body effective-interaction parameters α anb β are defined as follows: α is the parameter multiplying the $L(L+1)$ correction; β is the coefficient of the Q-correction (where Q is the seniority operator [16]). For the two three-body effective-interaction parameters, we shall only mention that T is the parameter which fully represents the perturbation of $3s^23d^n$ by $3s3d^{n+1}$, while Tx is an additional independent three-body-interaction parameter which is necessary in order to make the set of parameters complete. Its formal definition is also given in reference [1]. Px is the parameter representing the three-body effective interaction between $3d$ and $4s$ electrons. Its full definition is given in section 3. We would also like to emphasize that we measured the accuracy of the fit between the theoretical and experimental levels by the *rms error*[2] Δ which is defined by the equation:

$$\Delta = \left[\left(\sum_i \delta_i^2 \right) \Big/ (n-m) \right]^{1/2} \qquad (1)$$

where δ_i is a single deviation; n is the number of observed data; and m is the number of free parameters

*An invited paper. This paper was supported in part by the National Bureau of Standards, Washington, D.C. 20234.

**Present address: Goddard Space Flight Center, National Aeronautics and Space Administration, Greenbelt, Maryland 20770. (On sabbatical leave from The Hebrew University of Jerusalem, Israel.)

***The Hebrew University of Jerusalem, Israel.

[1] Figures in brackets refer to the literature references at the end of this paper.

[2] In all the references cited here, the expressions "mean error" and "mean deviation" were used for the presently defined "rms error" and "rms deviation," respectively.

used in the calculation. Contrary to the *rms deviation*[2] $\bar{\delta}$ which is defined by the equation

$$\bar{\delta}=\left[\left(\sum_i \delta_i^2\right)\Big/ n\right]^{1/2}, \qquad (2)$$

the rms error takes into account the effect of the addition of more free parameters. Thus, if the addition of a new parameter causes an essential decrease of the rms error, it means that this parameter really has physical significance. For a more detailed description of the above mentioned notations, definitions and considerations, the reader is referred to reference [1].

In sections 2 and 3 of this paper, the introduction of all the above mentioned effective-interactions is described. In section 4, we investigate the effects of also adding the effective-interaction between $3d$ and $4s$ electrons. The results achieved in this paper are summarized and discussed in section 5.

The main purposes of the calculations to be described in the following sections are:

(a) To check if the addition of the new effective-interactions actually improves our approximation (i.e., reduces the rms error); and if it does, to find the numerical values of the new parameters and to evaluate a new optimal set of numerical values for all the interaction parameters.

(b) To study the behavior of the parameters in different spectra and different configurations, and to evaluate the relative importance of the various effective-interaction parameters.

(c) To use the improved approximation for a more accurate prediction of the unobserved levels and in some cases, also, for a better critical examination of some experimental levels.

2. The Use of a Complete Set of Effective-Interactions Between 3*d* Electrons

The starting point for our present calculation was the final results of the first author's above mentioned paper [3] on the third spectra of the iron group. In that paper, the Slater approximation was improved by the addition of the $\alpha L(L+1)$ correction and the spin-orbit interaction. In this case, for each spectrum only two configurations, $3d^n$ and $3d^{n-1}4s$, were included in the calculation. The third configuration, $3d^{n-2}4s^2$, is very high and experimentally unknown. It is certain that its interaction with the two lower configurations is negligible. In fact, in that previous calculation, we didn't succeed in including the interaction between the two lower configurations, since its effect is apparently so small that in the least-squares calculation, it didn't determine the configuration interaction parameter H.

In the previous work [3], 483 levels were calculated and fitted to 322 observed levels with the use of 30 free parameters, and the rms error was 160 cm^{-1}.

The main source of the experimental material used in the previous work [3], as well as in our present paper, is Moore's compilation [17]. Additional sources not used in the previous work are explicitly referred to in appropriate paragraphs of our present paper.

It should be noted that in that calculation [3], the observed level $d^6\ a\ ^1S$ of Fe III was excluded from the least-squares fit because of a very large deviation. Had it been included in the least-squares fit, the rms error achieved with the previous approximation would have been 184 cm^{-1}. (For the detailed history of this $a\ ^1S$ see reference [18].)

We also have to mention that in the previous work [3], the calculation was concluded by expressing all the interaction parameters by simple interpolation formulas (usually linear functions of the atomic number, and in some cases, with a small quadratic correction). In this way, all the spectra of that sequence were simultaneously treated in one total least-squares calculation in which the coefficients of the interpolation formulas took the role of free parameters. For any interaction parameter P, such a formula was of the form

$$P=P(n)=P_0+P_1\cdot x+P_2\cdot y$$

where

$$x=n-6$$

$$y=x^2-10$$

and n is the total number of $3d$ and $4s$ electrons for each spectrum. For most of the parameters, we could put $P_2=0$. In the present calculation, we used the interpolative method from the beginning.

As initial values for the general parameters, we took the final values of the previous work [3] with the following changes: for the parameter T (which was not used in the previous work), we took a value which was the average between the value obtained by us in reference [1] and the one obtained by Trees in his paper on Fe III [8]. For β, we took the values obtained in reference [1]; and according to our experience with the second spectra of the iron group, we took an initial value for α only one-half of the value it assumed in the previous work [3]. For the same reason, we increased the value for the parameter C by about 10 percent. For the new parameter Tx, we assigned the initial value zero.

In principle, we allowed a maximum number of 44 free parameters, including 10 additive parameters, one for each spectrum, and 34 coefficients of the interpolation formulas for the interaction parameters. We call these coefficients "general parameters." It should be noted that in the previous work [3], we had only 30 free parameters. Later, we shall see that in the present work, too, the final number of meaningful parameters is much smaller than the maximum number of 44 just mentioned. The values assumed by the "general parameters" in our various L.S. calculations are given in table 1. We did not report the values of the 10 additive parameters.

The whole set of initial parameters for our first diagonalization is given in table 1 in the column headed Diag. I. The derivatives of Diag. I were used for three least-squares calculations designated by L.S. 1a, L.S. 1b and L.S. 1c. In all of these calculations, the observed levels fitted to the calculated ones are the

TABLE 1. *Parameters of the various stages of the calculation*
(parameter values are given in units of cm^{-1})

	Diag. 1	L.S. 1a	L.S. 1b	L.S. 1c	L.S. 2a	L.S. 2b	L.S. 2c	L.S. 3
D_0	56717	56721 ±12	56720 ±12	56713 ±15	56720 ±12	56720 ±12	56716 ±11	56717 ±9
D_1	5959	5965 ±4	5963 ±4	5967 ±5	5965 ±4	5964 ±4	5962 ±4	5960 ±3
D_2	−85	−83 ±2	−83 ±2	−82 ±2	−83 ±2	−83 ±2	−83 ±2	−84 ±1
B_0	970	972.5 ±1.4	972.5 ±1.0	973.2 ±1.3	972.4 ±1.4	972.5 ±1.0	972.2 ±0.9	972.4 ±0.8
B_0'	1052	1055.1 ±0.8	1055.5 ±0.7	1053.9 ±0.9	1055.0 ±0.8	1055.4 ±0.7	1054.8 ±0.7	1049.6 ±0.7
B_1	60	54.0 ±0.6	53.9 ±0.5	53.7 ±0.6	54.0 ±0.6	53.9 ±0.5	53.8 ±0.5	53.8 ±0.4
B_1'	59	55.1 ±0.6	54.7 ±0.5	56.4 ±0.6	55.2 ±0.6	54.7 ±0.5	54.4 ±0.5	54.5 ±0.4
C_0	3830	3766 ±9	3755 ±7	3750 ±9	3767 ±9	3755 ±7	3760 ±6	3760 ±5
C_0'	4183	4084 ±10	4099 ±6	4081 ±7	4082 ±10	4099 ±6	4103 ±6	4103 ±5
C_1	300	308 ±4	306 ±2	308 ±3	308 ±4	306 ±2	306 ±2	306 ±2
C_1'	298	290 ±4	295 ±2	291 ±3	291 ±4	295 ±2	293 ±2	293 ±2
G_0	1815	1809 ±2	1809 ±2	1809 ±3	1809 ±2	1809 ±2	1809 ±2	1812 ±2
G_1	25	30 ±2	30 ±2	29 ±2	29 ±2	30 ±2	30 ±2	9 ±2
α_0	39	35.5 ±1.1	37.2 ±0.9	40.1 ±1.0	35.5 ±1.1	37.3 ±0.9	37.0 ±0.8	37.1 ±0.6
α_0'	39	41.4 ±1.7			41.9 ±1.6			
α_1	3.9	3.1 ±0.7	3.2 ±0.2	4.0 ±0.3	3.0 ±0.7	3.2 ±0.3	3.3 ±0.3	3.4 ±0.2
α_1'	3.9	2.5 ±0.9			2.3 ±0.8			
β_0	−558	−429 ±20	−393 ±13	−371 ±15	−431 ±20	−398 ±12	−413 ±12	−411 ±9
β_0'	−558	−378 ±21			−374 ±20			
β_1	0	−8 ±11			−8 ±11			
β_1'	0	23 ±11			22 ±10			
T_0	−4.68	−4.61±0.12	−4.44±0.10	−4.86±0.12	−4.61±0.12	−4.43±0.10	−4.47±0.09	−4.47±0.07
T_0'	−4.68	−5.14±0.20	−5.67±0.12		−5.06±0.20	−5.64±0.12	−5.63±0.11	−5.63±0.07
T_1	0	−0.06±0.08			−0.06±0.08			
T_1'	0	−0.10±0.10			−0.13±0.10			
Tx_0	0	−2.08±0.23	−2.10±0.15	−2.17±0.19	−2.05±0.22	−2.09±0.15	−1.99±0.14	−1.98±0.11
Tx_0'	0	−1.85±0.23			−1.87±0.22			
Tx_1	0	−0.39±0.13	−0.32±0.06	−0.20±0.07	−0.40±0.12	−0.33±0.06	−0.36±0.06	−0.30±0.04
Tx_1'	0	−0.47±0.11			−0.48±0.11			
Px_0								−1930±160
ζ_0	491	509 ±8	509 ±8	509 ±10	509 ±8	509 ±8	510 ±7	509 ±6
ζ_0'	561	562 ±6	563 ±6	563 ±7	559 ±6	561 ±6	562 ±6	559 ±5
ζ_1	113	111 ±3	111 ±3	110 ±4	111 ±3	111 ±3	111 ±3	111 ±2
ζ_1'	125	117 ±2	117 ±2	117 ±2	118 ±2	117 ±2	118 ±2	119 ±2
ζ_2	9	9 ±1	9 ±1	9 ±1	9 ±1	9 ±1	9 ±1	9 ±1
ζ_2'								
Δ		±48.4	±49.8	±61.2	±48.2	±49.9	±46.0	±37.7

The parameter Px is constant for all $d^{n-1}s$ configurations, so that its linear coefficient Px_1 is equal to zero.

same as those used in the previous work [3]; except that the above mentioned $a\,^1S$ of Fe III was also included.

In L.S. 1a, all of the 44 parameters were free, and the rms error is 48.4 cm^{-1}. The parameters of this L.S. calculation are given in table 1 in the column headed L.S. 1a. A detailed examination of the results of this calculation shows that a great deal of unnecessary freedom was allowed to many of the parameters. Therefore, we performed L.S. 1b in which this extra freedom was eliminated by imposing the following restrictions on the parameters:

$$\alpha_0' = \alpha_0$$
$$\alpha_1' = \alpha_1$$
$$\beta_0' = \beta_0$$
$$\beta_1' = \beta_1 = 0$$
$$T_1' = T_1 = 0$$
$$Tx_0' = Tx_0$$
$$Tx_1' = Tx_1$$

In this way, the number of free parameters was reduced from 44 to 35. The rms error almost didn't increase, and it assumed the value of 49.8 cm^{-1}. In L.S. 1c where, in addition, we also imposed the requirement $T_0 = T_0'$, the rms error increased to 61.2 cm^{-1}. This means that these two parameters should be allowed to assume different values. In order to achieve convergence, we used the parameters of L.S. 1b for a second diagonalization, Diag. II.

The derivatives of Diag. II were also used for three L.S. calculations designated as L.S. 2a, L.S. 2b and L.S. 2c. In L.S. 2a, again, all the parameters were allowed to change freely and the rms error was 48.2 cm^{-1}. In L.S. 2b, we imposed the same requirements upon the parameters as in L.S. 1b, and the rms error was 49.9 cm^{-1}. The results of L.S. 2a and L.S. 2b are practically equal to those of L.S. 1a and L.S. 1b, respectively, which means that mathematical convergence was achieved. In this stage of the calculation, we noted that the level $d^7s(b\,^2D)\ ^3D_1$ of Ni III deviated from its calculated value by about +300 cm^{-1}, while the $^3D_2$ and $^3D_3$ of the same term had the deviations of −74

cm^{-1} and -52 cm^{-1}, respectively. In L.S. 2c, the same restrictions were imposed on the parameters as in L.S. 2b, but the above mentioned $^3D_1$ of Ni III was not included. The rms error was reduced to 46.0 cm^{-1}. The deviations of the $^3D_2$ and $^3D_3$ were reduced to -3 cm^{-1} and -17 cm^{-1}, respectively. The parameters didn't change within their uncertainties. The parameters of L.S. 2a, 2b, and 2c are given in table 1 under the corresponding columns. The fit between the observed and calculated levels in the above mentioned calculations is practically the same as in reference [3], except for the above mentioned $a\,^1S$ of Fe III which was reincluded in these calculations, and the $^3D_1$ of Ni III which was excluded from them.

3. The Interaction Between the Configurations $3d^n$ and $3d^{n-1}4s$

In the previous work [3], we could not determine the interaction between the configurations d^n and $d^{n-1}s$. One should remember that this interaction is determined by one Slater parameter, H, also defined in reference [1]. Since, in its algebraic matrix, all the diagonal elements are equal to zero, it follows that if the initial value zero is given to the parameter H, the derivatives of all the eigen-values of the energy matrix with respect to H are also zero; and the least-squares calculation, in which linear dependence of the levels upon the parameters is assumed, is not able to determine this parameter. Because of the above mentioned considerations, we tried, in the previous work, to assign various nonzero initial values to H, and to use the derivatives of the corresponding diagonalizations for making several least-squares calculations. In all of these calculations, H assumed unreasonable values (e.g., the value zero, or even changed its sign). In addition, the behavior of these values for the various spectra of the sequence was unsystematic. From these facts, we concluded that the actual interaction between the above mentioned configurations is so weak that, actually, H was determined by accidental features of the experimental material in the spectra. Therefore, in the final stages of our previous calculation [3], we did not include the interaction between the above mentioned configurations in the Hamiltonian.

Since, in the present calculation, we achieved a rms error four times smaller than in the previous paper, which means a corresponding increase in the sensitivity of our least-squares calculation for weaker interactions, we decided to try to reinclude the interaction between d^n and d^{n-1}s in our calculation. We performed a diagonalization in which we used the values obtained in our analogous calculation on the second spectra of the iron group [1] as initial values for H. In the resulting least-squares calculation, we again obtained nonreasonable, nonsystematic values for H.

At this stage, we considered the possibility that our failure to determine a significant value fot the parameter H was the result of our having ignored the interaction of the configurations d^n and d^{n-1}s with the third configuration $d^{n-2}s^2$. Fortunately, Shenstone sent us new levels of Cu III belonging to the configuration d^7s^2. This enabled us to make a calculation in which the interactions of the configurations $d^{n-2}s^2$ were also included just by estimating a value for the linear coefficient in the interpolation formula of the parameter D'' (for its definition, see reference [1]). Unfortunately, even this more complete calculation didn't improve the meaningfulness of the results obtained for H.

Finally, we made a third effort. From the Ph.D. thesis of C. Roth [18], in which he calculated the configurations d^np and $d^{n-1}sp$ for various second spectra of the iron group, we were able to obtain some information about the value of the parameter H. In this case, the interaction between the above mentioned configurations is represented by three parameters:

$$H = R^2\,(dd, ds)/35$$
$$J = R^2\,(dp, sp)/5$$
$$K = R^1\,(dp, ps)/3$$

J and K are much larger than H, and since they appear in the same nondiagonal elements of the energy matrix as does H, they also greatly increase the derivatives of the eigen-values with respect to H. Therefore, in the least-squares calculations performed by Roth, H was determined. So, we performed a new diagonalization in which H was given the values obtained in Roth's calculations. The derivatives of our new diagonalization were used for two least-squares calculations: In the first one, H was free, and it consistently assumed the value zero. In the second one, H was forced to maintain the value it was given in the diagonalization. This caused the rms error to increase from 46 to 51 cm^{-1}.

Thus at this stage of the present calculations H still remains undefined.

4. The Effective Interactions Between 3d and and 4s Electrons

In order to complete the process of describing all the perturbations of the configurations of the type $(d+s)^n$ by farlying perturbing configurations, one still has to consider that kind of effective-interactions which also include s electrons. Since, the configuration ds consists of only two terms, it is fully described by the two Slater parameters $F_0(ds)$ and $G_2(ds)$. Hence, it is evident that no additional two-body effective-interactions with s electrons exist. On the other hand, three-body effective-interactions of such a kind are mathematically possible, and it is very easy to demonstrate that they can really appear in an actual physical Hamiltonian just by considering a possible actual perturbing configuration. By using group-theoretical methods, Feneuille [15] was able to show that only five linearly independent three-body interaction operators can be added to the electrostatic Hamiltonian of a $(d+s)^n$ configuration, assuming that

all the two-body effective-interactions have already been added to it.

Since in our previous calculations we already used the two-body effective-interactions represented by α and β, and the three-body interactions represented by T and Tx, we had to build three additional three-body operators. We did it in the following way: following Racah and Stein [13], let us define $u_i^{(k)}$ and $Y_i^{(k)}$, which are the one-electron tensorial operators of the order k acting on the coordinates of the ith electron, by their reduced matrices:

TABLE 2. *Relative importance of the various effective interaction parameters*

No.	Effective interaction parameters included in the calculation	Total number of free parameters	Rms error
1	α	30	184 cm^{-1}
2	α, β	31	175 cm^{-1}
3	α, T	32	164 cm^{-1}
4	α, β, T	33	61 cm^{-1}
5	α, β, T, Tx	35	46 cm^{-1}
6	α, β, T, Tx, Px	36	38 cm^{-1}
7	α, β, Tx	33	165 cm^{-1}

$$(d||u_i^{(k)}||d)=1; \qquad (d||y_i^{(2)}||s)=1.$$

All the other elements of the reduced matrices are equal to zero. Now we can define the operators

$$U^{(k)}=\Sigma_i u_i^{(k)}; \qquad Y^{(2)}=\Sigma_i y_i^{(2)}.$$

By using the method developed in the above mentioned paper of Racah and Stein [13], one can easily show that all of the second order perturbations caused to the $(d+s)^n$ configurations can be represented by a zero order product of such operators, or by suitable linear combinations of such products. We are not interested in products consisting of $U^{(k)}$'s only, since interactions between only d electrons are already completely described. Thus the operators representing new interactions may be of the forms

(1) $$[U^{(k)} \times Y^{(2)} \times Y^{(2)\dagger}]^{(0)} + \text{h.c.}$$

(2) $$[U^{(k)} \times U^{(k')} \times Y^{(2)}]^{(0)} + \text{h.c.}$$

(3) $$[U^{(k)} \times Y^{(2)} \times Y^{(2)}]^{(0)} + \text{h.c.}$$

where "h.c." means "hermitian conjugate."
The first of these operators acts within the configuration $d^{n-1}s$. The second one contributes to the interaction between d^n and $d^{n-1}s$ or between $d^{n-1}s$ and $d^{n-2}s^2$. The third contributes to the interaction between the configurations d^n and $d^{n-2}s^2$.

An appropriate set of operators of the above mentioned types can be chosen by considering the configuration $(d+s)^3$. A simple counting of the terms of the configuration d^2s and of the nonzero, nondiagonal elements connecting the configurations d^3 and ds^2 shows that we have exactly one independent three-body operator acting within d^2s, and one such operator connecting the configurations d^3 and ds^2. Thus the third independent operator must connect the configurations d^3 and d^2s. It turns out that we have to add to our hamiltonian one operator of each of the above mentioned types. Since there are no more independent operators, it is unimportant if, in the formulas (1), (2), and (3), we set k and k' equal to 2 or 4. Thus we completed the definition of the operators by arbitrarily choosing for k and k' the value 2. Then we defined three parameters, Px, Py, and Pz which are the coefficients of the above mentioned operators numbered as 1, 2, and 3, respectively. Practically, Px, Py, and Pz are three additional correction-terms whose numerical values may be determined by the usual least-squares calculation method.

In our previous calculations, we could not include even the actual electrostatic interaction between the configurations d^n and $d^{n-1}s$. Hence, there is no hope that a much smaller correction of this interaction, represented by the parameter Py, will have any detectable effect. Thus, it seemed reasonable to introduce only the new effective-interaction parameter Px which "acts" within the configuration $d^{n-1}s$. In the column "L.S. 3" of table 1, the results of its introduction are reported. We see that the addition of only one parameter has reduced the rms error from 46 to 38 cm^{-1}. The new parameter is well defined. This is demonstrated by the fact that its numerical value is considerably larger than its corresponding uncertainty. It should be noted that at this final stage of the calculation we included 12 additional levels of Co III, which had been observed by A. G. Shenstone [19]. Thus, the total number of observed levels which were fitted to the calculated ones is 334. The observed and calculated levels as calculated in L.S. 3 are reported in tables 4 to 13.

TABLE 3. *Comparison of the configurations* $3d^n$ *and* $3d^{n-1}4s$ *for the various approximations*

Effective-interaction parameters included in the calculation	Rms-error for the obs. levels of $3d^n$	Rms-error for the obs. levels of $3d^{n-1}4s$
α	233 cm^{-1}	136 cm^{-1}
α, β, T	59 cm^{-1}	60 cm^{-1}
α, β, T, Tx	35 cm^{-1}	46 cm^{-1}
α, β, T, Tx, Px	35 cm^{-1}	32 cm^{-1}

TABLE 4. Sc III-*observed and calculated energy levels*

CONF.	TERM	J	OBS.	CALC.	O–C	CALC. g
d	^2D	3/2	0.0	−97	97	0.800
		5/2	197.5	130	68	1.200
s	^2S	1/2	25536.7	25701	−164	2.000

TABLE 5. Ti III-*observed and calculated energy levels*

CONF.	TERM	J	OBS.	CALC.	O–C	CALC. g
d^2	^3F	2	0.0	−34	34	0.667
		3	183.7	150	34	1.083
		4	421.9	390	32	1.250
d^2	^1D	2	8472.6	8456	17	1.002
d^2	^3P	0	10536.4	10546	−10	0.000
		1	10603.5	10611	−8	1.500
		2	10721.1	10744	−23	1.497
d^2	^1G	4	14398.5	14404	−6	1.000
d^2	^1S	0		32480		0.000
ds	$(^2D)^3D$	1	38063.50	38096	−33	0.500
		2	38197.98	38224	−26	1.166
		3	38425.19	38436	−11	1.333
ds	$(^2D)^1D$	2	41703.65	41705	−1	1.000

TABLE 6. V III-*observed and calculated energy levels*

CONF.	TERM	J	OBS.	CALC.	O–C	CALC. g
d^3	^4F	3/2	0.0	34	−34	0.400
		5/2	145.5	178	−33	1.029
		7/2	341.5	375	−34	1.238
		9/2	583.8	622	−38	1.333
d^3	^4P	1/2	11513.8	11544	−30	2.661
		3/2	11591.8	11610	−18	1.730
		5/2	11769.7	11773	−3	1.600
d^3	^2G	7/2	11966.3	11989	−23	0.889
		9/2	12187.0	12205	−18	1.111
d^3	^2P	3/2	15550.3	15563	−13	1.182
		1/2	15579.8	15600	−20	0.672
d^3	$a\ ^2D$	3/2	16330.5	16308	23	0.954
		5/2	16374.7	16349	26	1.200
d^3	^2H	9/2	16810.9	16831	−20	0.910
		11/2	16977.6	17000	−22	1.091
d^3	^2F	7/2	27727.8	27743	−15	1.143
		5/2	27846.8	27835	12	0.857
d^3	$b\ ^2D$	5/2	42267.4	42233	34	1.200
		3/2	42371.2	42352	19	0.800
d^2s	$(^3F)^4F$	3/2	43942.49	43945	−3	0.400
		5/2	44110.04	44104	6	1.028
		7/2	44345.84	44330	16	1.238
		9/2	44646.96	44621	26	1.333
d^2s	$(^3F)^2F$	5/2	49327.74	49332	−4	0.858
		7/2	49805.29	49786	19	1.143
d^2s	$(^1D)^2D$	5/2	56160.42	56148	12	1.262
		3/2	56256.75	56224	33	0.864
d^2s	$(^3P)^4P$	1/2	56529.7	56526	4	2.666
		3/2	56669.2	56657	12	1.671
		5/2	56922.7	56908	15	1.537
d^2s	$(^3P)^2P$	1/2	61578.74	61569	10	0.667
		3/2	61777.15	61776	1	1.332
d^2s	$(^1G)^2G$	7/2	63304.64	63268	37	0.889
		9/2	63313.90	63268	46	1.111
d^2s	$(^1S)^2S$	1/2		86152		2.000

TABLE 7. Cr III—*observed and calculated energy levels*

CONF.	TERM	J	OBS.	CALC.	O–C	CALC. g
d^4	^{5}D	0	0.0	−20	20	0.000
		1	59.9	42	18	1.500
		2	181.9	164	18	1.500
		3	355.8	342	14	1.500
		4	575.0	570	5	1.500
d^4	a ^{3}P	0	16770.9	16788	−17	0.000
		1	17167.4	17170	−3	1.499
		2	17850.0	17850	−0	1.500
d^4	^{3}H	4	17272.8	17297	−24	0.802
		5	17395.5	17431	−36	1.034
		6	17528.8	17583	−54	1.166
d^4	a ^{3}F	2	18451.0	18460	−9	0.667
		3	18510.0	18519	−9	1.078
		4	18581.6	18598	−16	1.245
d^4	^{3}G	3	20702.0	20741	−39	0.755
		4	20851.3	20900	−49	1.052
		5	20994.6	21049	−54	1.199
d^4	a ^{1}G	4		25092		1.001
d^4	^{3}D	3	25725.8	25741	−15	1.333
		2	25781.0	25794	−13	1.167
		1	25848.2	25848	0	0.501
d^4	^{1}I	6		25981		1.000
d^4	a^{1}S	0		27289		0.000
d^4	a^1D	2		32065		1.000
d^4	^{1}F	3		36938		1.000
d^4	b ^{3}F	4	43286.4	43281	5	1.250
		3	43321.7	43332	−10	1.083
		2	43304.1	43334	−30	0.684
d^4	b ^{3}P	2		43344		1.482
		1		43801		1.500
		0		44030		0.000
d^4	b ^{1}G	4		49594		1.000
d^3s	(^{4}F)^{5}F	1	49491.0	49479	12	0.000
		2	49626.8	49615	12	1.000
		3	49827.7	49817	11	1.250
		4	50089.2	50084	5	1.350
		5	50408.2	50413	−5	1.400
d^3s	(^{4}F)^{3}F	2	56650.5	56658	−8	0.667
		3	56992.2	56998	−6	1.083
		4	57422.1	57435	−13	1.250
d^3s	(^{4}P)^{5}P	1	63038.6	63052	−13	2.497
		2	63172.2	63167	5	1.831
		3	63420.3	63396	24	1.666
d^4	b ^{1}D	2		65585		1.000
d^3s	(^{2}G)^{3}G	3	65890.9	65855	36	0.750
		4	66027.8	65997	31	1.049
		5	66222.7	66196	27	1.199
d^3s	(^{2}G)^{1}G	4		69622		0.994
d^3s	60%(^{4}P) + 40%(^{2}P)^{3}P	0	69510.6	69594	−83	0.000
	58%(^{6}P)^{3}P + 34%(^{2}P)^{3}P	1	69780.9	69764	17	1.422
	70%(^{4}P)^{3}P + 13%(^{2}P)^{3}P	2	70291.8	70247	45	1.475

TABLE 7. Cr III—*observed and calculated energy levels*—Continued

CONF.	TERM	J	OBS.	CALC.	O−C	CALC. g
d^3s	60%(^{2}P)^{3}P + 40%(^{4}P)^{3}P	2		70155		1.445
	55%(^{2}P)^{3}P + 40%(^{6}P)^{3}P	1		70306		1.423
	86%(^{2}P)^{3}P + 7%(^{4}P)^{3}P	0		70445		0.000
d^3s	(a^2D)^{3}D	1	70980.2	70924	56	0.659
		2	71166.1	71255	−89	1.245
		3	71321.8	71269	53	1.333
d^3s	(^{2}H)^{3}H	4	71676.2	71602	74	0.807
		5	71736.0	71677	59	1.034
		6	71868.5	71822	47	1.167
d^3s	(^{2}P)^{1}P	1		73886		0.998
d^3s	(a ^{2}D)^{1}D	2		74678		1.004
d^3s	(^{2}H)^{1}H	5		75314		1.000
d^4	b ^{1}S	0		83901		0.000
d^3s	(^{2}F)^{3}F	4		84316		1.250
		3		84396		1.083
		2		84460		0.667
d^3s	(^{2}F)^{1}F	3		87723		1.000
d^3s	(b ^{2}D)^{3}D	3		102089		1.333
		2		102189		1.166
		1		102259		0.500
d^3s	(b ^{2}D)^{1}D	2		105516		1.000

TABLE 8. Mn III—*observed and calculated energy levels*

CONF.	TERM	J	OBS.	CALC.	O−C	CALC. g
d^5	^{6}S	5/2	0.0	−188	188	2.000
d^5	^{4}G	11/2	26824.5	26858	−34	1.273
		9/2	26852.4	26863	−11	1.172
		7/2	26860.3	26853	7	0.984
		5/2	26856.9	26836	21	0.572
d^5	^{4}P	5/2	29168.9	29194	−25	1.593
		3/2	29243.0	29234	9	1.722
		1/2		29274		2.650
d^5	^{4}D	7/2	32308.9	32324	−15	1.428
		5/2	32385.7	32401	−15	1.376
		3/2		32395		1.210
		1/2		32367		0.017
d^5	^{2}I	11/2		39144		0.924
		13/2		39188		1.077
d^5	77%a ^{2}D + 22%a ^{2}F	5/2		41199		1.124
	a ^{2}D	3/2		41543		0.788
d^5	a ^{2}F	7/2		42583		1.143
	75%a ^{2}F + 15%a ^{2}D	5/2		43064		0.933
d^5	^{4}F	9/2	43574.2	43650	−76	1.331
		7/2	43604.2	43679	−75	1.237
		5/2	43670.5	43740	−70	1.030
		3/2	43675.6	43762	−86	0.413

TABLE 8. Mn III—*observed and calculated energy levels*—Continued

CONF.	TERM	J	OBS.	CALC.	O–C	CALC. g
d^5	^{2}H	9/2		46477		0.926
		11/2		46648		1.090
d^5	$a\ ^2$G	7/2		47806		0.890
		9/2		47954		1.097
d^5	$b\ ^2$F	5/2		50938		0.858
		7/2		51013		1.143
d^5	^{2}S	1/2		55616		2.000
d^5	$b\ ^2$D	3/2		61466		0.800
		5/2		61521		1.199
d^4s	(^{5}D)^{6}D	1/2	62456.7	62427	30	3.332
		3/2	62567.9	62541	27	1.866
		5/2	62747.3	62727	20	1.657
		7/2	62988.9	62980	9	1.587
		9/2	63285.2	63295	−10	1.555
d^5	$b\ ^2$G	9/2		68802		1.111
		7/2		68821		0.889
d^4s	(^{5}D)^{4}D	1/2	71396.5	71359	38	0.001
		3/2	71565.5	71532	34	1.200
		5/2	71833.4	71809	24	1.371
		7/2	72184.8	72177	8	1.428
d^5	^{2}P	3/2		83144		1.332
		1/2		83172		0.667
d^4s	($a\ ^3$P)^{4}P	1/2		84598		2.659
		3/2		85154		1.731
		5/2		86043		1.599
d^4s	(^{3}H)^{4}H	7/2		84934		0.670
		9/2		85048		0.972
		11/2		85195		1.134
		13/2		85373		1.231
d^4s	($a\ ^3$F)^{4}F	3/2		86463		0.401
		5/2		86501		1.021
		7/2		86566		1.230
		9/2		86658		1.327
d^4s	(^{3}G)^{4}G	5/2		88847		0.582
		7/2		89033		0.990
		9/2		89204		1.172
		11/2		89324		1.267
d^5	$c\ ^2$D	5/2		89509		1.200
		3/2		89557		0.801
d^4s	($a\ ^3$P)^{2}P	1/2		90229		0.675
		3/2		91310		1.333
d^4s	(^{3}H)^{2}H	9/2		90432		0.914
		11/2		90770		1.095
d^4s	($a\ ^3$F)^{2}F	5/2		91888		0.855
		7/2		91941		1.132
d^4s	(^{3}G)^{2}G	7/2		94395		0.895
		9/2		94722		1.110
d^4s	(^{3}D)^{4}D	7/2		94709		1.428
		5/2		94776		1.371
		3/2		94842		1.200
		1/2		94886		0.003

331-607 O - 69 - 5

TABLE 8. Mn III—*Observed and calculated energy levels*—Continued

CONF.	TERM	J	OBS.	CALC.	O−C	CALC. g
d^4s	$(a\ ^1G)^2G$	9/2		96358		1.111
		7/2		96400		0.894
d^4s	$(^1I)^2I$	13/2		97192		1.077
		11/2		97202		0.924
d^4s	$(a\ ^1S)^2S$	1/2		98962		1.996
d^4s	$(^3D)^2D$	5/2		99976		1.200
		3/2		100057		0.801
d^4s	$(a\ ^1D)^2D$	5/2		104407		1.200
		3/2		104436		0.801
d^4s	$(^1F)^2F$	7/2		109792		1.143
		5/2		109783		0.858
d^4s	$(b\ ^3P)^4P$	5/2		115528		1.599
		3/2		116093		1.732
		1/2		116452		2.664
d^4s	$(b\ ^3F)^4F$	9/2		115650		1.333
		7/2		115718		1.237
		5/2		115734		1.028
		3/2		115725		0.401
d^4s	$(b\ ^3P)^2P$	3/2		120834		1.334
		1/2		121523		0.669
d^4s	$(b\ ^3F)^2F$	7/2		120919		1.142
		5/2		120993		0.857
d^4s	$(b\ ^1G)^2G$	9/2		124967		1.111
		7/2		124980		0.890
d^4s	$(b\ ^1D)^2D$	5/2		143467		1.200
		3/2		143469		0.800
d^4s	$(b\ ^1S)^2S$	1/2		165639		2.000

TABLE 9. Fe III—*Observed and calculated energy levels*

CONF.	TERM	J	OBS.	CALC.	O−C	CALC. g
d^6	^5D	4	0.0	−13	13	1.500
		3	436.2	419	17	1.500
		2	738.9	723	16	1.500
		1	932.4	918	14	1.500
		0	1027.3	1014	13	0.000
d^6	$a\ ^3P$	2	19404.8	19427	−22	1.499
		1	20688.4	20703	−15	1.499
		0	21208.5	21238	−30	0.000
d^6	^3H	6	20051.1	20090	−39	1.166
		5	20300.8	20307	−6	1.036
		4	20481.9	20464	18	0.810
d^6	$a\ ^3F$	4	21462.2	21481	−19	1.237
		3	21699.9	21708	−8	1.077
		2	21857.2	21867	−10	0.668
d^6	^3G	5	24558.8	24566	−7	1.198
		4	24940.9	24944	−3	1.053
		3	25142.4	25126	16	0.757
d^5s	$(^6S)^7S$	3	30088.84	29997	92	2.000

TABLE 9. Fe III—*Observed and calculated energy levels*—Continued

CONF.	TERM	J	OBS.	CALC.	O–C	CALC. g
d^6	^{1}I	6	30356.2	30336	20	1.000
d^6	^{3}D	1	30725.8	30690	36	0.501
		2	30716.2	30699	17	1.165
		3	30857.8	30837	21	1.333
d^6	$a\ ^1$G	4	30886.4	30838	48	1.001
d^6	$a\ ^1$S	0	34812.4	34715	97	0.000
d^6	$a\ ^1$D	2	35803.7	35787	17	1.002
d^5s	(^{6}S)^{5}S	2	40999.87	40866	134	2.000
d^6	^{1}F	3	42896.9	42801	96	1.001
d^6	$b\ ^3$P	0	49148	49168	−20	0.000
		1	49576.9	49574	3	1.500
		2	50412.3	50410	2	1.499
d^6	$b\ ^3$F	2	50184.9	50197	−12	0.667
		3	50295.2	50281	14	1.083
		4	50276.1	50242	34	1.249
d^6	$b\ ^1$G	4	57221.7	57121	101	1.001
d^5s	(^{4}G)^{5}G	6	63425.17	63504	−79	1.333
		5	63466.39	63510	−44	1.267
		4	63486.78	63501	−14	1.150
		3	63494.00	63485	9	0.917
		2	63494.56	63468	27	0.334
d^5s	(^{4}P)^{5}P	3	66464.64	66518	−53	1.658
		2	66522.95	66570	−47	1.819
		1	66591.68	66642	−50	2.482
d^5s	(^{4}D)^{5}D	4	69695.73	69746	−50	1.499
		3	69836.83	69885	−48	1.506
		2	69837.76	69872	−34	1.512
		1	69788.19	69808	−20	1.517
		0	69747.40	69757	−10	0.000
d^5s	(^{4}G)^{3}G	5	70694.03	70748	−54	1.200
		4	70728.75	70747	−18	1.051
		3	70725.01	70713	12	0.751
d^5s	(^{4}P)^{3}P	2	73727.64	73757	−29	1.482
		1	73849.10	73879	−30	1.471
		0	73935.96	73975	−39	0.000
d^6	$b\ ^1$D	2		76714		1.000
d^5s	(^{4}D)^{3}D	3	76956.79	76994	−37	1.332
		2	77102.43	77136	−34	1.180
		1	77075.30	77096	−21	0.526
d^5s	(^{2}I)^{3}I	7	79840.12	79885	−45	1.143
		6	79844.74	79842	3	1.025
		5	79860.42	79818	42	0.835
d^5s	76%($a\ ^2$D)^{3}D + 16%($a\ ^2$F)^{3}F	3	82382.87	82362	21	1.285
	69%($a\ ^2$D)^{3}D + 17%(^{4}F)^{5}F	2	82410.94	82399	12	1.077
	66%($a\ ^2$D)^{3}D + 34%(^{4}F)^{5}F	1	82494.88	82502	−7	0.332
d^5s	(^{4}F)^{5}F	5	83138.23	83208	−70	1.398
	(^{4}F)^{5}F	4	83161.48	83222	−61	1.347
	(^{4}F)^{5}F	3	83237.86	83289	−51	1.241
	77%(^{4}F)^{5}F + 15%($a\ ^2$F)^{3}F	2	83358.88	83395	−36	0.964
	66%(^{4}F)^{5}F + 34%($a\ ^2$D)^{3}D	1	83646.98	83680	−33	0.172
d^5s	(^{2}I)^{1}I	6	83429.61	83450	−20	1.002

TABLE 9. Fe III—*Observed and calculated energy levels*—Continued

CONF.	TERM	J	OBS.	CALC.	O–C	CALC. g
d^5s	$(a\ ^2F)^3F$	4	84159.55	84162	−3	1.251
	$77\%(a\ ^2F)^3F + 18\%(a\ ^2D)^3D$	3	84671.87	84656	16	1.131
	$60\%(a\ ^2F)^3F + 17\%(a\ ^2D)^3D$	2	84369.92	84347	23	0.834
d^5s	$(a\ ^2D)^1D$	2	86847.11	86856	−9	0.958
d^5s	$(a\ ^2F)^1F$	3	87901.87	87889	13	1.003
d^5s	$(^2H)^3H$	4	88663.87	88612	52	0.835
		5	88694.67	88666	29	1.058
		6	88923.07	88921	2	1.164
d^5s	$(a\ ^2G)^3G$	3	89697.52	89698	−1	0.783
		4	89783.59	89786	−3	1.044
		5	89907.85	89906	2	1.172
d^5s	$(^4F)^3F$	2	90423.68	90499	−75	0.673
		3	90483.94	90551	−67	1.058
		4	90472.53	90534	−62	1.216
d^5s	$(^2H)^1H$	5	92523.91	92526	−2	1.004
d^5s	$58\%(b\ ^2F)^3F + 41\%(a\ ^2G)^1G$	4	93388.75	93409	−20	1.193
	$(b\ ^2F)^3F$	3	93392.45	93381	11	1.084
	$(b\ ^2F)^3F$	2	93412.93	93387	26	0.668
d^5s	$55\%(a\ ^2G)^1G + 40\%(b\ ^2F)^3F$	4	93512.64	93498	15	1.064
d^5s	$(b\ ^2F)^1F$	3	97041.38	97038	3	1.001
d^6	b^1S	0		98216		0.000
d^5s	$(^2S)^3S$	1		98666		2.000
d^5s	$(^2S)^1S$	0		102289		0.000
d^5s	$(b^2D)^3D$	1	105895.35	105829	66	0.500
		2	105906.23	105864	42	1.166
		3	105929.16	105924	5	1.332
d^5s	$(b^2D)^1D$	2	109570.84	109507	64	1.000
d^5s	$(b^2G)^3G$	5	114325.35	114284	41	1.200
		4	114339.95	114307	33	1.050
		3	114351.92	114325	27	0.750
d^5s	$(b\ ^2G)^1G$	4	117950.32	117922	28	1.000
d^5s	$(^2P)^3P$	2		130711		1.499
		1		130741		1.499
		0		130761		0.000
d^5s	$(^2P)^1P$	1		134330		0.996
d^5s	$(c\ ^2D)^3D$	3		138594		1.333
		2		138644		1.167
		1		138694		0.506
d^5s	$(c\ ^2D)^1D$	2		142241		1.000

TABLE 10. Co III—*Observed and calculated energy levels*

CONF.	TERM	J	OBS.	CALC.	O–C	CALC. g
d^7	^4F	9/2	0.0	−17	17	1.333
		7/2	841.2	819	22	1.238
		5/2	1451.3	1432	19	1.029
		3/2	1866.8	1851	16	0.401

TABLE 10. Co III—*Observed and calculated energy levels*—Continued

CONF.	TERM	J	OBS.	CALC.	O−C	CALC. g
d^7	^4P	5/2	15201.9	15200	2	1.599
		3/2	15428.2	15447	−19	1.715
		1/2	15811.4	15861	−50	2.631
d^7	^2G	9/2	16977.6	16950	28	1.108
		7/2	17766.2	17751	15	0.889
d^7	^2P	3/2	20194.9	20196	−1	1.306
		1/2	20918.5	20931	−13	0.702
d^7	^2H	11/2	22720.3	22703	17	1.091
		9/2	23434.3	23415	19	0.913
d^7	$a\ ^2D$	5/2	23058.8	23032	27	1.201
		3/2	24236.8	24217	20	0.845
d^7	^2F	5/2	37021.0	36946	75	0.858
		7/2	37316.5	37302	15	1.143
d^6s	$(^5D)^6D$	9/2	46438.3	46444	−6	1.555
		7/2	47003.1	46997	6	1.587
		5/2	47415.4	47404	11	1.657
		3/2	47698.6	47686	13	1.866
		1/2	47864.8	47851	14	3.331
d^6s	$(^5D)^4D$	7/2	55729.2	55705	24	1.428
		5/2	56373.8	56347	27	1.371
		3/2	56794.8	56770	25	1.200
		1/2	57036.8	57014	23	0.003
d^7	$b\ ^2D$	3/2		57142		0.800
		1/2		57567		1.200
d^6s	$(a\ ^3P)^4P$	5/2	70934.1	70933	1	1.599
		3/2	72341.9	72337	5	1.722
		1/2	73214.5	73225	−11	2.653
d^6s	$(^3H)^4H$	13/2	71623.1	71683	−60	1.230
		11/2	71873.7	71890	−16	1.135
		9/2	72083.3	72063	20	0.978
		7/2	72270.5	72222	49	0.676
d^6s	$(a\ ^3F)^4F$	9/2	73286.0	73311	−25	1.322
		7/2	73540.2	73546	−6	1.225
		5/2	73726.6	73724	3	1.021
		3/2	73861.8	73856	6	0.402
d^6s	$(^3G)^4G$	11/2	76518.9	76564	−45	1.222
		9/2	77121.1	77153	−32	1.133
		7/2	77383.1	77405	−22	0.994
		5/2	77472.3	77470	2	0.596
d^6s	$(a\ ^3P)^2P$	3/2	76791.1	76786	5	1.341
		1/2	78434.3	78444	−10	0.679
d^6s	$(^3H)^2H$	11/2	77411.6	77464	−52	1.138
		9/2	77622.9	77624	−1	0.955
d^6s	$(a\ ^3F)^2F$	7/2	78927.8	78940	−12	1.126
		5/2	79425.3	79436	−11	0.843
d^6s	$(^3G)^2G$	9/2	82363.3	82409	−46	1.108
		7/2	82920.7	82947	−26	0.897
d^6s	$(^3D)^4D$	1/2	83789.3	83796	−7	0.006
		3/2	83773.4	83795	−22	1.199
		5/2	83799.6	83837	−37	1.370
		7/2	83938.9	83982	−43	1.428
d^6s	$(^1I)^2I$	13/2	85474.1	85468	6	1.077
		11/2	85517.3	85486	31	0.924

TABLE 10. Co III—*Observed and calculated energy levels*—Continued

CONF.	TERM	J	OBS.	CALC.	O−C	CALC. g
d^6s	$(a\ ^1G)^2G$	9/2	86283.8	86291	−7	1.111
		7/2	86327.1	86317	10	0.892
d^6s	$(^3D)^2D$	3/2		89277		0.802
		5/2		89535		1.199
d^6s	$(a\ ^1S)^2S$	1/2		90884		1.996
d^6s	$(a\ ^1D)^2D$	5/2	91715.1	91673	42	1.201
		3/2		91780		0.802
d^6s	$(^1F)^2F$	7/2		99597		1.144
		5/2		99588		0.859
d^6s	$(b\ ^3P)^4P$	1/2		105113		2.661
		3/2		105671		1.731
		5/2		106698		1.598
d^6s	$(b\ ^3F)^4F$	3/2		106482		0.401
		5/2		106565		1.029
		7/2		106607		1.237
		9/2		106528		1.333
d^6s	$(b\ ^3P)^2P$	1/2		111013		0.672
		3/2		112214		1.334
d^6s	$(b\ ^3F)^2F$	7/2		112119		1.140
		5/2		112144		0.858
d^6s	$(b\ ^1G)^2G$	9/2		116336		1.112
		7/2		116365		0.892
d^6s	$(b\ ^1D)^2D$	3/2		138788		0.800
		5/2		138785		1.200
d^6s	$(b\ ^1S)^2S$	1/2		164007		2.000

TABLE 11. Ni III—*Observed and calculated energy levels*

CONF.	TERM	J	OBS.	CALC.	O−C	CALC. g
d^8	^3F	4	0.0	−12	12	1.250
		3	1360.7	1361	−0	1.083
		2	2269.8	2284	−14	0.669
d^8	^1D	2	14031.6	14039	−7	1.078
d^8	^3P	2	16661.6	16705	−43	1.420
		1	16977.8	16955	23	1.500
		0	17230.7	17216	15	0.000
d^8	^1G	4	23108.7	23091	18	1.000
d^8	^1S	0		52564		0.000
d^7s	$(^4F)^5F$	5	53703.7	53722	−18	1.399
		4	54657.9	54659	−1	1.349
		3	55406.1	55399	7	1.249
		2	55952.0	55941	11	1.000
		1	56308.2	56296	12	0.002
d^7s	$(^4F)^3F$	4	61339.2	61338	1	1.249
		3	62606.3	62602	4	1.084
		2	63472.6	63472	1	0.669
d^7s	$(^4P)^5P$	3	71067.0	71061	6	1.666
		2	71383.7	71397	−13	1.822
		1	71841.9	71886	−44	2.479

TABLE 11. *Observed and calculated levels*—Continued

CONF.	TERM	J	OBS.	CALC.	O−C	CALC. g
d^7s	$(^2G)^3G$	5	75123.8	75141	−17	1.197
		4	75646.9	75652	−5	1.045
		3	76237.8	76246	−8	0.751
d^7s	$47\%(^4P)^3P + 53\%(^2P)^3P$	2	78303.1	78285	18	1.488
	$52\%(^4P)^3P + 35\%(^2P)^3P$	1	78482.9	78465	18	1.441
	$48\%(^4P)^3P + 46\%(^2P)^3P$	0	78657.8	78647	11	0.000
d^7s	$47\%(^2P)^3P + 53\%(^4P)^3P$	2	79143.3	79129	14	1.492
	$56\%(^2P)^3P + 39\%(^4P)^3P$	1		79758		1.469
	$43\%(^2P)^3P + 51\%(^4P)^3P$	0		80669		0.000
d^7s	$(^2G)^1G$	4	79250.8	79248	3	0.993
d^7s	$(^2H)^3H$	6	81686.9	81703	−16	1.167
		5	82194.3	82191	3	1.035
		4	82826.9	82821	6	0.814
d^7s	$(a\ ^2D)^3D$	3	82172.9	82183	−10	1.334
	$(a\ ^2D)^3D$	2	83033.8	83038	−4	1.177
	$54\%(a\ ^2D)^3D + 41\%(^2P)^1P$	1	82277.0	82273	4	0.852
d^7s	$48\%(^2P)^1P + 40\%(a\ ^2D)^1D$	1	84604.8	84628	−23	0.758
d^7s	$(^2H)^1H$	5	85834.8	85838	−3	1.002
d^7s	$(a\ ^2D)^1D$	2	86646.2	86646	0	1.019
d^7s	$(^2F)^3F$	2	97841.4	97796	45	0.668
		3	97996.3	97989	7	1.083
		4	98238.2	98294	−56	1.250
d^7s	$(^2F)^1F$	3		101989		1.001
d^7s	$(b\ ^2D)^3D$	1		121189		0.500
		2	121412.2	121401	11	1.166
		3	121802.8	121770	33	1.333
d^7s	$(b\ ^2D)^1D$	2		125444		1.001

TABLE 12. Cu III—*Observed and calculated energy levels*

CONF.	TERM	J	OBS.	CALC.	O−C	CALC. g
d^9	^2D	5/2	0.0	30	−30	1.200
		3/2	2071.8	2111	−39	0.800
d^8s	$(^3F)^4F$	9/2	60803.68	60785	19	1.333
		7/2	62063.64	62036	28	1.235
		5/2	63142.16	63114	28	1.027
		3/2	63884.97	63860	25	0.403
d^8s	$(^3F)^2F$	7/2	67015.29	66992	23	1.145
		5/2	68962.23	68951	11	0.863
d^8s	$50\%(^1D)^2D + 50\%(^3P)^4P$	5/2	77966.37	77979	−13	1.402
	$78\%(^1D)^2D + 18\%(^3P)^4P$	3/2	78778.22	78761	17	0.989
d^8s	$(^3P)^4P$	1/2	80421.57	80386	36	2.664
	$82\%(^3P)^4P + 17\%(^1D)^2D$	3/2	80303.83	80283	21	1.558
	$50\%(^3P)^4P + 49\%(^1D)^2D$	5/2	80550.29	80589	−39	1.393
d^8s	$(^3P)^2P$	3/2	85445.42	85515	−70	1.316
		1/2	86131.99	86142	−10	0.670
d^8s	$(^1G)^2G$	9/2	89016.57	89032	−16	1.111
		7/2	89044.87	89037	8	0.889
d^8s	$(^1S)^2S$	1/2		122865		2.000

TABLE 13. Zn III—*Observed and calculated energy levels*

CONF.	TERM	J	OBS.	CALC.	O–C	CALC. g
d^{10}	^1S	0	0	88	−88	0.000
d^9s	$(^2D)^3D$	3	78105	78092	13	1.333
		2	79283	79255	28	1.148
		1	80859	80817	42	0.500
d^9s	$(^2D)^1D$	2	83509	83505	4	1.018

5. Discussion of the Results

In L.S. 3 where the β, T, Tx, and Px corrections were included, we used 36 free parameters for fitting 334 observed levels to the calculated ones, and the rms error is 38 cm^{-1}. In the calculation, analogous to reference [3], where these new corrections were not included, and the same experimental levels were fitted to the theoretical ones, the rms error is 184 cm^{-1}. This drastic difference in the mean error is a definite proof of the importance of the new corrections. Comparing these results with the analogous ones of the second spectra of the iron group, we see that in the third spectra, the effect of the new corrections is much stronger.

Now let us examine in more detail the behavior of the various effective interaction parameters: The mean value of the parameter α, which was already included in the previous work [3], is now halved, while its linear coefficient doesn't change considerably. This parameter still assumes equal values for the two configurations d^n and $d^{n-1}s$. The parameter β is constant for all the spectra, and also assumes the same value for both configurations. The parameter T is constant for all spectra, but assumes a larger value for the configurations $d^{n-1}s$ than it does for the configurations of the type d^n. The parameter Tx is equal for both configurations, but changes linearly with the atomic number. The parameter Px, by its very definition, is defined only for the $d^{n-1}s$ configurations. This parameter is constant along the sequence. The average value of the parameter G doesn't change considerably, but the addition of Px greatly reduced its linear coefficient, so that now it is almost constant along the sequence, which is more analogous to the behavior of G in the second spectra. The behavior of all of the other parameters is practically the same as in reference [3].

The values which we obtained in the present paper for the parameters α, β and T are of the same order of magnitude as those obtained for them in the calculations given in references [20] and [21]. The above mentioned behavior of the parameters α, β and T is consistent with our efforts to explain them as mainly representing the perturbations caused to a configuration of the type $3s^23p^63d^n$ by configurations characterized by the same set of principle quantum numbers [20, 21].

We will now examine the relative importance of the various effective interaction parameters in improving our approximation. In table 2, the results of various least-squares calculations are reported. In all of them, the same experimental material is included, and the same restrictions as in L.S. 3 are imposed on all of the parameters used in any of these calculations. They differ from each other by the set of effective interaction parameters used in them.

In column 1 of table 2, numbers are assigned to the various least-squares calculations. In the second column, we report which effective-interaction parameters were included in each calculation. In the third column, the total number of free parameters is given; and in the fourth column, we report the rms error. Row I is analogous to reference [3], except for the above mentioned changes in the experimental material. The results of calculations 2 and 3 show that the introduction of each of the parameters B or T alone, doesn't reduce the rms error considerably. However, in calculation 4, we see that the simultaneous introduction of β and T causes a drastic decrease of the rms error from 184 to 61 cm^{-1}. The calculation reported in row 5 is identical with L.S. 2c, and we see that the addition of the second three-body parameter Tx causes an additional reduction of the rms error from 61 to 46 cm^{-1}. In Row 6, we see the effect of also using the parameter Px which is a three-body effective-interaction between two d electrons and one s electron. The rms error is reduced to 38 cm^{-1}. Remembering that this parameter can improve only the levels belonging to the $d^{n-1}s$ configurations, it follows that the actual average improvement achieved by the addition is considerably larger than 8 cm^{-1} (which is the difference between the rms errors of calculations 5 and 6). Calculation 7 was performed in order to compare the relative importance of the two parameters T and Tx, which represent three-body effective-interactions only between equivalent d electrons. Calculation 7 is analogous to calculation 4, except that the three-body parameter T was replaced by the three-body parameter Tx. Comparison of the rms errors definitely shows how much more important T is than Tx. It should be noted that the conclusions obtained in reference [1] are qualitatively equal to our analogous present conclusions. However, in the present paper, the final agreement achieved between

theory and experiment is much better than the agreement achieved in the second spectra.

It is also interesting to compare the effectiveness of the above mentioned various approximations for each of the two configurations d^n and $d^{n-1}s$. In table 3, we describe the results of the least-squares calculations performed separately for the observed levels of the d^n and $d^{n-1}s$ configurations. For each of them, four different least-squares calculations were performed. In the first one, only the parameter α was included. In the second one, the parameters α, β, and T were included; in the third one, the complete set of effective-interaction parameters between d electrons, α, β, T, and Tx, was included. In the fourth calculation, the parameter Px was also added. We see that in the first calculation which is analogous to that used in the previous paper [3], the calculated levels of the $d^{n-1}s$ configurations are much more accurately calculated than those of d^n. However, during the two following stages of improving our approximation, as reported in Rows 2 and 3, the d^n configurations are much more strongly effected than are the $d^{n-1}s$ configurations. Thus, the rms error is 35 cm^{-1} for all of the levels of the d^n configurations, and 46 cm^{-1} for all of the levels of the $d^{n-1}s$ configurations. This result is very plausible since α, β, T and Tx constitute a complete set of effective-interactions between $3d$ electrons only. In the calculation reported in Row 4, where the effective-interaction which includes an s electron was also added, the $d^{n-1}s$ configurations were strongly improved, and are even somewhat better than the d^n configurations.

We would like to note that after the addition of Px, we again tried to include in our calculations also the electrostatic interaction between the configurations d^n and $d^{n-1}s$. This was done by the same procedures as those described in section 3. The effect of the improvement of the approximation was that, in the least-squares calculation, H assumed more or less consistent values, with uncertainties somewhat smaller that the values themselves. These values of H are quite similar to those obtained for H in the second spectra of the iron group. Although this behaviour of H is a remarkable improvement in comparison to its behaviour in the calculations described in section 3 of the present paper, its introduction into our calculation hardly reduced the rms error.

In these circumstances, we thought it unreasonable to add the parameter Py and Pz (defined in section 4) which represent correction terms to the electrostatic configuration interaction. Thus, we have the impression that the process of improving the approximation by adding electrostatic effective-interaction correction terms has come to a standstill, at least at the present stage.

A Remark on the Second Spectra. We would like to note that we also tried to use the new parameter Px in our calculations of the second spectra of the iron group. It didn't cause any significant improvement in the approximation; and naturally, also couldn't unambiguously determine the value of the parameter Px. This negative result was actually anticipated, since in reference [1], where Px was not included, the $d^{n-1}s$ configurations are already more accurately approximated than are the d^n configurations.

We thank Serge Feneuille for the information with which he kindly supplied us.

6. References

[1] Shadmi, Y., Oreg, J., and Stein, J., J. Opt. Soc. Am. **58**, 909(1968).
[2] Racah, G., and Shadmi, Y., Bull. Res. Council Israel **8F**, 15(1959).
[3] Shadmi, Y., Bull. Res. Council Israel **10F**, 3(1962).
[4] Shadmi, Y., Bull. Res. Council Israel **9F**, 4 (1961).
[5] Shadmi, Y., J. Res. NBS **70A** (Phys. and Chem) No. 5, 435 (1966).
[6] Bacher, R. F., and Goudsmit, S. A., Phys. Rev. **46**, 948 (1934).
[7] Trees, R. E., Phys. Rev. **83**, 756 (1951).
[8] Trees, R. E., Phys. Rev. **84**, 1089 (1951).
[9] Trees, R. E., Phys. Rev. **129**, 1220 (1963).
[10] Racah, G., Phys. Rev. **85**, 381 (1952).
[11] Racah, G., and Shadmi, Y., Phys. Rev. **119**, 156 (1960).
[12] Rajnak, K., and Wybourne, B. G., Phys. Rev. **132**, 280 (1963).
[13] Racah, G., and Stein, J., Phys. Rev. **156**, 58 (1967).
[14] Judd, B. R., Physica **33**, 174 (1967).
[15] Feneuille, S., C. R. Acad. Sc. Paris **262**, 23 (1966).
[16] Racah, G., Phys. Rev. **63**, 367 (1943).
[17] Moore, C. E., Atomic Energy Levels, NBS Circ. No. 467, **1** and **2** (1949, 1952).
[18] Roth, C., Ph. D. Thesis, The Hebrew University of Jerusalem, (1967).
[19] Shenstone, A. G., Can. J. Phys. **38**, 677 (1960).
[20] Shadmi, Y., Phys. Rev. **139**, A43 (1965).
[21] Shadmi, Y., Physica **33**, 183 (1967).

(Paper 73A2–542)

JOURNAL OF RESEARCH of the National Bureau of Standards—A. Physics and Chemistry
Vol. 73A, No. 2, March–April 1969

Test of a Kinetics Scheme: Emission in $H(^2S) + NO(^2\Pi)$*

M. Krauss

Institute for Materials Research, National Bureau of Standards, Washington, D.C. 20234

(November 27, 1968)

The mechanism to explain the afterglow in the collision of $H(^2S)$ and $NO(^2\Pi)$ is critically examined by calculating part of the energy surface of the $^3A''$ state. It is found that the long range interaction energies are consistently repulsive even though at shorter distances attractive ionic interactions dominate. It is concluded that the essential feature of the Clyne and Thrush mechanism is missing; intimate interaction of $H(^2S)$ and $NO(^2\Pi)$ is not possible at room temperature along the $^3A''$ surface. This study was undertaken to provide an example where a theoretical calculation is required to critically test a kinetics mechanism.

Key words: Hartree-Fock; $HNO(^1A', ^3A'', ^1A')$; interaction energy; ionic state; radiative recombination; reaction barrier.

1. Introduction

The understanding of the kinetics of reaction often depends upon a knowledge of the energy surface or surfaces accessible to the reactants. When theoretical information is lacking, the available experimental information is often used to construct a schematic representation. A particular example of this is seen in the mechanism proposed by Clyne and Thrush [1] to explain the afterglow in the collision of $H(^2S)$ and $NO(^2\Pi)$. Four molecular states correlate with these asymptotic fragments. There is a X^1A' ground state and $^3A''$, $^1A''$, and $^3A'$ excited states. The $^1A''$ is known [2] to have a considerable barrier to the interaction of H and NO. Clyne and Thrush therefore proposed that the rate determining step is a radiationless transition

$$HNO(^3A'') \rightarrow HNO(^1A'')$$

which is followed by

$$HNO(^1A'') \rightarrow HNO(^1A') + h\nu.$$

No barrier is presumed to impede the close approach of H and NO in the continuum of the $^3A''$ state. The $^3A''$ state provides a path for an intimate collision and ultimate curve crossing to the $^1A''$.

This study will directly test this mechanism by determining the $^3A''$ energy surface especially at large interfragment distances. The $^3A''$ energy surface will be calculated in the H.F. approximation [3]. Asymptotically only one configuration will determine the energy behavior since the H.F. wave function behaves correctly as the fragments separate. At shorter distances there is no low lying excited state that can qualitatively modify the H.F. surface. Since we are looking for a yes-no answer the qualitatively correct H.F. surface will suffice.

2. Hartree-Fock Calculation

The Gaussian-type function (GTF) basis is obtained from Huzinaga [4]. A contracted set of the 9*s* and 5*p* atom GTF basis is used for N and O and three *s* GTF are used for the H atom. The NO internuclear distance is fixed at 2.1747 a.u. which is the $X^2\Pi$ ground state equilibrium value. The H atom approaches the NO molecule along four lines. Two are collinear. The H atom approaches from the N or O side. The main calculation effort is along a line which is directed at the N atom and at an angle of 110°. Points along this line will be close to the equilibrium geometry of the $^1A'$ and $^1A''$ states. Two points were calculated on a line between the H and O atoms with an angle of 150°. Cost will not permit a more complete determination of the surface. Nontheless the results in table 1, which are illustrated in figure 1, are sufficient to test the Clyne and Thrush mechanism.

One of the features of the calculations at 110° is the sudden change of wave function when R(NH) is about 3.0 a.u. Nonetheless the H.F. equations still converged smoothly although somewhat slowly to a solution. For linear encounters of H with O at 150° the convergence proved to be extremely slow but the barrier at 110° is duplicated on the 150° line.

*This Research was supported by the Advanced Research Projects Agency of the Department of Defense under the Strategic Technology Office.

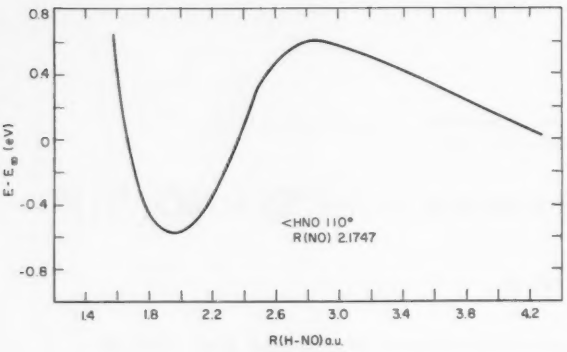

FIGURE 1

TABLE 1. *Calculated interaction energies for* H + NO

Linear	$E-E_\infty$ (a.u.)		
R(HN)	$^3\Pi$	$^1\Delta$	$^3\Sigma^-$
2.	0.1673	0.0535	0.0110
4.	.0088		
5.	.0016		
6.	.0002		
R(HO)			
3.5	0.0137		
4.	.0050		
4.3	.0034		
4.5	.0024		
5.0	.0009		

110° < HNO

R(HN)	$^1A'$	$^1A''$	$^3A''$
1.6			0.0147
1.8			−.0166
2.0	−0.0363	0.0141	−.0211
2.2			−.0132
3.0			.0209
4.0			.0051

150° < HON

R(HO)			$^3A''$
3.0			0.0279
4.5			.0011

For sake of comparison, the ground state X^1A' with a configuration

$$1a'^2\ 2a'^2\ 3a'^2\ 4a'^2\ 5a'^2\ 6a'^2\ 1a''^2\ 7a'^2,\ X^1A'$$

was calculated as well as the $^1A''$ in which, analogously to the $^3A''$, the $7a'$ orbital is excited to a $2a''$. In addition to the $^3\Pi$ two other states were calculated for the linear HNO conformation, the $^1\Delta$ and $^3\Sigma^-$. All of these states were calculated for R(HN) equal to 2.0 a.u. which is close to the observed [5] internuclear distance in the ground state HNO.

3. Conclusion

When the H(^{2}S) and NO($^2\Pi$) interaction is collinear only $^3\Pi$ and $^1\Pi$ molecular states will arise. In the H.F. approximation the $^1\Pi$ is almost invariably above the $^3\Pi$ state so calculation of the $^3\Pi$ will determine the character of both states. The approach from the N side yields a repulsive curve even to the close approach of R(HN) equal to 2.0 a.u. At this distance the $^1\Delta$ and $^3\Sigma^-$ states are much more stable but in a linear correlation they can not dissociate to ground state fragments. From the O side the interaction curve is also repulsive. At R(HO) equal to 3.5 a.u. the repulsion energy is already 0.35 eV.

Along the 110° line the barrier height for the $^3A''$ reaches about 0.6 eV which certainly precludes penetration for all but very energetic H atoms. At R(HN) equal to 3.0 a.u. the wave function suddenly changes character. The $7a'$ orbital which is primarily a H 1s function shifts charge to the NO Π type functions. The total wave function at R(HN) = 2.0 a.u. is best described as a predominately ionic interaction between an H^+ and a NO^-. At this point the $^3A''$ is 0.6 eV stable relative to the asymptotic fragments. The $^1A''$ is almost 1.0 eV above the $^3A''$ at this point or about 0.4 eV above the asymptote. Correlation energy can be large in this case since all the open shell orbitals are valence in character and penetrate the closed shell core. The extent to which the correlation and H. F. errors cancel is difficult to estimate. But it is clear [2] that the $^1A''$ has a minimum 0.45 eV below the asymptote since there is no activation energy for the emission. If the $^1A''$ is displaced downward by 0.85 eV and the $^1A'$ by about 1.1 eV then the observed excitation energy and dissociation energies are satisfied. Such values are consonant with electron-pair correlation energies but in this case are an amalgam of correlation and H.F. errors.

The maximum observed in the $^3A''$ along the 110° line will be relatively unaffected by the correlation energy since the ionic charge transfer has not yet occurred. Since the $^1A''$ barrier is expected to remain above the $^3A''$ at these distances, the observation of vibrational bands well above the dissociation limit is expected.

The approach along the H–O line also exhibits a barrier that is at least 0.6 eV high. This barrier is again sufficient to preclude penetration.

The barriers that are calculated on all four lines of approach of the H atom are representative of the $^3A''$ Hartree-Fock energy surface. It is difficult to envisage another result for any other angle of attack. From the present results one would be reluctant to consider the $^3A''$ surface as an important path for the population of $^1A''$ HNO molecules. It should be noted that radiationless transitions could occur from vibrationally excited X^1A' or even from the continuum of X^1A' which is the one remaining bimolecular pathway that is energetically accessible.

4. References

[1] Clyne, M. A. A., and Thrush, B. A., Discussions Faraday Soc. **33**, 139 (1962).

[2] Clement, M. J. Y., and Ramsay, D. A., Can. J. Phys. **39**, 205 (1961).

[3] The present calculations were made with a computer program, IBMOL2, that was written by E. Clementi and A. Veillard which was modified to suit the open-shell problem considered here.

[4] Huzinaga, S., J. Chem. Phys. **42**, 1293 (1965).

[5] Herzberg, G., Electronic Spectra of Polyatomic Molecules (D. Van Nostrand Co., Inc., New York, 1967).

(Paper 73A2–543)

JOURNAL OF RESEARCH of the National Bureau of Standards—A. Physics and Chemistry
Vol. 73A, No. 2, March–April 1969

A Nuclear Magnetic Resonance and Relaxation Study of Dimethoxyborane

T. C. Farrar and T. Tsang

Institute for Materials Research, National Bureau of Standards, Washington, D.C. 20234

(December 10, 1968)

Proton and boron-11 c.w. nuclear magnetic resonances have been studied in solid $H^{11}B(OCD_3)_2$ and $H^{10}B(OCD_3)_2$. For ^{11}B, only the $-\frac{1}{2}\rightarrow\frac{1}{2}$ transition, broadened by second order quadrupolar effects and by proton dipolar interaction can be seen; from the spectrum at several rf frequencies, the quadrupolar coupling constant $|e^2qQ/h|$ was found to be 3.0 ± 0.2 MHz ($\pm$ always refers to rms errors). In $H^{10}B(OCD_3)_2$, the proton line shapes at 53 and 10 MHz are considerably different; this may be interpreted as due to changes in the directions of ^{10}B nuclear quantization. Nuclear magnetic relaxation studies have been made in the liquid phase. From the ^{10}B and ^{11}B relaxation times, the activation energy for molecular reorientation was found to be 8.7 ± 0.4 kJ/mol (2.1 ± 0.1 kcal/mol). Consistent values for $|e^2qQ/h|$ were obtained from relaxation measurements in liquid phase and from c.w. spectra in solid phase. The temperature dependence of proton relaxation times deviates significantly from the activation energy model at higher temperatures, where spin-rotation interactions may be important. Proton transverse relaxation times (T_2) have also been measured and are consistent with the Allerhand-Thiele theory.

Key words: Boron-10; boron-11; dimethoxyborane; proton; pulsed nuclear magnetic resonance; scalar and quadrupolar coupling constants and relaxation effects.

1. Introduction

In the past few years, several experimental wide-line NMR studies [1–3][1] of two-spin systems ($I=\frac{1}{2}$, $S>\frac{1}{2}$) have been reported. The early experimental work [1, 2] was initiated in an attempt to determine metal-hydrogen bond distances in transition-metal carbonyl hydrides. If one assumes, as everyone did at that time, that the Van Vleck moment theory [4] is valid for such systems, then in some cases metal-hydrogen bond distances can be obtained from the low-temperature proton wide-line NMR data. In studies of $HMn(CO)_5$ and $HCo(CO)_4$, values of 1.3 and 1.2 A, respectively, were obtained for the metal-hydrogen bond distances. The subsequent observation in this laboratory that the proton line shapes for $HCo(CO)_4$ and $H^{10}B(OC^2H_3)_2$ are frequency dependent indicates that factors other than the direct dipole-dipole interaction can play an important role in determining the proton line shape and second moment of such systems. Since that time it has been shown theoretically [3, 5, 6] that this is indeed the case. In this paper, we have examined the various interactions that may contribute to proton NMR line shapes and moments by studying the systems $H^{11}B(OC^2H_3)_2$ and $H^{10}B(OC^2H_3)_2$ rather carefully. These molecules are not ideal, since the principal z-axis of the electric field gradient tensor does not coincide with the H-B internuclear vector. Consequently, detailed line shape calculations are not possible. Nevertheless, they do afford us the opportunity to determine some of the NMR and NQR parameters by at least two independent techniques. In this way, one can assess experimentally the accuracy of some of the newer pulse techniques to determine such parameters as spin-spin coupling constants J_{ij} and electric quadrupole coupling constants e^2qQ/h (in *liquid* samples), and one can check the validity of the approximations made in the analysis of two-spin systems and some of the predictions made by the theory. If these new pulse techniques can be shown to be valid and reliable, they can then be used with confidence to determine, for example, $J_{H\text{-}Mn}$ in $HMn(CO)_5$; in such two spin ($I=\frac{1}{2}$, $S>\frac{1}{2}$) systems, conventional c.w. techniques (high resolution and wide-line NMR) give no information about the coupling constants. In this paper, we would like to call attention to the various interactions which can contribute to the proton NMR line shapes and moments, to show how the magnitudes of these interactions can be determined *experimentally* using pulsed and wide-line NMR techniques and to demonstrate the validity of these techniques.

[1] Figures in brackets indicate the literature references at the end of this paper.

2. Theory

The second moment M_2 of the proton NMR absorption spectrum in two-spin systems (e.g., $HMn(CO)_5$, $HCo(CO)_4$, $H^{11}B(OC^2H_3)_2$, etc.) with spins $I=\frac{1}{2}$ and $S>\frac{1}{2}$ arises from several sources [1, 2, 7]:

(a) *The direct dipole-dipole interactions (Van Vleck's result* [4]). For a two spin system, this is given by:

$$M_2^{d-d}=(4/15)\hbar^2\gamma_s^2S(S+1)r^{-6} \tag{1}$$

(b) *The chemical-shift anisotropy interaction.* This will be small for protons and may be neglected.

(c) *Indirect dipole-dipole interaction.* For a two-spin system $I=\frac{1}{2}$ and $S>\frac{1}{2}$, the nuclear spin I is quantized along the magnetic field H_0. On the other hand, the direction of quantization of the spin S lies between H_0 and the principal z axis of the electric field gradient tensor. For convenience, we define the parameter

$$\alpha=|4S(2S-1)\gamma_s\hbar H_0/(e^2qQ)|.$$

In the limit $\alpha \ll 1$, the spin S is quantized along the z axis of the field gradient tensor and for $\alpha \gg 1$, S is quantized along H_0. As has been pointed out [3, 6], both the line shape shape and second moment for the nucleus I change considerably in the region $\alpha \approx 4$. The direct (Van Vleck) interaction limit corresponds to $\alpha=\infty$.

(d) *The spin spin coupling interaction.* The contribution to M_2 is given [8] by

$$M_2^{s.c.}=\frac{S(S+1)}{3}J^2. \tag{2}$$

For $H^{11}B(OCD_3)_2$ where the ^{11}B-H spin-spin coupling constant $J_{H\text{-}B}=164$Hz, the contribution to the second moment is very small. $J_{H\text{-}Mn}$ in $HMn(CO)_5$ and $J_{H\text{-}Co}$ in $HCo(CO)_4$ are unknown, but could be rather large. In order to be significant, J would have to be greater than 1 kHz. Similarly, the contribution to M_2 from the anisotropic part of spin-spin coupling is also very small [6].

In 2-spin systems where the fine-structure has been partially or completely wiped out because of rapid quadrupole relaxation of one of the nuclei, the spin-spin coupling constant J_{IS} can, in principle still be obtained by pulsed NMR measurements. Following Abragam's notation [8], the relaxation rates, $R_1(R_1=1/T_1)$ and R_2 of the nucleus I(I = 1/2, S > 1/2) for dipolar relaxation are given by:

$$R_2^I=R_1^I=\gamma_I^2\gamma_S^2\hbar^2S(S+1)$$
$$\{\tfrac{1}{12}J^{(0)}(\omega_I-\omega_S)+\tfrac{3}{2}J^{(1)}(\omega_I)+\tfrac{3}{4}J^{(2)}(\omega_I+\omega_S)\} \tag{3}$$

For $^1H=I$, $^{11}B=S$ and $\omega\tau_c \ll 1$, we get:

$$R_2^I=R_1^I=\frac{5\gamma_H^2\gamma_B^2\hbar^2}{r_{H\text{-}B}^6}\tau_c \equiv DD \tag{4}$$

where γ_H and γ_B are the magnetogyric ratios of ^{1}H and ^{11}B, $r_{H\text{-}B}=1.25\times10^{-8}$ cm, is the H-B bond distance [7], τ_c is the correlation time for the isotropic reorientation of the molecule.

The proton relaxation times arising from the indirect scalar coupling interactions are given by [8]

$$R_1^I=\frac{2A^2}{3}S(S+1)\frac{\tau_s}{1+(\omega_I-\omega_S)^2\tau_s^2} \tag{5}$$

$$R_2^I=\frac{A^2}{3}S(S+1)\left\{\frac{\tau_s}{1+(\omega_I-\omega_S)^2\tau_s^2}+\tau_s\right\} \tag{6}$$

where A is the spin-spin coupling constants in radians/s ($2\pi J=A$), and τ_s in this case is just the relaxation time of the nucleus $S(R_1^S=R_2^S=\tau_s^{-1})$ which is dominated by quadrupole relaxation effects [8]:

$$R_1^S=R_2^S=\frac{3}{40}\frac{2S+3}{S^2(2S-1)}\left(1+\frac{\eta^2}{3}\right)\left(\frac{eqQ}{\hbar}\right)^2\tau_c \tag{7}$$

The total proton (or nucleus I) relaxation times then are given by

$$R_1^I=DD+\frac{2A^2}{3}S(S+1)\frac{\tau_s}{1+(\omega_I-\omega_S)^2\tau_s^2} \tag{8}$$

$$R_2^I=DD+\frac{A^2}{3}S(S+1)\left[\frac{\tau_s}{1+(\omega_I-\omega_S)^2\tau_s^2}+\tau_s\right]. \tag{9}$$

For our experiments, $\omega \sim 10^8 s^{-1}$, $\tau_s \sim 10^{-4}$ s, hence

$$R_1^I=DD \tag{10}$$

$$R_2^I-R_1^I=\tfrac{1}{3}A^2S(S+1)\tau_s=\tfrac{1}{3}A^2S(S+1)(R_1^S)^{-1}. \tag{11}$$

For very fast quadrupole relaxation of nucleus S (e.g., $Mn(CO)_5$ where $T_1^{Mn}\approx 90\ \mu$s), a simple spin-echo experiment will give an accurate value of R_2^I. For slower quadrupole relaxation (e.g., $H^{11}B(OCD_3)_2$ where $T_1B\approx 3$ ms), Carr-Purcell experiments are required to overcome the residual spin-spin coupling interaction.

The spin-spin coupling constant, J, then is given by:

$$2\pi J=\left[\frac{3(R_2^I-R_1^I)}{S(S+1)R_1^S}\right]^{1/2}. \tag{12}$$

To obtain $e^2qQ/\hbar$ is also relatively easy. If we know the I-S bond distance and R_1^I, then from eq (4) we obtained τ_c. From the value of τ_c and R_1^S we can obtain $e^2qQ/\hbar$ from eq (7) (in most of the simple cases with which we are concerned the asymmetry parameters, η, is approximately zero).

3. Experimental Procedure

The synthesis [10] of the molecules $H^{11}B(OC^2H_3)_2$ and $H^{10}B(OC^2H_3)_2$ and a preliminary NMR study [7]

have already been reported. The proton and ^{11}B c.w. line shape studies were performed using a modified marginal oscillator [11], a gas-flow cryostat and a commercial magnet, magnet power supply and field sweep system. The field sweep was calibrated by the audio side-band technique. The pulsed NMR experiments were done using a spectrometer designed and built in this laboratory. The $\pi/2$ pulse-widths were about 1 μs in duration for protons and the overall system recovery time was about 16 μs. The T_1 values at each temperature were determined via the $\pi - \pi/2$ pulse sequence; a least square fit of the data to the equation

$$\ln[I(\infty) - I(t)] = (-t/T_1) + K \tag{13}$$

was used to obtain T_1. At least ten data points were used to obtain each T_1 value. A rms deviation of about 3 percent was typical for the T_1 values. The temperature of the gas-flow cryostat system was controlled by a servo-device which employed a platinum resistor as a sensing element. The temperature could be held constant to about 0.01 °C. The sample temperature was measured with a copper-constantan thermocouple placed near the sample coil. Since the samples were synthesized in a high vacuum system the presence of even minute amounts of dissolved oxygen can be discounted. The final samples for our experiments were distilled in the high-vacuum system into 10 mm quartz sample tubes and sealed off. (Borosilicate glass containers are not suitable in this case because of the intense ^{11}B resonance from the glass.)

4. Results and Discussion

4.1. Line-Shape Studies

Proton NMR spectra of $H^{11}B(OCD_3)_2$ were recorded from 9.7 MHz ($0.23T = 2.3$kG) to 53 MHz. All of them are quite similar to the previously recorded spectra [7] at 30 MHz. This reflects the fact that even at $0.23T$, $\alpha \cong 14$ and consequently no appreciable indirect dipolar interaction is to be expected.

For the $H^{10}B(OCD_3)_2$ molecule, the situation is quite different. Although the details are obscured due to the larger spin quantum number ($S = 3$ for ^{10}B) and the smaller magnetogyric ratio $\gamma(^{11}B)/\gamma(^{10}B) \cong 3$, there is a considerable difference in the proton spectra recorded at 10 and at 53 MHz; these spectra are shown in figure 1. The predicted trends [3, 6] and the observed spectra are in good general agreement. A detailed comparison of the theory and the experimental results is not possible since the magnetic dipole-dipole vector does not coincide with the principal axis of electric field gradient and the calculations are therefore intractable.

The quadrupolar coupling constant e^2qQ/h for boron-11 may be determined directly from the NMR spectra in the solid phase [12]. The spectra at 18.8, 12.7, and 9.7 MHz are shown in figure 2. Only the central ($-\frac{1}{2} \rightarrow \frac{1}{2}$) component, broadened by second order quadrupole splitting, can be seen. The spectra are in general agreement with the calculated line shape for a symmetric field gradient, indicating $\eta \ll 1$. However, fine structures due to the magnetic dipole interactions between ^{11}B and proton nuclei are also observed. Including the magnetic dipolar contributions, the total splitting (in Hz) is $(25/192)(e^2qQ/h)^2\nu_L^{-1} + (\xi/h)$, where ν_L is the rf oscillator frequency, $\xi = \gamma_B\gamma_H\hbar^2 r^{-3}$, $\xi/h = 20$ KHz. The dipolar contribution, ξ/h, is about 10 percent of the total splitting. From figure 2, we get $|e^2qQ/h| = 3.0 \pm 0.2$ MHz for ^{11}B in the solid phase of $H^{11}B(OCD_3)_2$. (In this paper, $\pm$ refers to rms deviations).

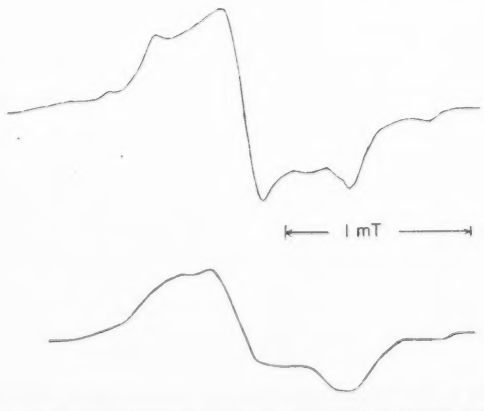

FIGURE 1. *Proton absorption derivative spectra in solid* $H^{10}B(OCD_3)_2$.
At 52.8 (top) and 9.8 (bottom) MHz.

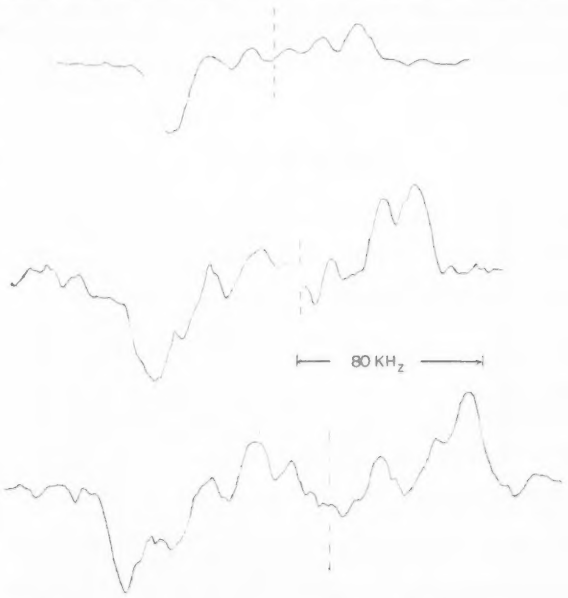

FIGURE 2. ^{11}B *spectra, absorption derivative,* $HB(OCD_3)_2$ *in quartz tube.*
Top to bottom, 18.8, 12.7 and 9.7 MHz. Dashed lines indicate unshifted ^{11}B resonance position. Magnetic field decreases from left to right.

331-607 O - 69 - 6

Slightly lower values ($|e^2qQ/h| = 2.5$ MHz) have been reported [13] for ^{11}B coupling constants at triangularly coordinated sites in borates.

4.2. Relaxation Studies

Spin-lattice relaxation time (T_1) data at various temperatures in the liquid phase are summarized in figure 3. The proton relaxation times T_{1H} at 4.2 and 19

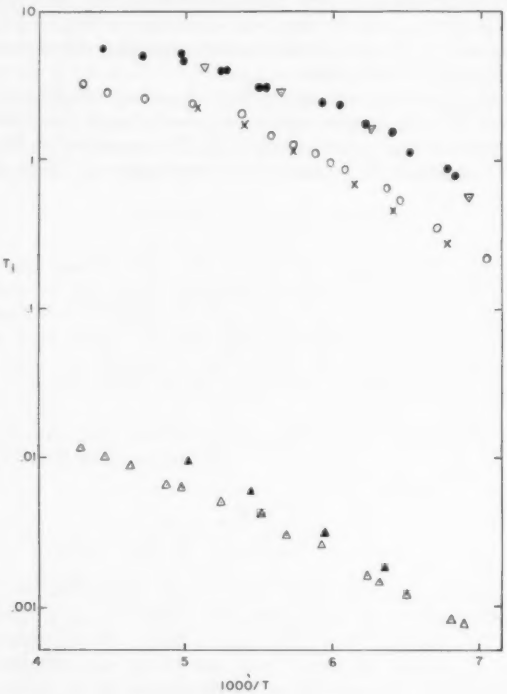

FIGURE 3. *Spin-lattice relaxation times* T_1 *(in s) versus inverse temperature on semilogarithm scale.*

$H^{11}B(OCD_3)_2$: proton at 19 MHz, ○; proton at 4.2 MHz, ×; ^{11}B at 19 MHz, △. $H^{10}B(OCD_3)_2$: proton at 19 MHz, ●; proton at 4.2 MHz, ▽; ^{10}B at 4.2 MHz, ▲.

MHz are not very different. Also, we observe that T_{1H} for $H^{10}B(OCD_3)_2$ is a factor of 2.5 ± 0.3 longer than T_{1H} for $H^{11}B(OCD_3)_2$ over the experimental temperature range 140–240 K, and that the ^{10}B relaxation time $T_{1B\text{-}10}$ in $H^{10}B(OCD_3)_2$ is a factor of 1.4 ± 0.2 longer than the ^{11}B relaxation time $T_{1B\text{-}11}$ in $H^{11}B(OCD_3)_2$.

We shall consider the nuclear magnetic relaxation due to molecular rotation only, the rotational correlation time τ_c being very short ($\tau_c \ll 10^{-8}$ sec). Then the proton relaxation time T_{1H} due to H-B dipolar interaction and the boron relaxation time due to electric quadrupole interaction are given by [8]:

$$(T_{1H})^{-1} = \tfrac{4}{3}\gamma_B^2\hbar^2 r^{-6} S(S+1)\tau_c \qquad (14)$$

$$(T_{1B})^{-1} = \frac{3(2S+3)}{40\,S^2(2S-1)}\left(\frac{e^2qQ}{\hbar}\right)^2\left(1+\frac{\eta^2}{3}\right)\tau_c \qquad (15)$$

where γ_B, S, e^2qQ/h and η are the magnetogyric ratio, spin, quadrupolar coupling constant and asymmetry parameter of the boron nucleus, and r is the H-B distance. From (15), T_1 for ^{10}B is expected to be a factor of 1.54 longer than T_1 for ^{11}B, this ratio being independent of q, η and τ_c; experimentally, we find the ratio to be 1.4 ± 0.2. From (14), we expect T_{1H} in $H^{10}B(OCD_3)_2$ to be a factor of 2.78 longer than T_{1H} in $H^{11}B(OCD_3)_2$, in reasonable agreement with the ratio 2.5 ± 0.3 observed experimentally.

Since $\eta^2 \ll 1$, the quadrupolar coupling constant e^2qQ/h may be calculated from the ratio T_{1H}/T_{1B} which is independent of τ_c. In $H^{11}B(OCD_3)_2$, we find $T_{1H}/T_{1B} = 360 \pm 40$ over our experimental temperature range in figure 3, T_{1B} being the ^{11}B relaxation time. Using B-H bond distance $r = 1.25$ A from the proton c.w. resonance data [8], we get $e^2qQ/h = 2.7 \pm 0.2$ MHz for ^{11}B in $H^{11}B(OCD_3)_2$ from (14) and (15). This calculated value is expected to be slightly lower than the true ^{11}B quadrupolar coupling constant, since we have considered only the intra molecular rotational ^{11}B-H dipolar relaxation for protons in (14). From the second order quadrupolar splitting in polycrystalline solids, we found $e^2qQ/h = 3.0 \pm 0.2$ MHz. A previous estimate of 2.6 MHz has been given by Boden, Gutowsky, Hansen, and Farrar [9] from pulse measurements in liquids.

Rotational correlation times for liquids $HB(OCD_3)_2$ from T_1 data using (14) and (15) are summarized in figure 4, using the B-H bond distance $r = 1.25$ A and

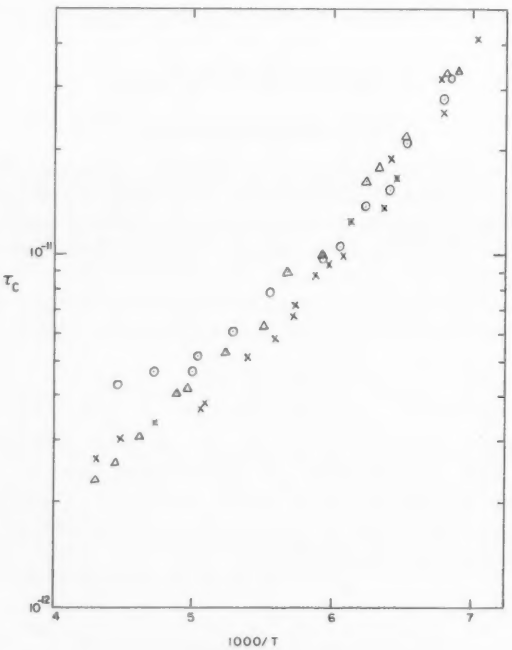

FIGURE 4. *Rotational correlation time (in s) in liquid* $HB(OCD_3)_2$ *versus inverse temperature on semilogarithm scale: from proton data in* $H^{11}B(OCD_3)_2$, ×; *from proton data in* $H^{10}B(OCD_3)_2$, ⊙; *from* ^{11}B *data in* $H^{11}B(OCD_3)_2$, △.

$e^2qQ/h = 2.7$ MHz for ^{11}B. The agreement between various methods is satisfactory, indicating that (14) and (15) are in general correct, although the problem is somewhat oversimplified. We expect the boron nuclear relaxation to be dominated by quadrupolar interaction. The correlation times from the boron relaxation can be fitted to usual form:

$$\tau_c = \tau_0 e^{V/RT} \tag{16}$$

where V is the activation energy, with $V = (8.7 \pm 0.4) \times 10^3$ J/mol (2.1 ± 0.1 kcal/mol). Previous studies [9] over a narrower temperature range gave a somewhat lower activation energy, $(5.5 \pm 0.4) \times 10^3$ J/mol.

On the other hand, the proton relaxation times in $H^{11}B(OCD_3)_2$ and $H^{10}B(OCD_3)_2$ cannot be fitted to the activation energy from (16); whereas the fit is reasonably good in the low temperature region, the T_1 versus $1/T$ curve is considerably flatter than expected in the $10^3/T > 5$ region. Similar behaviors have been reported, for example, by Powles and co-workers [14], and their results have been interpreted through spin-rotation interactions. This may well be the cause of the nonlinear high-temperature dependence of T_{1H} versus temperature for $H^{11}B(OCD_3)_2$.

Transverse proton relaxation times T_{2H} have been measured by the Carr-Purcell pulse sequence in the liquid phase of $H^{11}B(OCD_3)_2$, and the results are summarized in figure 5. At 147 K, our results are in good agreement with the fast quadrupolar relaxation limit [15] when $\tau_{cp} \geqq T_{1S}$:

$$(T_{2H})^{-1} = (T_{1H})^{-1} + \tfrac{1}{3}S(S+1)A^2T_{1S}(2T_{1S}/t_{cp}) \tanh (t_{cp}/2T_{1S})]$$

where S refers to ^{11}B, $T_{1S} = 6.2 \times 10^{-4}$ sec. and $T_{1H} = 0.2$ sec. from figure 3, $A = 2\pi J$. From our data, we estimate the ^{11}B-H spin-spin coupling constant $J = 170$ Hz, in agreement with the previous high resolution studies [9].

In conclusion, we believe that these results demonstrate that pulsed NMR techniques can, in favorable cases be used to obtain reliable, reasonably accurate values for spin-spin and quadrupole coupling constants in liquids.

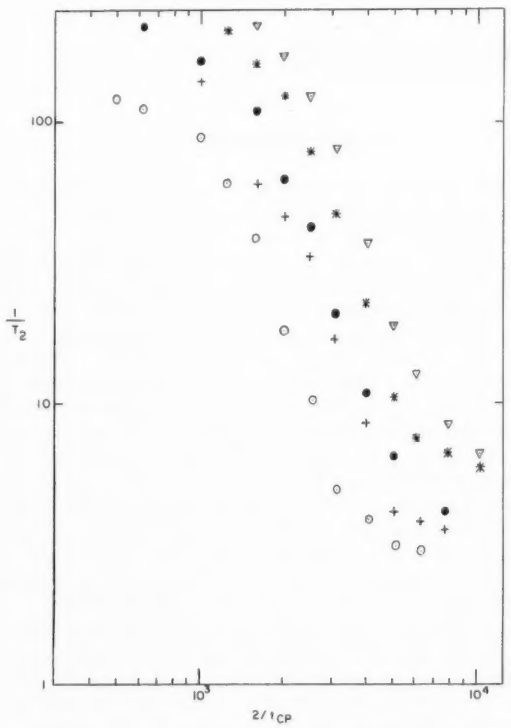

FIGURE 5. $1/T_2$ *versus* $1/t_{cp}$ *for proton in* $H^{11}B(OCD_3)_2$.
198 K, ⊙; 175 K, +; 167 K, ●; F55 K, *; 147 K, ▽.

5. References

[1] Farrar, T. C., Ryan, W., Davison, A., and Faller, J. W., J. Am. Chem Soc. **88,** 184 (1966).
[2] Farrar, T. C., Brinckman, F. E., Coyle, T. D., Davison, A., and Faller, J. W., Inorg. Chem. **6,** 161 (1967).
[3] Vander Hart, D. L., Gutowsky, H. S., and Farrar, T. C., J. Am. Chem. Soc. **89,** 5056 (1967).
[4] Van Vleck, J. H., Phys. Rev. **74,** 1168 (1948).
[5] Sheldrick, G. M., Chem. Comm., 751 (1967); Mol. Phys. **13,** 399 (1967).
[6] Vander Hart, D. L., and Gutowsky, H. S., J. Chem. Phys. **49,** 261 (1968); Vander Hart, D. L., Gutowsky, H. S., and Farrar, T. C., J. Chem. Phys. (to be published, 1969).
[7] Farrar, T. C., Cooper, J., and Coyle, T. D., Chem. Comm. 610 (1966).
[8] Abragam, A., The Principles of Nuclear Magnetism (Clarendon Press, London (1961), pp. 294, 299, 311, 314, 331 and 438; his notation will be followed here in general.
[9] Boden, N., Gutowsky, H. S., Hansen, J. R., and Farrar, T. C., J. Chem. Phys. **46,** 2849 (1967).
[10] Burg, A. B., and Schlesinger, H. I., J. Am. Chem. Soc. **55,** 4020 (1933).
[11] Gutowsky, H. S., Meyer, L. H., and McClure, R. E., Rev. Sci. Instr. **24,** 644 (1953).
[12] Cohen, M. H., and Reif, F., Solid State Physics **5,** 339 (1957); their notation will be followed here in general.
[13] Cuthbert, J. D., MacFarlane, W. T., and Petch, H. E., J. Chem. Phys. **43,** 173 (1965); Lal, K. C., and Petch, H. E., J. Chem. Phys. **43,** 178 (1965).
[14] Powles, J. G., and Figgins, R., Molecular Physics **13,** 253 (1967); Green, D. K., and Powles, J. G., Proc. Phys. Soc. (London) **85,** 87 (1965); Aksnes, D. W., Rhodes, M., and Powles, J. G., Molecular Physics **14,** 333 (1968).
[15] Allerhand, A., and Thiele, E., J. Chem. Phys. **45,** 902 (1966); Alger, T. D., and Gutowsky, H. S., J. Chem. Phys. **48,** 4625 (1968).

(Paper 73A2–544)

JOURNAL OF RESEARCH of the National Bureau of Standards—A. Physics and Chemistry
Vol. 73A, No. 2, March–April 1969

The Effects of Low Energy Irradiation on Organometallics. Organometal Halides of Group IVA[1]

F. E. Brinckman, Gerald F. Kokoszka,[2] and Norman K. Adams, Jr.

Institute for Materials Research, National Bureau of Standards, Washington, D.C. 20234

(November 27, 1968)

A group of selected group IVA halides of the type $(CH_3)_nMCl_{4-n}$, where $n = 0, 1, 3$ and M = Si, Ge, Sn have been subjected to low-energy irradiation (254 and 370 nm) in the condensed phase at −196 °C. This survey also examined related compounds including $HSiCl_3$, $CH_2ClSiCl_3$, CH_3SiF_3, CH_3SiHCl_2 as well as cocondensed mixtures. It is demonstrated by EPR spectroscopy that these conditions suffice to cleave M—C bonds. By following spectral changes during or following irradiation, as a function of time, it is demonstrated that both primary and secondary reactions occur. Some general features of the spectra are discussed and certain conclusions are projected to additional studies on low temperature reactions in 1:1 cocondensed mixtures of organometal halides. Some preliminary supporting evidence from mass spectrometric observations is discussed.

Key words: EPR; free radicals; germanium; irradiation; low-temperature reaction; organometallic compounds; silicon; tin.

1. Introduction

Numerous examples of organic free radicals arising from organometallic compounds have been shown by various spectroscopic techniques [1][3]; however, relatively few data are presently available concerning those radicals produced from organometal halides [2a]. This class of compounds is particularly interesting to us since under suitable conditions of excitation its members might serve as precursors to reactive organic, inorganic, or organometallic radical species whose existence is suggested from bulk product characterization in a variety of decomposition reactions.

In addition, considerable data are available on organic free radicals in the solid state. The review by Morton [3] discusses some of the studies on single cyrstals and the recent book by Atkins and Symons [4] also covers references in this area. The general electron paramagnetic resonance properties of this class of radicals have been known for some time. More recently a number of studies have been reported which characterize essentially inorganic free radicals [3, 6]. Often these studies are carried out on rather small quantities of the parent material imbedded in a rare gas matrix. Such conditions are generally believed to be important since they produce a reasonably isotropic local environment which fosters rapid rotation of the molecular fragments. This situation is desirable since a rapidly rotating radical generally is characterized by relatively narrow electron paramagnetic resonance lines which often aid in the identification of the radical.

High-energy irradiation sources seem to predominate in the study of radicals; often γ-irradiation is a convenient source while x-ray irradiation has also been widely used. The utilization of relatively low-energy sources does not seem to have been widely exploited. It appeared that consideration should be given to this technique since low-energy irradiation might be expected to disrupt the parent material much less than higher energy sources with fewer bonds cleaved and/or fragments ionized. This should result in fewer, relatively simpler species which might be more easily characterized. Further, when more complicated spectra arise it may be possible to identify the nature of the reaction. In this connection, the interesting work of Roncin [2b] deserves comment. Some of the systems which we have investigated using low energy irradiation have been simultaneously investigated by Roncin with γ irradiation. This higher energy source has produced some additional radicals which we do not observe, but this work bears a complementary relation to the work discussed in the present paper.

As a part of a more general study dealing with free radicals incorporating elements other than carbon [5], we have recently turned to an investigation of the consequences of low energy irradiation of polycrystal-

[1] Portions of this work were presented at the Symposium on Organometallic Radicals, Am. Chem. Soc., 153rd Nat'l. Mtg., Miami Beach, Fla., April 1967.
[2] Present address: Dept. of Chemistry, State Univ. of N.Y., Plattsburgh, N.Y. 12901.
[3] Figures in brackets indicate the literature references at the end of this paper.

line organometallic halide substrates. These studies have been carried out chiefly at liquid nitrogen temperature. Our principal interest was to gain information about the nature of bond cleavage in these compounds when they are subjected to low energy irradiation. In organometal halides such as we are considering here low symmetries in the condensed phase, and the expected comparative immobility of large halometalloid radicals, such as that recently described [7] for $\cdot SiCl_3$ below -150 °C, encouraged our starting point at liquid nitrogen temperature. In this way, concurrent small, possibly mobile, but hopefully rotating species could be identified, and ultimately the more complex spectral elements associated with large fragments could be characterized under a variety of conditions.

Once the comparative modes of fragmentation in these compounds have been ascertained, this knowledge could be used to obtain a wide variety of new radicals by properly selecting the appropriate isolation matrix and/or the correct temperature. Our studies along these lines will be the subject of a future paper. For the present survey purposes we have chosen the stated conditions so as to minimize complicating spectral features since the parent compounds are, by choice, rather complex molecules.

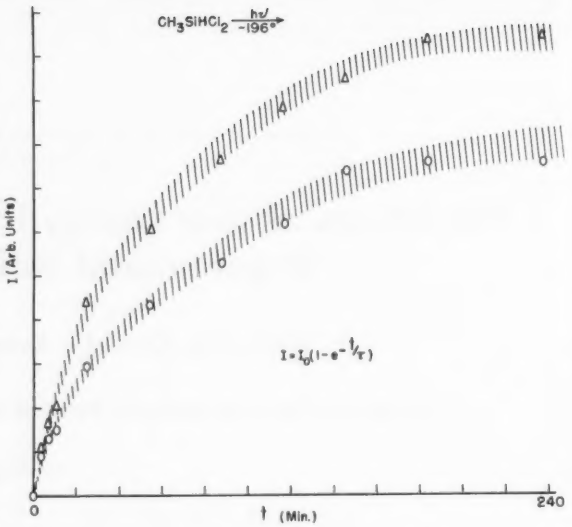

FIGURE 1. *Build up curve for* CH_3SiHCl_2.
Upper curve developed from central component, lower curve developed from sum of two outer peak intensities. Vertical hatch marks represent maximum estimated uncertainty, in intensity.

2. Experimental Procedures

2.1. Organometal Halides

All compounds studied were obtained from commercial suppliers or synthesized by literature methods in this laboratory. Purification and other manipulations were accomplished in an efficient recirculating drybox and a conventional high-vacuum system. Purity is estimated (by infrared spectra, vapor pressure, NMR spectra) at about 99 percent with obvious contaminants (i.e., HCl, oxygen) absent prior to sealing off in vacuo at -196 °C in 4 mm O.D. fused silica tubes. The 1:1 cocondensed samples were frozen into sample tubes at a slow rate from low pressure gas mixtures.

2.2. Electron Paramagnetic Resonance

The EPR data were obtained at liquid nitrogen temperature with an X-band spectrometer. The cavity was equipped with irradiation slots allowing a continual monitoring of the EPR signal as a function of time for continuous irradiation. In general the rate of build up of spectral intensity followed first-order kinetics, namely $I = I_0(1-e^{-t/\tau})$. In this expression, I_0 represents the intensity expected with $t \to \infty$ and τ is a characteristic time which is a function of the experimental configuration. In these experiments, τ was in the range of 20 min to 100 min, thus allowing adequate data to be gathered in a single day. A typical build up curve is shown in figure 1. The sample is CH_3SiHCl_2 irradiated by the commercial high-pressure 200 W mercury lamp (300–600 nm with λ max $\approx$ 370 nm) used in all of these experiments. Since no change in line width of the spectra was observed over the period indicated in the figure, it is sufficient to plot the peak height. The width of the lines represents the maximum estimated uncertainty in intensity.

Samples which were studied over longer periods were initially irradiated by the high pressure mercury lamp for a period of about 4 hr. The EPR spectrum was then immediately obtained. The samples were stored at liquid nitrogen temperature and examined every 24 to 48 hr in most cases. The day-to-day reproducibility of a comparison sample of DPPH was better than 8 percent with relatively little special care and it is assumed that this sort of peak height reproducibility is also characteristic of the organometallic samples.

2.3. Macro-Irradiation of Methyldichlorosilane

One additional experiment with CH_3SiHCl_2 utilized a small ultraviolet source (2.5 W with 92% at 253.7 nm) in conjunction with an analytical mass spectrometer $\left(180°\text{ single-focusing, magnetic scan, resolution} = \frac{M}{\Delta M} \geq 250\ [8]\right)$ for determining non-condensible products formed during photolysis at -196 °C. The apparatus used provided insertion coaxially of the ultraviolet probe lamp into a borosilicate glass sample tube, achieving a vacuum-tight seal with polyfluorocarbon O-ring joints. This arrangement permitted a purified sample of CH_3SiHCl_2 (*ca.* 1 mmol) to be condensed directly from the high-vacuum line as a thin film on the walls of the sample tube. Following this, the apparatus was valved off (polyfluorocarbon valve stopcocks only) and then attached to the mass spectrometer in a direct inlet mode while the sample was maintained at -196 °C. Examination of background gases ($2–3 \times 10^{-8}$ torr) in this irradiation setup indicated only traces of

N_2 ($m/e = 28$) greater (~ 15 scale divisions) than baseline noise (2–3 scale divisions).

Within several minutes of turning on the ultraviolet lamp, appreciable amounts of H_2 ($m/e = 2$) formed, reaching a maximum value (~ 330 scale divisions, $\sim 1 \times 10^{-7}$ torr) in 40–50 min followed by diminution of H_2 as starting material reacted. An evaluation of comparable formation of noncondensible CH_4 ($m/e = 15$–16) maxima revealed in several runs the same pattern of rapid, dominant H_2 production over that of CH_4.

3. Results

3.1. Methylchlorometallic Compounds

The compounds chiefly studied were of the group $(CH_3)_nMCl_{4-n}$ for $n = 1$ and 3 and M = Si, Ge, and Sn. A number of additional compounds such as CH_3SiF_3, $CHCl_2SiCl_3$, $(CH_2Cl)SiCl_3$, CH_3SiHCl_2 and a number of mixtures (vide infra) were also irradiated under comparable conditions in order to assess limits of the low-energy method. With one notable exception (see para. 3.2), in all compounds containing a CH_3 moiety, evidence for the formation of methyl radical was unambiguous [9]. The four-line pattern with relative intensities in the ratio of about 1:3:3:1, the separation between the four components of about 23×10^{-4} T and the g-value close to the spin-only value are the characteristics of this well-known radical species. The peak-to-peak linewidth varied slightly from precursor to precursor but the range from 1 to 4×10^{-4} T easily included them all. Data were usually obtained using a modulation amplitude somewhat larger than these values in order to maximize the signal-to-noise ratio. The magnetic parameters for the methyl radicals produced from the various sources are listed in table 1. No dramatic change in the g or A values is noted as the host lattice is changed. It seems likely that the small rapidly rotating methyl radical is trapped on surfaces or in vacancies in the lattice or any other place where a sufficiently large hole is available.

TABLE 1. *Summary of magnetic parameters for* CH_3MCl_3 *and* $(CH_3)_3MCl$ [a]

	g	H_{pp} [b]	A [b]
CH_3SiCl_3	2.0025	3.2	22.8
CH_3GeCl_3	2.0036	2.9	23.3
CH_3SnCl_3	2.0033	4.7	22.6
CH_3SiF_3	2.0030	4.6	23.1
$(CH_3)_3SiCl$	2.0032	4.3	22.7
$(CH_3)_3GeCl$	2.0031	4.4	23.0
$(CH_3)_3SnCl$	2.0032	3.4	22.7

[a] The uncertainties in the g values are estimated to be less than 0.0003 and for the A values and for H_{pp}, the peak-to-peak line width, less than 0.3×10^{-4} T.
[b] The units for H_{pp} and A are 10^{-4} T.

3.2. Special Case of Methyldichlorosilane

A compound excepted from the general trend of CH_3 production is CH_3SiHCl_2 where simple Si—C fission cannot explain the triplet spectrum observed with components separated by $\sim 20 \times 10^{-4}$ T. That the observed result stems from rapid secondary or competitive processes involving *both* Si—C and Si—H bonds was considered in the macro-irradiation experiment, and the interesting apparent [4] dominance of H_2 production over CH_4 definitely requires consideration of an additional consecutive mechanism involving possibly *both* H—C and Si—H bonds [10]. Thus, if we assume initial Si—C cleavage analogous to that of CH_3SiCl_3

$$CH_3SiHCl_2 \xrightarrow{h\nu} CH_3\cdot + \cdot SiHCl_2$$

and the $CH_3\cdot$ is sufficiently mobile to immediately abstract a proton from a nearby parent molecule [2], several reaction courses are possible:

$$CH_3\cdot + CH_3SiHCl_2 \xrightarrow{(1)} CH_4 + CH_3\dot{S}iCl_2$$

$$\xrightarrow{(2)} CH_4 + \cdot CH_2SiHCl_2, \text{ as well as}$$

$$\xrightarrow{(3)} C_2H_6 + \cdot SiHCl_2.$$

Although reaction (3) would appear unlikely, some mass spectrometric evidence was obtained suggesting presence of small amounts of C_2H_6 ($m/e = 29$–30) on slight warming of sample (5×10^{-7} torr). Reaction (2) seems least likely in view of rather slow diminution of $CH_3\cdot$ from analogous CH_3SiCl_3.

However, since H_2 is rapidly formed during photolysis an alternate explanation is necessary for its production which also explains the absence of $CH_3\cdot$ quartet:

$$\text{initiation: } CH_3SiHCl_2 \xrightarrow{h\nu} CH_3\dot{S}iCl_2 + H\cdot$$

$$\text{propagation: } H\cdot + CH_3SiHCl_2 \xrightarrow{(4)} \cdot CH_2SiHCl_2 + H_2$$

$$\xrightarrow{(5)} CH_3\dot{S}iCl_2 + H_2$$

$$\xrightarrow{(6)} H\dot{S}iCl_2 + CH_4$$

Reactions (4) and (6) are preferred since these explain not only the observed H_2 and CH_4 production, but also (4) offers a reasonable radical species giving rise to a triplet spectrum (vide infra).

3.3. α-Chloromethylchlorosilanes

The compound $CH_2ClSiCl_3$ produced a three-line pattern with relative intensities 1:2:1. The separation

[4] While $CH_3\cdot$ production rate could even exceed that of $H\cdot$, relative mobilities of $H\cdot$ or H_2 and $CH_3\cdot$ or CH_4 in the host lattice followed by degassing under these experimental conditions are not known, hence only an "apparent" difference is suggested.

between the components was about 18×10^{-4} T and the outer two components were somewhat broader than the inner one. This pattern is assigned to the radical $CH_2Cl\cdot$ where chlorine structure is not resolved. This result is also consistent with the hypothesis that the primary cleavage is that of the carbon-silicon bond. A further test of this idea might be exemplified by irradiation of $CHCl_2SiCl_3$, where in the most obvious process the α-proton radical $CHCl_2$ should afford a *two*-line spectrum, consistent with our earlier observations. However, to date experimental results have not yielded results as conclusive as in the $CH_2ClSiCl_3$ case.

3.4. General Trends

For those neat organometal chlorides producing methyl radicals on irradiation, examination of the spectral features seen in addition to the $\cdot CH_3$ quartet permits classification of each parent compound into one of three distinct modes of behavior. The first group is characterized by the irradiation products of $(CH_3)_3GeCl$ and $(CH_3)_3SiCl$. In both of these cases, a seven-line pattern seems to be the dominant spectral feature in addition to the methyl signal. The patterns in both cases are nearly identical with $A \approx 17 \times 10^{-4}$ T and an example of $(CH_3)_3SiCl$ is shown in figure 2. An additional residual component may also be present in the $(CH_3)_3SiCl$ spectrum since the central peak is enhanced over that of the Ge analog.

A typical representative of the second group is provided by irradiation of CH_3GeCl_3. The spectrum obtained from this compound on the first day consists essentially of the four-line $CH_3\cdot$ pattern with no underlying components apparent, while that obtained on the ninth day after irradiation is shown in figure 3. Over this period of time the intensity of the methyl radical signal was roughly constant while the additional spectral components built up according to the rate law previously mentioned with a characteristic

FIGURE 2. *EPR spectra obtained from irradiated* $(CH_3)_3SiCl$ *as a function of time.*

time (τ) of about three days. A similar time-intensity relationship was also observed after irradiation of CH_3SnCl_3 or $(CH_3)_3SnCl$.

A third mode of behavior is represented by only a single compound, CH_3SiCl_3. Following irradiation of this material as a function of time, the methyl signal decays over a period of days revealing an underlying triplet pattern not dissimilar to that of CH_3SiHCl_2. Figure 4 shows typical spectra obtained immediately after irradiation and 18 hr after irradiation.

FIGURE 3. *EPR spectrum of* CH_3GeCl_3 *obtained on ninth day after irradiation.*

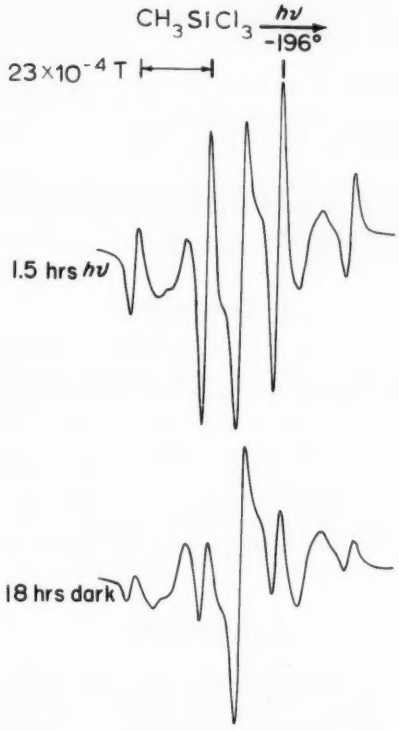

FIGURE 4. *EPR spectra obtained from irradiated* CH_3SiCl_3 *as a function of time.*

3.5. Irradiation of Mixtures

Since our experience with photolysis of CH_3SiHCl_2 indicated both primary and secondary processes might involve either Si—C or Si—H scission, a number of experiments emphasizing intermolecular processes were conducted (table 2). If the idealized 1:1 cocondensates afforded sufficient homogeniety, a possibility of processes uncharacteristic of either addend might ensue, indicative of the new reaction course(s) available. Table 2 summarizes our results compared with additive or no interaction behavior.

4. Discussion

The evidence presented in the previous section strongly indicates that the primary process which occurs upon irradiation is the cleavage of the metalloid-carbon. In this connection, we might also note that no radicals were observed when the halides MCl_4 (M = Si, Ge, or Sn) were irradiated under comparable conditions. The results with the compounds in the second group, as typified by CH_3GeCl_3, further suggest that secondary processes might be quite important in producing noticeable spectral changes over comparatively brief periods of time.

The results on the compounds in category one may be rationalized in terms of a rather simple scheme

$$(CH_3)_3MCl \xrightarrow{h\nu} \cdot CH_3 + (CH_3)_2\dot{M}Cl \qquad M = Si, Ge.$$

The dimethylchloro-silyl or -germyl radical would be expected to produce a symmetric seven-line pattern if the unpaired electron primarily interacts equivalently with the protons in the two methyl groups [11]. The remaining four-line pattern is associated with the methyl radical. As a function of time, spectral features associated with the larger radical alter very slowly compared to the methyl radical spectral decay pattern. Indeed, in the germanium compound the methyl signal is very small even after the first day. This suggests the possiblity of secondary recombination reactions, perhaps between two methyls excluding the larger metalloid-containing radicals. The decay of the signal associated with methyl radicals as a function of time is no doubt affected by a number of reactions.

In the second group, the evidence for secondary processes is more pronounced. The initial M—CH_3 cleavage results in the production of methyl radicals while the assumed $GeCl_3$ radical is not likely to be freely rotating and thus no sharp line spectrum is expected. The absence of a spectrum due to this species is not surprising when the results of Leray and Roncin [7] are taken into account. The growth of a secondary spectrum as a function of time, while the methyl spectrum remains essentially constant in intensity, suggests a process involving the $GeCl_3$ species. Two possible mechanisms can be illustrated:

TABLE 2. *Reactions of mobile radicals in "mixed" systems*

	Source	Result expected if no interaction	Result observed
(1)	CH_3SiHCl_2	$CH_3\cdot$ or possibly $H\cdot$	No $CH_3\cdot$, no $H\cdot$, triplet component.
(2)	CH_3SiCl_3 + $HSiCl_3$ 1:1	$CH_3\cdot$, $H\cdot$ unlikely, triplet from $\cdot CH_2Si\leqslant$	No $CH_3\cdot$, no $H\cdot$, anisotropic spectrum similar to CH_3GeCl_3 and CH_3SnCl_3.
(3)	CH_3GeCl_3 + $HSiCl_3$ 1:1	$CH_3\cdot$, $H\cdot$ unlikely, anisotropic spectrum underlying.	Very small $CH_3\cdot$ component, no $H\cdot$ anisotropic CH_3GeCl_3 spectrum.

$$CH_3GeCl_3 \xrightarrow[-196\,^\circ C]{h\nu} CH_3\cdot + \cdot GeCl_3$$

$$\cdot GeCl_3 + CH_3GeCl_3 \xrightarrow{(1)} HGeCl_3 + \cdot CH_2GeCl_3$$
$$\xrightarrow{(2)} GeCl_4 + CH_3\dot{G}eCl_2$$

The anisotropic nature of the spectrum and the lack of any clear cut proton hyperfine interaction, particularly when the parent material is $(CH_3)_3SnCl$ indicates that mechanism (2) is more realistic, but no definite assignment is proposed at this time. This view is further borne out by observations with the last group.

The results for CH_3SiCl_3, the only example in the third category, are consistent with proton abstraction by the methyl radicals on neutral CH_3SiCl_3 to produce CH_2SiCl_3. This process is similar to that described by Kerr, Slater, and Young in the gas phase [2a]. The time-intensity curves indicated that additional recombination process may also be present. For comparative purposes, we wish to point out some of the differences noted by Roncin [2b] in his investigations with γ-irradiation. With trimethylchlorosilane, the $CH_2(CH_3)_2SiCl$ radical is somewhat similar to the radical CH_2SiHCl_2 radical discussed earlier in this paper and believed to be formed by a slower secondary reaction. In methyltrichlorosilane Roncin observed $\cdot CH_2SiCl_3$ and $\cdot SiCl_3$ in a ratio of 2.5 to 1 and in tetramethylsilane the radical $CH_2Si(CH_3)_3$ is found. This points out the greater importance of initial C—H and Si—Cl bond cleavage at the higher energies.

The importance of these trends is amplified by some preliminary studies on cocondensed 1:1 mixtures. As noted previously, CH_3SiCl_3 produces a strong methyl signal and somewhat weaker triplet spectrum immediately upon irradiation. No spectrum is observed when $HSiCl_3$ is irradiated under comparable conditions. However, when the two materials are cocondensed and irradiated neither the methyl nor the triplet spectrum is observed. Rather, an anisotropic spectrum somewhat similar to that obtained in CH_3GeCl_3 after nine days is observed.

Similarly for $CH_3GeCl_3 + HSiCl_3$ a nonadditive spectrum occurs, and again as with the two previous cases noted in the table very considerable depletion or absence of $CH_3\cdot$ is obtained. Presently it is consistent to presume intermolecular processes occur, initiated by M—CH_3 cleavage:

$$CH_3MCl_3 \longrightarrow CH_3\cdot + \cdot MCl_3 \quad (M = Si, Ge), \text{ and}$$

$$CH_3\cdot + HSiCl_3 \longrightarrow CH_4 + \cdot SiCl_3.$$

Future efforts will thus be directed to evaluating possible CH_4 production by the mass spectrometric method described in this paper.

5. Conclusions

The irradiation of organometallic compounds has demonstrated that only low energy irradiation is required to break the M—C bond. By following the spectral changes as a function of time it has been demonstrated that primary and secondary processes can both be important at liquid nitrogen temperature. Furthermore, the importance of low temperature reactions in order to produce new or novel compounds or radicals has been suggested by the studies of cocondensed mixtures.

6. References

[1] Friswell, N. J., and Gowenlock, B. G., Advances in Free Radical Chemistry, Vol. **1**, p. 39, G. H. Williams, ed. (Academic Press, N.Y., 1965).

[2a] Kerr, J. A., Slater, D. H., and Young, J. C., J. Chem. Soc. (A) **1966** 104.

[2b] Roncin, J., Mol. Cryst. **3**, 117 (1967).

[3] Morton, J. R., Chem. Rev. **64**, 453 (1964).

[4] Symons, M. C. R., and Atkins, P. W., Inorganic Free Radicals (American Elsevier Press, N.Y. 1967).

[5] Kokoszka, G. F., and Brinckman, F. E., Chem. Comm. **1968**, 349.

[6] Fessenden, R. W., and Schuler, R. H., J. Chem. Phys. **45**, 1845 (1966).

[7] Leray, N., and Roncin, J., J. Chem. Phys. **42**, 800 (1965).

[8] Ten percent valley definition. See J. H. Beynon, Mass Spectrometry and Its Applications to Organic Chemistry, p. 51–54 (Elsevier Publ. Co., Amsterdam, 1960).

[9] Shrader, D. M., J. Chem. Phys. **46**, 3895 (1967) and references cited therein.

[10] Nay, M. A., Woodall, G. N. C., Strausz, O. P., and Gunning, H. E., J. Amer. Chem. Soc. **87**, 179 (1965).

[11] See for example, Tench, A. J., J. Chem. Phys. **38**, 593 (1963) and references cited therein.

(Paper 73A2–545)

JOURNAL OF RESEARCH of the National Bureau of Standards—A. Physics and Chemistry
Vol. 73A, No. 2, March–April 1969

Measurements of Gaseous Diffusion Coefficients by a Gas Chromatographic Technique

S. P. Wasik and K. E. McCulloh

Institute for Materials Research, National Bureau of Standards, Washington, D.C. 20234

(November 1, 1968)

A method is presented for measuring gaseous diffusion coefficients using a gas chromatographic technique. Diffusion coefficients were measured for the systems: argon, krypton, oxygen, and nitrogen diffusing into helium at temperatures from 77 to 400 K.

Key words: Argon; diffusion coefficient; gas chromatography; helium; krypton; nitrogen; oxygen.

1. Introduction

Accurate knowledge of molecular diffusion coefficients and their temperature dependence is important in obtaining fundamental information on forces between unlike molecules. Until recently most diffusion measurements were conducted over short temperature intervals because the conventional methods such as the Loschmidt or the Stefan, require the thermostating of large, static systems. Walker and Westenberg [1][1] have developed a method which involves measuring concentration profiles downstream of a point source of tracer gas in a uniform laminar jet of carrier gas. Diffusion coefficient for permanent gas pairs over a temperature interval 300 to 1100 K have been measured using this technique.

Determining diffusion coefficients using gas cromatographic techniques is relatively new. Taylor [2] derived an expression for the radial diffusion term for a liquid dispersion flowing in a tube. The same expression was derived by Giddings [3] and Golay [4] as a special case of a general theory of gas chromatography. Giddings and Seager [5] have measured diffusion coefficients using this method.

The method reported in this paper is also based on gas chromatography techniques. In brief, a trace amount of one gas was injected into a carrier gas stream of different composition flowing through a column at a constant flow rate. The concentration profile of the gas dispersion was determined at two points downstream from the point of sample injection by thermal conductivity detectors. The binary diffusion coefficients were calculated from the dimensions of the recorded peaks and time required for the peak maximum to travel the distance between the two detectors.

Diffusion coefficients were measured for the systems: argon, krypton, oxygen and nitrogen diffusing into helium at temperatures from 77 to 400 K.

2. Theoretical

2.1. Fundamental Relations

As has been shown by theoretical studies [2, 3, 4] when a nonuniform gaseous dispersion flows through a cylindrical tube, the effect of radial diffusion acting in conjunction with the parabolic velocity profile is accounted for by an effective longitudinal diffusion coefficient α^2, given by

$$\alpha^2 = D + \frac{1}{48}\frac{v^2 a^2}{D}, \tag{1}$$

where v is the mean flow velocity, a is the inside radius of the tube, and D is the diffusion coefficient. If c represents the mean concentration in a cross section at distance x from the moving centroid of the dispersion (x is taken positive downstream from the centroid) then c satisfies the one-dimensional diffusion equation

$$\frac{\partial c}{\partial t} = \alpha^2 \frac{\partial^2 c}{\partial x^2}. \tag{2}$$

First let us assume an ideal system in which the experiment is initiated by instantaneous injection at time $t=0$ of n moles of diffusing substance into the carrier gas stream at a fixed injection point, and

[1] Figure in brackets indicate the literature references at the end of this paper.

further assume that the external parameters affecting the flow (e.g., temperature, pressure, and tube radius) are all constant. Equation (2) applies after a time which is long compared with a^2/D. Its solution appropriate to these initial conditions is given by

$$c=\frac{n}{\pi a^2}\frac{1}{2\alpha\sqrt{\pi t}}e^{-x^2/4\alpha^2 t} \tag{3}$$

Equation (3) defines a concentration distribution which is instantaneously Gaussian and spreading with time. In the actual system the assumption of constant flow parameters applies only to the diffusion column proper. However, the experimental system was designed such that the concentration distribution was always instantaneously Gaussian within the diffusion column. Equation (3) can be applied under these conditions if the zero of time is redefined. Instead of taking $t=0$ as the instant of sample injection, it must be so defined that eq (3) is consistent with an analysis of the peaks recorded from two or more separate detectors along the tube.

Equation (3) expresses concentration in terms of a frame of reference that moves with the mean velocity of the carrier gas stream. In order to express concentration as a function of time at a fixed detector, we must transform eq (3) by means of the relation

$$x=v(t_0-t), \tag{4}$$

where t_0 is that time at which the centroid of the dispersion arrives at the detector. When we make this substitution, the concentration at a fixed detector is given by

$$c=\frac{n}{\pi a^2}\frac{1}{2\alpha\sqrt{\pi t}}e^{-v^2(t_0-t)^2/4\alpha^2 t} \tag{5}$$

2.2. Peak Analysis

Assuming linear detector response, the height h of a recorder trace of the signal at time t is proportional to c as expressed by eq (5). If h_0 is the height at time t_0, it follows from eq (5) that

$$t\ln\frac{\sqrt{t_0}h_0}{\sqrt{t}h}=\frac{v^2}{4\alpha^2}(t_0-t)^2. \tag{6}$$

From this equation it is seen that a straight line with the slope $v^2/4\alpha^2$ should be obtained when

$$t\left(\ln\frac{h_0}{h}+\frac{1}{2}\ln\frac{t_0}{t}\right)$$

is plotted versus $(t_0-t)^2$. Such a plot is useful for demonstrating that the peak shape conforms to theory. However, for determining the diffusion coefficient an approximation based on eq (6) is easier to apply while providing sufficient accuracy.

This approximation can be derived by introducing the characteristic diffusion distance s defined by

$$s=\alpha\sqrt{t_0}, \tag{7a}$$

the dimensionless variable η defined by

$$v(t-t_0)=2\eta s, \tag{7b}$$

and the small dimensionless parameter ϵ defined by

$$s=\epsilon v t_0. \tag{7c}$$

When eq (6) is rewritten in terms of ϵ and η, the result is

$$(1+2\epsilon\eta)\left[\ln\frac{h_0}{h}-\frac{1}{2}\ln(1+2\epsilon\eta)\right]=\eta^2 \tag{8}$$

Since ϵ is small (typically, $\epsilon^2<10^{-3}$), eq (8) can be expanded in powers of ϵ. Neglecting powers higher than the second,

$$(1+\epsilon^2)\eta^2-\epsilon\left(2\ln\frac{h_0}{h}-1\right)\eta-\ln\frac{h_0}{h}\cong 0.$$

This equation is quadratic in η. Let $\Delta\eta$ be the difference of its two roots. Expanding $\ln\frac{h_0}{h}$ as a power series in ϵ^2, the solution of eq (8), correct through terms in ϵ^2, can be written

$$4\ln\frac{h_0}{h}=(\Delta\eta)^2+\epsilon^2[2(\Delta\eta)^2-\frac{1}{4}(\Delta\eta)^4-1]. \tag{9}$$

Taking typical values for ϵ and $\Delta\eta$ (typically, $\Delta\eta^2<10$), it can be readily seen that all but the first term on the right side of this equation can be neglected when accuracy to a few parts per thousand is adequate. If we let Δt represent the width of the recorder trace at height h, we can make use of eqs (7a) and (7b) to write

$$\Delta\eta=\frac{v}{\alpha\sqrt{t_0}}\frac{\Delta t}{2}.$$

Substituting in eq (9) and retaining only the first term on the right we obtain the approximation

$$t_0\ln\frac{h_0}{h}=\frac{v^2}{4\alpha^2}\left(\frac{\Delta t}{2}\right)^2. \tag{10}$$

If $t_0\ln\frac{h_0}{h}$ is plotted versus $\left(\frac{\Delta t}{2}\right)^2$, it is seen that a straight line with the slope $v^2/4\alpha^2$ should be obtained. This plot should superimpose accurately on that based on eq (6). It is obvious that eq (10) is easier to apply in determining α.

Since t_0, the time of arrival of the peak at a detector, appears on the left in eq (10), it is still necessary to define the zero of time. The difference of the t_0 values

at two detectors along the tube can be measured directly. Their ratio can be obtained by applying eq (10) to each of the detectors. Solving for the two t_0 from their difference and their ratio is equivalent to determining the effective zero of time.

Another method which, although tedious, yields α with good precision because random fluctuations in the recorder signal are smoothed by integration, is based on the ratio of peak area to peak height. The equation

$$h = h_0 \sqrt{\frac{t_0}{t}}\, e^{-v^2(t_0-t)^2/4\alpha^2 t}$$

equivalent to eq (6), can be reduced to a standard integral form (7), by the substitution $y^2 = v^2 t/4\alpha^2$, with the result

$$\left(\frac{\int_0^\infty h\,dt}{h_0}\right)^2 = \frac{4\alpha^2\pi t_0}{v^2}. \tag{11}$$

2.3. Experimental Procedure

In figure 1 is shown a schematic drawing of the apparatus. A 150-ft empty 1/4-in O.D. copper column was divided into three equal segments; a thermostatic column, C_1, the diffusion column, C_2, and a third column, C_3, which allowed the carrier gas to come to room themperature before its flow rate was measured by a soap-bubble flowmeter, F. The thermostating and diffusion columns were immersed in liquid nitrogen for the low temperature measurements and an oil thermostat, controlled to ± 0.02 °C, for the other measurements. At the beginning and end of the diffusion column were thermal conductivity detectors, D_1 and D_2, located in line with the incoming gas flow. The detectors, shown in figure 2, were constructed from 1/4-in Tee connectors for tubing in which one arm was cut off to allow the sensing element, a Gow Mac type 9225 filament support (see footnote 2) to be soldered into position so that the sensing element was on the central axis of the diffusion column. The two

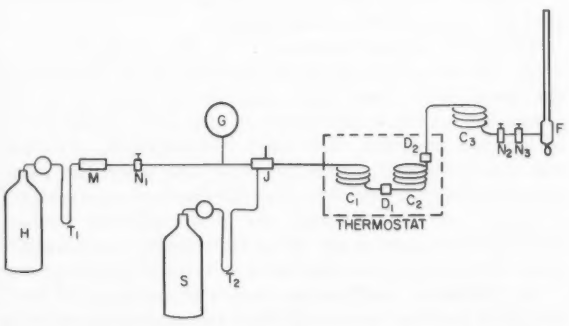

FIGURE 1. *Schematic diagram of flow system for measuring diffusion coefficients.*

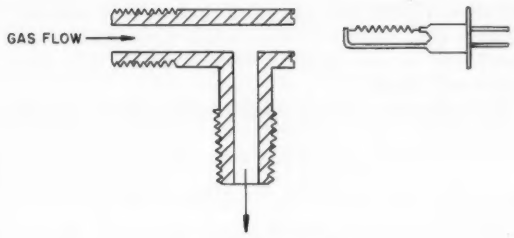

FIGURE 2. *Detector.*

detectors formed adjacent arms of a Wheatstone bridge circuit. The resultant voltages were plotted as a function of time using a 1 mV full scale recorder.

The flow of helium carrier gas from a high pressure tank, H, was controlled by a Moore [6] [2] constant-differential type flow controller, M, a needle valve, N_1, upstream from the diffusion column and two needle valves, N_2 and N_3, downstream from the diffusion column. An 0.1 ml of sample gas from a high pressure tank, S, was injected into the thermostating column by means of a F & M [8] gas injection valve, J. Commercially available gases with a stated purity of better than 99 mole percent were dried by passing them through a molecular sieve column (T_1 and T_2). The column pressure was read from a Wallace and Tiernan [9] absolute aneroid barometer, G.

The effective radius, a, was calculated at room temperature by equating the mass flow rate measured by the soap-bubble meter to the mass flow rate in the diffusion column, $\pi P_c a^2 L/t$, where P_c is the pressure of the carrier gas in atmospheres and t is the time required for an air peak to travel the distance, L, between the two detectors. The value of a agreed within one part in two hundred for all the measurements taken.

For the high and low temperature measurements the mass flow rate in the diffusion column was used to determine the temperature of the carrier gas, the column's dimensions being corrected for thermal expansion. If the carrier gas was not at the temperature of the thermostat the flow rate was reduced until it was.

A preliminary diffusion measurement was made for each system to determine peak heights. The attenuation was then adjusted by means of a 10-turn, 10,000 Ω Heli-pot so that for all the following measurements the peak heights would be the maximum height allowed by the recorder chart paper. Duplicate runs were made by injecting successive amounts of sample gas into the carrier gas stream, the injections being at a time interval such that no overlapping of peaks occurred. At liquid nitrogen temperature, it was possible for as many as four peaks to be in the diffusion column simultaneously. This enables four velocity measurements to be made during the course of a run. The time

[2] Certain commercial materials and equipment are identified in this paper in order to specify adequately the experimental procedure. In no case does such identification imply recommendation or endorsement by the National Bureau of Standards, nor does it imply that the material or equipment identified is necessarily the best available for the purpose.

between peaks was checked with a stop watch. The heights and widths of the peaks were measured to a precision of one part in two hundred fifty with an engineer's scale.

The quantity α^2 was calculated from the expression

$$\alpha^2=\left(\frac{1}{S_2}-\frac{1}{S_1}\right)\frac{v^2}{16(t_{02}-t_{01})} \tag{13}$$

where S_2 and S_1 are the slopes of the ln $H_0/h-(\Delta t)^2$ plots and $(t_{02}-t_{01})$ is the time required for the peak maximum to travel the distance between detectors.

The quantity α^2 was also calculated from

$$\left(\frac{A_2}{h_{02}}\right)^2-\left(\frac{A_1}{h_{01}}\right)^2=\frac{4\alpha^2\pi(t_{02}-t_{01})}{v^2} \tag{14}$$

where A_2 and A_1 are the areas under the second and first peak respectively and v the velocity of the carrier gas in the diffusion column. Equation (14) which follows from eq (11), gave the same values for α^2 as eq (13).

3. Results and Discussion

In figure 3 are shown plots of eqs (6) and (10) for one experiment on the diffusion of nitrogen in helium at 30 psia and 25°. The filled squares represent values calculated from eq (10) for the first peak with t_{01} equal to 23.59 min and the open squares are values obtained from the second peak with t_{02} equal to 48.81 min. The open circles represent values calculated from eq (6) from the leading half of the first peak while the filled circles are those of the leading half of the second peak. The half-filled circles right represent values calculated from eq (6) from the trailing half of the first peak while the half-filled circles left are the corresponding values for the second peak. All experimental points fit the theoretical line within a precision of 0.5 percent.

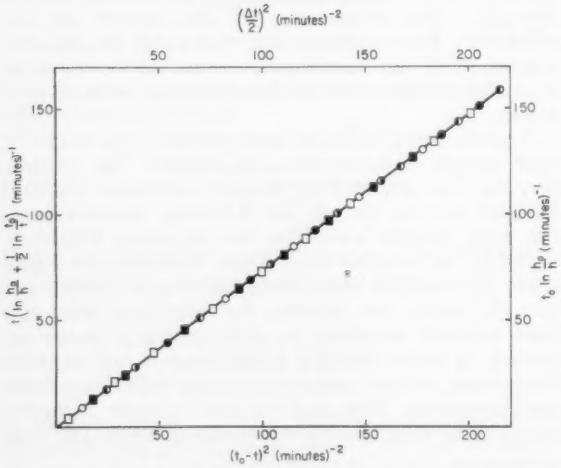

FIGURE 3. *Plot of eqs (6) and (10) for the diffusion of nitrogen in helium at 30 psia and 25 °C.*

There are no indications of skewing or tailing of either peak.

Values for the diffusion coefficients at different temperatures are given in table 1. The pressure of the carrier gas in the diffusion column varied from 1.1 to 1.6 atm for these determinations. These values have been corrected to standard atmospheric pressure. Each diffusion coefficient was obtained as an average of eight separate determinations. The values of 0.732 and 0.688 cm²/s for the diffusion of argon in helium and nitrogen in helium at 25 °C respectively compare favorably with values of 0.725 and 0.688 cm²/s obtained by Walker and Westenberg [1] for the same gas pairs.

TABLE 1. *Effect of Temperature on the Diffusion Coefficient*

Gas pair	Temp. K	D(cm²/s)
He-A	77.2	0.0710 ± 0.0009*
He-A	298	.7335 ± .004
He-A	334	.8890 ± .006
He-A	357	.9917 ± .006
He-N_2	77.2	.0725 ± .001
He-N_2	296	.678 + .005
He-N_2	321	.8171 ± .005
He-N_2	348	.9251 ± .007
He-N_2	370	1.030 ± .006
He-Kr	298	.6491 ± .004
He-Kr	322	.7372 ± .004
He-Kr	341	.813 ± .005
He-Kr	366	.904 ± .006
He-O_2	298	.7361 ± .005
He-O_2	320	.8472 ± .006
He-O_2	365	1.041 ± .008

*90% confidence limits for the mean.

A least square calculation for the expression

$$\log\frac{D_{298}}{D_T}=m\log\frac{298}{T}$$

where D_{298} is the diffusion coefficient at 298 K, D_T is the diffusion coefficient at temperature, T, and m is a constant. The following values for m were obtained with indicated precision being for a 90 percent confidence limit: He-N_2, 1.69 ± 0.02; He-O_2, 1.67 ± 0.06; He-Kr, 1.71 ± 0.06 and He-Ar, 1.72 ± 0.006. These values may be compared with values obtained by Seager, Geerston, and Giddings [5]: He-N_2, 1.75 ± 0.12; He-O_2, 1.70 ± 0.08 and He-Ar, 1.73 ± 0.07. The two sets agree within the given experimental errors. In figure 4 is shown the log diffusion coefficient-log temperature plot for argon diffusing into helium.

There are several advantages to this method.

(a) The use of two detectors instead of one eliminates the need for a zero time correction, since it is not necessary to know the shape of the peak at the point of sample injection. The only requirements are that the concentration profile be Gaussian when the peak reaches the first detector, that the thermal conductivity detectors do not distrub the concentration profile, and that the carrier gas be at thermostat temperature since the sample injection value is at room temperature.

(b) Diffusion coefficients over a wide range of temperature may be measured since the apparatus may be used in a liquid nitrogen bath or in an oven without any change in design.

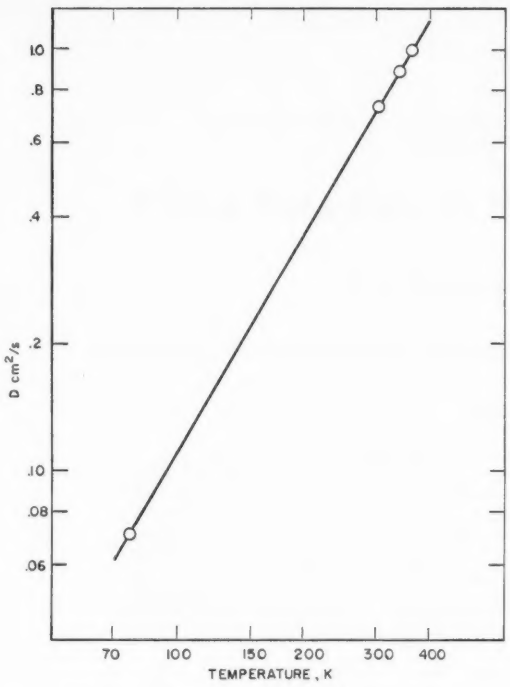

FIGURE 4. *Plot of log diffusion coefficient-log temperature for argon diffusing into helium.*

(c) Time measurements may be made accurately. Since the velocity of the carrier gas appears as a square term in the diffusion equation it is important to be able to measure this quantity accurately. This can be done by measuring the time required for the peak maxima to travel the measured distance between the two detectors. By injecting more than one peak into the diffusion column it is possible to determine whether the velocity of the carrier gas has changed during a measurement.

(d) Deviations of experiment from the assumed model may be determined. Equation (6) provides a means for analyzing the peak for any disturbance due to gas absorption on the walls of the diffusing column or for any disturbance to the concentration profile due to the gas injection and detection systems.

It is conluded that this is a simple, rapid, widely applicable method for the determination of gaseous diffusion coefficients.

4. References

[1] Walker, R. E., and Westenberg, H. A., J. Chem. Phys. **31,** 519 (1959).
[2] Taylor, G. I., Proc. Roy. Soc. **A223,** 446 (1954).
[3] Giddings, J. C., J. Chem. Phys. **26,** 169 (1957).
[4] Golay, M., Gas Chromatography (butterworths, London, 1958), p. 35, (editor, D. H. Desty).
[5] Seager, S. L., Geertson, L. R., and Giddings, J. C., J. Chem. Eng. Data **8,** 168 (1963).
[6] Moore Products Co., Philadelphia, Pa.
[7] Gow-Mac Instrument Co., Madison, New Jersey.
[8] F & M Scientific Corp., Avondale, Pa.
[9] Wallace and Tiernan Inc., Belleville, New Jersey.

(Paper 73A2–546)

JOURNAL OF RESEARCH of the National Bureau of Standards—A. Physics and Chemistry
Vol. 73A, No. 2, March–April 1969

Phase Relations in the Ru-Ir-O_2 System in Air

C. L. McDaniel and S. J. Schneider

Institute for Materials Research, National Bureau of Standards, Washington, D.C. 20234

(November 27, 1968)

The equilibrium phase relations were determined in an air environment for the system Ru-Ir-O_2. In air Ru oxidizes at moderate temperatures, to form RuO_2, which in turn dissociates at 1405 °C. Similarly Ir oxidizes to form IrO_2 and dissociates at 1020 °C. The dissociation of RuO_2 and IrO_2 are reversible processes. A ternary equilibrium phase diagram was constructed indicating selected oxygen reaction lines and isotherms. A binary representation of the Ru-Ir-O_2 system in air is given. Up to 1020 °C, RuO_2 reacts with IrO_2 to form a complete solid solution series having the rutile-type structure. At 1345 °C three solid phases, $rutile_{ss}$, Ru_{ss}, and Ir_{ss}, exist in equilibrium for compositions between approximately 2 and 45 mole percent IrO_2. Above 1405 °C dissociation is complete for all compositions and the phase relations are represented by the Ru-Ir system. At 1500 °C solid solution of Ru and Ir occurs with the addition of up to 45 mole percent Ir and up to 44 mole percent Ru, respectively.

Key words: Dissociation; oxidation; phase relations; Ru-Ir-O_2 system; RuO_2-IrO_2 system; solid solution.

1. Introduction

The present study is part of a program to better understand the behavior of various Pt-group metals heated in an oxidizing environment. Considering the fact that several of these metals are used as secondary standards on the International Practical Temperature Scale (IPTS)[1] [1][2] as well as container materials for high temperature applications, knowledge of the phase relations between these metals, oxygen, and other materials becomes important. This work presents the results of an investigation of the equilibrium relationships between the condensed phases in the system ruthenium (Ru)-iridium (Ir)-oxygen (O_2) in air. Several of the Pt group metals have a strong tendency to oxidize when heated in air at moderate temperatures forming stable condensed phases. At higher temperatures in air, the oxides volatilize and /or dissociate to oxygen and one solid phase, the metal [2].

Even though powdered Ru and Ir oxidize to ruthenium dioxide (RuO_2) and iridium dioxide (IrO_2), when heated in air, complete oxidation is often difficult to obtain. By utilizing RuO_2 and IrO_2 rather than their respective metals as starting materials, an approach to equilibrium could be achieved more readily. The study would still reflect, however, the behavior of the metals in air.

Ruthenium has a hexagonal, magnesium-type structure with $a = 2.7058$ Å and $c = 4.2819$ Å [3]. The freezing point of Ru has been reported as 2280 °C [4]. Ruthenium dioxide, similar to IrO_2 in having the tetragonal, rutile structure, has unit cell dimensions of $a = 4.491$ Å and $c = 3.107$ Å [5]. Upon heating, RuO_2 has been reported to dissociate to Ru metal and a vapor phase at 1540 °C in 1 atm oxygen [6].

Iridium has a face-centered cubic, copper-type structure with $a = 3.8394$ Å [7]. The freezing point of Ir is given as a secondary reference point on the IPTS. The unit cell dimensions of IrO_2 are reported as $a = 4.4983$ Å and $c = 3.1544$ Å [8]. Iridium dioxide dissociates to Ir metal and a vapor phase at 1100 °C in 1 atm oxygen [9] and 1020 °C in air [10].

2. Materials

The starting materials used in this study were found by general quantitative spectrochemical analyses[3] to have the following impurities:

Ru: 0.01–0.1% Pd;
0.001–0.01% each Al, Au, Ca, Cr, Fe, and Pt;
< 0.001% each Ag, Cu, K, Mg. Mn, Na, Pb, Si, and Sn;

RuO_2: 0.01–0.1% each Au, Cr, Pd, Pt, Sn, and Zn;
0.001–0.01% each Al, Ca, Co, Cu, Fe, Mg, Pb, Si, V, and Zr;
< 0.001% each Ag, Ir, and Mn;

[1] This scale (IPTS) applies to all temperatures listed in this paper.
[2] Figures in brackets indicate the literature references at the end of this paper.
[3] The spectrochemical analyses were performed by the Spectrochemical Analysis Section of the National Bureau of Standards.

331-607 O - 69 - 7

Ir: 0.01–0.1% each Pd, Pt, and Si;
0.001–0.01% each Ag, Cu, and Fe;
0.0001–0.001% each Al and Mg;
< 0.0001% Ca;

IrO_2: 0.01–0.1% Pt;
0.001–0.01% each Al, Cu, Fe, Pd, and Si;
0.0001–0.001% Mg;
< 0.0001% Ca.

3. Experimental Procedure

Specimens were prepared from 0.4 g batches of various combinations of the end member oxides. Calculated amounts of each oxide, corrected for ignition loss, were weighed to the nearest milligram. Each batch was thoroughly hand mixed, placed in fused silica tubes (sealed at one end) and fired in a muffle furnace for a minimum of 18 hr at 800 and then at 1000 °C. Following the preliminary heat treatment the materials were again thoroughly hand mixed. Portions of each batch were then fired in a platinum alloy wire-wound quench furnace at various temperatures for different periods of time, again using fused silica tubes as the containers. The specimens were air quenched by quickly pulling the silica tube from the furnace. Equilibrium was assumed to have been achieved when the x-ray pattern showed no change after successive heat treatment of the specimen or when the data were consistent with the results from a previous set of experiments.

Sealed platinum tubes were employed as specimen containers for the experiments requiring prolonged heat treatments at temperatures below the dissociation temperatures. Because of volatility, sealed Pt tubes were sometimes utilized in an attempt to maintain composition and to obtain equilibrium more readily. The use of fused silica tubes instead of platinum, at the higher temperatures, was necessary because the metals, frequently found as decomposition products, readily react with platinum. On the other hand, the silica tube did not appear to influence or react with the various oxide samples.

Temperatures in the quench furnace were measured with a 100 percent Pt versus 90 percent Pt–10 percent Rh calibrated thermocouple. All reported temperatures pertaining to quench furnace data are considered accurate to within ±5 °C. The precision of the measurements was estimated to be ±2 °C.

Several experiments were conducted at 1500 °C with mixtures using the metals as the starting materials. Specimens weighing 0.3 g were thoroughly hand mixed, pressed into pellets, and heat treated in an induction vacuum furnace utilizing an iridium crucible as both the susceptor and specimen container. No change in composition was detected due to the iridium crucible. At 1500 °C the normal operating pressure of the system was nominally 7×10^{-5} torr. Temperatures were measured with a calibrated optical pyrometer sighted through a window in the vacuum enclosure into a small hole in the cricible cover. The susceptor-container acted as the blackbody for temperature measurement. This arrangement achieved measurements estimated to be accurate to within ±25 °C or better.

All specimens were examined by x-ray diffraction at room temperature using a high-angle-recording Geiger counter diffractometer and Ni-filtered Cu radiation.

4. Results and Discussion

The equilibrium phase diagram for the Ru-Ir-O_2 system in air is given in figure 1. The diagram was constructed from the data listed in table 1. The solid circles illustrate the compositions and temperatures of the experiments conducted. The open circles indicate phase boundaries determined from a plot of the unit cell dimensions. In the ternary plot the dashed lines represent oxygen reaction lines and the heavy lines indicate isotherms. The oxygen reaction lines connect the O_2 apex and the final composition attained upon complete dissociation of the oxide mixture. The dissociation products are either Ru_{ss},[4] Ir_{ss},[5] or Ru_{ss} plus Ir_{ss}. It should be emphasized that these dissociation products are the condensed phases of the system and are always in equilibrium with oxygen. Prior to any dissociation, complete solid solution exists between RuO_2 and IrO_2 (rutile solid solution).[6] The isotherms (heavy lines) represent joins for a given temperature for any series of intersecting oxygen reaction lines. The possible equilibrium assemblages may consist of any combination of $rutile_{ss}$, Ru_{ss}, and Ir_{ss}, depending upon the oxygen reaction line under consideration. The isotherms illustrated were arbitrarily chosen except for those which represent the dissociation temperatures of IrO_2 (1020 °C) and RuO_2 (1405 °C) and that indicating the temperature at which three phases coexist (1345 °C).

Proper interpretation of the diagram can best be accomplished by example. Consider for instance a 50:50 mole percent mixture on the RuO_2-IrO_2 join (25 mole percent Ru: 25 mole percent Ir: 50 mole percent O_2). At all temperatures below approximately 1090 °C, the mixture contains only one solid phase, rutile solid solution ($rutile_{ss}$). As this single phase is heated to higher temperatures, oxygen loss occurs, producing a situation in which two or three solid phases are in equilibrium for a given temperature. These equilibrium assemblages always contain at least one reduced phase, a metal. By following the oxygen reaction lines in figure 1, the specific phases in equilibrium can be established. The oxygen reaction line for the 50:50 mole percent composition is seen from figure 1 to cross a number of isotherms. The intersection of these isotherms with the RuO_2-IrO_2 and Ru-Ir joins indicates the compositions of the phases in equilibrium. At 1100 °C, for example, an original $50RuO_2$:$50IrO_2$ mole percent composition

[4] Ru_{ss} = ruthenium solid solution having hexagonal structure (Ru_xIr_{1-x}).
[5] Ir_{ss} = iridium solid solution having cubic structure (Ir_xRu_{1-x}).
[6] $Rutile_{ss}$ = solid solution phases having rutile-type structure ($Ru_xIr_{1-x}O_2$).

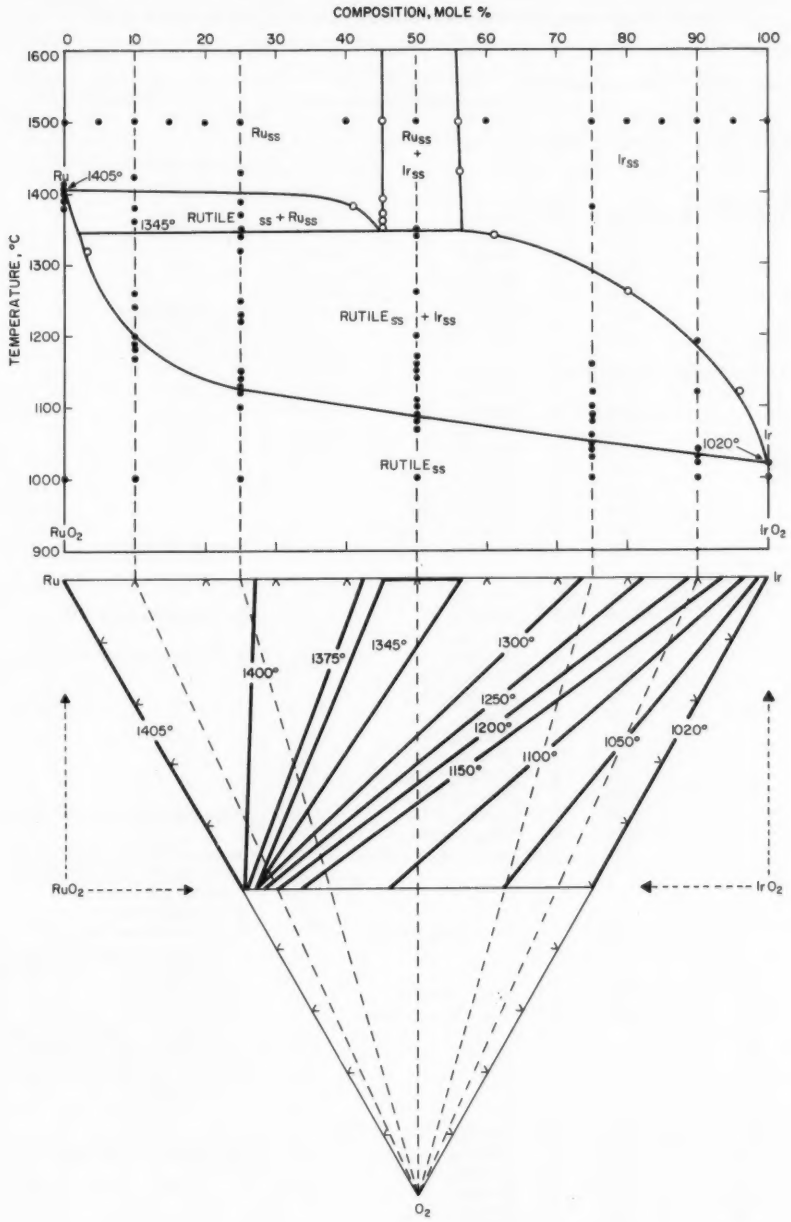

FIGURE 1. *Phase equilibrium diagram for the* Ru-Ir-O_2 *system in air.*

Dashed lines represent oxygen reaction lines. Heavy lines indicate isotherms. ● – compositions and temperatures of experiments conducted. ○ – phase boundaries determined from a plot of the unit cell dimensions, ss – solid solution. $Rutile_{ss}$ – phases having rutile-type structure ($Ru_xIr_{1-x}O_2$).

TABLE 1. *Experimental data for compositions in the* Ru-Ir-O_2 *system in air*

Composition		Heat treatment [a]		X-ray diffraction analyses [b]	Remarks
RuO_2	IrO_2	Temp.	Time		
mole %	*mole %*	*°C*	*hr*		
100	0	1000	18	RuO_2	
		[c] 1000	20	RuO_2	Quenched in ice water.
		1375	2	RuO_2	
		1385	2	RuO_2	
		1400	2.5	RuO_2	
		1405	2	$RuO_2 + Ru$	Nonequilibrium.
		1410	2	$RuO_2 + Ru$	Nonequilibrium.
90	10	1000	18	$Rutile_{ss}$	
		1170	2	$Rutile_{ss}$	
		1180	2	$Rutile_{ss}$	
		1190	2	$Rutile_{ss}$	
		1200	2	$Rutile_{ss} + Ir_{ss}$	
		1240	2	$Rutile_{ss} + Ir_{ss}$	
		1260	2	$Rutile_{ss} + Ir_{ss}$	
		1360	1	$Rutile_{ss} + Ru_{ss}$	
		1380	0.25	$Rutile_{ss} + Ru_{ss}$	
		1425	0.25	$Rutile_{ss} + Ru_{ss}$	Nonequilibrium.
75	25	1000	18	$Rutile_{ss}$	
		[c] 1100	192	$Rutile_{ss}$	Quenched in ice water.
		1120	2	$Rutile_{ss}$	
		1135	2	$Rutile_{ss}$	Ir not detected by x-rays.[d]
		1140	2	$Rutile_{ss} + Ir_{ss}$	
		1150	1	$Rutile_{ss} + Ir_{ss}$	
		1220	1	$Rutile_{ss} + Ir_{ss}$	
		1230	2	$Rutile_{ss} + Ir_{ss}$	
		1250	2	$Rutile_{ss} + Ir_{ss}$	
		1320	2	$Rutile_{ss} + Ir_{ss}$	
		1340	2	$Rutile_{ss} + Ir_{ss}$	
		1350	2	$Rutile_{ss} + Ir_{ss}$	Nonequilibrium; trace of Ir_{ss}.
		1370	0.5	$Ru_{ss} + rutile_{ss}$	
		1370	2	$Ru_{ss} + Ir_{ss} + rutile_{ss}$	Nonequilibrium; apparent change in composition due to differential volatilization.
		1390	2	$Ir_{ss} + Ru_{ss} + rutile_{ss}$	Nonequilibrium; apparent change in composition due to differential volatilization.
		1430	0.5	$Ru_{ss} + rutile_{ss}$	Nonequilibrium.
		1430	2	$Ir_{ss} + Ru_{ss} + rutile_{ss}$	Nonequilibrium; apparent change in composition due to differential volatilization; $rutile_{ss}$ probably formed on cooling.
50	50	1000	18	$Rutile_{ss}$	
		[c] 1000	18	$Rutile_{ss}$	Quenched in ice water.
		1070	2.5	$Rutile_{ss}$	
		1080	2	$Rutile_{ss}$	
		1090	2	$Rutile_{ss} + Ir_{ss}$	
		1100	2	$Rutile_{ss} + Ir_{ss}$	
		1110	2	$Rutile_{ss} + Ir_{ss}$	
		1140	3	$Rutile_{ss} + Ir_{ss}$	
		1150	2	$Rutile_{ss} + Ir_{ss}$	
		1160	2	$Rutile_{ss} + Ir_{ss}$	
		1170	2	$Rutile_{ss} + Ir_{ss}$	
		1200	2	$Rutile_{ss} + Ir_{ss}$	
		1260	2	$Rutile_{ss} + Ir_{ss}$	
		1340	2	$Ir_{ss} + rutile_{ss}$	
		1350	1	$Ir_{ss} + Ru_{ss} + rutile_{ss}$	Nonequilibrium.
25	75	1000	18	$Rutile_{ss}$	
		1030	2	$Rutile_{ss}$	
		1040	2	$Rutile_{ss}$	

TABLE 1. *Experimental data for compositions in the* Ru-Ir-O_2 *system in air*—Continued

Composition		Heat treatment [a]		X-ray diffraction analyses [b]	Remarks
RuO_2	IrO_2	Temp.	Time		
mole %	*mole %*	*°C*	*hr*		
		1050	2	$Rutile_{ss}$	
		1060	2	$Rutile_{ss}$	Ir not detected by x-rays.[d]
		1080	2	$Rutile_{ss} + Ir_{ss}$	
		1090	2	$Rutile_{ss} + Ir_{ss}$	
		1100	46	$Rutile_{ss} + Ir_{ss}$	
		1120	2	$Rutile_{ss} + Ir_{ss}$	
		1160	4	$Rutile_{ss} + Ir_{ss}$	
		1380	2	Ir_{ss}	
10	90	1000	18	$Rutile_{ss}$	
		[c] 1000	20	$Rutile_{ss}$	Quenched in ice water.
		1020	2	$Rutile_{ss}$	
		1030	2	$Rutile_{ss}$	
		1040	2	$Rutile_{ss} + Ir_{ss}$	
		1120	2	$Rutile_{ss} + Ir_{ss}$	
		1190	3	Ir_{ss}	
Ru	**Ir**				
100	0	1500	4	Ru	
95	5	1500	4	Ru_{ss}	
90	10	1500	4	Ru_{ss}	
85	15	1500	2	Ru_{ss}	
80	20	1500	2	Ru_{ss}	
75	25	1500	2	Ru_{ss}	
		[e] 1500	2	Ru_{ss}	
		[e] 1500	4	Ru_{ss}	
60	40	1500	2	Ru_{ss}	
		[e] 1500	2	Ru_{ss}	
50	50	1500	2	$Ru_{ss} + Ir_{ss}$	
		[e] 1500	2	$Ru_{ss} + Ir_{ss}$	
		[e] 1500	4	$Ru_{ss} + Ir_{ss}$	
40	60	1500	2	Ir_{ss}	
		[e] 1500	2	Ir_{ss}	
		[e] 1500	2	Ir_{ss}	
25	75	1500	2	Ir_{ss}	
		[e] 1500	2	Ir_{ss}	
		[e] 1500	4	Ir_{ss}	
20	80	1500	2	Ir_{ss}	
15	85	1500	2	Ir_{ss}	
10	90	1500	4	Ir_{ss}	
5	95	1500	4	Ir_{ss}	
0	100	1500	4	Ir	

[a] All oxide specimens were heat treated at 800 °C a minimum of 18 hr; unless otherwise indicated, fused silica tubes (sealed at one end) were used for specimen containers and were air quenched. The 1500 °C experiments were conducted in the iridium induction furnace; operating pressure of the system was nominally 7×10^{-5} torr.

[b] The phases identified are given in order of the relative amount present at room temperature.

[c] Sealed platinum tubes were used for specimen containers.

[d] Small amounts of dissociation products (metals) tend to segregate and evade detection by x-ray diffraction. Microscopic examination of the specimens in conjunction with x-ray diffraction data give consistent dissociation temperatures.

[e] Reheat of specimen from previous experiment.

would contain two phases, rutile$_{ss}$ and Ir$_{ss}$. The composition of the rutile$_{ss}$ is estimated to be 58 mole percent RuO_2:42 mole percent IrO_2, while that of Ir$_{ss}$ is about 3 mole percent Ru:97 mole percent Ir. The intersection of the oxygen reaction line and the 1100 °C isotherm represents the total bulk composition (Ru 27, Ir 27, O_2 46 mole percent) at that temperature. At 1345 °C and only this temperature, three solid phases (rutile$_{ss}$, Ru$_{ss}$, Ir$_{ss}$) exist in equilibrium, as illustrated by the triangular isotherm. Above 1345 °C the dissociation is complete for the original 50RuO_2: 50IrO_2 mole percent mixture and the phase relations can be established from the true binary Ru-Ir system. Phase relations for other compositions are interpreted in a similar manner by following the appropriate oxygen reaction lines.

The binary-type phase diagram given in the top portion of figure 1 is a projection of certain elements of the three dimensional ternary system Ru-Ir-O_2 on a two-dimensional plane figure. The diagram in effect represents a composite of the true binary system Ru-Ir and the pseudobinary system, RuO_2-IrO_2. By representing the dissociation of RuO_2 and IrO_2 as a type of phase transition in which the vapor phase is ignored, a simple binary representation of the phase relations of the ternary system can be given. This method of illustration has been employed by a number of investigators [11, 12]. The diagram can be interpreted as a binary diagram and the application of the lever law is valid.

Ruthenium dioxide was found to dissociate to Ru metal and presumably oxygen at 1405 °C in air at atmospheric pressure. This value compares favorably with the data (1540 °C in one atm oxygen) given by Bell and Tagami in their study of the Ru-oxygen system [6]. The dissociation of RuO_2 is a reversible process; that is, oxidation of Ru occurs readily at temperatures below 1405 °C. At temperatures of 1300 °C and above RuO_2 becomes very volatile. Bell and Tagami conclude that RuO_3 and RuO_4, stable only in the gaseous state, form on heating Ru in one atm of oxygen [6]. Several experiments were conducted in an effort to produce a stable solid $RuO_{2\pm x}$ in an air environment without success. In one experiment it was observed that prolonged heating of RuO_2 at 1300 °C produced a trace of an unidentified phase. Additional experiments revealed that the RuO_2 volatilized, leaving a phase assumed to be a reaction product of a mixture of RuO_2 and the impurities listed in the spectrochemical analysis. This became evident when a different but purer source of RuO_2 was used. The unidentified phase did not form under the same experimental conditions. Stoichiometric RuO_2 appears to be the only stable condensed phase in an air environment.

It was found in earlier work that IrO_2 dissociates to Ir metal and oxygen at 1020 °C in air [10]. This dissociation is also a reversible process. Other investigators [9, 13] have reported that IrO_2 combines with oxygen to form IrO_3, which is stable only in the gaseous state. Several experiments conducted in this study revealed that IrO_2, similar to RuO_2, is the only stable condensed oxide in an air environment.

This study did not detect any oxygen-deficient rutile solid solution or oxygen-rich metal solid solution. It is possible that nonstoichiometric ternary solid solutions should be indicated in figure 1 (bottom portion) adjacent to the RuO_2-IrO_2 join and likewise the Ru-Ir join. It appears unlikely that this occurs, inasmuch as deviation from stoichiometry was not detected in this study for the uncombined end members.

At temperatures up to 1020 °C in air the RuO_2-IrO_2 system (fig. 1, top portion) acts as a true binary. Above 1020 °C and below 1405 °C, portions of the system become pseudobinary. Above 1405 °C all compositions can be indicated by the true binary Ru-Ir system.

Complete solid solution was found at the lower temperatures between the two rutile end member oxides. Solid solution of Ir in Ru (hexagonal symmetry) occurs with the addition of up to 45 mole percent Ir at 1500 °C. Solid solution of Ru in Ir (cubic symmetry) extends up to 44 mole percent Ru at 1500 °C.

The complete binary representation of the condensed ternary system Ru-Ir-O_2 in air is given in figure 2. The diagram up to 1500 °C was constructed from data obtained in this study and is a reproduction of the binary presented in figure 1. Subsolidus data above 1600 °C were taken from the work of Raub [14]. Solidus and liquidus lines are strictly postulated as a reasonable facsimile of what might actually occur. Except for the melting points of the metallic end members, there are no data available for a more accurate construction.

Unit cell dimensions for the solid solution region between RuO_2 and IrO_2 are plotted in figure 3. The data were obtained from specimens heat treated at 1000 °C. Both *a* and *c* dimensions deviate as expected from the linear line predicted by Vegard's Law. However, for unknown reasons the deviations are not in the same direction. It is also evident that the a dimension for compositions rich in RuO_2 changes very little until about 40 mole percent IrO_2 is added.

Inasmuch as both RuO_2 and IrO_2 have the tetragonal, rutile-type structure and similar reported cationic radii (0.67, 0.68 Å, respectively) [15], it would be expected the unit cell dimensions should be similar. The dimensions for the *a* parameters, however, differ only by 0.005 Å, while the difference for the *c* parameters is 0.05 Å. The larger deviation in the *c* parameters are probably due to crystal field effects resulting from the additional *d*-electron of Ir.

5. Summary

Equilibrium phase relations were determined for the system Ru-Ir-O_2 in air up to 1500 °C. A ternary equilibrium phase diagram was constructed, indicating selected oxygen reaction lines and isotherms. A binary representation of the Ru-Ir-O_2 system in air is given. The diagram represents a composite of the true binary system Ru-Ir and the pseudobinary RuO_2-IrO_2 system. Selected mixtures in the system

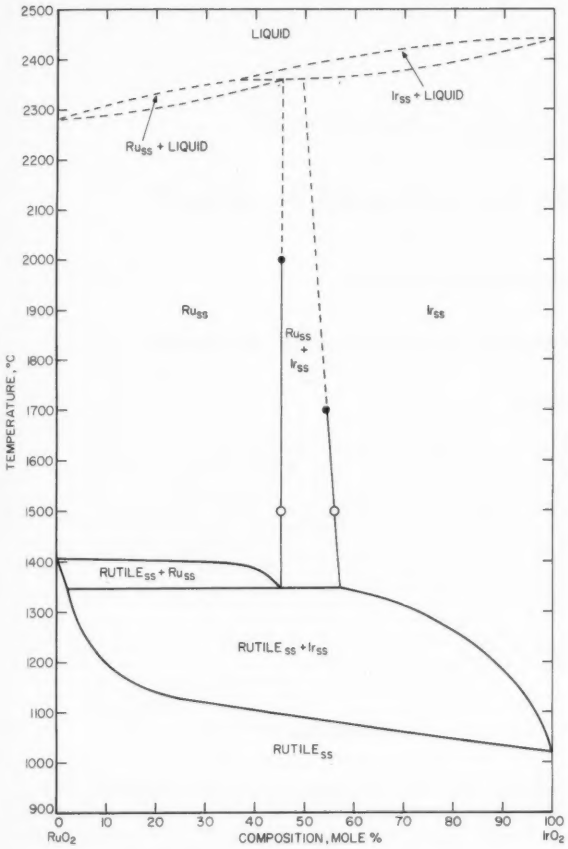

FIGURE 2. *Binary representation of the condensed ternary system* Ru-Ir-O_2.

Lower portion is a reproduction of the binary presented in figure 1. Dashed lines represent postulated portion of the diagram. ● – data taken from work of Raub [14]. ○ – data obtained is this study. ss – solid solution.

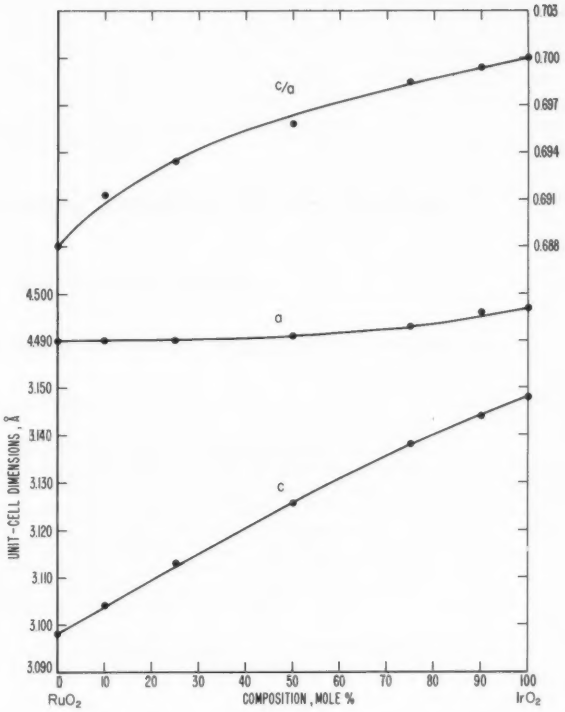

FIGURE 3. *Unit cell dimensions for rutile$_{ss}$ as a function of composition.*

The data were obtained from specimens heat treated at 1000 °C.

were studied by x-ray diffraction techniques after various heat treatments. The dissociation temperatures of RuO_2 and IrO_2 in air were established at 1405 and 1020 °C, respectively. Both the dissociations were found to be reversible. The oxides react to form complete solid solution at temperatures up to 1020 °C. At 1345 °C, three solid phases, rutille$_{ss}$, Ru_{ss}, and Ir_{ss}, exist in equilibrium for compositions between 2 and 45 mole percent IrO_2. Above 1405 °C dissociation is complete for all compositions and the phase relations are represented by the true binary Ru-Ir system. At 1500 °C, solid solution of Ru and Ir occur with the addition of up to 45 mole percent Ir and up to 44 mole percent Ru, respectively.

6. References

[1] Stimson, H. F., J. Res. NBS **65A** (Phys. and Chem.), No. 3, 139–45 (1960).

[2] Krier, C. A., and Jaffee, R. I., J. Less-Common Metals **5,** 411–31 (1963).

[3] Swanson, H. E., Fuyat, F. K., and Ugrinic, G. M., NBS Circ. 539, Vol. **4,** 5 (1955).

[4] Rudy, E., Kieffer, B., and Frohlich, H., Z. Metallk. **53,** 90 (1962).

[5] Cotton, F. A., and Mague, J. T., Inorg. Chem. **5,** No. 2, 317–8 (1966).

[6] Bell, W. E., Tagami, M., J. Phys. Chem. **67,** No. 11, 2432–6 (1963).

[7] Swanson, H. E., Fuyat, R. K., and Ugrinic, G. M., NBS Circ. 539, Vol. **4,** 9–10 (1955).

[8] Swanson, H. E., Morris, M. C., and Evans, E. H., NBS Mon. 25, Sec. 4 (1965).

[9] Cordfunke, E. H. P., and Meyer, G., Rec. Trav. Chim. **81,** 495–504 (1962).

[10] McDaniel, C. L., and Schneider, S. J., J. Res. NBS **71A** (Phys. and Chem.), No. 2, 119–23 (1967).

[11] Muan, A., Am. J. Sci. **256,** 171–207 (1958).

[12] Negas, T., J. Am. Ceram. Soc., to be published.

[13] Schafer, H., and Heitland, H. J., Z. Anorg. Allgem. Chem. **304,** 249 (1960).

[14] Raub, E., Z. Metallk. **55,** 316–9 (1964).

[15] Ahrens, L. H., Geochim. et Cosmochim. Acta **2,** 155–69 (1952).

(Paper 73A2–547)

JOURNAL OF RESEARCH of the National Bureau of Standards—A. Physics and Chemistry
Vol. 73A, No. 2, March-April 1969

Heats of Reaction of Natural Rubber With Sulfur

Norman Bekkedahl * and James J. Weeks

Institute for Materials Research, National Bureau of Standards, Washington, D.C. 20234

(December 16, 1968)

An adiabatic copper calorimeter was used to determine the heats of vulcanization of pale crepe natural rubber with sulfur for mixtures varying in composition from 0 to 32 percent added sulfur. The side reaction that produces hydrogen sulfide was avoided by using reaction temperatures near 155 °C. Heats of reaction at 25 °C and at 155 °C are reported. The enthalpy change at 25 °C for compounds containing up to about 18 percent sulfur is given in joules per gram of vulcanizate by the equation, $\Delta H_{25} = -21.1 \cdot S$ with a standard deviation of 11 J/g. Here S is the percentage of combined sulfur. Above 18 percent sulfur the heat of reaction at 25 °C remains approximately constant at 380 ±8 J/g. A comparison is made between the heat of vulcanization and the volume change on vulcanization, both as functions of combined sulfur, by making use of data in the literature.

Key words: Aneroid calorimeter; calorimeter; heat of vulcanization; heat measurements; rubber; rubber-sulfur reaction; volume change on vulcanization; vulcanization.

1. Introduction

The generally accepted theory of the vulcanization of natural rubber with sulfur is that a chemical reaction takes place in which intermolecular sulfur crosslinks are formed, giving the product a three-dimensional network structure. However, neither the details of this structure nor the mechanism of the chemical reaction is entirely understood, in spite of the vast amount of research work that has taken place in this field.

It has been known for many years that the vulcanization of natural rubber with sulfur involves an exothermic reaction, but very little careful work has been done to measure the quantity of heat involved. Most of the thermal studies have been only of a qualitative nature, in which thermometers or thermocouples have been imbedded in mixtures of rubber with vulcanizing ingredients and observed for temperature rise during the chemical reaction [1–14].[1] These rather crude experiments were made chiefly for the purpose of comparing the efficiencies of various types of accelerators, evaluating raw rubbers, or searching for the best temperature conditions for vulcanization.

However, several investigators have obtained quantitative data for the heat liberated from similar experiments involving differential calorimetry [15–22] and by means of direct measurements [23]. Indirect means have also been employed [24–26], in which measurements of the heats of combustion have been made both on the reactants and the products of reaction, but this method has the disadvantage of requiring extremely high accuracy of calorimetric measurements because the heats of reaction are obtained as the differences between relatively large values of heats of combustion.

For a good review and discussion of the earlier work on the subject of the heat of reaction of the vulcanization process reference should be made to the articles of Oberto [17] and Hock and Schroeter [19]. The published results, however, have been anything but harmonious, even with respect to the general shape of the curve obtained when the heat of reaction is plotted as a function of the composition of the product. The present investigation was undertaken primarily with the hope that more precise calorimetric measurements might aid in bringing about a better understanding of the mechanism of the vulcanization process.

2. Method

A calorimeter of large heat capacity was designed and constructed so that samples of convenient size, at 25 °C, can be inserted into the calorimeter at vulcanization temperatures without lowering its temperature by more than a few degrees. In addition, this large heat capacity keeps the temperature change, arising from the vulcanization reaction, small enough for convenient measurement.

By using a reaction temperature of about 165 °C for the mixtures containing less than about 20 percent

*Present address: Nassau House, 301 N. Ocean Blvd., Apt. 1103, Pompano Beach, Fla. 33062.

[1] Figures in brackets indicate the literature references at the end of this paper.

sulfur the reaction rate was rapid enough to permit one sample to be run during a single day. However, it was found that for very high percentages of sulfur appreciable portions of the sample would be lost by the formation of H_2S. By lowering the reaction temperature to about 145 °C this H_2S formation was reduced in all cases to negligible amounts. Of course, the time interval needed for complete reaction at this lower temperature was considerably lengthened, to as much as four days in some instances.

Since enthalpy is a function of the state of a system only, the heat of the vulcanization reaction at 25 °C may be determined by subtracting the energy absorbed by the products of the reaction, in going from 25.0 °C to the final equilibrium temperature of the reaction, from the energy absorbed by the reactants in going through the same temperature interval. Figure 1 is a schematic diagram which aids in the explanation of the experiments and in the derivation of the equations used to calculate the results of the experiments.

At a recorded time the reactants, a mixture of natural rubber and sulfur at temperature T_1', are dropped into the calorimeter at temperature T_4'. The temperature of the calorimeter and its contents would then, exclusive of any heat of reaction, come to an equilibrium temperature T_2'. The heat liberated by the vulcanization reaction causes a rise in the temperature of the calorimeter and its contents to T_3'.

The products of the completed reaction are removed from the calorimeter and allowed to return to room temperature. The calorimeter temperature is then readjusted to a temperature near T_4', but is measured as T_4'' at the time that the reaction products at T_1'' are inserted into it. The equilibrium temperature of the calorimeter and contents is now measured as T_2''. A measured quantity of electrical energy, q, is then added to the calorimeter to bring it up to a temperature T_3'', where should be quite near the previously measured temperature T_3'. The symbol T_v denotes the average temperature of vulcanization, ΔT_v the temperature rise which occurs during the vulcanization, and ΔT_q the temperature change from adding the quantity of heat, q.

Sample temperatures T_1' and T_1'' are measured to the nearest 0.1 °C, and differences in the calorimeter temperature, e.g. $T_4'-T_3'$, to the nearest 0.001 °C. Temperature T_2' needs not, and usually cannot, be measured because of lack of time for complete equilibrium before the vulcanization reaction begins.

From the first law of thermodynamics, the following general equation is obtained for the heat of the vulcanization reaction at 25 °C,

$$\Delta H_{25}=\int_{T_3'}^{T_4'} C\,dT-\int_{T_3''}^{T_4''} C\,dT+\int_{25}^{T_1'} c'\,dT - \int_{25}^{T_1''} c''\,dT+\int_{T_3'}^{T_3''} c''\,dT-q. \qquad (1)$$

In this equation C represents the heat capacity of the empty calorimeter and c refers to the heat capacity of the sample plus its container. Single primes are used in referring to experiments involving the mixed reactants, and the double primes to those on the reaction products. When the temperatures T_1' and T_1'' are adjusted to 25 ° ±0.1 °C, as was done in most of the experiments in the present investigation, the third and fourth terms on the right side of the equation are eliminated.

For reasons that will be explained later in the discussion, it is actually more meaningful to report the heats of reaction with reference to a higher vulcanization temperature than to 25 °C. It can be seen from figure 1 that the heat of the reaction, ΔH_v, at this higher temperature, T_v, can be obtained from

$$\Delta H_v=\int_{T_3'}^{T_4'} C\,dT-\int_{T_1'}^{T_v} c'\,dT-\int_{T_v}^{T_3'} c''\,dT. \qquad (2)$$

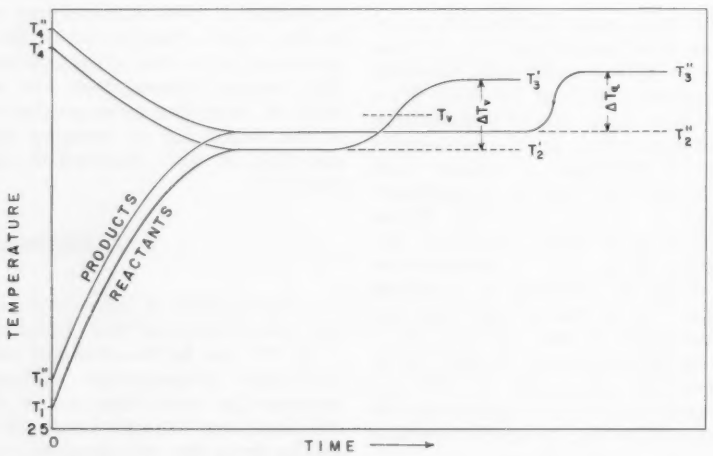

FIGURE 1. *Diagram showing the course of the experiments for both the reactants and the products of reaction.*

The diagram is not drawn to scale. See text for explanation

Here, the mean heat capacities of rubber, sulfur, and the sample container must be known between room temperature and the temperature of vulcanization. This can be determined for each of the materials separately in the same calorimeter by applying the equation

$$\int_{T_1}^{T_2} cdT = \int_{T_2}^{T_4} CdT. \tag{3}$$

3. Experimental Detail

3.1. Calorimeter Assembly

A diagram of the apparatus is given in figure 2. A cylindrical block of copper, C, 6.7 cm in diameter and 22.2 cm long, is supported on glass wool in the bottom of a 1-liter wide-mouth dewar flask, D1. The block contains a circular well, W, about 3.8 cm in diameter, extending from the top to within 1.2 cm of the bottom. A copper tube of 2.5 cm inside diameter, with constantan heating-wire wound around it, is of such wall thickness that it fits snugly into the copper block. The heating-wires are represented by open circles. This whole unit then serves as the heater, H4, of the calorimeter. The space within this heater, which is about 20 cm in length, holds the sample container during an experiment. A small plug of glass wool is placed at the bottom of the well for protection of this container, which is made of glass.

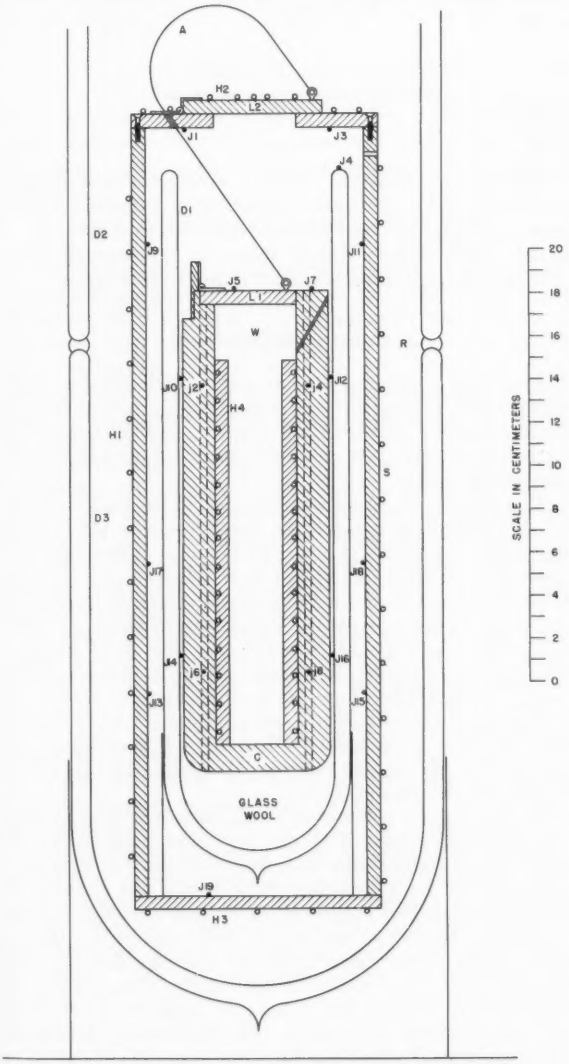

FIGURE 2. *Diagram of the calorimeter used to measure the heats of vulcanization.*

The temperature of the calorimeter is measured by means of an 8-junction copper-constantan thermopile, whose junctions are represented by solid circles and are referred to as j2, j4, j6, and j8. The other four junctions are in similar positions 90 degrees from those shown in the diagram. A hinged lid, L1, covers the sample-well in order to prevent the loss of heat by convection currents from the sample compartment, which may be at a temperature several degrees higher than that of the calorimeter.

A copper jacket, S, having a 0.6-cm wall thickness surrounds the calorimeter and serves as a thermal shield. A hinged lid, L2, is placed at the top to allow introduction of the sample. Both the lids L1 and L2 can be opened simultaneously by pulling on the loop of fine wire, A. Three separate heaters, H1, H2, and H3 are wound on the side, top, and bottom of the jacket, respectively, as are shown by the open circles in the diagram. It was later found, however, that the bottom heater, H3, was unnecessary. Thermal insulation of the jacket from the surroundings is provided by two 4-liter dewar flasks, D2 and D3, one inverted over the other. An asbestos ring, R, acts as a cushion between the two flasks. In order to lower the sample into the calorimeter or to remove it, the top dewar D2 must, of course, be temporarily removed.

The thermal head between the shield and the calorimeter is measured by an 8-junction copper-constantan thermopile located in various positions as indicated by the closed circles J1 to J16. Several other thermocouples were used to balance the heat input to H1 and H2.

In the earlier experiments, the sample was initially equilibrated to room temperature in a large copper block inside a wide-mouth dewar and was quickly transferred into the calorimeter. Later, a vertical tube oven was mounted above the calorimeter, so that the sample container could be maintained at 25.0 °C and then dropped directly into the calorimeter.

a. Jacket Temperature Control

Except for a short interval of time when the upper dewar flask is removed, the jacket temperature is automatically held very nearly equal to that of the calorimeter by the jacket temperature controller. Figure 3 is a schematic diagram of the system, which also records the differential thermopile emf. A cam is attached to the shaft of the large drive gear of the potentiometer in such a position that it will just touch a

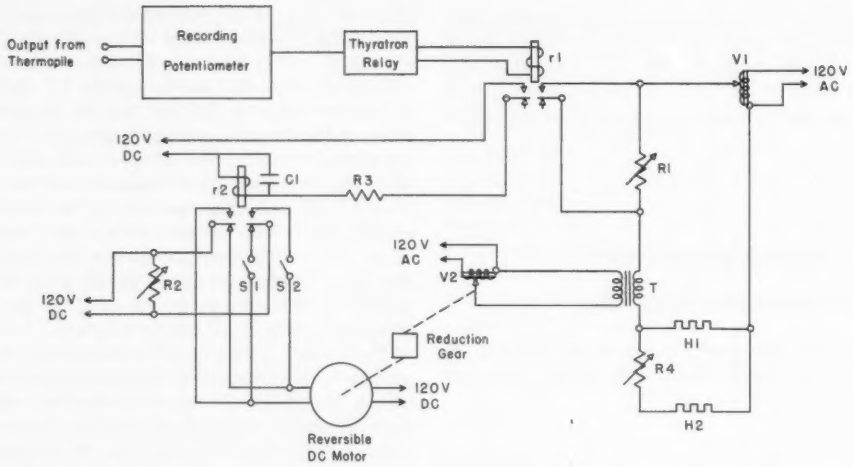

FIGURE 3. *Schematic diagram of the apparatus that controls the differential temperature between the jacket and the calorimeter.*

spring contactor when the input voltage exceeds zero (or any other desired value). This action shorts out the bias on a 2050 thyratron, which fires and thereby closes a double-pole-double-throw relay, r1. Closing of this relay does two things: first, the variable resistance, R1, that was initially in series with the jacket heaters, H1 and H2, is shorted out; and second, the circuit to the coil of another double-pole-double-throw relay r2, is completed. The position of this second relay, determines the direction of rotation of a reversible d-c motor, which in turn operates, through a reduction gear, a variable transformer, V2, across the input of a 6-volt transformer, T. The output of this transformer is in series with the heaters. Two micro-switches, S1 and S2, are used to limit the rotation of the transformer shaft. By adjusting the slack in the linkage between the reduction box and the variable transformer, or by adjusting the speed of the motor, a normal high-low heating period is allowed without any change in the transformer setting. This period was found to be about 40 s for the present setup. Should the demand for heater power change, as, for example, it does during the vulcanization, the setting of the transformer will automatically be changed to the proper value. The overall system provides high-low control with automatic reset.

With a zero emf input to the jacket temperature controller, it was found that the empty calorimeter would drop slowly in temperature, at a rate of about 0.00012 °C/min. By measuring this average rate of temperature change overnight on a number of occasions, an indication of the reliability of the jacket control was obtained. The standard deviation of 67 measurements of the rate was found to be 8 μ°C/min. The rate of temperature change for the calorimeter plus a sample is equal to that for the empty calorimeter times the ratio of the heat capacity of the calorimeter to that of the calorimeter plus sample and sample container.

The cooling constant of the calorimeter was measured to be 2.3×10^{-3} min^{-1} by utilizing various control point settings of the jacket temperature controller. If the upper dewar (D2 in figure 2) is removed, the cooling constant is increased by about 10 percent.

b. Calibration of Calorimeter

The heat capacity of the empty calorimeter was determined by two different methods: (a) from measured additions of electrical energy, and (b) from the enthalpy change in a calorimetric standard sample of aluminum oxide.

The usual procedure was followed in the first method in that direct current from batteries was used, the energy being obtained from the product of the voltage, current, and time of current flow. Most of the voltage (120 volts) supplied by the batteries was dropped by resistors in series with the calorimeter heater, so that 0.1 to 0.2 amp would flow through the 80-Ω heater. The current was obtained from voltage measurements, using a Rubicon Type-B potentiometer, across a calibrated 1-Ω resistor in series with the heater. Durations of time were measured to 0.1 s with a timer run on the regular ac line voltage. Heating intervals of 45 to 90 min were used.

In the second method of calibration a known weight of standard sample of aluminum oxide, contained in a thin-walled copper tube, was dropped into the calorimeter; and the heat capacity of the latter was calculated from its observed temperature change and the known enthalpy changes in the copper tube and in the aluminum oxide. The value used for the specific heat of copper was that given in the International Critical Tables [27]. Values for aluminum oxide as a function of temperature are given by Furukawa, Douglas, McCoskey, and Ginnings [28, 29].

In order to convert the measured thermocouple voltage, e, for the 8-junction thermopile into degrees

Celsius when using an ice bath to maintain the reference junctions at 0 °C, the equation

$$e = 312.64t + 0.2925t^2 + 0.1784 \times 10^{-4}t^3 \quad (4)$$

was used. It was obtained from the calibration values of emf at 120, 140, and 160 °C for the spool of thermocouple wire used in the calorimeter. The derivative of this equation, evaluated at the mean temperature of the experiment, was divided into the emf difference to obtain the temperature difference. This procedure for converting Δe into Δt produces an error no larger than 10 μ °C.

Assuming the electrical and the Al_2O_3 measurements to be equally valid, the linear regression of the heat capacity as a function of temperature was found to be, in J/°C,

$$C = 2494.2 + 1.53(t - 155.00), \quad (5)$$

with a standard deviation of 3.0 J/°C. This equation was obtained from eleven electrical and seven Al_2O_3 measurements in the temperature range from 143 to 166 °C.

3.2. Samples and Container Materials

The samples were prepared from No. 1 pale latex crepe and commercial powdered rhombic sulfur. One kilogram of the rubber was thoroughly blended on a compounding mill. One-half of this rubber was mixed with sulfur to give a masterbatch containing 32.1 percent sulfur. The other half was used to add to portions of the masterbatch when mixtures of other compositions were required.

In preliminary experiments the samples were allowed to vulcanize while exposed to air in the calorimeter, but the susceptibility of the rubber to oxidation prevented a final equilibrium temperature from being reached. The samples in all later experiments were sealed in a glass container, and the air surrounding them was replaced by helium.

In spite of this treatment some reaction still took place within the rubber, as was shown by measurements of the enthalpy change of sulfur-free rubber between 25 and 165 °C. The initial average specific heat, $\bar{s}$, of seven such samples in this temperature range was 2.154 ± 0.007 J·g^{-1}·°C^{-1}*; but when the same samples were run a second time the $\bar{s}_{95}$ values were found to be higher by 0.020 J·g^{-1}·°C^{-1}. No further increases were obtained on subsequent runs. Several variations in the methods of preparation of the rubber, including vacuum molding, did not eliminate the reaction that occurs the first time the sample is raised to the elevated temperatures. In measurements of the specific heats of organic polymeric materials Furukawa [30] has reported a similar evolution of heat above about 65 to 70 °C from polymers containing double bonds. Since the total heat evolved in this reaction of the rubber, which amounts to about 2.8 J/g for the 140 °C difference in temperature, is small compared with that produced by the rubber-sulfur vulcanization reaction, no further attempt was made to eliminate it.

The recommended values [31] for the specific heat of natural rubber in the temperature range from about 50 to 175 °C, in J · g^{-1} · °C^{-1}, are given by

$$s(\text{rubber}) = 1.917 + 0.00344(t - 25). \quad (6)$$

This equation gives a value of 2.158 J · g^{-1} · °C^{-1} for $\bar{s}_{95}$, which agrees very well with that determined by the measurements described earlier. Later in this paper calculations are made for the heats of vulcanization at 155 °C, which require specific heat values between 25 and 155 °C. We will use eq (6) which gives for $\bar{s}_{90}$ a value of 2.141 J · g^{-1} · °C^{-1}.

Sulfur is also part of the rubber sample, being present in a simple mixture prior to the vulcanization reaction and as part of the rubber-sulfur compound after the reaction. In calculating the heat of reaction at vulcanization temperatures, for example at 155 °C, from experimental data using eq (2) the difference in the heat content of the rubber-sulfur mixture must be known between 25 and 155 °C. For elemental sulfur West [32] reported a value of 174.1 J/g for $H_{155} - H_{25}$. Measurements by means of our own calorimeter gave good agreement with this, a value of 174.6 J/g. The former value, which is used for the present calculations, is equivalent to a mean specific heat of 1.339 J · g^{-1} · °C^{-1} at 90 °C. The mean specific heat of the rubber-sulfur mixture between 25 and 155 °C, in J · g^{-1} · °C^{-1}, can therefore be obtained from

$$\bar{s}_{90}(\text{mixture}) = 2.141 - 0.00802 \cdot S \quad (7)$$

in which S is the percentage of sulfur in the mixture.

In order to evaluate the last integral in either eq (1) or eq (2), we need an estimate of the specific heats of the vulcanizates, s'', in the temperature range 145 to 165 °C. Direct measurement of s'' was not possible in this temperature range because the vulcanization reaction continues to a slight extent when high percentage sulfur compounds are heated to these temperatures. First, we approximate the dependence of s'' on the combined sulfur by measuring the mean specific heats of rubber vulcanizates between 25 and 155 °C and use this value at the higher temperatures. For compounds containing from 0 to 18 percent sulfur, the results, in J · g^{-1} · °C^{-1}, can be represented by

$$\bar{s}''_{90} = 2.156 - 0.478x \quad (8)$$

in which x is the fraction of an atom of combined sulfur per unit of C_5H_8 in the compound. Compounds containing more than 18 percent sulfur gave $\bar{s}''_{90}$ values which deviated from this relation and which appeared not to be given by a linear function of the combined sulfur.* Secondly, we assume the temperature derivative of the compounds to be the same as

*Earlier work in our laboratory [23] using a less precise calorimeter gave a value of 2.16 J·g^{-1}·°C^{-1} for the mean specific heat of natural rubber between 25 and 175 °C, which is equivalent to a $\bar{s}_{95}$ of 2.14 J·g^{-1}·°C^{-1}

*For the cause of the deviation from linearity see section 4.2c.

that of rubber alone, which we derive as follows. An average value of s (rubber) at 155 °C was found to be 2.435 $J \cdot g^{-1} \cdot °C^{-1}$. When this value is combined with our previously mentioned value of 2.174 at 95 °C, an average temperature derivative of 0.0044 $J \cdot g^{-1} \cdot °C^{-2}$ is obtained. We therefore estimate s'' in the temperature range near 155 °C to be given by

$$s'' = 2.435 - 0.478\,x + 0.0044\,(t - 155). \qquad (9)$$

It is also necessary to know the specific heat of the Pyrex glass that was used as a sample container. We measured its $H_{165} - H_{25}$ to be 122.7 J/g which, when combined with the ds/dt of 0.001311 $J \cdot g^{-1} \cdot °C^{-2}$ determined by de Vries [33], gives the equation

$$s(\text{Pyrex}) = 0.7521 + 0.001311t \qquad (10)$$

for the specific heat of Pyrex glass in $J \cdot g^{-1} \cdot °C^{-1}$.

3.3. Illustrative Example

Details of the measurements are illustrated by the following history of one of the samples that was used in this study of the heat of reaction.

Five grams of the blended pale crepe were thoroughly mixed with 15g of the 32.1 percent sulfur masterbatch on a cold laboratory mill. This sample which contained 24.1 percent S, was removed in the form of a thin sheet and rolled into a cylinder. After its surface was lubricated with water, the sample was slipped into a 22-mm Pyrex glass tube which had a short capillary tube attached at one end. A plug of Pyrex glass wool was added above the sample, and the tube was sealed while the lower part of the tube containing the sample was cooled with ice water. The tube was then evacuated through the capillary for 6 hr at room temperature, then overnight at 70 °C, after which helium was admitted. The capillary was finally sealed close to its entrance to the tube and formed into a small hook which enabled the tube to be lifted by a loop of fine wire. The mass of the glass container was 57.41g.

Over a period of 24 hr the average rate of thermal emf change in the empty calorimeter was measured to be -0.0475μV/min. At zero time the calorimeter thermopile emf was 50,767 μV. The sample was quickly transferred from its 25 °C chamber into the calorimeter. This opening and closing of the calorimeter disturbs its temperature, so a correction was made to the initial emf reading. A number of experiments of opening the calorimeter just as is done when inserting the sample, but without actually inserting it, showed that the correction is -3 μV.

Corrections were also made for the heat exchange between the calorimeter and the jacket during the experiment. First, there is a correction for the interval when the jacket controller cannot maintain the differential emf at the control point setting. Figure 4 is a diagram prepared from an automatic recording sheet showing the differential emf. A reading to the left of the zero indicates that the jacket is at a lower temperature than the calorimeter. Each microvolt

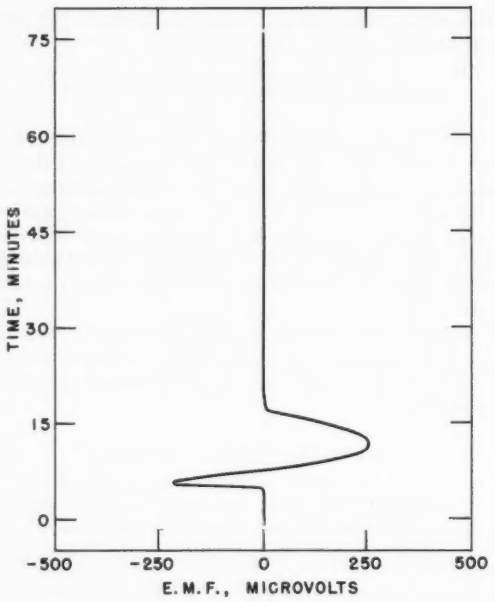

FIGURE 4. *Automatic recording of the differential emf between the calorimeter and the jacket.*

represents about 0.0025 °C. As may be seen, the jacket temperature falls rapidly until the sample starts to cool the calorimeter. Then the calorimeter cools more rapidly than the jacket, in spite of the electric current in the jacket heater being completely off, until the sample approaches the calorimeter temperature. After a period of about 15 min the rates of change are slow enough so that the jacket temperature controller automatically keeps the differential thermopile voltage at a constant zero value for the rest of the experiment. The correction for the interval during which the jacket was out of control was calculated to be -1μV. This value was obtained by multiplying the integrated area of the curve in figure 4 by the cooling constant of the calorimeter (sec. 3.1a).

The second correction, necessitated by the intrinsic heat transfer between calorimeter and jacket, even when the jacket is in temperature control, was derived in the following manner. On the third day of the experiment the observed rate of voltage change of the calorimeter thermopile had reached a value of -0.036 μV/min, which by comparison with the value of -0.0475 μV/min, noted just prior to the experiment, indicated that the reaction was essentially complete. The final calorimeter thermopile emf was read as 50,210 μV after 4740 min of reaction time, and the sample was removed. Over the following day the average rate of voltage change with the calorimeter empty was found to be -0.0491 μV/min. This value was averaged with the rate determined just prior to the experiment, and the result multiplied by $C/(C+c')$, (in this case 2475/2569), to account for the increased heat capacity of the calorimeter when it contained the sample. This gives a value of -0.0465 μV/min for the drift rate of the calorimeter during the measurement on the

rubber. When this drift rate is multiplied by 4725 min, the time during which the jacket was in temperature control, a correction of $+220$ μV is obtained. The total correction to be added to the final thermopile emf is thus 219 μV, making the corrected final emf equal to 50,438 μV.

The average temperature of the calorimeter during the experiment was 142.65 °C. At this temperature (by eq (5)) the heat capacity of the calorimeter is 2475 J/°C. The derivative of eq (4) for this temperature gives a value of 397.2 μV/°C as the conversion factor for changing the observed emf difference of 326 μV into the temperature difference $T_4' - T_3'$. The calorimeter temperature change was 0.821 °C. Thus the first integral term of eq (1) is

$$\int_{T_3'}^{T_4'} C dT = 2475 \times 0.821 = 2032 \pm 100 \text{ J.}^*$$

The same procedure was carried out on the products, with the exception that 1321 J of electrical energy, q, was added to the calorimeter and sample in order to bring the final equilibrium temperature, T_3'', close to that attained by the reactants, T_3'. The observed calorimeter thermopile emf was corrected for heat exchange with the surroundings in the same manner as previously described. However, the rate of emf change recorded just prior to completion of the vulcanization run was used for the correction so that if the sample should still have been reacting to a slight extent the heat evolved would not be included in the enthalpy change of the products. Of course, the reaction must have been carried very nearly to completion in the first place or else a significant amount of additional sulfur would combine when the products are brought up to the calorimeter temperature. The total heat loss correction was found to be $+5$ μV, giving a corrected emf change of 1368 μV, which is equivalent to 3.437 °C for $T_4'' - T_3''$. The mean temperature of the calorimeter was 144.02 °C, at which temperature its heat capacity is 2477 J/°C. The enthalpy change in the calorimeter during this experiment was

$$\int_{T_3''}^{T_4''} C dT = 2477 \times 3.437 = 8513 \pm 12 \text{ J.}$$

The final temperature of the run, T_3'', was 142.30 °C, as compared with the T_3' of 142.24 °C for the vulcanization experiment. The correction that must be applied to bring the reactants and the products to the same final temperature is calculated from the specific heat of the rubber vulcanizate, eq (9), and the specific heat of the Pyrex glass container, eq (10), as

$$\int_{T_3'}^{T_3''} c'' dT = [(20.00 \times 2.0) + (57.41 \times 0.93)]0.06 = 6 \text{ J.}$$

The two remaining terms in eq (1) that are necessary for calculating the heat of reaction are both zero because the samples were at 25.0 °C when introduced into the calorimeter.

The total heat exchange during the vulcanization reaction calculated at 25 °C from eq (1) is thus

$$\Delta H_{25} = 2032 - 8513 + 0 - 0 + 6 - 1321 = -7796 \pm 101 \text{ J}$$

for the whole sample of rubber vulcanizate. Assuming that oxidation took place in the rubber to the same extent as measured previously for the rubber alone (2.8 J/g) a correction of 43 J is needed for the 15.2 g of rubber present in the sample. For the vulcanization reaction at 25 °C, therefore, the corrected value is -7753 J for the sample, or

$$\begin{aligned}\Delta H_{25} &= -388 \pm 5 \text{ J/g of vulcanizate} \\ &= -34.7 \pm 0.4 \text{ kJ/mole of } C_5H_8 \\ &= -51.7 \pm 0.7 \text{ kJ/atom of S.}\end{aligned}$$

In calculating the heat of the vulcanizing reaction at a temperature of 155 °C from eq (2)

$$\begin{aligned}\Delta H_{155} = {} & 2032 - 130[(20.00 \times 1.948) + \\ & (57.41 \times 0.8701)] + 12.8[(20.00 \times 2.02) + \\ & (57.41 \times 0.9469)] \\ = {} & -8314 \pm 101 \text{ J for the sample,} \\ = {} & -416 \pm 5 \text{ J/g of vulcanizate.}\end{aligned}$$

Subsequent analysis for free sulfur [34] in the vulcanizate showed the presence of 0.08 percent S, indicating that 24.0 percent sulfur had combined with the rubber, which is equivalent to an x value of 0.671 atom of S per C_5H_8 unit.

4. Results and Discussion

4.1. The Vulcanization Reaction

As early as 1902 Weber [35], in vulcanizing rubber-sulfur mixtures containing from 33 to 50 percent sulfur, found that the amount of combined sulfur increased with time and higher temperatures but that under no condition was it possible to obtain a combined sulfur content of more than about 32 percent. Under normal conditions of vulcanization it was therefore assumed that sulfur adds chemically to the double bonds of the rubber hydrocarbon molecule until the saturation point is reached, which gives the formula $(C_5H_8S)_n$. This assumption was strengthened when it was found that for every atom of sulfur that was added to a molecule of rubber in soft-rubber vulcanization a double bond was lost [36–38]. However, this loss of a double bond for each sulfur atom over the complete range of sulfur additions was later questioned by the infrared studies of Sheppard and Sutherland [39] and of Linnig and Stewart [40], who found that a considerable number of double bonds still remain in hard-rubber vulcanizates, even in those containing 32 percent combined sulfur.

Other studies of the rubber vulcanization process, both with and without accelerators and other additives, indicate that the molecular structure of the vul-

*The value following the ± symbol here and in the rest of this section is the estimated standard deviation of a single measurement. It results primarily from the previously given standard deviation of the drift rate and heat capacity of the calorimeter.

canizate is not as simple as it was once thought to be. Recent review articles, such as those of Moore and collaborators [41, 42], Scheele [43], and Saville and Watson [44], point out that although the primary purpose of the vulcanization process is to interlink the rubber molecules so as to form a three-dimensional network, other sulfur addition reactions take place that lower the efficiency of the desired reaction. The unaccelerated rubber-sulfur reactions are very inefficient in the formation of good vulcanizates because most of the sulfur atoms add as intramolecular monosulfides rather than as cross-links. The function of accelerators and other additives is not only to increase the rate of the chemical reactions but also to increase the efficiency of the crosslinking reactions by decreasing the intramolecular cyclic monosulfide formations. The crosslinks enter as long polysulfide chains, but as the reaction proceeds they decrease in length and finally end up primarily as monosulfide crosslinks. Even under the best conditions of acceleration 100 percent efficiency of crosslinking has not yet been achieved with sulfur vulcanizations. Although the system, rubber-sulfur without accelerators or other additives, is the least efficient of the vulcanizing formulas, it was chosen for the present study because of fewer complications from reactions involving other materials.

4.2. Heat of Vulcanization

a. Reaction Conditions

Compromises had to be made in the selection of temperatures for conducting the vulcanization reactions. It was desired to have the reaction take place at as high a temperature as possible in order to decrease the overall time for completion and thus to reduce the error of measurement caused by heat leakage in the calorimeter. On the other hand, the reaction should not be forced to proceed too rapidly because of introducing undesirable side reactions, such as the production of hydrogen sulfide at the higher concentrations of sulfur.

Because of the low thermal conductivity of the rubber the exothermic vulcanization reaction causes the temperature of the reactants to become higher than that of the surroundings. When a rubber-sulfur mixture containing 24 percent sulfur, about the size and shape of the usual sample used in the vulcanization experiments, was placed in an oven maintained at 175 °C, the center of this sample attained a maximum temperature of 276 °C, which resulted in a large amount of hydrogen sulfide being formed. However, in a similar experiment in an oven at 143 °C the temperature rose to only 154 °C, which is low enough to avoid the H_2S side reaction. For an 8 percent sulfur mixture in a 161 °C oven the temperature rose to only 169 °C. Similar results had previously been obtained by Daynes [11] and by Winspear and coworkers [14].

In a number of experiments on samples with a high sulfur content the sample containers were broken open and weighed immediately, and in no case was there a weight loss of more than 0.1 percent of that of the sample. Neither was there any odor present that indicated an appreciable quantity of hydrogen sulfide gas in the container. It was found that for the rubber samples containing less than about 20 percent of sulfur, a calorimeter temperature of 165 °C was suitable and that the reaction under these conditions was usually complete within a single day. For samples containing higher percentages of sulfur, however, the calorimetric measurements were conducted at temperatures near 145 °C. These lower-temperature experiments required more time for the completion of the reaction, but this procedure was found to be necessary in order to prevent side reactions from taking place.

Although the evolution of hydrogen sulfide from a rubber-sulfur compound is increased by either an increase in temperature or sulfur content [45, 46], it can also be increased by subjecting the rubber to direct sunlight and, conversely, can be greatly reduced in darkness [47, 48]. Other studies [49] have shown that the production of hydrogen sulfide becomes much greater if a stream of air of some other gas is passed over the sample while it is being vulcanized or while the vulcanized product is held at elevated temperatures.

The conditions under which the samples were vulcanized in the present investigation were therefore optimum, in that no flow of gas was present over the sample, the samples were kept in complete darkness, and vulcanization temperatures were relatively low.

b. Results of the Measurements

The results obtained from direct measurements of the heat of reaction of natural rubber with sulfur, for mixtures varying in composition from 0 to 32 percent added sulfur, are given in table 1. Figure 5 also presents the

TABLE 1. *Results of experiment*

Sulfur			Heat of Reaction	
Added	Combined		$-\Delta H_{25}$	$-\Delta H_{155}$
percent	*percent*	x [1]	kJ/C_5H_8	kJ/C_5H_8
1.01	1.00	0.021	1.04	1.08
2.01	1.99	.043	2.53	2.54
2.99	2.96	.065	3.79	3.94
4.00	3.96	.088	5.15	5.12
5.00	4.94	.110	6.26	6.40
6.01	5.89	.133	8.35	8.76
8.00	7.70	.178	12.18	12.30
10.03	9.54	.225	14.45	14.87
13.00	12.34	.301	21.52	22.01
16.06	15.46	.391	27.15	27.88
[2] 19.00	17.83	.468	32.49	33.64
16.04	15.82	.400	26.22	26.85
19.03	18.85	.494	31.34	32.56
[3] 24.08	23.98	.671	34.74	37.20
27.98	27.81	.820	36.92	39.96
32.08	31.09	.973	37.63	40.68
32.08	30.97	.969	37.49	41.01

[1] Atom of sulfur per C_5H_8 unit.

[2] This sample and all previously listed ones were vulcanized at temperatures near 165 °C; all following ones near 145 °C.

[3] Used as illustrative example in section 3.3.

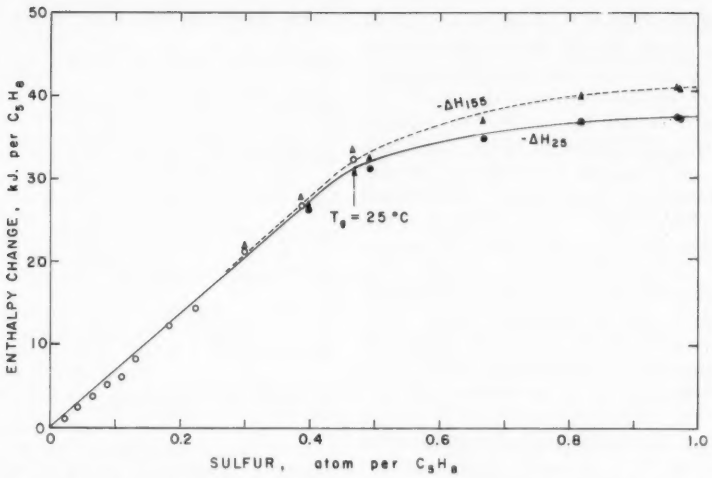

FIGURE 5. *Heat of vulcanization of rubber-sulfur mixtures as a function of composition expressed as the fraction of an atom of sulfur per* C_5H_8 *unit of the rubber.*

results in graphical form, in which the enthalpy change in kilojoules per mole of C_5H_8 units is plotted as a function of the fraction of an atom of combined sulfur in the vulcanizate, assuming that the rubber is all hydrocarbon. The solid circles and triangles represent measurements that were made with the vulcanization reaction taking place near 145 °C, and the open circles and triangles for those near 165 °C. The circles and the solid curve represent values for the heat of reaction calculated to 25 °C, while the triangles and broken curve are for the values at 155 °C.

Data from table 1 were also used to plot figure 6, which shows the heat of reaction as a function of sulfur concentration, but in this case the units for the abscissa and ordinate are different from those of figure 5. In this plot it seems as though the heat of vulcanization at 25 °C, ΔH_{25}, levels off to a value of about -380 ± 8 J/g above 18 percent combined sulfur by weight. Below the 18 percent sulfur the heat change in J/g can be obtained, with a standard deviation of 11 J/g, from the formula

$$\Delta H_{25} = -21.2 \cdot S$$

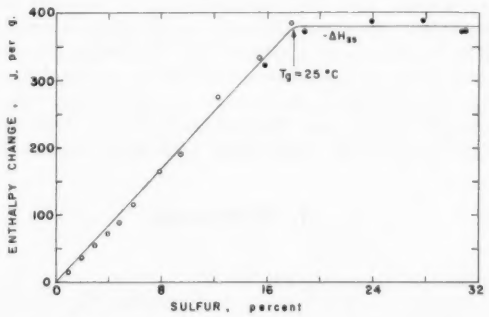

FIGURE 6. *Heat of vulcanization of rubber-sulfur mixtures as a function of composition expressed as percent of sulfur by weight.*

in which S is the percentage of combined sulfur by weight. McPherson [50] found that when variations were made in the temperature and time of vulcanization the same density values were always obtained provided the reaction had been run to completion. The same should probably be true for the enthalpy; however, there is some slight indication in our data (see fig. 6) that the 25 °C heat of reaction is greater when vulcanization takes place at 165 °C than when it occurs at 145 °C, at least for compounds containing about 16 percent combined sulfur.

C. Comment on ΔH_{25}

The obvious change in slope of the $-\Delta H_{25}$ curve at $x \simeq .47$ in figure 5 can be only partially accounted for. Martin and Mandelkern [51] have shown that the glass temperature, T_g, of a natural rubber vulcanizate is dependent on the percentage of combined sulfur. For a vulcanizate having a composition of 18 percent combined sulfur, which is equivalent to 0.466 atom of sulfur per C_5H_8 unit, the T_g is about 25 °C. (This point is marked by a vertical arrow in figure 5.) At this temperature, and below this concentration of sulfur, both the raw rubber reactant and the vulcanized rubber product exist in liquid states above their glass transition temperatures. However, at the same temperature of 25 °C but above this sulfur concentration, the product of the reaction is in the glassy state, while the rubber reactant is in a liquid state. Therefore an abrupt change in slope would be expected in the curve for the heat of vulcanization at 25 °C at a concentration of 0.466 atom of S per C_5H_8 because of the discontinuity at T_g in the specific heat curve of any vulcanized rubber having more than 18 percent combined sulfur.

The highest T_g value for any rubber-sulfur vulcanizate is about 95 °C, which is that for 32 percent sulfur or $x = 1.0$ [51]. Thus, a curve for ΔH at any temperature above 95 °C would not be biased by a specific heat change at T_g in some of the products.

331-607 O - 69 - 8

We chose to obtain ΔH at 155 °C not only because all the reactants and products would be liquids at that temperature, but also because the heat corrections to bring the products to 155 °C from the final vulcanization temperature would be small. The experimental values for ΔH_{155} are given in table 1 but are plotted in figure 5 only where the curves exhibit appreciable separation from each other. Since both the ΔH_{25} and ΔH_{155} curves are very similar to each other, it indicates that the T_g transition has only a small effect on the shape of the ΔH_{25} curve. Apparently, its effect is overshadowed by a change in the shape of the curve due to another cause. This could be either a change in the type of chemical reaction taking place or the simultaneous occurrence of an endothermic reaction. It is probably only coincidental that these two different causes for a change of slope should arise at or near the same concentration of combined sulfur.

Bhaumik, Banderjee, and Sircar [21, 22] obtained a linear curve through the 0.466 S region and suggested that earlier work done at the National Bureau of Standards [23] must have allowed an endothermic reaction, the formation of hydrogen sulfide, to take place with the higher percentages of sulfur and thus cause the curve to deviate from the linearity that it has below about 18 percent of combined sulfur. Care was taken in the present investigation, however, not to permit this side reaction to take place, but the shape of the curve in figure 5 still resembles that obtained previously [23], indicating again that the curve does not have the same slope for the higher concentrations of combined sulfur as it does for the lower.

4.3. Vulcanization Volume Change

Further indication that changes of slope actually do take place in the curves for the heat of vulcanization as a function of combined sulfur both at 25 °C and 155 °C results from work done by McPherson [50] and by Martin and Mandelkern [51] on the measurement of the densities of rubber-sulfur mixtures at various concentrations and their vulcanizates. The changes of volume on vulcanization, shown in figure 7, were calculated from data obtained in the publication of the latter investigators [51]. From data given in table 1 and in figure 3 of their paper it was determined that the specific volumes of the unvulcanized rubber-sulfur mixtures, V_{25} (mix), in cm³/g at 25 °C, can be obtained from the equation

$$V_{25}\,(\text{mix}) = 1.095 - 0.0060 \cdot S \qquad (11)$$

in which S is the percentage by weight of sulfur. The specific volumes of the corresponding vulcanizates, V_{25} (vulc), given in column 3 of their table 1, after being corrected for the amount of free sulfur present, were subtracted from the V_{25} (mix) values obtained for the corresponding concentrations of sulfur and were then computed per gram of isoprene. The values of volume change on vulcanization are plotted as $-\Delta V_{25}$ in figure 7 as a function of the bound sulfur recalculated to the fraction of an atom per C_5H_8 unit.

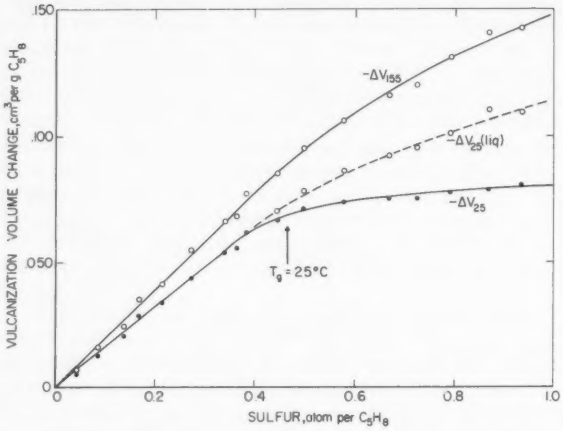

FIGURE 7. *Change in volume of rubber-sulfur mixtures during vulcanization as a function of composition.*

Data for the curves are taken from a paper by Martin and Mandelkern [51].

It can be seen that the $-\Delta V_{25}$ curve of figure 7 has a shape similar to that of the $-\Delta H_{25}$ curve of figure 5 in that they both deviate from linearity at about the same sulfur concentration and that both the changes in volume and the changes in heat of vulcanization are much less per sulfur atom at the higher concentrations of sulfur.

The $-\Delta V_{25}$(liq) curve of figure 7 was derived from the data plotted in figure 3 of reference 51 expressed in the same units as before. Now the vulcanization volume change is given with all the products in a liquid state but a change of slope at higher concentrations of sulfur is still observed. We also calculated the volume changes which would occur from vulcanization at 155 °C by making use of the volume-temperature derivatives given in tables 1 and 2 of Martin and Mandelkern's paper [51]. These changes are shown in figure 7 and labeled $-\Delta V_{155}$. The change in slope for $x > .47$ is less obvious but still similar to that occurring in the plot of ΔH_{155}.

In conclusion, both heat and volume measurements have shown that the vulcanization of natural rubber with sulfur does not proceed to 32 percent combined sulfur by means of a single type of chemical reaction. Other kinds of measurements will be needed to elucidate the detailed molecular combinations but any proposed theory for the vulcanization of this system should at least be compatible with these observations.

5. References

[1] Seidl, E., Gummiztg. **25,** 710, (1911).
[2] Kirchhof, F., and Wagner, A., Gummiztg. **39,** 537, 572, 892 (1925).
[3] Perks, A. A., J. Soc. Chem. Ind. **45,** 142T (1926).
[4] Kimishima, T., Memoirs of the College of Engineering, Kyushu Imperial University, Fukuoka, Japan **4,** 193 (1927); Rubber Chem. and Technol. **1,** 307 (1928).

[5] Toyabe, Y., J. Soc. Chem. Ind. Japan **33,** 96B (1930); Rubber Chem. and Technol. **3,** 384 (1930).
[6] Toyabe, Y., J. Rubber Soc. Japan **2,** 251 (1930); Rubber Chem. and Technol. **4,** 514 (1931).
[7] Toyabe, Y., J. Soc. Chem. Ind. Japan **33,** 275B (1930); Rubber Chem. and Technol. **4,** 190 (1931).
[8] Riding, H., Trans. Inst. Rubber Ind. **6,** 230 (1931).
[9] Hada, K., and Nakajima, T., J. Soc. Rubber Ind. Japan **5,** 288 (1932); Rubber Chem. and Technol. **6,** 56 (1933).
[10] Horie, H., and Morikawa, K., J. Soc. Rubber Ind. Japan **7,** 5 (1934); Rubber Chem. and Technol. **8,** 514 (1935).
[11] Daynes, H. A., Trans. Inst. Rubber Ind. **11,** 336 (1935); Rubber Chem. and Technol. **9,** 444 (1936).
[12] Numaziri, S., J. Soc. Chem. Ind. Japan **43,** 285 (1940); Chem. Abs. **35,** 6145 (1941).
[13] Church, H. F., and Daynes, H. A., J. Rubber Research **13,** 55 (1944); Rubber Chem. and Technol. **17,** 923 (1944).
[14] Winspear, G. G., Herrmann, D. B., Malm, F. S., and Kemp, A. R., Ind. Eng. Chem. **38,** 687 (1946).
[15] Williams, I., and Beaver, D. J., Ind. Eng. Chem. **15,** 255 (1923).
[16] Blake, J. T., Ind. Eng. Chem. **26,** 1283 (1934) Rubber Chem. and Technol. **8,** 112 (1935).
[17] Oberto, S., Gomma **1,** 38 (1937); Rubber Chem. and Technol. **10,** 725 (1937).
[18] Bruce, P. L., Lyle, R., and Blake, J. T., Ind. Eng. Chem. **36,** 37 (1944); Rubber Chem. and Technol. **17,** 404 (1944).
[19] Hock, L., and Schroeter, G., Kolloid-Z. **152,** 98 (1957).
[20] Bhaumik, M. L., Sircar, A. K., and Banderjee, D., J. Appl. Polymer Sci. **4,** 366 (1960).
[21] Bhaumik, M. L., Banderjee, D., and Sircar, A. K., J. Appl. Polymer Sci. **6,** 674 (1962) Rubber Chem. and Technol. **36,** 1059 (1963).
[22] Bhaumik, M. L., Banderjee, D. and Sircar, A. K., Proc. Fourth Rubber Technol. Conf. London, May 22–25, 1962 Institution of the Rubber Industry, London, p. 80.
[23] McPherson, A. T., and Bekkedahl, N., J. Res. NBS **14,** No. 5, 601 (1935) RP 791. Ind. Eng. Chem. **27,** 597 (1935). Rubber Chem. and Technol. **8,** 456 (1935).
[24] Blake, J. T., Ind. Eng. Chem. **22,** 737 (1930). Rubber Chem. and Technol. **3,** 631 (1930).
[25] Hada, K., Fukaya, K., and Nakajima, T., J. Soc. Rubber Ind. Japan **2,** 389 (1931); Rubber Chem. and Technol. **4,** 507 (1931).
[26] Jessup, R. S., and Cummings, A. D., J. Res. NBS **13,** No. 3, 357 (1934) RP713; Rubber Chem. and Technol. **8,** 44 (1935).
[27] Rolla, L., and Piccardi, G., International Critical Tables **5,** 92 (1929).
[28] Furukawa, G. T., Douglas, T. B., McCoskey, R. E., and Ginnings, D. C., J. Res. NBS **57,** No. 2, 67 (1956) RP2694.
[29] Ginnings, D. C., and Furukawa, G. T., J. Am. Chem. Soc. **75,** 522 (1953).
[30] Furukawa, G. T., National Bureau of Standards, private communication.
[31] Wood, L. A., and Bekkedahl, N., J. Polymer Sci. Part B, (Polymer Letters) **5,** 169 (1967).
[32] West, E. D., J. Am. Chem. Soc. **81,** 29 (1959).
[33] de Vries, T., Ind. Eng. Chem. **22,** 617 (1930).
[34] Chemical Analysis of Rubber Products, A.S.T.M. Designation: D 297–67T.
[35] Weber, C. O., Chemistry of India Rubber, Charles Griffin and Co., London (1902) p. 91.
[36] Spence, D., and Scott, J. H., Kolloid-Z. **8,** 304 (1911).
[37] Brown, J. R., and Hauser, E. A., Ind. Eng. Chem. **30,** 1291 (1938). Rubber Chem. and Technol. **12,** 43 (1939).
[38] Hauser, E. A., and Brown, J. R., Ind. Eng. Chem. **31,** 1225 (1939), Rubber Chem. and Technol. **13,** 65 (1940).
[39] Sheppard, N., and Sutherland, G. B. B. M., J. Chem. Soc. **1947,** 1699; Rubber Chem. and Technol. **21,** 799 (1948).
[40] Linnig, F. J., and Stewart, J. E., J. Res. NBS **60,** No. 1, 9 (1958) RP2816; Rubber Chem. and Technol. **31,** 719 (1958).
[41] Bateman, L., Moore, C. G., Porter, M., and Saville, B., Chapter 15 in L. Bateman's The Chemistry and Physics of Rubberlike Substances, John Wiley and Sons, New York, New York p. 449 (1963).
[42] Moore, C. G., Chapter in L. Mullins' Proceedings of the Natural Rubber Procedures Research Association Jubilee Conference, Cambridge (1964) Maclaren and Sons, Ltd., London, England, p. 167.
[43] Scheele, W., Rubber Chem. and Technol. **40,** 849 (1967).
[44] Saville, B., and Watson, A. A., Rubber Chem. and Technol. **40,** 100 (1967).
[45] Wolesensky, E., J. Res. NBS **4,** 501 (1930) RP 162; Rubber Chem. and Technol. **3,** 386 (1930).
[46] Cummings, A. D., Bur. Std. J. Res. NBS **9,** 163 (1932) R.P. 464; Rubber Chem. and Technol. **6,** 46 (1933).
[47] Fry, J. D., and Porritt, B. D., India Rubber J. **78,** 307 (1929).
[48] Webster, D. M., and Porritt, B. D., India Rubber J. **79,** 239 (1930); Rubber Chem. and Technol. **3,** 618 (1930).
[49] J. Franklin Inst. **219,** 607 (1935).
[50] McPherson, A. T., NBS Sci. Pap. **22,** 385 (1927).
[51] Martin, G. M., and Mandelkern, L., J. Res. NBS **62,** No. 4, 141 (1959) RP 2944.

(Paper 73A2–548)

JOURNAL OF RESEARCH of the National Bureau of Standards—A. Physics and Chemistry
Vol. 73A, No. 2, March–April 1969

A Table of Rotational Constants of Symmetric Top Molecules Giving Rise to Microwave Spectra*

Matthew S. Lojko

Environmental Science Services Administration, Boulder, Colorado 80302

and

Yardley Beers

National Bureau of Standards, Boulder Colorado 80302

(December 23, 1968)

This paper lists, in order of increasing value, the "B" rotational constants of most of the linear and symmetric top molecules which have been observed by microwave spectroscopy. Also are listed the microwave spectral lines which have been observed for the asymmetric tops water and formaldehyde. These data are useful for making a quick selection of a molecule which has a spectral line close to some previously selected frequency.

Key words: Asymmetric, linear, and symmetric top molecules; "B" rotational constants; formaldehyde; microwave spectra; spectral lines; water.

Nowadays there are a number of actual and potential situations in which one would like to select a molecule to have a spectral line close to some previously specified frequency. For one thing, the transitions of light linear or symmetric top molecules, which lie in almost but not exact harmonic relationship, are used to tune up millimeter wave spectrographs. For another, there is a great interest in devising experiments, many involving lasers, in which a spectral line, or one of the harmonics of its frequency, nearly coincides with a spectral line of another substance. In addition there might be practical applications, such as in a communications system, in which it may be desired to build a molecular frequency standard with its fundamental close to some previously chosen frequency.

As an aid to making such a selection, herewith in table 1 is presented, in order of increasing value, the "B" rotational constants of most of the linear and symmetric top molecules which are listed in "Microwave Spectral Tables," National Bureau of Standards, Monograph 70.[1] From the simple well-known formula given in eq (1) it is possible to get a very good approximation of the frequencies of nearly all of the rotational lines of these molecules. The frequency

$$f = 2BJ, \tag{1}$$

where J is any integer, which is the quantum number giving the total angular momentum (not including nuclear spin) of the upper state giving rise to the transition. In table 1, values of B are given for only one isotopic species of each molecule, generally the most abundant one. The values for other isotopic species may be easily determined from the fact that B is inversely proportional to the reduced mass of the molecule. Also listed in table 1 are the common names of the molecules to aid in referring to handbooks giving physical properties and to the catalogs of chemical companies.

The values of B given in table 1 were obtained from the same punched computer cards which served as the basis of the "Microwave Spectral Tables." A program was written for selecting the values in accordance with the present philosophy, arranging the values in ascend-

*Contribution of National Bureau of Standards and Environmental Science Services Administration, not subject to copyright.

[1] These Tables may be obtained through the Superintendent of Documents, U.S. Government Printing Office, Washington, D.C. 20402.
The following volumes have been published:
Volume I: Diatomic Molecules, by P. F. Wacker, M. Mizushima, J. D. Petersen, and J. R. Ballard, December 15, 1964.
Volume II: Line Strengths of Asymmetric Rotors, by P. F. Wacker and M. R. Pratto, December 15, 1964.
Volume IV: Polyatomic Molecules Without Internal Rotation, M. S. Cord, J. D. Petersen, M. S. Lojko, and R. H. Haas, October 1968.
Volume V: Spectral Line Listing, by M. S. Cord, M. S. Lojko, and J. D. Petersen, June 1968.
Publication of the remaining volume is expected shortly:
Volume III: Polyatomic Molecules With Internal Rotation, P. F. Wacker, M. S. Cord, D. G. Burkhard, J. D. Petersen, and R. F. Kukol.

ing order, and printing out the result. In this tabulation, it has not been practical to distinguish between ground vibrational state (B_0) and equilibrium state (B_e) values. In most cases, however, for polyatomic molecules the values given pertain to the ground vibrational state while for diatomic molecules they pertain to the equilibrium state. However, the difference between values of these quantities for the same molecule is probably smaller than the errors associated with eq (1) which result from the neglect of such effects as centrifugal distortion and hyperfine effects.

Accordingly, it is appropriate to give some general discussion of the tables. The present series of volumes are based upon a thorough search of the literature of microwave spectroscopy. The cut-off date of the search differs slightly from volume to volume but is approximately 1961 for all of them. In addition, through the cooperation of numerous investigators, much unpublished data and data published in sources not widely available have been included. In a number of cases where important data after the official cut-off date happened to be conveniently available, they were included, but inclusion of post-cut-off data was determined by convenience and nothing else. A critical selection was made, and the selected data on frequencies and molecular constants were transcribed upon punched cards. The cards were checked against the original sources. Except for a few nonstandard situations, all final print-out was made direct from the cards by use of suitable programs. The present series of volumes were carried out in accordance with a plan developed by Paul W. Wacker. It received sponsorship of the Office of Standard Reference Data of the National Bureau of Standards when it became established. It is likely that in due time supplements to the present series will be published under sponsorship of the Office.

Volume V, which lists the measured frequencies of spectral lines in order of frequency, is also useful in giving direct answers to questions of the type described in the opening paragraph above. Indeed most of the time it may be more useful than table 1 and eq (1). However, the present material is useful in providing some answers not contained in Volume V, and therefore availability of the present material is highly desirable. One reason is that Volume V contains only lines that have actually been observed and measured accurately. However, there exist many lines which are observable but which have not been observed, and there are others which have been observed but not measured accurately and not published. In addition, Volume V contains very few entries above 300 GHz and none above 500 GHz. At the same time, the development of submillimeter lasers has stimulated a great interest in the frequencies of spectral lines up to a few thousand megahertz. The material given here can be used to give good approximations of the frequencies of many spectral lines which are involved in either of these two categories. Once eq (1) has been used to select a molecular transition, the frequency may be computed more exactly by including such effects as centrifugal distortion and hyperfine interactions by methods contained in textbooks but beyond the scope of this paper.

TABLE 1. *"B" Rotational constants of symmetric top and linear molecules*

B(MHz)	Molecule name	Isotopic species [a]
708.3579	Cesium Iodide	$Cs^{133}I^{127}$
725.9	1-Bromo-Bicyclo(2,2,2)Octane	$C_8^{12}H_{13}Br^{79}$
729.8	Benzene Chromium Tricarbonyl	$C_6^{12}H_6Cr^{52}(C^{12}O^{16})_3$
788.0	Methyl Mercuric Iodide	$C^{12}H_3Hg^bI^b$
817.510	Thallium Iodide	$Tl^{205}I^{127}$
891.69	1-Chloro-3,3-Dimethyl-1-Butyne	$(C^{12}H_3)_3C^{12}C^{12}\equiv C^{12}Cl^{35}$
984.3166	Rubidium Iodide	$Rb^{85}I^{127}$
996.4	Phosphorus Tribromide	$P^bBr_3^{79}$
1081.343	Cesium Bromide	$Cs^{133}Br^{79}$
1096.42	Trimethyliodosilane	$(C^{12}H_3)_3Si^{28}I^{127}$
1104.95	Indium Iodide	$In^{115}I^{127}$
1142.86	Methyl Mercuric Bromide	$C^{12}H_3Hg^{198}Br^{79}$
1247.61	Tribromomethane	$C^{12}HBr_3^{79}$
1259.02	1-Iodopropyne	$H_3C^{12}C^{12}\equiv C^{12}I^{127}$
1259.25	Nickel Cyclopentadienyl Nitrosyl	$C_5^{12}H_5N^{14}Ni^{58}O^{16}$
1297.409	Thallium Bromide	$Tl^{205}Br^{79}$
1369.70	1,1,1-Trifluoro-2-Butyne	$C^{12}H_3C^{12}\equiv C^{12}C^{12}F_3^{19}$
1402.64	Thiophosphoryl Chloride	$S^{32}P^{31}Cl_3^{35}$
1424.840	Rubidium Bromide	$Rb^{85}Br^{79}$
1461.95	Trimethylbromosilane	$(C^{12}H_3)_3Si^{28}Br^{79}$
1467.98	Cyclopentadienyl Thallium	$C_5^{12}H_5Tl^{203}$
1497.	Bismuth Trichloride	$Bi^{209}Cl_3^{35}$
1516.018	Silyl Isothiocyanate	$Si^{28}H_3N^{14}C^{12}S^{32}$
1523.23	Trifluoroiodomethane	$C^{12}F_3^{19}I^{127}$
1549.98	Bromotrifluorosilane	$Si^{28}F_3^{19}Br^{79}$
1561.11	1-Bromopropyne	$H_3C^{12}C^{12}\equiv C^{12}Br^{79}$

[a] The superscript b means that the particular isotope was not specified.

TABLE 1. *"B" Rotational constants of symmetric top and linear molecules*—Continued

B(MHz)	Molecule name	Isotopic species [a]
1562.	2-Iodo-2-Methylpropane	$(C^{12}H_3)_3C^{12}I^{127}$
1573.7	Trimethylamine-Trimethylborane	$(C^{12}H_3)_3N^{14} \cdot B^{11}(C^{12}H_3)_3$
1584.122	Thiocarbonyl Telluride	$S^{32}C^{12}Te^{122}$
1599.3	Methyltrichlorogermane	$C^{12}H_3Ge^bCl_3^{35}$
1667.2	Trichloroacetonitrile	$C^{12}Cl_3^{35}C^{12}N^{14}$
1670.14	Indium Bromide	$In^{115}Br^{79}$
1706.86	Gallium Monoiodide	$Ga^{69}I^{127}$
1750.	Trifluoroborane-trimethylamine	$F_3^{19}B^b \cdot N^b(C^{12}H_3)_3$
1753.9	Antimony Trichloride	$Sb^{121}Cl_3^{35}$
1769.836	Methyltrichlorosilane	$C^{12}H_3Si^{28}Cl_3^{35}$
1825.012	Potassium Iodide	$K^{39}I^{127}$
2001.56	Thiocarbonyl Selenide	$S^{32}C^{12}Se^{82}$
2015.20	Phosphoryl Chloride	$P^{31}O^{16}Cl_3^{35}$
2035.741	Penta-1,3-Diyne	$H_3C^{12}C^{12} \equiv C^{12}C^{12} \equiv C^{12}H$
2044.2	2-Bromo-2-Methylpropane	$(C^{12}H_3)_3C^{12}Br^{79}$
2065.73	2-Butynenitrile	$H_3C^{12}C^{12} \equiv C^{12}C^{12}N^{14}$
2077.48	Methyl Mercuric Chloride	$C^{12}H_3Hg^{198}Cl^{35}$
2094.20	Rhenium Trioxychloride	$Re^{185}O_3^{16}Cl^{35}$
2098.06	Bromotrifluoromethane	$C^{12}F_3^{19}Br^{79}$
2147.2	Arsenic Trichloride	$As^{75}Cl_3^{35}$
2161.208	Cesium Chloride	$Cs^{133}Cl^{35}$
2168.52	Chlorotrifluorogermane	$Ge^{70}F_3^{19}Cl^{35}$
2172.75	Trichlorogermane	$Ge^{70}HCl_3^{35}$
2197.441	Trimethylchlorosilane	$(C^{12}H_3)_3Si^{28}Cl^{35}$
2232.271	1-Chloropropyne	$C^{12}H_3C^{12} \equiv C^{12}Cl^{35}$
2326.	Phosphorus Tricyanide	$P^b(C^{12}N^{14})_3$
2372.6	1,1,1-Trichloroethane	$C^{12}H_3C^{12}Cl_3^{35}$
2431.4	Quinuclidine	$C_7^{12}H_{13}N^{14}$
2434.953	Potassium Bromide	$K^{39}Br^{79}$
2438.57	Bromogermane	$Ge^{70}H_3Br^{79}$
2465.39	Trichlorofluoromethane	$C^{12}Cl_3^{35}F^{19}$
2472.489	Trichlorosilane	$Si^{28}HCl_3^{35}$
2477.79	Chlorotrifluorosilane	$Si^{28}F_3^{19}Cl^{35}$
2481.99	Gallium Monobromide	$Ga^{69}Br^{79}$
2617.1	Phosphorus Trichloride	$P^{31}Cl_3^{35}$
2657.63	Thiophosphoryl Fluoride	$S^{32}P^{31}F_3^{19}$
2683.18	1,1-Dimethyl-3-Butyne	$(C^{12}H_3)_2C^{12}C^{12} \equiv C^{12}H$
2743.913	Thallium Chloride	$Tl^{203}Cl^{35}$
2749.89	2,2-Dimethylpropanenitrile	$(C^{12}H_3)_3C^{12}C^{12}N^{14}$
2767.414	Rubidium Chloride	$Rb^{85}Cl^{35}$
2877.93	3,3,3-Trifluoro-1-Propyne	$C^{12}F_3^{19}C^{12} \equiv C^{12}H$
2945.528	Trifluoroacetonitrile	$C^{12}F_3^{19}C^{12}N^{14}$
3017.69	2-Chloro-2-Methylpropane	$(C^{12}H_3)_3C^{12}Cl^{35}$
3215.52	Iodosilane	$Si^{28}H_3I^{127}$
3225.578	Cyanogen Iodide	$I^{127}C^{12}N^{14}$
3257.	Methyltrifluorogermane	$C^{12}H_3Ge^bF_3^{19}$
3269.47	Indium Chloride	$In^{115}Cl^{35}$
3301.94	Trichloromethane	$C^{12}HCl_3^{35}$
3335.56	Chlorotrifluoromethane	$C^{12}F_3^{19}Cl^{35}$
3411.00	Trimethylfluorosilane	$(C^{12}H_3)_3Si^{28}F^{19}$
3422.300	Iodine Monochloride	$I^{127}Cl^{35}$
3531.778	Sodium Iodide	$Na^{23}I^{127}$
3566.801	Rhenium Trioxyfluoride	$Re^{185}O_3^{16}F^{19}$
3715.66	Methyltrifluorosilane	$C^{12}H_3Si^{28}F_3^{19}$
3856.399	Potassium Chloride	$K^{39}Cl^{35}$
4095.786	Carbonyl Selenide	$O^{16}C^{12}Se^{74}$
4120.230	Cyanogen Bromide	$Br^{79}C^{12}N^{14}$
4129.106	Manganese Trioxyfluoride	$Mn^{55}O_3^{16}F^{19}$
4321.72	Bromosilane	$Si^{28}H_3Br^{79}$
4401.71	Chlorogermane	$Ge^{70}H_3Cl^{35}$
4493.73	Gallium Monochloride	$Ga^{69}Cl^{35}$
4534.52	Sodium Bromide	$Na^{23}Br^{79}$
4549.07	Propiolonitrile	$HC^{12} \equiv C^{12}C^{12}N^{14}$
4570.92	Bromine Monochloride	$Br^{79}Cl^{35}$
4594.262	Phosphoryl Fluoride	$P^{31}O^{16}F_3^{19}$
4636.24	Trifluorosulfur Nitride	$N^{14}S^{32}F_3^{19}$

[a] The superscript b means that the particular isotope was not specified.

TABLE 1. *"B" Rotational constants of symmetric top and linear molecules*—Continued

B(MHz)	Molecule name	Isotopic species [a]
4712.15	2-Fluoro-2-Methylpropane	$(C^{12}H_3)_3C^{12}F^{19}$
4724.98	Trimethylarsine	$(C^{12}H_3)_3As^{75}$
4972.7	Silyl Cyanide	$H_3Si^{28}C^{12}N^{14}$
5185.14	1,1,1-Trifluoroethane	$C^{12}H_3C^{12}F_3^{19}$
5260.66	Perchlorylfluoride	$Cl^{35}O_3^{16}F^{19}$
5273.6	1,3,5-Trioxane	$O^{16*}C^{12}H_2O^{16}C^{12}H_2O^{16}C^{12*}H_2$
5345.15	Trimethylsilane	$(C^{12}H_3)_3Si^{28}H$
5527.34	Cesium Fluoride	$Cs^{13}F^{19}$
5684.24	Chloroacetylene	$HC^{12}\equiv C^{12}Cl^{35}$
5816.24	Trimethylphosphine	$(C^{12}H_3)_3P^{31}$
5878.971	Arsenic Trifluoride	$As^{75}F_3^{19}$
5970.831	Cyanogen Chloride	$Cl^{35}C^{12}N^{14}$
6081.480	Carbonyl Sulfide	$O^{16}C^{12}S^{32}$
6537.07	Sodium Chloride	$Na^{23}Cl^{35}$
6673.8	Chlorosilane	$Si^{28}H_3Cl^{35}$
6695.46	Thallium Fluoride	$Tl^{203}F^{19}$
6906.35	Methyltin	$C^{12}H_3Sn^{118}H_3$
7208.049	Trifluorosilane	$Si^{28}F_3^{19}H$
7501.30	Iodomethane	$C^{12}H_3I^{127}$
7789.45	2-Methylpropane	$(C^{12}H_3)_3C^{12}H$
7819.900	Phosphorus Trifluoride	$P^{31}F_3^{19}$
8545.84	Propyne	$C^{12}H_3C^{12}\equiv C^{12}H$
8710.65	Methylgermane	$C^{12}H_3Ge^{70}H_3$
8720.86	Trimethylamine	$(C^{12}H_3)_3N^{14}$
8979.94	Carbonyl Borane	$H_3B^{10}C^{12}O^{16}$
9198.83	Acetonitrile	$C^{12}H_3C^{12}N^{14}$
9568.20	Bromomethane	$C^{12}H_3Br^{79}$
9706.22	Fluoroacetylene	$HC^{12}\equiv C^{12}F^{19}$
10052.88	Methyl Isocyanide	$C^{12}H_3N^{14}C^{12}$
10348.74	Trifluoromethane	$C^{12}HF_3^{19}$
10554.20	Cyanogen Fluoride	$F^{19}C^{12}N^{14}$
10680.96	Nitrogen Trifluoride	$N^{14}F_3^{19}$
10706.9	Bromine Monofluoride	$Br^{79}F^{19}$
10968.96	Methylsilane	$C^{12}H_3Si^{28}H_3$
12561.64	Nitrous Oxide	$N_2^{14}O^{16}$
13292.84	Chloromethane	$C^{12}H_3Cl^{35}$
14327.9	Fluorosilane	$Si^{28}H_3F^{19}$
15381.99	Lithium Iodide	Li^6I^{127}
15483.69	Fluorine Chloride	$F^{19}Cl^{35}$
19162.32	Lithium Bromide	Li^6Br^{81}
24584.35	Carbon Monosulfide	$C^{12}S^{32}$
25530.59	Fluoromethane	$C^{12}H_3F^{19}$
43100.5	Oxygen	O_2^{16}
44315.99	Hydrocyanic Acid	$HC^{12}N^{14}$
51109.51	Nitric Oxide	$N^{14}O^{16}$
57898.568	Carbon Monoxide	$C^{12}O^{16}$
88031.92	Stibine	$Sb^{121}H_3$
112468.5	Arsine	$As^{75}H_3$
128600	Hydrogen Bromide	DBr^{79}
133478.3	Phosphine	$P^{31}H_3$
163340.1	Hydrogen Chloride	DCl^{35}
195229.1	Hydrogen Iodide	HI^{127}
298000	Ammonia	$N^{14}H_3$

[a] The superscript b means that the particular isotope was not specified.

Of course, there are molecular transitions other than the rotational ones of symmetric top molecules that can serve the purposes alluded to in the introductory paragraph. The well known inversion spectrum of ammonia has been used for this purpose. The frequencies of the lines are tabulated in Volume V and elsewhere. The lines of asymmetric tops may be used too, if they are listed in Volume V or known by some other means. However, the calculation of their frequencies from molecular data cannot be done in closed form, and even rough estimates can sometimes be very laborious. Two of these molecules, water and formaldehyde, deserve special mention because samples are easy to obtain, and the lines from them are very strong and distributed widely over the spectrum. For convenience, the listings of spectral lines of these molecules, contained in Volume IV of NBS Monograph 70, are reprinted here in tables 2 and 3 respectively.

TABLE 2. *Microwave spectral lines of water*

The Rotational Quantum Numbers are, respectively, J, K_{-1}, *and* K_{+1} upper state followed by J, K_{-1}, and K_{+1} of the lower state.

All transitions pertain to ground vibrational state.

Isotopic species	Rotational quantum Nos.	Hyperfine				Frequency MHz	Acc. ± MHz
		F_1'	F'	F_1	F		
H_2O^{16}	3, 1, 3 ← 2, 2, 0					183 311.30	.30
	6, 1, 6 ← 5, 2, 3					22 235.22	.05
HDO^{16}	1, 1, 0 ← 1, 1, 1					80 578.15	
	2, 1, 1 ← 2, 1, 2					241 561.3	
	2, 2, 1 ← 2, 2, 0	1	3/2	2	5/2	10 278.0796	.001
	2, 2, 1 ← 2, 2, 0	3	5/2	3	7/2	10 278.1365	.001
	2, 2, 1 ← 2, 2, 0	1	1/2	1	3/2	10 278.1681	.001
	2, 2, 1 ← 2, 2, 0	3	5/2	1	3/2	10 278.2255	.001
	2, 2, 1 ← 2, 2, 0					10 278.2455	.001
	2, 2, 1 ← 2, 2, 0	1	3/2	3	5/2	10 278.2643	.001
	2, 2, 1 ← 2, 2, 0	1	3/2	1	1/2	10 278.3234	.001
	2, 2, 1 ← 2, 2, 0	3	7/2	3	5/2	10 278.3554	.001
	2, 2, 1 ← 2, 2, 0	2	5/2	1	3/2	10 278.4126	.001
	3, 2, 1 ← 3, 2, 2					50 236.30	
	3, 3, 0 ← 3, 3, 1	3	5/2	2	3/2	824.4754	.002
	3, 3, 0 ← 3, 3, 1	4	9/2	4	7/2	824.5074	.002
	3, 3, 0 ← 3, 3, 1	3	5/2	4	7/2	824.5247	.002
	3, 3, 0 ← 3, 3, 1	3	7/2	3	5/2	824.5488	.002
	3, 3, 0 ← 3, 3, 1	3	7/2	4	9/2	824.5685	.002
	3, 3, 0 ← 3, 3, 1	2	5/2	4	7/2	824.6042	.002
	3, 3, 0 ← 3, 3, 1					824.6706	.002
	3, 3, 0 ← 3, 3, 1	2	5/2	4	7/2	824.7419	.002
	3, 3, 0 ← 3, 3, 1	3	7/2	4	9/2	824.7730	.002
	3, 3, 0 ← 3, 3, 1	3	7/2	3	5/2	824.7904	.002
	3, 3, 0 ← 3, 3, 1	3	5/2	4	7/2	824.8136	.002
	3, 3, 0 ← 3, 3, 1	4	9/2	4	7/2	824.8341	.002
	3, 3, 0 ← 3, 3, 1	3	5/2	2	3/2	824.8637	.002
	3, 2, 1 ← 4, 1, 4					20 460.40	
	4, 2, 2 ← 4, 2, 3					143 727.2	
	4, 3, 1 ← 4, 3, 2					5 702.78	
	5, 0, 5 ← 4, 2, 2					2 887.4	.1
	5, 1, 5 ← 4, 2, 2					120 778.2	
	5, 3, 2 ← 5, 3, 3					22 307.67	.05
	5, 4, 1 ← 5, 4, 2	5	11/2	5	9/2	486.266	.002
	5, 4, 1 ← 5, 4, 2	5	11/2	4	9/2	486.450	.002
	5, 4, 1 ← 5, 4, 2	5	11/2	6	13/2	486.487	.002
	5, 4, 1 ← 5, 4, 2					486.528	.002
	5, 4, 1 ← 5, 4, 2	5	11/2	6	13/2	486.569	.002
	5, 4, 1 ← 5, 4, 2	5	11/2	4	9/2	486.606	.002
	6, 1, 6 ← 5, 2, 3					138 530.4	
	6, 4, 2 ← 6, 4, 3					2 394.56	.05
	7, 1, 7 ← 6, 2, 4					26 880.38	.05
	7, 4, 3 ← 7, 4, 4					8 577.7	.1
	8, 4, 4 ← 8, 4, 5					24 884.77	.05
	9, 5, 4 ← 9, 5, 5					3 044.71	.10
	10, 5, 5 ← 10, 5, 6					8 836.95	.1
	11, 5, 6 ← 11, 5, 7					22 581.1	.2
	12, 6, 6 ← 12, 6, 7					2 961.	1.
D_2O^{16}	3, 1, 3 ← 2, 2, 0	7/2	3	5/2	2	10 919.301	.001
	3, 1, 3 ← 2, 2, 0	9/2	5	7/2	4	10 919.357	.001
	3, 1, 3 ← 2, 2, 0	5/2	4	3/2	3	10 919.521	.001
	3, 1, 3 ← 2, 2, 0	9/2	3	7/2	2	10 919.603	.001
	4, 2, 3 ← 3, 3, 0					43 414.57	

TABLE 2. *Microwave spectral lines of water*—Continued

Isotopic species	Rotational quantum Nos.	Hyperfine				Frequency MHz	Acc. ± MHz
		F_i'	F'	F_i	F		
—Continued	4, 4, 0 ← 5, 3, 3					55 482.32	
	4, 4, 1 ← 5, 3, 2					10 947.13	.05
	6, 1, 6 ← 5, 2, 3					90 916.8	
HDO^{17}	2, 2, 0 ← 2, 2, 1					10 374.56	
	3, , ← 2, ,					23 374.4	.05
	3, , ← 2, ,					23 481.6	.05
	3, , ← 2, ,					23 585.6	.05
	3, , ← 2, ,					23 646.3	.05
	3, , ← 2, ,					24 256.0	.05
	3, , ← 2, ,					24 280.5	.05
	3, , ← 2, ,					24 384.9	.5
	3, , ← 2, ,					24 472.6	.5
	3, , ← 2, ,					24 528.8	.5

TABLE 3. *Microwave spectral lines of formaldehyde*

The Rotational Quantum Numbers are, respectively, J, K_{-1}, and K_{+1} upper state followed by J, K_{-1}, and K_{+1} of the lower state.

All transitions pertain to ground vibrational state.

Isotopic species	Rotational quantum Nos.	Hyperfine				Frequency MHz	Acc. ± MHz
		F_i'	F'	F_i	F		
$HC^{12}HO^{16}$	1, 0, 1 ← 0, 0, 0					72 838.14	
	1, 1, 0 ← 1, 1, 1					4 829.73	.01
	2, 0, 2 ← 1, 0, 1					145 603.1	.73
	2, 1, 1 ← 1, 1, 0					150 498.2	.75
	2, 1, 2 ← 1, 1, 1					140 839.3	.70
	2, 1, 1 ← 2, 1, 2					14 488.65	
	3, 0, 3 ← 2, 0, 2					218 221.6	1.1
	3, 1, 2 ← 2, 1, 1					225 698.2	1.1
	3, 1, 3 ← 2, 1, 2					211 210.6	1.1
	3, 2, 0 ← 2, 2, 0					218 759.4	1.1
	3, 2, 2 ← 2, 2, 1					218 475.1	1.1
	3, 1, 2 ← 3, 1, 3					28 974.85	
	3, 2, 1 ← 3, 2, 2					355.586	.005
	4, 1, 3 ← 4, 1, 4					48 284.60	
	4, 2, 2 ← 4, 2, 3					1 065.85	.02
	5, 1, 4 ← 5, 1, 5					72 409.35	
	6, 2, 4 ← 6, 2, 5					4 954.76	.01
	7, 2, 5 ← 7, 2, 6					8 884.87	
	8, 2, 6 ← 8, 2, 7					14 726.74	
	8, 3, 5 ← 8, 3, 6					301.10	.01
	9, 2, 7 ← 9, 2, 8					22 965.71	
	9, 3, 6 ← 9, 3, 7					601.07	.005
	11, 2, 9 ← 11, 2,10					48 612.70	.1
	12, 3, 9 ← 12, 3,10					3 225.58	.01
	13, 3,10 ← 13, 3,11					5 136.58	.01
	14, 3,11 ← 14, 3,12					7 892.03	
	15, 3,12 ← 15, 3,13					11 753.13	
	16, 3,13 ← 16, 3,14					17 027.60	
	17, 3,14 ← 17, 3,15					24 068.31	
	19, 3,16 ← 19, 3,17					45 063.10	.1

TABLE 3. *Microwave spectral lines of formaldehyde*—Continued

Isotopic species	Rotational quantum Nos.	Hyperfine				Frequency MHz	Acc. ± MHz
		F_1'	F'	F_1	F		
$HC^{12}HO^{16}$—Con.	20, 4,16 ← 20, 4,17					3 518.85	.5
	21, 4,17 ← 21, 4,18					5 138.57	.5
	22, 4,18 ← 22, 4,19					7 362.60	
	23, 4,19 ← 23, 4,20					10 366.51	
	24, 4,20 ← 24, 4,21					14 361.54	
	25, 4,21 ← 25, 4,22					19 595.23	
	26, 4,22 ← 26, 4,23					26 358.82	
	28, 4,24 ← 28, 4,25					45 835.58	
	31, 5,26 ← 31, 5,27					7 833.20	
	1, 1, 0 ← 1, 1, 1					4 593.26	.5
	2, 1, 1 ← 2, 1, 2					13 778.86	
	3, 1, 2 ← 3, 1, 3					27 555.73	
	4, 1, 3 ← 4, 1, 4					45 920.08	
	7, 2, 5 ← 7, 2, 6					8 012.56	.5
	9, 2, 7 ← 9, 2, 8					20 736.30	
	14, 3,11 ← 14, 3,12					6 752.31	.5
	16, 3,13 ← 16, 3,14					14 592.44	
	17, 3,14 ← 17, 3,15					20 649.30	
	18, 3,15 ← 18, 3,16					28 582.40	
$HC^{12}HO^{18}$	1, 1, 0 ← 1, 1, 1					4 388.85	.5
$DC^{12}DO^{16}$	1, 1, 0 ← 1, 1, 1					6 096.10	.02
	2, 1, 1 ← 2, 1, 2					18 287.90	
	4, 2, 2 ← 4, 2, 3					3 687.28	.04
	5, 2, 3 ← 5, 2, 4					8 519.10	
	6, 2, 4 ← 6, 2, 5					16 759.64	
	8, 3, 5 ← 8, 3, 6					2 850.62	.03
	9, 3, 6 ← 9, 3, 7					5 636.98	
	10, 3, 7 ← 10, 3, 8					10 304.64	
	13, 4, 9 ← 13, 4,10					3 079.48	.03
	14, 4,10 ← 14, 4,11					5 461.54	
	15, 4,11 ← 15, 4,12					9 259.88	
	16, 4,12 ← 16, 4,13					15 080.34	
	19, 5,14 ← 19, 5,15					4 508.39	.04
$HC^{12}DO^{16}$	1, 1, 0 ← 1, 1, 1					5 346.64	.03
	2, 1, 1 ← 2, 1, 2					16 038.06	
	3, 2, 1 ← 3, 2, 2					644.893	.005
	5, 2, 3 ← 5, 2, 4					4 489.08	.03
	6, 2, 4 ← 6, 2, 5					8 922.59	
	7, 2, 5 ← 7, 2, 6					15 907.38	
	10, 3, 7 ← 10, 3, 8					3 283.09	.03
	11, 3, 8 ← 11, 3, 9					5 702.6	
	12, 3, 9 ← 12, 3,10					9 412.51	
	13, 3,10 ← 13, 3,11					14 873.02	
	16, 4,12 ← 16, 4,13					2 946.67	.03
	17, 4,13 ← 17, 4,14					4 713.90	
	18, 4,14 ← 18, 4,15					7 322.35	
	19, 4,15 ← 19, 4,16					11 074.30	
	23, 5,18 ← 23, 5,19					3 330.66	.04
	24, 5,19 ← 24, 5,20					5 018.25	
$HC^{12}DO^{16}$	1, 1, 0 ← 1, 1, 1					5 156.19	.10

(Paper 73A2–549)

JOURNAL OF RESEARCH of the National Bureau of Standards—A. Physics and Chemistry
Vol. 73A, No. 2, March–April 1969

Energy Levels, Wave Functions, Dipole and Quadrupole Transitions of Fe^{+++} Ions in Sapphire*

Jacques Lewiner**

Physics Department, Catholic University of America, Washington, D.C. 20017

Paul H. E. Meijer

Institute for Basic Standards, National Bureau of Standards, Washington, D.C. 20234

and

Physics Department, Catholic University of America, Washington, D.C. 20017

(December 26, 1968)

A computation is made of energy levels, wave functions and transition probabilities of the Fe^{3+} ion in Al_2O_3. The crystal field parameters used were those determined by Symmons and Bogle at 4 K. The magnetic field direction is described by the angles θ and φ indicating the directions with respect to and around the c axis of the crystal. The values of θ go from 0 to $\pi/2$ with $\pi/12$ intervals, the angles φ are 0 and $2\pi/3$ corresponding to the two nonequivalent sites of the crystal. The transition probabilities are given for dipole radiation in three polarization directions and for ultrasonic work the six components of the quadrupole transitions were computed.

Key words: Energy levels of Fe^{+++} in Al_2O_3; iron doped Al_2O_3; magneto elastic tensor; paramagnetic resonance; quadrupole transitions; spin hamiltonian; transition probabilities; ultrasonic (paramagnetic) resonance; ultrasonic transition probabilities; wave functions of Fe^{+++}

1. Introduction

As a result of recent work in ultrasonic paramagnetic resonance [1],[1] it became desirable to obtain a complete set of transition probabilities for quadrupole radiation, besides the known values for the dipolar transitions. We have programmed the calculations of these and related quantities in order to select *a priori* angles and field strengths that would enable us to observe specific components of the transition probabilities. There are some uncertainties with regard to the selection rules for ultrasonic absorption [2–4]. The first question is whether dipolar, quadrupolar, or a combination of these determines the line strength of the absorption. The next question is whether components of other multipoles are playing a role in the process.

In the available literature [5–8] the wave functions are never quoted. Consequently, it was necessary to recalculate these quantities in order to evaluate the transition probabilities. A new program was constructed for that purpose; the details are described in appendix I.

The physical properties and the spin hamiltonian are described in Sections 2 and 3.

The angle θ is the angle between the magnetic field and the c axis of the lattice which is a three-fold axis oriented along a body diagonal of the crystal field. There are two nonequivalent sites in the lattice. The angle φ depends on the ion in the unit cell. The crystal field is rotated over $\pi/3$ if one goes from one ion site to the other. Hence the spectrum is actually a superposition of two spectra. The differences are in general small, but noticeable.

The values for θ in which the calculation was performed are 0, $\pi/12$ . . . $\pi/2$ rad. for $\varphi=0$ and $\pi/3$. The field was varied from 0 to 0.5 Teslas (5000 Gauss) in steps of 0.025 T, but not all values are incorporated in

*This work was supported by NSG 647/07–05–008.
**Present address: Laboratoire d'Electricité Générale Ecole Supérieure de Physique et de Chimie 10 Rue Vauquelin—PARIS 5e.
[1] Figures in brackets indicate the literature references at the end of this paper.

the tables. At low field values and or near the crossing points, 10^{-3} T steps were used.

The crossing or non-crossing of the levels constitutes a certain practical difficulty in the labelling of the wave functions. We decided simply to list the levels in increasing order and label the wave functions accordingly.

2. Properties of the Crystal and Discussion of Previous Work

The free ion Fe^{3+} has the configuration $3d^5$. The $3d$ electron shell is half filled and the resultant orbital momentum L is equal to zero. The singlet ground state ^6S has a six-fold spin degeneracy. The first four excited states of the free ion are ^4G, ^4P, ^4D, and ^4F [9]. The optical spectrum has been studied by Moorjani and McAvoy [10].

The Al_2O_3 lattice, as described by Geschwind and Remeika [11] is shown in figure 1. It exhibits a three-fold symmetry around an axis perpendicular to the plane of the O^{2-}. The lattice presents the properties of the 3 m point group (D_{3d} in the Schoenflies notation) but each site has only a 3 (C_3) point of symmetry.

The specific directions for the propagation of sound waves have been studied by Borgnis [12]. The c axis and also the x axis (two-fold rotational symmetry often called "a" axis) are directions for purely compressional waves. There are two nonequivalent sites, which are identical except for a rotation of $\pi/6$ around the c axis. Consequently, the spectrum consists of the superposition of two slightly different spectra. The differences are large enough to be seen, i.e., the lines are clearly separated in certain directions and for certain fields. Ultrasonic propagation and absorption in Al_2O_3 were studied by Brian and Meister [13]. The velocity of sound for longitudinal waves is 10.9×10^5 cm/s, for shear waves, 6.41×10^5 cm/s. The Fe^{3+} ion, when introduced in the Al_2O_3 lattice occupies the sites of an Al ion. It is surrounded by 6 ions that are held responsible for the electric field: the O^{2-} ions. The positions of these ions determine the symmetry of the crystal field. Although deviations are known, the site symmetry can be considered bo be C_3 as mentioned above.

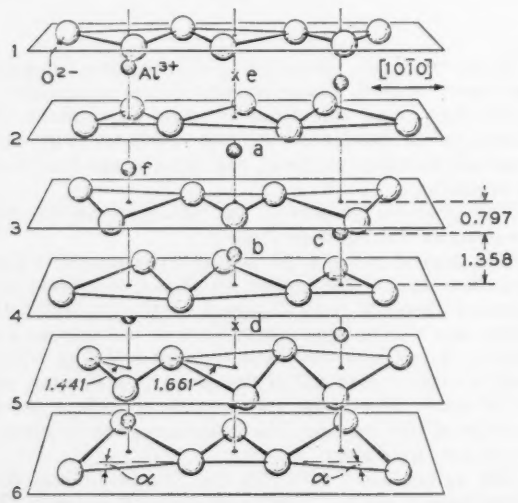

FIGURE 1. *Portion of the Al_2O_3 lattice, the two inequivalent sites are located in two adjacent planes for instance a and b (ref. [10]).*

The crystal field has a main component of trigonal symmetry and a smaller component of cubic symmetry. The total angular momemtum $J = S = 2\frac{1}{2}$ is split into three Kramers doublets whose degeneracy can be removed only by a magnetic field. For fields large compared to the zero field splitting the ion will be virtually free. Although the zero field splitting is small for S-state ions, most of the ultrasonic work was done in the low field region; hence we are mainly interested in the numerical values of the transition probabilities when magnetic field and crystal field are comparable.

This level structure is confirmed by many paramagnetic experiments [14–16]. The energy levels are most conveniently described by a spin hamiltonian with an effective spin $S = 5/2$. Abragam and Pryce proposed [7] the following expression:

$$\mathcal{H} = g\beta \mathbf{B} \cdot \mathbf{S} + D[S_z^2 - 35/12] + E[S_x^2 - S_y^2] + (a/6)[S_\xi^4 + S_\eta^4 + S_\zeta^4].$$

The D term corresponds to the trigonal or tetragonal crystalline field components and incorporates a part of the spin-spin interactions. A slight distortion from cylindrical symmetry around the z axis is described by the E term. The cubic field is described on a set of orthogonal axes such that the z axis (trigonal axis of the crystal) lies in the (111) direction. They considered the E term of no importance. Bleaney and Trenam [18] introduced another term for the fourth degree part of the trigonal field and wrote the spin hamiltonian

$$\mathcal{H} = g\beta \mathbf{B} \cdot \mathbf{S} + D[S_z^2 - (1/3)S(S+1)] + (F/180)[35S_z^4 - 30S(S+1)S_z^2 + 25S_z^2 - 6S(S+1) + 3S^2(S+1)^2] + (a/6)[S_\xi^4 + S_\eta^4 + S_\zeta^4 - (1/5)S(S+1)(3S^2 - 3S - 1)],$$

which became the generally accepted form. Basically, this is the most general form if one imposes the following conditions:

(1) The triangular rule requires that the main quantum number of the spin hamiltonian for d-electrons should be 4 or less.

(2) Inversion symmetry rules out even values for the main quantum number.

(3) The C_3 symmetry implies that the azimuthal quantum number can only take the values $0, \pm 3$.

For sufficiently high fields ($g\beta B \gg a$) the energy levels have been calculated. Bleaney and Ingram [19] obtained by perturbation calculation the matrix elements of the allowed transition in the absence of the

fourth order terms. This calculation was completed by Bleaney and Trenam [18]. The results are:

$$\pm 5/2 \leftrightarrow \pm 3/2: \quad g\beta B = g\beta B_0$$
$$\mp [2D(3\cos^2\theta - 1) + 2pa + 1/6Fq] - 32\delta_1 + 4\delta_2 + \epsilon_1$$
$$\pm 3/2 \leftrightarrow \pm 1/2: \quad g\beta B = g\beta B_0$$
$$\mp [D(3\cos^2\theta - 1) - 5/2pa - 5/24Fq] + 4\delta_1 - 5\delta_2 + \epsilon_2$$
$$+1/2 \leftrightarrow -1/2: \quad g\beta B = g\beta B_0 + 16\delta_1 - 8\delta_2 + \epsilon_3.$$

In these expressions B is the magnetic field corresponding to a transition at the frequency ν and $B_0 = h\nu/g\beta$.

Following Kronig and Bouwkamp [20] we introduced

$$p = (1 - 5\phi),\ \phi = (l^2m^2 + m^2n^2 + n^2l^2),$$

where (l, m, n) are the directions cosines of H referred to the axes of the cubic crystalline field. θ is the angle between H and the trigonal axis and

$$\epsilon_1 = \frac{a^2}{g\beta H_0}\,[(5/3)\phi(1 - 7\phi)]$$

$$\epsilon_2 = -\frac{a^2}{g\beta H_0}\,[(5/4)\delta(3 + 16\delta\phi - 625\phi^2)]$$

$$\epsilon_3 = \frac{a^2}{g\beta H_0}\,[(10/3)\phi(7 - 25\phi)]$$

$$q = 35\cos^4\theta - 30\cos^2\theta + 3$$
$$\delta_1 = (D^2/g\beta H_0)\cos^2\theta\sin^2\theta$$
$$\delta_2 = (D^2/4g\beta H_0)\sin^4\theta.$$

3. Calculation of Eigenvalues and Eigenfunctions of the Spin Hamiltonian

The general expression for spin hamiltonians, using the conventions introduced by Stevens [21] as reviewed by Hutchings [22], is given by

$$\mathcal{H} = \sum_n \sum_{m=0}^{n} B_n^m O_n^m,$$

where n is the "length" of the vector, m the azimuthal quantum number of its projection. The three restrictions mentioned in section 2 lead to a spin hamiltonian with three undetermined parameters

$$\mathcal{H} = B_2^0\,O_2^0 + B_4^0\,O_4^0 + B_4^3\,O_4^3 \qquad (1)$$

On the basis of the description of the crystal some coefficients are dominant, in particular, the term representing the trigonal field called $D = 3\,B_2^0$. Next in importance is probably the field of cubic symmetry, oriented in such a way that a body diagonal of the cube coincides with the three-fold axis of the trigonal field.

This field can be described in a coordinate system with the axes along the four-fold axes of the cube or in a system with the axes along the three-fold axis (plus two orthogonal axes, to be defined) of the crystal.

On the first set of axes we have in operator polynomials

$$\frac{a}{6}\left[S_\xi^4 + S_\eta^4 + S_\zeta^4 - \frac{1}{5}\,S(S+1)(3S^2 + 3S - 1)\right]$$
$$= \frac{a}{120}\,[O_4^0 + 5O_4^4]$$

This expression can be transformed into the second set of axes [22]. In figure 2 the z axis is in the (111) direction. The x axis is in the $z\zeta$ plane (fig. 3) and y is in the $\eta\xi$ plane:

$$(O_4^0 + 5O_4^4)_{\xi\eta\zeta} = -\frac{2}{3}\,(O_4^0 - 20\sqrt{2}\,O_4^3)_{xyz}$$

Finally it is assumed that the cube is distorted (elongated or compressed) along the z axis. This is accom-

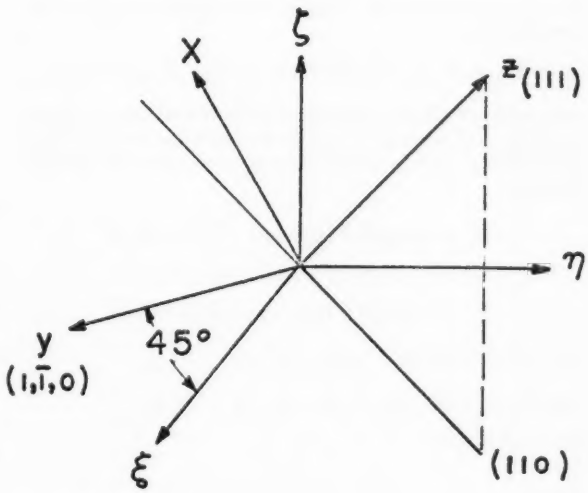

FIGURE 2. *Orientation of the* x y z *reference axes with respect to the* ξ, η, ζ *axes.*
The x axes is in the plane defined by ζ and (110) (see fig. 3).

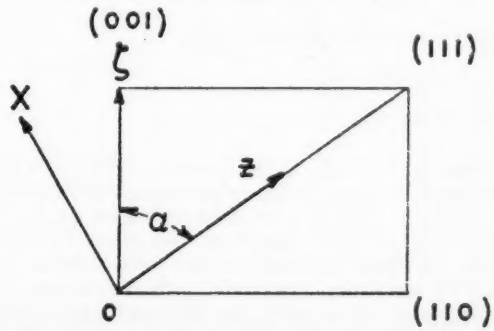

FIGURE 3. *Plane* $\zeta 0$ (110) *the angle* α *is defined by* $\mathrm{tg}\alpha = \sqrt{2}$.

plished by adding a term $F/180 = B_4^0$. Adding all contributions we have for the coefficients in eq (1)

$$B_2^0 = D/3,\ B_4^0 = (F-a)/180,\ B_4^3 = (\sqrt{2}/9)\ a.$$

$\|5/2\rangle$	$\|3/2\rangle$	$\|1/2\rangle$	$\|-1/2\rangle$	$\|-3/2\rangle$	$\|-5/2\rangle$
$10D/3-(a-F)/3$	0	0	$2\sqrt{5}\ a/3$	0	0
0	$-2D/3+(a-F)$	0	0	0	0
0	0	$-\pi\delta D/3-2(a-F)/3$	0	0	$-2\sqrt{5}\ a/3$
$2\sqrt{5}\ a/3$	0	0	$-8D/3-2(a-F)/3$	0	0
0	0	0	0	$-2D/3+(a-F)$	0
0	0	$-2\sqrt{5}\ a/3$	0	0	$10D/3-(a-F)/3$

To insert the magnetic field in this matrix we use polar coordinates:

$$B_z = B\cos\theta;\ B_x = B\sin\theta\cos\varphi;\ B_y = B\sin\theta\sin\varphi$$

where φ is the angle between the field and the xz plane as defined in figures 2 and 3. In the case of $\theta = 0$ the eigenvalues and eigenfunctions can be calculated directly:

$$E_{1,2} = \pm g\beta B + D/3 - (a-F)/2 - \Delta_\pm/2$$
$$E_{3,4} = \mp 3g\beta B/2 - 2D/3 + (a-F)$$
$$E_{5,6} = \mp g\beta B + D/3 - (a-F)/2 + \Delta_\mp/2$$
$$|\psi_{1,6}\rangle = 2\sqrt{5}/3\ aC_\pm\,|5/2\rangle \mp A_\pm/C_\pm\,|-1/2\rangle$$
$$|\psi_{2,5}\rangle = 2\sqrt{5}/3\ aD_\pm\,|1/2\rangle + B_\pm/D_\pm\,|-5/2\rangle$$
$$|\psi_{3,4}\rangle = |\mp 3/2\rangle$$

where

$$\Delta_\pm = [[3g\beta H \pm 6D \pm (a-F)/3]^2 + 80a^2/g]^{1/2}$$
$$A_\pm = [3g\beta H/2 + 3D + (a-F)/6 \pm \Delta_+]$$
$$B_\pm = [g\beta H/2 - 3D - (a-F)/6 \pm \Delta_-]$$
$$C_\pm = 20a^2/9 + A_\pm^2$$
$$D_\pm = 20a^2/9 + B_\pm^2$$

Note that for $\theta = 0$ (fig. 4) the levels $|-5/2\rangle$ and $|1/2\rangle$ do not cross, contrary to figures published elsewhere [5]. For θ different from zero the diagonalization cannot be accomplished by simple algebraic operations. The computation of these orientations is conveniently performed by computer. Moreover, each calculation has to be repeated for at least two different values of φ, differing by 60°, in order to obtain the spectra of both sites.

These coefficients can be easily translated in experimentally observable quantities with the exception of the sign of a.

The matrix describing the crystalline field expressed on the basis of the free spin eigenfunctions is:

4. Transition Probabilities

If the spin system previously described is placed in an rf magnetic field, B_{rf}, the time dependent interaction hamiltonian

$$\mathscr{H}_{int} = -\mu B_{rf} = g\beta B_{rf} \cdot S$$

will induce transitions between the energy levels.

The probability of a transition between the level E_i characterized by a wave function ψ_i and the level E_j characterized by ψ_j is proportional to the square of the matrix element of H_{int} between ψ_i and ψ_j:

$$W_{ij} \sim |\langle\psi_i|\mathscr{H}_{int}|\psi_j\rangle|^2$$

Since the ψ_i in most cases are not pure spin states, we have

$$|\psi_i\rangle = \sum_{n=-s}^{s} a_{in}|n\rangle$$

and

$$W_{ij} \sim |\sum_n \sum_m a_{in}^* a_{jm} \langle n|\mathscr{H}_{int}|m\rangle|^2 \qquad (2)$$

This expression was calculated for three polarizations of the magnetic field, along x, y, and z.

If an ultrasonic wave is applied to the lattice the periodic displacement of the ions will induce transitions between the energy levels, through the modulation of the crystalline electric field. This can be described assuming an interaction hamiltonian including two terms, one describing the modulation of the g-factor, the second one the modulation of the crystalline field parameters.

In the case of the Fe^{3+}, since the static spin hamiltonian includes, besides B_2^0, two other terms, B_4^0 and B_4^3, one would expect them to be also modulated by the ultrasonic wave. We have, however, neglected these

two terms on the basis that the ratios B_4^0/B_2^0 and B_4^3/B_2^0 are very small (of the order of 2 and 5%) provided that considerations about the static behavior can be carried over to the dynamic one. With these hypotheses the interaction hamiltonian can be written:

$$\mathcal{H}_{\text{int}} = \beta \mathbf{B} d g \mathbf{S} + \mathbf{S} \mathbf{d} \mathbf{S}$$

The first term is referred in the literature as the dipolar term, the second as the quadrupolar one. The relative importance of these two terms was discussed by Mattuck and Strandberg [3] who showed that in most cases the second one is dominant and experimental data seemed to confirm that fact [23–27] in the case of non-S state ions. In this expression δg and d| are two second rank tensors related to the lattice strain ϵ as

$$dg_{ij} = \sum_{kl} F_{ijkl} \epsilon_{kl} \qquad \text{and} \qquad \mathbf{d}_{ij} = \sum_{kl} G_{ijkl} \epsilon_{kl}$$

where F_{ijkl} and G_{ijkl} are two fourth rank tensors (called the magnetoelastic tensors). Using the Voigt notation [28], they can be written as 6 by 6 matrices. Considering the fact that the point group symmetry at each Fe^{3+} site is C_3 the number of independent components of F or G is only 10. For the first site the G tensor can be written:

G_{11}	G_{12}	$-G_{33}/2$	G_{14}	$-G_{25}$	G_{16}
G_{12}	G_{11}	$-G_{33}/2$	$-G_{14}$	G_{25}	$-G_{16}$
$-(G_{11}+G_{12})$	$-(G_{11}+G_{12})$	G_{33}	0	0	0
G_{41}	$-G_{41}$	0	G_{44}	G_{45}	G_{52}
$-G_{52}$	G_{52}	0	$-G_{45}$	G_{44}	G_{41}
$-G_{16}$	G_{16}	0	G_{25}	G_{14}	$(G_{11}-G_{12})/2$

The tensor for the second site is similar except for the sign of G_{52}, G_{25}, G_{45}, and G_{16}. The interaction hamiltonian describing the "quadrupolar" term can now be written:

$$\mathcal{H}_{\text{quad}} = \mathbf{d}_{xx} S_x^2 + \mathbf{d}_{yy} S_y^2 + \mathbf{d}_{zz} S_z^2 + \mathbf{d}_{yz}(S_y S_z + S_z S_y) + \mathbf{d}_{zx}(S_z S_x + S_x S_z) + \mathbf{d}_{xy}(S_x S_y + S_y S_x).$$

Since the d's (or the G's) are not known for Fe^{3+} in Al_2O_3 and since we want to make it possible through a comparison with experimental data to evaluate the G's, we have calculated the matrix elements between the different wave functions of each term:

$$|\langle \psi_i | S_x^2 | \psi_j \rangle|^2, \ldots, |\langle \psi_i | S_x S_y + S_y S_x | \psi_j \rangle|^2, \ldots \quad (3)$$

the six (symmetrized) quadrupole moments.

5. Presentation of the Data

The energy level diagrams (figs. 4–10) were obtained by plotting the results of the calculation using steps of 0.025T (250G) except near crossover or noncrossover points, where the steps were decreased. The dotted lines represent the data for $\phi = 60°$.

The tables of numerical results use intervals for: θ, φ, and B (in 10^{-4} Tesla) larger than the ones computed in order to save space, but still maintain a representative sample. Each table consists of two parts:

(a) The normalized wave functions, where every other column gives the real part, alternated by the imaginary part. The first column is the corresponding energy in cm^{-1}. Note that the levels are arranged in ascending order. The lowest value is then called number one, the next lowest number two, etc. . . . This is

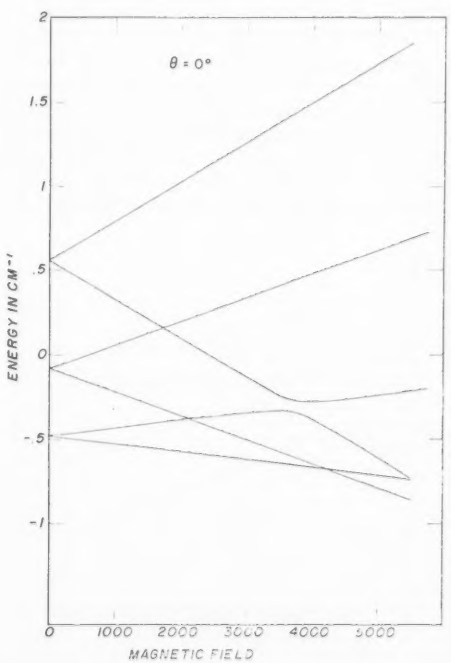

FIGURE 4. *Plot of the energy levels of* Fe^{3+} *in* Al_2O_3.
The solid line corresponds to $\varphi = 0$, the dotted line to $\varphi = 60°$. The Magnetic Field is in 10^{-4} Tesla.

331-607 O - 69 - 9

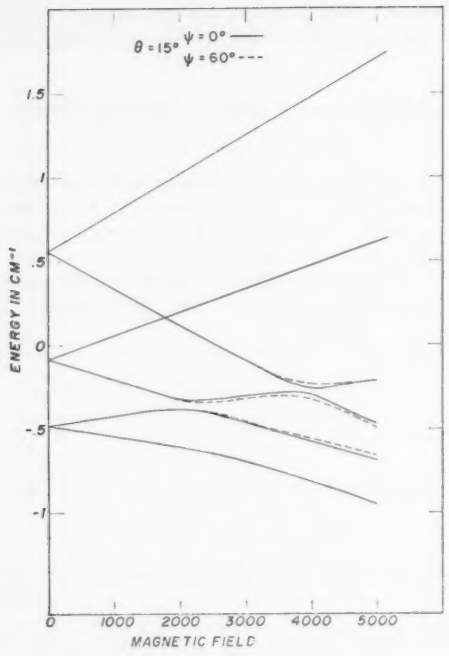

FIGURE 5. *Plot of the energy levels of* Fe^{3+} *in* Al_2O_3.

The solid line corresponds to $\varphi = 0$, the dotted line to $\varphi = 60°$. The Magnetic Field is in 10^{-4} · Tesla.

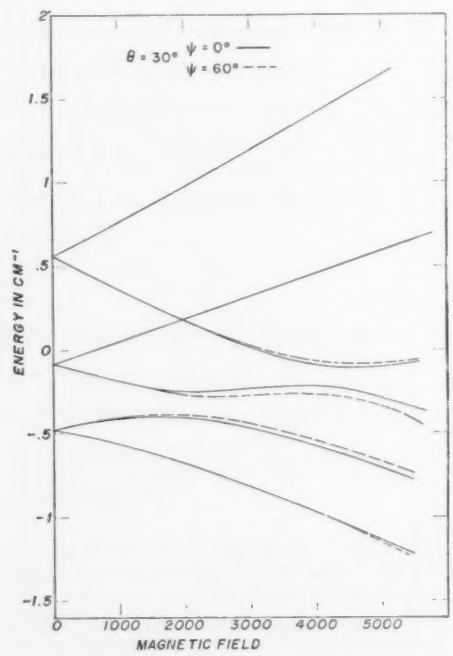

FIGURE 6. *Plot of the energy levels of* Fe^{3+} *in* Al_2O_3.

The solid line corresponds to $\varphi = 0$, the dotted line to $\varphi = 60°$. The Magnetic Field is in 10^{-4} · Tesla.

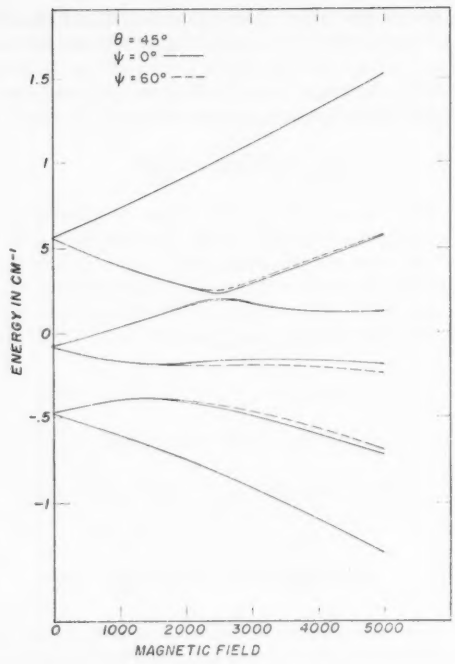

FIGURE 7. *Plot of the energy levels of* Fe^{3+} *in* Al_2O_3.

The solid line corresponds to $\varphi = 0$, the dotted line to $\varphi = 60°$. The Magnetic Field is in 10^{-4} · Tesla.

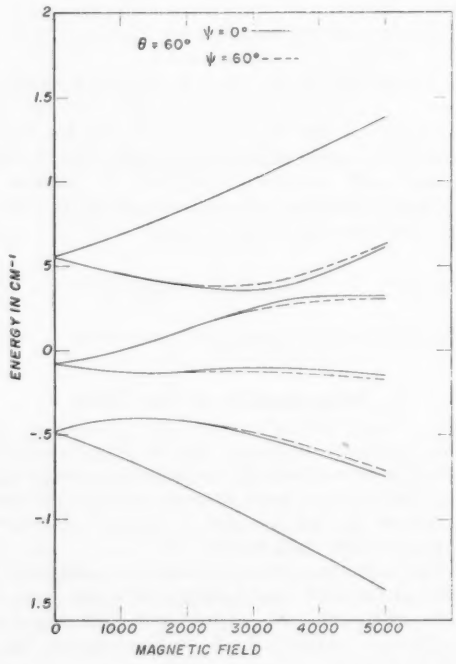

FIGURE 8. *Plot of the energy levels of* Fe^{3+} *in* Al_2O_3.

The solid line corresponds to $\varphi = 0$, the dotted line to $\varphi = 60°$. The Magnetic Field is in 10^{-4} · Tesla.

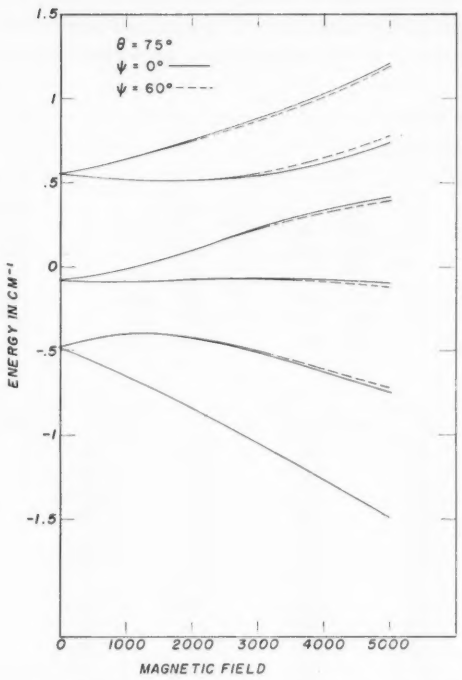

FIGURE 9. *Plot of the energy levels of* Fe^{3+} *in* Al_2O_3.

The solid line corresponds to $\varphi = 0$, the dotted line to $\varphi = 60°$. The Magnetic Field is in 10^{-4} · Tesla.

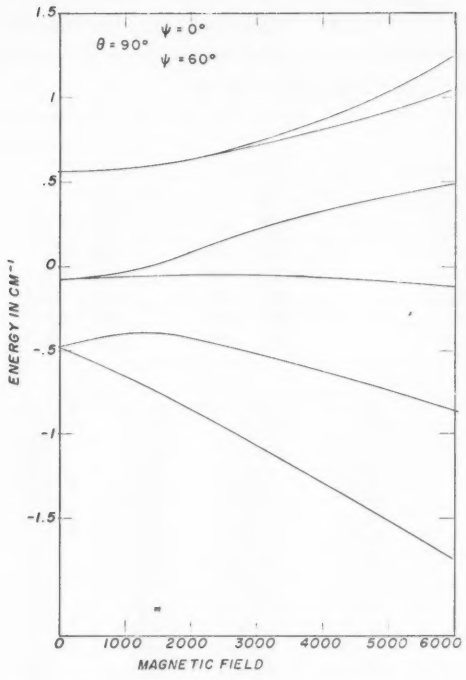

FIGURE 10. *Plot of the energy levels of* Fe^{3+} *in* Al_2O_3.

The solid line corresponds to $\varphi = 0$, the dotted line to $\varphi = 60°$. The Magnetic Field is in 10^{-4} · Tesla.

to establish the correspondence with the next part of each table.

(b) Tables that give the probabilities, i.e., absolute square of the matrix elements for dipole and quadrupole transitions between the energy level differences indicated. The column on the left gives the initial value i and the final value j which are of course interchangeable. The next column gives the positive energy difference in Gigahertz. The multiplication factor is 28.05 GHz/Tesla. The next three columns indicate the probabilities for a dipole transition in the x direction, the y direction, and the z direction. For $\theta = 0$, the first two are equal. The last six columns are the quadrupolar transition probabilities. The symbol PSXSX stands for the probability corresponding to an $S_X S_X$ transition. Similarly, PSXSY corresponds to $\frac{1}{2}(S_x S_y + S_y S_x)$. The tables are for $\varphi = 0$, except for $\theta = 45°$, where $\varphi = 0, 30, 60, 90$ is used to indicate the variation with φ.

TABLE 1. *Energy levels, wave functions, and transition probabilities for angles and field strengths indicated*

THETA = .00 PHI = .00 B = .0

Energy levels and wave functions

E(CM-1)	(5/2)		(3/2)		(1/2)		(−1/2)		(−3/2)		(−5/2)	
−.4823	.000	.000	.000	.000	.999	.000	.000	.000	.000	.000	.033	.000
−.4823	.033	.000	.000	.000	.000	.000	.999	.000	.000	.000	.000	.000
−.0805	.000	.000	.000	.000	.000	.000	.000	.000	1.000	.000	.000	.000
−.0805	.000	.000	1.000	.000	.000	.000	.000	.000	.000	.000	.000	.000
.5628	.999	.000	.000	.000	.000	.000	.033	.000	.000	.000	.000	.000
.5628	.000	.000	.000	.000	−.033	.000	.000	.000	.000	.000	.999	.000

Transition probabilities

I, J	D(GC)	PSX	PSY	PSZ	PSXSX	PSYSY	PSZSZ	PSYSZ	PSXSZ	PSXSY
1–2	.00	2.245	2.245	.000	.000	.000	.000	.000	.000	.000
1–3	12.06	.001	.001	.000	4.495	4.495	.000	.005	.005	4.495
1–4	12.06	1.998	1.998	.000	.000	.000	.000	1.998	1.998	.000
1–5	31.35	.002	.002	.000	2.500	2.500	.000	.000	.000	2.500
1–6	31.35	.000	.000	.010	.010	.010	.039	.000	.000	.000
2–3	12.06	1.998	1.998	.000	.000	.000	.000	1.998	1.998	.000
2–4	12.06	.001	.001	.000	4.495	4.495	.000	.005	.005	4.495
2–5	31.35	.000	.000	.010	.010	.010	.039	.000	.000	.000
2–6	31.35	.002	.002	.000	2.500	2.500	.000	.000	.000	2.500
3–4	.00	.000	.000	.000	.000	.000	.000	.000	.000	.000
3–5	19.30	.002	.002	.000	.000	.000	.000	.002	.002	.000
3–6	19.30	1.249	1.249	.000	.005	.005	.000	4.995	4.995	.005
4–5	19.30	1.249	1.249	.000	.005	.005	.000	4.995	4.995	.005
4–6	19.30	.002	.002	.000	.000	.000	.000	.002	.002	.000
5–6	−.00	.000	.000	.000	.000	.000	.000	.000	.000	.000

THETA = .00 PHI = .00 B = 1000.0

Energy levels and wave functions

E(CM-1)	(5/2)		(3/2)		(1/2)		(−1/2)		(−3/2)		(−5/2)	
−.5289	.026	.000	.000	.000	.000	.000	1.000	.000	.000	.000	.000	.000
−.4360	.000	.000	.000	.000	.999	.000	.000	.000	.000	.000	.045	.000
−.2207	.000	.000	.000	.000	.000	.000	.000	.000	1.000	.000	.000	.000
.0598	.000	.000	1.000	.000	.000	.000	.000	.000	.000	.000	.000	.000
.3294	.000	.000	.000	.000	−.045	.000	.000	.000	.000	.000	.999	.000
.7964	1.000	.000	.000	.000	.000	.000	.026	.000	.000	.000	.000	.000

Transition probabilities

I, J	D(GC)	PSX	PSY	PSZ	PSXSX	PSYSY	PSZSZ	PSYSZ	PSXSZ	PSXSY
1–2	2.79	2.244	2.244	.000	.001	.001	.000	.000	.000	.001
1–3	9.24	1.999	1.999	.000	.000	.000	.000	1.999	1.999	.000
1–4	17.66	.001	.001	.000	4.497	4.497	.000	.003	.003	4.497
1–5	25.75	.004	.004	.000	2.499	2.499	.000	.000	.000	2.499
1–6	39.76	.000	.000	.006	.006	.006	.024	.000	.000	.000
2–3	6.46	.003	.003	.000	4.491	4.491	.000	.010	.010	4.491
2–4	14.87	1.996	1.996	.000	.000	.000	.000	1.996	1.996	.000
2–5	22.96	.000	.000	.018	.018	.018	.072	.000	.000	.000
2–6	36.97	.001	.001	.000	2.499	2.499	.000	.000	.000	2.499
3–4	8.42	.000	.000	.000	.000	.000	.000	.000	.000	.000
3–5	16.50	1.247	1.247	.000	.009	.009	.000	4.990	4.990	.009
3–6	30.51	.001	.001	.000	.000	.000	.000	.001	.001	.000
4–5	8.09	.004	.004	.000	.000	.000	.000	.004	.004	.000
4–6	22.10	1.249	1.249	.000	.003	.003	.000	4.997	4.997	.003
5–6	14.01	.000	.000	.000	.001	.001	.000	.000	.000	.001

TABLE 1. *Energy levels, wave functions, and transition probabilities for angles and field strengths indicated*—Continued

THETA = .00 PHI = .00 B = 2000.0

Energy levels and wave functions

E(CM−1)	(5/2)		(3/2)		(1/2)		(−1/2)		(−3/2)		(−5/2)	
−.5755	.021	.000	.000	.000	.000	.000	−1.000	.000	.000	.000	.000	.000
−.3901	.000	.000	.000	.000	.998	.000	.000	.000	.000	.000	.070	.000
−.3610	.000	.000	.000	.000	.000	.000	.000	.000	1.000	.000	.000	.000
.0965	.000	.000	.000	.000	−.070	.000	.000	.000	.000	.000	.998	.000
.2001	.000	.000	1.000	.000	.000	.000	.000	.000	.000	.000	.000	.000
1.0300	1.000	.000	.000	.000	.000	.000	.021	.000	.000	.000	.000	.000

Transition probabilities

I, J	D(GC)	PSX	PSY	PSZ	PSXSX	PSYSY	PSZSZ	PSYSZ	PSXSZ	PSXSY
1–2	5.56	2.238	2.238	.000	.006	.006	.000	.000	.000	.006
1–3	6.43	1.999	1.999	.000	.000	.000	.000	1.999	1.999	.000
1–4	20.16	.011	.011	.000	2.494	2.494	.000	.000	.000	2.494
1–5	23.27	.001	.001	.000	4.498	4.498	.000	.002	.002	4.498
1–6	48.16	.000	.000	.004	.004	.004	.016	.000	.000	.000
2–3	.87	.006	.006	.000	4.478	4.478	.000	.025	.025	4.478
2–4	14.60	.000	.000	.044	.044	.044	.178	.000	.000	.000
2–5	17.71	1.990	1.990	.000	.000	.000	.000	1.990	1.990	.000
2–6	42.60	.001	.001	.000	2.494	2.494	.000	.000	.000	2.494
3–4	13.73	1.244	1.244	.000	.022	.022	.000	4.975	4.975	.022
3–5	16.83	.000	.000	.000	.000	.000	.000	.000	.000	.000
3–6	41.73	.001	.001	.000	.000	.000	.000	.001	.001	.000
4–5	3.11	.010	.010	.000	.000	.000	.000	.010	.010	.000
4–6	28.00	.000	.000	.000	.006	.006	.000	.000	.000	.006
5–6	24.90	1.249	1.249	.000	.002	.002	.000	4.998	4.998	.002

THETA = .00 PHI = .00 B = 3000.0

Energy levels and wave functions

E(CM−1)	(5/2)		(3/2)		(1/2)		(−1/2)		(−3/2)		(−5/2)	
−.6221	.018	.000	.000	.000	.000	.000	−1.000	.000	.000	.000	.000	.000
−.5013	.000	.000	.000	.000	.000	.000	.000	.000	1.000	.000	.000	.000
−.3466	.000	.000	.000	.000	.987	.000	.000	.000	.000	.000	.163	−.000
−.1340	.000	.000	.000	.000	−.163	.000	.000	.000	.000	.000	.987	.000
.3404	.000	.000	1.000	.000	.000	.000	.000	.000	.000	.000	.000	.000
1.2637	1.000	.000	.000	.000	.000	.000	.018	.000	.000	.000	.000	.000

Transition probabilities

I, J	D(GC)	PSX	PSY	PSZ	PSXSX	PSYSY	PSZSZ	PSYSZ	PSXSZ	PSXSY
1–2	3.63	1.999	1.999	.000	.000	.000	.000	1.999	1.999	.000
1–3	8.27	2.189	2.189	.000	.053	.053	.000	.000	.000	.053
1–4	14.64	.060	.060	.000	2.447	2.447	.000	.000	.000	2.447
1–5	28.87	.000	.000	.000	4.499	4.499	.000	.002	.002	4.499
1–6	56.57	.000	.000	.003	.003	.003	.012	.000	.000	.000
2–3	4.64	.033	.033	.000	4.380	4.380	.000	.133	.133	4.380
2–4	11.02	1.217	1.217	.000	.120	.120	.000	4.867	4.867	.120
2–5	25.25	.000	.000	.000	.000	.000	.000	.000	.000	.000
2–6	52.95	.001	.001	.000	.000	.000	.000	.001	.001	.000
3–4	6.38	.000	.000	.233	.233	.223	.932	.000	.000	.000
3–5	20.61	1.947	1.947	.000	.000	.000	.000	1.947	1.947	.000
3–6	48.31	.001	.001	.000	2.447	2.447	.000	.000	.000	2.447
4–5	14.23	.053	.053	.000	.000	.000	.000	.053	.053	.000
4–6	41.93	.000	.000	.000	.053	.053	.000	.000	.000	.053
5–6	27.70	1.250	1.250	.000	.001	.001	.000	4.998	4.998	.001

TABLE 1. *Energy levels, wave functions, and transition probabilities for angles and field strengths indicated*—Continued

THETA = .00 PHI = .00 B = 4000.0

Energy levels and wave functions

E(CM−1)	(5/2)		(3/2)		(1/2)		(−1/2)		(−3/2)		(−5/2)	
−.6688	.016	.000	.000	.000	.000	.000	−1.000	.000	.000	.000	.000	.000
−.6416	.000	.000	.000	.000	.000	.000	.000	.000	1.000	.000	.000	.000
−.3862	.000	.000	.000	.000	.348	.000	.000	.000	.000	.000	.937	.000
−.2815	.000	.000	.000	.000	−.937	.000	.000	.000	.000	.000	.348	.000
.4806	.000	.000	1.000	.000	.000	.000	.000	.000	.000	.000	.000	.000
1.4974	1.000	.000	.000	.000	.000	.000	.016	.000	.000	.000	.000	.000

Transition probabilities

I. J	D(GC)	PSX	PSY	PSZ	PSXSX	PSYSY	PSZSZ	PSYSZ	PSXSZ	PSXSY
1–2	.82	2.000	2.000	.000	.000	.000	.000	2.000	2.000	.000
1–3	8.48	.273	.273	.000	2.170	2.170	.000	.000	.000	2.170
1–4	11.62	1.976	1.976	.000	.330	.330	.000	.000	.000	.330
1–5	34.48	.000	.000	.000	4.499	4.499	.000	.001	.001	4.499
1–6	64.98	.000	.000	.002	.002	.002	.009	.000	.000	.000
2–3	7.66	1.098	1.098	.000	.546	.546	.000	4.393	4.393	.546
2–4	10.80	.152	.152	.000	3.954	3.954	.000	.607	.607	3.954
2–5	33.67	.000	.000	.000	.000	.000	.000	.000	.000	.000
2–6	64.17	.000	.000	.000	.000	.000	.000	.000	.000	.000
3–4	3.14	.000	.000	.960	.960	.960	3.841	.000	.000	.000
3–5	26.00	.243	.243	.000	.000	.000	.000	.243	.243	.000
3–6	56.51	.000	.000	.000	.330	.330	.000	.000	.000	.330
4–5	22.86	1.757	1.757	.000	.000	.000	.000	1.757	1.757	.000
4–6	53.37	.000	.000	.000	2.170	2.170	.000	.000	.000	2.170
5–6	30.50	1.250	1.250	.000	.001	.001	.000	4.999	4.999	.001

THETA = .00 PHI = .00 B = 5000.0

Energy levels and wave functions

E(CM−1)	(5/2)		(3/2)		(1/2)		(−1/2)		(−3/2)		(−5/2)	
−.7818	.000	.000	.000	.000	.000	.000	.000	.000	1.000	.000	.000	.000
−.7155	.014	.000	.000	.000	.000	.000	−1.000	.000	.000	.000	.000	.000
−.6105	.000	.000	.000	.000	.094	.000	.000	.000	.000	.000	.996	.000
−.2442	.000	.000	.000	.000	−.996	.000	.000	.000	.000	.000	.094	.000
.6209	.000	.000	1.000	.000	.000	.000	.000	.000	.000	.000	.000	.000
1.7311	1.000	.000	.000	.000	.000	.000	.014	.000	.000	.000	.000	.000

Transition probabilities

I. J	D(GC)	PSX	PSY	PSZ	PSXSX	PSYSY	PSZSZ	PSYSZ	PSXSZ	PSXSY
1–2	1.99	2.000	2.000	.000	.000	.000	.000	2.000	2.000	.000
1–3	5.14	1.239	1.239	.000	.040	.040	.000	4.956	4.956	.040
1–4	16.13	.011	.011	.000	4.460	4.460	.000	.044	.044	4.460
1–5	42.08	.000	.000	.000	.000	.000	.000	.000	.000	.000
1–6	75.39	.000	.000	.000	.000	.000	.000	.000	.000	.000
2–3	3.15	.020	.020	.000	2.471	2.471	.000	.000	.000	2.471
2–4	14.14	2.230	2.230	.000	.029	.029	.000	.000	.000	.029
2–5	40.09	.000	.000	.000	4.499	4.499	.000	.001	.001	4.499
2–6	73.40	.000	.000	.002	.002	.002	.007	.000	.000	.000
3–4	10.99	.000	.000	.078	.078	.078	.314	.000	.000	.000
3–5	36.94	.018	.018	.000	.000	.000	.000	.018	.018	.000
3–6	70.25	.000	.000	.000	.029	.029	.000	.000	.000	.029
4–5	25.95	1.982	1.982	.000	.000	.000	.000	1.982	1.982	.000
4–6	59.26	.000	.000	.000	2.471	2.471	.000	.000	.000	2.471
5–6	33.31	1.250	1.250	.000	.001	.001	.000	4.999	4.999	.001

TABLE 1. *Energy levels, wave functions, and transition probabilities for angles and field strengths indicated*—Continued

THETA = 15.00 PHI = .00 B = 1000.0

Energy levels and wave functions

E(CM−1)	(5/2)		(3/2)		(1/2)		(−1/2)		(−3/2)		(−5/2)	
−.5435	.025	.000	−.020	.000	.327	.000	−.939	.000	.097	.000	.010	.000
−.4276	.008	.000	.066	.000	−.941	.000	−.323	.000	.058	.000	−.044	.000
−.2134	−.004	.000	−.003	.000	.025	.000	.111	.000	.992	.000	−.047	.000
.0564	−.037	.000	.997	.000	.069	.000	.002	.000	.001	.000	.008	.000
.3387	.000	.000	−.005	.000	−.044	.000	.000	.000	.049	.000	.998	.000
.7894	−.999	.000	−.037	.000	−.002	.000	−.026	.000	−.001	.000	.000	.000

Transition probabilities

I, J	D(GC)	PSX	PSY	PSZ	PSXSX	PSYSY	PSZSZ	PSYSZ	PSXSZ	PSXSY
1–2	3.48	1.212	2.326	.099	.062	.058	.000	.002	.036	.169
1–3	9.90	1.639	1.586	.008	.449	.740	.036	1.866	1.664	.554
1–4	18.00	.153	.115	.000	3.914	4.091	.002	.168	.265	3.930
1–5	26.46	.011	.000	.001	2.198	2.001	.005	.022	.024	2.108
1–6	39.99	.000	.000	.005	.137	.267	.021	.001	.001	.197
2–3	6.43	.435	.316	.007	4.008	3.515	.016	.137	.307	3.779
2–4	14.52	1.825	1.890	.005	.476	.315	.017	1.837	1.715	.378
2–5	22.99	.004	.000	.016	.230	.547	.067	.015	.010	.366
2–6	36.51	.000	.004	.001	2.362	2.209	.003	.009	.010	2.297
3–4	8.09	.003	.002	.000	.146	.142	.000	.004	.000	.142
3–5	16.56	1.221	1.266	.002	.031	.000	.035	4.957	4.914	.074
3–6	30.08	.001	.001	.000	.004	.002	.000	.002	.002	.003
4–5	8.47	.004	.004	.001	.000	.001	.002	.004	.004	.000
4–6	21.99	1.256	1.240	.001	.057	.008	.022	4.977	4.972	.003
5–6	13.52	.000	.000	.000	.001	.001	.000	.000	.000	.001

THETA = 15.00 PHI = .00 B = 2000.0

Energy levels and wave functions

E(CM−1)	(5/2)		(3/2)		(1/2)		(−1/2)		(−3/2)		(−5/2)	
−.6144	.021	.000	−.027	.000	.307	.000	−.920	.000	.240	.000	−.003	.000
−.3891	.000	.000	.101	.000	−.858	.000	−.168	.000	.462	.000	−.109	.000
−.3277	−.007	.000	−.051	.000	.390	.000	.353	.000	.846	.000	−.074	.000
.1183	−.004	.000	.058	.000	−.058	.000	.005	.000	.115	.000	.990	.000
.1952	−.066	.000	.989	.000	.120	.000	.008	.000	−.004	.000	−.051	.000
1.0176	.998	.000	.066	.000	.004	.000	.022	.000	.001	.000	−.000	.000

Transition probabilities

I, J	D(GC)	PSX	PSY	PSZ	PSXSX	PSYSY	PSZSZ	PSYSZ	PSXSZ	PSXSY
1–2	6.76	.247	3.392	.145	.092	.007	.048	.352	.644	1.155
1–3	8.60	2.012	.282	.007	.546	1.319	.168	1.583	.977	.128
1–4	21.98	.052	.000	.002	2.334	2.240	.001	.162	.125	1.498
1–5	24.29	.080	.065	.000	3.226	3.458	.004	.134	.245	3.908
1–6	48.96	.000	.000	.004	.088	.175	.015	.002	.001	.128
2–3	1.84	.299	.529	.565	2.265	.469	.672	.089	.136	3.215
2–4	15.22	.162	.287	.050	.078	.654	.280	.917	1.103	.158
2–5	17.53	1.564	1.474	.008	.058	.000	.053	1.665	1.329	.029
2–6	42.20	.000	.006	.000	1.907	1.865	.000	.017	.018	1.904
3–4	13.38	.997	1.004	.000	.503	.209	.063	3.888	3.539	.505
3–5	15.69	.315	.468	.003	.847	.703	.007	.220	.380	.896
3–6	40.36	.000	.000	.001	.477	.414	.002	.010	.011	.450
4–5	2.31	.008	.007	.044	.023	.001	.034	.009	.005	.003
4–6	26.98	.004	.004	.000	.002	.004	.000	.014	.014	.003
5–6	24.67	1.253	1.231	.004	.134	.011	.070	4.938	4.902	.020

TABLE 1. *Energy levels, wave functions, and transition probabilities for angles and field strengths indicated*—Continued

THETA = 15.00 PHI = .00 B = 3000.0

Energy levels and wave functions

E(CM-1)	(5/2)		(3/2)		(1/2)		(−1/2)		(−3/2)		(−5/2)	
−.7021	.016	.000	−.028	.000	.267	.000	−.862	.000	.428	.000	−.044	.000
−.4709	−.009	.000	.049	.000	−.374	.000	.312	.000	.842	.000	−.228	.000
−.3138	.002	.000	.139	.000	−.868	.000	−.399	.000	−.258	.000	−.044	.000
−.0946	.002	.000	−.028	.000	.114	.000	−.017	.000	−.205	.000	−.972	.000
.3345	−.089	.000	.984	.000	.151	.000	.014	.000	.001	.000	−.011	.000
1.2470	.996	.000	.089	.000	.007	.000	.019	.000	.001	.000	−.000	.000

Transition probabilities

I, J	D(GC)	PSX	PSY	PSZ	PSXSX	PSYSY	PSZSZ	PSYSZ	PSXSZ	PSXSY
1-2	6.93	.119	2.702	.233	.007	.483	.603	1.818	1.377	1.474
1-3	11.65	1.243	.602	.018	.979	1.454	.047	.251	.001	.863
1-4	18.22	.147	.005	.001	1.763	1.982	.006	.482	.426	1.112
1-5	31.10	.040	.031	.000	2.727	2.930	.004	.107	.169	2.957
1-6	58.47	.000	.000	.002	.047	.096	.009	.002	.001	.070
2-3	4.71	.777	.802	.286	.964	1.799	.129	.019	.164	2.152
2-4	11.29	.786	1.184	.100	.386	.130	.966	3.990	3.450	.258
2-5	24.16	.207	.177	.001	.815	1.042	.014	.313	.285	.951
2-6	51.54	.001	.002	.000	.253	.295	.002	.002	.002	.276
3-4	6.58	.179	.208	.060	.591	1.265	.127	.438	.415	1.054
3-5	19.45	1.695	1.778	.020	.851	.419	.076	1.581	1.448	.649
3-6	46.83	.000	.003	.001	2.131	2.035	.001	.042	.044	2.102
4-5	12.87	.024	.023	.004	.020	.018	.000	.031	.027	.019
4-6	40.25	.000	.001	.000	.019	.022	.000	.002	.002	.021
5-6	27.38	1.255	1.232	.008	.209	.010	.127	4.923	4.853	.041

THETA = 15.00 PHI = .00 B = 4000.0

Energy levels and wave functions

E(CM-1)	(5/2)		(3/2)		(1/2)		(−1/2)		(−3/2)		(−5/2)	
−.8139	.013	.000	−.024	.000	.211	.000	−.754	.000	.609	.000	−.124	.000
−.5767	−.011	.000	.046	.000	−.342	.000	.520	.000	.689	.000	−.367	.000
−.3012	−.002	.000	−.040	.000	.225	.000	.239	.000	.391	.000	.859	.000
−.2598	.004	.000	−.166	.000	.870	.000	.322	.000	.021	.000	−.335	.000
.4744	.108	.000	−.978	.000	−.177	.000	−.020	.000	−.002	.000	.007	.000
1.4772	.994	.000	.107	.000	.010	.000	.017	.000	.001	.001	−.000	.000

Transition probabilities

I, J	D(GC)	PSX	PSY	PSZ	PSXSX	PSYSY	PSZSZ	PSYSZ	PSXSZ	PSXSY
1-2	7.11	.003	2.437	.344	.216	.418	1.234	2.220	1.010	1.784
1-3	15.38	.015	.123	.001	.218	.396	.026	.426	.758	1.352
1-4	16.62	.882	.334	.009	2.543	3.531	.081	.587	.016	.842
1-5	38.65	.014	.011	.000	1.794	1.923	.002	.062	.099	1.923
1-6	68.73	.000	.000	.001	.018	.042	.005	.001	.001	.029
2-3	8.26	1.232	.331	.078	1.606	.008	1.838	2.901	2.216	.087
2-4	9.51	.512	1.995	.329	.062	1.002	.565	.604	.120	1.380
2-5	31.53	.114	.095	.001	1.739	2.059	.013	.249	.255	1.942
2-6	61.62	.000	.001	.001	.150	.195	.003	.001	.001	.173
3-4	1.24	.143	.288	.602	3.159	.007	2.876	.260	.001	1.495
3-5	23.27	.147	.160	.001	.467	.325	.013	.100	.089	.403
3-6	53.35	.000	.000	.000	.201	.182	.000	.004	.005	.193
4-5	22.02	1.683	1.740	.031	.445	.126	.097	1.630	1.465	.274
4-6	52.11	.001	.005	.000	2.055	2.022	.000	.055	.057	2.061
5-6	30.09	1.252	1.231	.012	.282	.010	.186	4.899	4.789	.062

TABLE 1. *Energy levels, wave functions, and transition probabilities for angles and field strengths indicated*—Continued

THETA = 15.00 PHI = .00 B = 5000.0

Energy levels and wave functions

E(CM−1)	(5/2)		(3/2)		(1/2)		(−1/2)		(−3/2)		(−5/2)	
−.9509	.009	.000	−.018	.000	.156	.000	−.626	.000	.725	.000	−.242	.000
−.6870	−.011	.000	.045	.000	−.326	.000	.625	.000	.421	.000	−.570	.000
−.4692	−.006	.000	.022	.000	−.133	.000	.283	.000	.535	.000	.784	.000
−.2154	.007	.000	−.191	.000	.902	.000	.370	.000	.105	.000	−.047	.000
.6145	.123	.000	−.972	.000	−.197	.000	−.024	.000	−.002	.000	.005	.000
1.7080	.992	.000	.123	.000	.012	.000	.015	.000	.001	.000	.000	.000

Transition probabilities

I, J	D(GC)	PSX	PSY	PSZ	PSXSX	PSYSY	PSZSZ	PSYSZ	PSXSZ	PSXSY
1–2	7.92	.027	2.315	.401	.713	.348	2.056	2.914	.814	2.178
1–3	14.45	.256	.002	.001	.598	1.290	.131	.635	.622	.072
1–4	22.06	.369	.220	.002	2.151	2.872	.052	.258	.049	2.017
1–5	46.96	.004	.003	.000	1.010	1.072	.001	.029	.049	1.074
1–6	79.77	.000	.000	.001	.005	.014	.003	.001	.001	.009
2–3	6.53	.151	1.005	.509	1.454	1.042	4.957	2.968	.515	.601
2–4	14.15	1.073	1.295	.167	.000	.053	.054	.000	.000	.100
2–5	39.04	.072	.060	.000	2.073	2.420	.013	.213	.231	2.293
2–6	71.85	.000	.000	.001	.104	.143	.003	.001	.001	.123
3–4	7.62	.579	.676	.012	1.916	1.602	.014	.224	.146	1.984
3–5	32.51	.008	.006	.001	.718	.760	.001	.044	.045	.752
3–6	65.32	.000	.000	.000	.008	.014	.001	.000	.000	.010
4–5	24.90	1.868	1.936	.039	.658	.190	.141	1.762	1.566	.404
4–6	57.70	.001	.004	.000	2.284	2.268	.000	.072	.074	2.301
5–6	32.81	1.249	1.230	.016	.349	.009	.244	4.879	4.728	.082

THETA = 30.00 PHI = .00 B = 1000.0

Energy levels and wave functions

E(CM−1)	(5/2)		(3/2)		(1/2)		(−1/2)		(−3/2)		(−5/2)	
−.5737	.024	.000	−.054	.000	.483	.000	−.860	.000	.152	.000	.009	.000
−.4144	.008	.000	.124	.000	−.862	.000	−.464	.000	.156	.000	−.049	.000
−.1925	−.007	.000	−.017	.000	.066	.000	.209	.000	.972	.000	−.088	.000
.0462	−.073	.000	.988	.000	.135	.000	.013	.000	.006	.000	.014	.000
.3655	.001	.000	−.009	.000	−.043	.000	.004	.000	.092	.000	.995	.000
.7689	.997	.000	.072	.000	.005	.000	.027	.000	.002	.000	.000	.000

Transition probabilities

I, J	D(GC)	PSX	PSY	PSZ	PSXSX	PSYSY	PSZSZ	PSYSZ	PSXSZ	PSXSY
1–2	4.78	.400	2.445	.204	.075	.058	.001	.010	.211	.565
1–3	11.44	1.197	1.018	.013	.999	1.665	.085	1.643	1.277	1.087
1–4	18.60	.279	.238	.002	3.118	3.537	.013	.403	.528	3.263
1–5	28.18	.013	.000	.003	1.691	1.480	.007	.046	.054	1.597
1–6	40.28	.000	.001	.004	.317	.490	.019	.007	.005	.400
2–3	6.66	.891	.772	.049	3.189	2.134	.106	.361	.576	2.847
2–4	13.82	1.668	1.741	.016	.934	.528	.058	1.605	1.405	.662
2–5	23.40	.019	.004	.014	.598	1.075	.070	.099	.076	.794
2–6	35.50	.000	.008	.001	2.127	1.938	.004	.032	.035	2.055
3–4	7.16	.026	.021	.001	.523	.485	.001	.016	.001	.494
3–5	16.74	1.190	1.272	.007	.178	.006	.120	4.839	4.730	.188
3–6	28.84	.001	.001	.001	.026	.015	.001	.005	.005	.021
4–5	9.58	.002	.002	.003	.001	.008	.004	.005	.006	.004
4–6	21.68	1.261	1.228	.005	.174	.016	.085	4.929	4.893	.025
5–6	12.10	.000	.000	.000	.001	.001	.000	.001	.001	.001

TABLE 1. *Energy levels, wave functions, and transition probabilities for angles and field strengths indicated*—Continued

THETA = 30.00 PHI = .00 B = 2000.0

Energy levels and wave functions

E(CM−1)	(5/2)		(3/2)		(1/2)		(−1/2)		(−3/2)		(−5/2)	
−.6862	.022	.000	−.072	.000	.442	.000	−.838	.000	.311	.000	−.021	.000
−.4005	−.009	.000	.181	.000	−.765	.000	−.207	.000	.561	.000	−.152	.000
−.2551	−.003	.000	−.128	.000	.405	.000	.502	.000	.737	.000	−.154	.000
.1738	.096	.000	−.712	.000	−.137	.000	−.049	.000	−.152	.000	−.663	.000
.1870	.087	.000	−.650	.000	−.189	.000	−.006	.000	.145	.000	.716	.000
.9810	.991	.000	.129	.000	.015	.000	.023	.000	.002	.000	.000	.000

Transition probabilities

I, J	D(GC)	PSX	PSY	PSZ	PSXSX	PSYSY	PSZSZ	PSYSZ	PSXSZ	PSXSY
1–2	8.57	.039	3.046	.298	.070	.006	.117	.391	1.187	2.434
1–3	12.93	1.047	.064	.002	1.122	2.420	.246	1.438	.445	.127
1–4	25.80	.148	.045	.005	3.729	4.134	.010	.498	.034	.256
1–5	26.20	.011	.066	.000	.048	.106	.011	.005	.562	3.646
1–6	50.02	.000	.000	.003	.173	.278	.012	.009	.006	.223
2–3	4.36	.248	1.141	.668	.997	.006	.850	.276	.254	1.907
2–4	17.23	.227	1.353	.074	.166	.334	.029	.001	2.443	.162
2–5	17.62	1.259	.143	.002	.022	.775	.536	2.841	.010	.180
2–6	41.45	.002	.010	.000	1.533	1.538	.000	.059	.061	1.560
3–4	12.87	1.457	.012	.001	3.332	1.587	.320	2.782	.631	.065
3–5	13.26	.028	1.652	.040	.009	.141	.079	.817	2.518	2.649
3–6	37.08	.000	.002	.001	.656	.580	.002	.052	.056	.632
4–5	.40	.002	.001	3.796	.918	.923	3.681	.011	.256	.054
4–6	24.22	.685	.666	.010	.234	.009	.150	2.583	2.501	.050
5–6	23.82	.571	.548	.008	.225	.015	.124	2.235	2.166	.056

THETA = 30.00 PHI = .00 B = 3000.0

Energy levels and wave functions

E(CM−1)	(5/2)		(3/2)		(1/2)		(−1/2)		(−3/2)		(−5/2)	
−.8195	.019	.000	−.073	.000	.390	.000	−.795	.000	.452	.000	−.074	.000
−.4764	−.018	.000	.159	.000	−.593	.000	.130	.000	.715	.000	−.307	.000
−.2352	−.014	.000	.248	.000	−.639	.000	−.578	.000	−.391	.000	.208	.000
.0162	−.005	.000	.014	.000	−.015	.000	.111	.000	.361	.000	.925	.000
.3172	.175	.000	−.937	.000	−.295	.000	−.064	.000	−.012	.000	.023	.000
1.1976	.984	.000	.174	.000	.025	.000	.022	.000	.003	.000	.000	.000

Transition probabilities

I, J	D(GC)	PSX	PSY	PSZ	PSXSX	PSYSY	PSZSZ	PSYSZ	PSXSZ	PSXSY
1–2	10.29	.000	2.686	.390	.092	.208	.576	1.116	1.714	3.428
1–3	17.53	.707	.081	.006	1.550	2.991	.235	1.035	.017	.208
1–4	25.07	.037	.004	.001	.794	.959	.008	.275	.279	.684
1–5	34.10	.048	.046	.002	1.707	2.081	.018	.211	.305	2.101
1–6	60.51	.000	.000	.002	.083	.144	.008	.007	.005	.112
2–3	7.24	.105	1.553	.750	.034	.462	.745	.267	.097	.931
2–4	14.78	.457	.535	.105	.087	.789	1.401	2.799	2.033	.026
2–5	23.81	.525	.455	.012	.416	1.039	.140	.935	.708	.715
2–6	50.22	.001	.005	.000	.675	.752	.002	.034	.033	.724
3–4	7.54	.625	.696	.052	2.827	.641	.776	1.495	.954	1.728
3–5	16.57	1.333	1.468	.088	1.918	.890	.195	.958	.720	1.507
3–6	42.99	.004	.010	.001	1.477	1.468	.000	.155	.164	1.510
4–5	9.03	.004	.006	.004	.339	.247	.007	.009	.005	.302
4–6	35.44	.001	.001	.000	.007	.003	.001	.000	.000	.005
5–6	26.41	1.244	1.203	0.33	.765	.028	.499	4.704	4.405	.198

TABLE 1. *Energy levels, wave functions, and transition probabilities for angles and field strengths indicated*—Continued

THETA = 30.00 PHI = .00 B = 4000.0

Energy levels and wave functions

E(CM−1)	(5/2)		(3/2)		(1/2)		(−1/2)		(−3/2)		(−5/2)	
−.9716	.017	.000	−.068	.000	.338	.000	−.740	.000	.558	.000	−.145	.000
−.5848	−.021	.000	.146	.000	−.530	.000	.310	.000	.633	.000	−.447	.000
−.2160	.028	.000	−.290	.000	.659	.000	.451	.000	.027	.000	−.526	.000
−.1014	−.009	.000	.123	.000	−.229	.000	−.380	.000	−.535	.000	−.708	.000
.4563	.211	.000	−.911	.000	−.342	.000	−.086	.000	−.020	.000	.011	.000
1.4175	.977	.000	.211	.000	.036	.000	.021	.000	.003	.000	−.000	.000

Transition probabilities

I, J	D(GC)	PSX	PSY	PSZ	PSXSX	PSYSY	PSZSZ	PSYSZ	PSXSZ	PSXSY
1–2	11.60	.005	2.352	.467	.311	.268	1.157	1.545	1.722	3.456
1–3	22.67	.513	.105	.009	2.158	4.000	.282	1.214	.014	.312
1–4	26.11	.002	.023	.000	.012	.013	.000	.027	.289	.767
1–5	42.84	.019	.018	.001	1.163	1.419	.013	.137	.196	1.397
1–6	71.67	.000	.000	.001	.037	.070	.005	.005	.003	.052
2–3	11.06	.117	2.238	.853	.247	.741	1.844	1.069	.536	.271
2–4	14.50	.573	.044	.019	.191	.679	1.590	2.173	.801	.009
2–5	31.23	.260	.225	.006	.978	1.784	.120	.712	.600	1.410
2–6	60.07	.000	.002	.000	.380	.453	.003	.022	.020	.422
3–4	3.44	.143	.815	.910	2.838	.202	4.557	.961	.000	2.078
3–5	20.17	1.268	1.334	.111	.720	.102	.280	1.211	.831	.382
3–6	49.01	.007	.012	.000	1.375	1.484	.002	.186	.191	1.467
4–5	16.73	.340	.380	.022	1.582	.997	.067	.088	.047	1.338
4–6	45.57	.001	.001	.000	.341	.341	.000	.047	.050	.351
5–6	28.84	1.231	1.199	.050	1.053	.030	.729	4.603	4.151	.288

THETA = 30.00 PHI = .00 B = 5000.0

Energy levels and wave functions

E(CM−1)	(5/2)		(3/2)		(1/2)		(−1/2)		(−3/2)		(−5/2)	
−1.1395	.014	.000	−.060	.000	.292	.000	−.682	.000	.629	.000	−.224	.000
−.7079	−.022	.000	.136	.000	−.492	.000	.418	.000	.493	.000	−.567	.000
−.2889	−.027	.000	.208	.000	−.492	.000	−.110	.000	.393	.000	.740	.000
−.1000	.034	.000	−.297	.000	.535	.000	.580	.000	.454	.000	.286	.000
.5964	−.241	.000	.888	.000	.377	.000	.103	.000	.025	.000	−.006	.000
1.6398	−.969	.000	−.241	.000	−.046	.000	−.022	.000	−.003	.000	.000	.000

Transition probabilities

I, J	D(GC)	PSX	PSY	PSZ	PSXSX	PSYSY	PSZSZ	PSYSZ	PSXSZ	PSXSY
1–2	12.95	.026	2.120	.526	.708	.273	1.861	1.916	1.571	3.473
1–3	25.52	.284	.066	.007	1.485	3.047	.278	.993	.052	.145
1–4	31.19	.091	.056	.001	.565	.954	.051	.157	.190	1.087
1–5	52.08	.007	.007	.001	.753	.913	.008	.084	.122	.896
1–6	83.38	.000	.000	.001	.015	.033	.003	.003	.002	.023
2–3	12.57	.026	1.974	.892	.785	1.392	4.268	2.482	.535	.075
2–4	18.24	.597	.310	.061	.006	.475	.372	.726	.006	.013
2–5	39.13	.141	.121	.003	1.218	2.024	.102	.565	.504	1.665
2–6	70.43	.000	.001	.000	.232	.290	.003	.015	.013	.263
3–4	5.67	.381	1.062	.982	.017	2.645	2.239	.714	.733	2.125
3–5	26.56	.431	.434	.041	.048	.386	.162	.802	.583	.170
3–6	57.86	.003	.006	.000	.510	.594	.003	.071	.071	.565
4–5	20.89	1.280	1.388	.128	2.432	.992	.318	.730	.416	1.743
4–6	52.19	.006	.009	.000	1.284	1.421	.003	.224	.229	1.389
5–6	31.30	1.217	1.196	.065	1.312	.030	.947	4.516	3.916	.369

TABLE 1. *Energy levels, wave functions, and transition probabilities for angles and field strengths indicated*—Continued

THETA = 45.00 PHI = .00 B = 1000.0

Energy levels and wave functions

E(CM−1)	(5/2)	(3/2)	(1/2)	(−1/2)	(−3/2)	(−5/2)
−.6051	.025 .000	−.087 .000	.561 .000	−.804 .000	.176 .000	.006 .000
−.4058	.004 .000	.175 .000	−.797 .000	−.525 .000	.235 .000	−.056 .000
−.1616	.007 .000	.047 .000	−.095 .000	−.277 .000	−.947 .000	.120 .000
.0296	.105 .000	−.974 .000	−.196 .000	−.033 .000	−.020 .000	−.014 .000
.4072	−.001 .000	.009 .000	.040 .000	−.009 .000	−.126 .000	−.991 .000
.7357	.994 .000	.104 .000	.011 .000	.028 .000	.003 .000	−.000 .000

Transition probabilities

I, J	D(GC)	PSX	PSY	PSZ	PSXSX	PSYSY	PSZSZ	PSYSZ	PSXSZ	PSXSY
1–2	5.98	.125	2.520	.269	.042	.024	.003	.018	.439	1.024
1–3	13.30	.913	.647	.011	1.384	2.285	.112	1.505	.984	1.257
1–4	19.04	.321	.295	.005	2.509	3.106	.032	.544	.694	2.847
1–5	30.37	.011	.000	.003	1.326	1.142	.007	.053	.064	1.242
1–6	40.22	.000	.002	.004	.411	.602	.018	.016	.012	.504
2–3	7.32	1.068	1.107	.108	2.405	1.170	.220	.509	.747	2.199
2–4	13.06	1.588	1.606	.032	1.123	.515	.117	1.471	1.172	.681
2–5	24.39	.034	.012	.012	.823	1.397	.076	.213	.171	1.043
2–6	34.24	.002	.012	.002	1.938	1.763	.004	.066	.072	1.883
3–4	5.74	.071	.063	.007	.961	.848	.004	.029	.001	.885
3–5	17.06	1.166	1.269	.013	.371	.019	.223	4.697	4.517	.298
3–6	26.92	.000	.000	.001	.061	.041	.002	.015	.017	.052
4–5	11.33	.001	.001	.003	.008	.026	.005	.010	.011	.017
4–6	21.18	1.263	1.214	.012	.344	.027	.179	4.854	4.767	.067
5–6	9.86	.000	.000	.000	.000	.000	.000	.001	.001	.000

THETA = 45.00 PHI = .00 B = 2000.0

Energy levels and wave functions

E(CM−1)	(5/2)	(3/2)	(1/2)	(−1/2)	(−3/2)	(−5/2)
−.7552	.027−.000	−.116−.000	.518−.000	−.785−.000	.317−.000	−.030−.000
−.4139	−.022−.000	.257−.000	−.714−.000	−.276−.000	.565−.000	−.167−.000
−.1827	−.012−.000	.210−.000	−.328−.000	−.543−.000	−.709−.000	.226−.000
.1554	−.188−.000	.916−.000	.333−.000	.100−.000	.057−.000	.040−.000
.2748	.008 .000	−.046 .000	−.045 .000	.052 .000	.273 .000	.958 .000
.9215	.981 .000	.188 .000	.030 .000	.027 .000	.004 .000	−.001 .000

Transition probabilities

I, J	D(GC)	PSX	PSY	PSZ	PSXSX	PSYSY	PSZSZ	PSYSZ	PSXSZ	PSXSY
1–2	10.24	.013	2.776	.385	.044	.013	.106	.273	1.520	3.170
1–3	17.17	.681	.034	.000	1.500	3.114	.292	1.524	.278	.149
1–4	27.32	.122	.119	.005	1.826	2.447	.045	.415	.510	2.138
1–5	30.90	.013	.003	.002	.740	.713	.000	.110	.171	.909
1–6	50.30	.000	.001	.002	.205	.324	.014	.019	.014	.261
2–3	6.94	.246	1.581	.671	.625	.016	.843	.412	.550	1.101
2–4	17.08	1.109	1.087	.052	.073	.062	.270	1.300	1.091	.012
2–5	20.66	.236	.137	.030	.263	1.419	.460	1.514	1.012	.566
2–6	40.06	.006	.016	.000	1.363	1.427	.001	.123	.129	1.432
3–4	10.14	.745	.622	.092	2.699	1.617	.138	.388	.068	1.923
3–5	13.73	.865	1.177	.060	1.691	.166	.797	3.160	2.739	1.264
3–6	33.13	.007	.010	.001	.568	.562	.000	.154	.164	.593
4–5	3.58	.005	.006	.038	.135	.285	.028	.027	.054	.217
4–6	22.98	1.242	1.180	.040	.982	.051	.586	4.563	4.225	.264
5–6	19.40	.002	.002	.000	.000	.000	.001	.018	.017	.000

TABLE 1. *Energy levels, wave functions, and transition probabilities for angles and field strengths indicated*—Continued

THETA = 45.00 PHI = .00 B = 3000.0

Energy levels and wave functions

E(CM−1)	(5/2)	(3/2)	(1/2)	(−1/2)	(−3/2)	(−5/2)
−.9238	.027 .000	−.122 .000	.475 .000	−.758 .000	.422 .000	−.078 .000
−.4953	−.036 .000	.260 .000	−.632 .000	−.039 .000	.663 .000	−.301 .000
−.1643	−.046 .000	.349 .000	−.438 .000	−.609 .000	−.434 .000	.353 .000
.1754	−.009 .000	.062 .000	−.002 .000	−.163 .000	−.436 .000	−.883 .000
.2908	−.254 .000	.853 .000	.424 .000	.156 .000	.065 .000	.000 .000
1.1172	−.965 .000	−.254 .000	−.054 .000	−.030 .000	−.005 .000	.001 .000

Transition probabilities

I. J	D(GC)	PSX	PSY	PSZ	PSXSX	PSYSY	PSZSZ	PSYSZ	PSXSZ	PSXSY
1–2	12.86	.003	2.501	.480	.096	.103	.398	.632	2.082	4.072
1–3	22.79	.486	.017	.003	1.749	3.787	.389	1.528	.028	.037
1–4	32.98	.006	.002	.001	.312	.345	.001	.092	.187	.560
1–5	36.44	.042	.048	.003	1.127	1.575	.037	.262	.369	1.550
1–6	61.23	.000	.000	.001	.097	.167	.010	.015	.009	.128
2–3	9.93	.001	1.998	.928	.201	.326	1.039	.459	.634	.311
2–4	20.12	.294	.172	.043	.011	1.329	1.097	2.188	1.161	.222
2–5	23.58	.588	.499	.025	.149	.944	.343	1.216	.849	.534
2–6	48.37	.003	.009	.000	.781	.909	.005	.096	.096	.866
3–4	10.19	.632	1.039	.229	2.873	.063	2.088	2.068	1.082	1.685
3–5	13.65	1.164	1.192	.224	2.282	.812	.371	.740	.254	1.571
3–6	38.44	.021	.027	.001	.938	1.134	.009	.367	.377	1.089
4–5	3.46	.074	.088	.020	.851	.740	.004	.024	.050	.845
4–6	28.25	.001	.001	.000	.028	.036	.001	.026	.026	.034
5–6	24.79	1.211	1.157	.077	1.673	.068	1.068	4.288	3.644	.493

THETA = 45.00 PHI = 30.00 B = 3000.0

Energy levels and wave functions

E(CM−1)	(5/2)	(3/2)	(1/2)	(−1/2)	(−3/2)	(−5/2)
−.9262	.013 −.013	−.067 .099	.422 −.219	−.754 −.043	.351 .239	−.027 −.093
−.4840	.003 .039	.124 −.238	−.540 .342	−.040 −.029	.596 .294	−.182 −.202
−.1776	−.060 .014	.281 .183	−.181 −.384	−.003 −.609	.183 −.388	−.347 .168
.1743	.058 −.004	−.186 −.112	−.009 −.009	−.091 .123	−.387 .174	−.859 −.086
.2970	.203 −.130	−.828 .067	−.383 −.189	−.080 −.162	.037 −.112	.141 −.047
1.1166	.030 .965	−.119 .224	−.039 .030	−.008 .021	−.004 .003	.000 −.001

Transition probabilities

I. J	D(GC)	PX1SX	PY1SY	PZ1SZ	P2SXX	P2SYY	P2SZZ	PSXSY	PSXSZ	PSYSZ
1–2	13.27	.600	1.860	.492	3.211	2.991	.422	1.068	1.705	.886
1–3	22.46	.387	.083	.003	.283	1.449	.451	1.884	.387	1.245
1–4	33.02	.021	.012	.004	.976	.946	.011	.122	.168	.151
1–5	36.70	.038	.044	.001	.995	1.215	.038	1.592	.351	.245
1–6	61.28	.000	.000	.001	.107	.161	.006	.131	.007	.011
2–3	9.19	.480	1.632	.897	.470	.422	.985	.098	.662	.569
2–4	19.75	.246	.322	.026	.084	.835	.890	.380	1.521	1.791
2–5	23.43	.572	.448	.032	.394	.987	.277	.393	.801	1.271
2–6	48.02	.002	.007	.000	.833	.892	.008	.881	.118	.117
3–4	10.56	.834	.790	.388	3.213	1.781	2.242	.728	1.183	1.829
3–5	14.24	.984	1.222	.146	1.519	.897	.684	1.855	.511	.560
3–6	38.83	.023	.028	.003	1.011	1.025	.039	1.054	.342	.323
4–5	3.68	.123	.133	.504	1.010	.752	.184	.795	.095	.088
4–6	28.27	.056	.055	.003	.050	.013	.053	.019	.217	.224
5–6	24.59	1.158	1.104	.066	1.263	.462	.952	.528	3.644	3.958

TABLE 1. *Energy levels, wave functions, and transition probabilities for angles and field strengths indicated*—Continued

THETA = 45.00 PHI = 60.00 B = 3000.0

Energy levels and wave functions

E(CM-1)	(5/2)	(3/2)	(1/2)	(−1/2)	(−3/2)	(−5/2)
−.9286	.000 .000	.097 −.064	−.425 −.214	.042 .750	.358 −.234	−.100 −.050
−.4720	−.025 .033	.275 .036	−.248 −.598	.023 −.031	−.662 −.087	.090 .216
−.1917	.062 −.039	−.282 −.151	.014 .408	−.518 .323	−.372 −.199	.014 .418
.1734	.049 .060	.102 −.270	.017 −.003	−.091 −.111	.146 −.387	.836 −.137
.3029	−.133 .187	.809 .075	.180 .391	−.116 .164	−.147 −.014	−.084 −.182
1.1160	−.966 −.028	−.120 −.222	.024 −.038	−.012 −.000	−.001 −.002	−.001 .001

Transition probabilities

I, J	D(GC)	PSX	PSY	PSZ	PSXSX	PSYSY	PSZSZ	PSYSZ	PSXSZ	PSXSY
1–2	13.70	1.820	.610	.505	3.126	3.188	.440	1.634	.829	1.021
1–3	22.11	.111	.317	.000	1.342	.197	.513	.469	1.247	1.919
1–4	33.06	.038	.017	.005	.934	.913	.022	.248	.102	.320
1–5	36.95	.036	.040	.000	1.237	.990	.039	.229	.339	1.[illegible]1
1–6	61.34	.000	.001	.001	.125	.147	.004	.007	.005	.135
2–3	8.41	1.715	.572	.861	.475	.398	.912	.685	.713	.074
2–4	19.36	.177	.479	.001	.672	.126	.667	1.167	2.130	.375
2–5	23.25	.535	.428	.038	.766	.522	.179	1.233	.839	.422
2–6	47.64	.002	.004	.000	.933	.836	.010	.140	.145	.896
3–4	10.95	1.052	.525	.531	1.921	2.920	2.419	1.346	1.533	.881
3–5	14.84	.822	1.255	.084	.675	2.065	.997	.321	.814	1.666
3–6	39.23	.026	.029	.005	1.134	.871	.068	.281	.304	1.011
4–5	3.88	.159	.170	.868	1.164	.673	.318	.202	.067	.785
4–6	28.28	.102	.100	.006	.043	.015	.096	.369	.400	.007
5–6	24.39	1.108	1.064	.056	.505	1.183	.848	3.516	3.813	.572

THETA = 45.00 PHI = 90.00 B = 3000.0

Energy levels and wave functions

E(CM-1)	(5/2)	(3/2)	(1/2)	(−1/2)	(−3/2)	(−5/2)
−.9262	.013 −.013	−.001 −.119	−.475 −.007	−.002 .755	.425 −.006	−.018 −.095
−.4840	.000 .039	.268 −.006	−.016 −.639	.038 −.032	−.001 −.665	−.269 −.039
−.1776	.015 −.060	−.335 .012	.028 .424	−.609 −.014	.043 −.427	−.385 .021
.1743	.046 .036	.119 −.181	.009 .010	−.006 −.153	.424 −.012	.021 .863
.2970	−.002 −.241	−.831 −.022	.005 −.427	.180 −.022	.043 .110	−.106 .105
1.1166	−.966 .001	.001 −.254	.049 .004	−.021 .009	−.002 −.004	−.001 −.001

Transition probabilities

I, J	D(GC)	PX1SX	PY1SY	PZ1SZ	P2SXX	P2SYY	P2SZZ	PSXSY	PSXSZ	PSYSZ
1–2	13.27	2.455	.004	.492	.083	.133	.422	4.060	.528	2.064
1–3	22.46	.018	.452	.003	3.807	1.653	.451	.020	1.580	.051
1–4	33.02	.026	.006	.004	.189	.148	.011	.914	.057	.261
1–5	36.70	.040	.042	.001	1.706	1.236	.038	1.226	.331	.265
1–6	61.28	.000	.000	.001	.140	.128	.007	.132	.009	.008
2–3	9.19	2.110	.002	.897	.328	.178	.985	.291	.573	.657
2–4	19.75	.110	.458	.026	1.260	.054	.890	.182	2.391	.920
2–5	23.43	.536	.484	.032	.767	.139	.277	.630	.933	1.139
2–6	48.02	.006	.004	.000	.957	.789	.008	.870	.121	.114
3–4	10.56	1.176	.449	.388	.028	2.398	2.242	2.011	1.856	1.156
3–5	14.24	.888	1.317	.146	.812	2.976	.684	1.169	.892	.179
3–6	38.83	.025	.025	.003	1.220	.863	.039	1.030	.342	.324
4–5	3.68	.121	.134	.504	1.096	.600	.184	.827	.013	.170
4–6	28.27	.056	.055	.003	.044	.015	.053	.021	.236	.205
5–6	24.59	1.140	1.121	.066	.075	1.556	.952	.575	4.110	3.492

TABLE 1. *Energy levels, wave functions, and transition probabilities for angles and field strengths indicated*—Continued

THETA = 45.00 PHI = .00 B = 4000.0

Energy levels and wave functions

E(CM−1)	(5/2)	(3/2)	(1/2)	(−1/2)	(−3/2)	(−5/2)
−1.1058	.026 .000	−.120 .000	.436 .000	−.729 .000	.496 .000	−.131 .000
−.6053	−.043 .000	.254 .000	−.592 .000	.108 .000	.634 .000	−.411 .000
−.1639	−.073 .000	.407 .000	−.465 .000	−.556 .000	−.168 .000	.525 .000
.1237	−.041 .000	.192 .000	−.066 .000	−.322 .000	−.561 .000	−.734 .000
.4311	−.304 .000	.790 .000	.483 .000	.206 .000	.091 .000	.020 .000
1.3202	.948 .000	.308 .000	.077 .000	.034 .000	.007 .000	−.000 .000

Transition probabilities

I, J	D(GC)	PSX	PSY	PSZ	PSXSX	PSYSY	PSZSZ	PSYSZ	PSXSZ	PSXSY
1–2	15.02	.008	2.240	.554	.251	.147	.781	.896	2.261	4.315
1–3	28.26	.355	.045	.007	1.817	4.144	.473	1.598	.002	.174
1–4	36.89	.001	.005	.000	.009	.004	.001	.004	.200	.538
1–5	46.11	.015	.019	.002	.734	1.038	.026	.173	.236	.989
1–6	72.78	.000	.000	.001	.046	.086	.006	.010	.006	.062
2–3	13.24	.042	2.286	1.060	.324	.506	1.641	.788	.929	.018
2–4	21.87	.321	.019	.011	.000	1.480	1.451	2.233	.453	.043
2–5	31.09	.298	.257	.013	.454	1.491	.299	.981	.774	1.027
2–6	57.77	.001	.005	.000	.478	.594	.006	.068	.065	.545
3–4	8.63	.166	1.195	.760	2.136	.236	3.793	1.451	.135	1.869
3–5	17.85	1.126	1.102	.230	1.206	.084	.654	1.170	.392	.523
3–6	44.52	.023	.029	.000	.925	1.277	.028	.436	.435	1.150
4–5	9.22	.348	.397	.151	1.924	1.437	.035	.000	.055	1.827
4–6	35.89	.011	.011	.000	.137	.244	.015	.177	.170	.201
5–6	26.67	1.174	1.138	.116	2.312	.079	1.538	4.015	3.076	.718

THETA = 45.00 PHI = .00 B = 5000.0

Energy levels and wave functions

E(CM−1)	(5/2)	(3/2)	(1/2)	(−1/2)	(−3/2)	(−5/2)
−1.2979	.025 .000	−.115 .000	.402 .000	−.701 .000	.548 .000	−.183 .000
−.7289	−.046 .000	.247 .000	−.569 .000	.206 .000	.570 .000	−.496 .000
−.1989	−.085 .000	.405 .000	−.465 .000	−.447 .000	.071 .000	.638 .000
.1229	−.080 .000	.315 .000	−.134 .000	−.454 .000	−.599 .000	−.559 .000
.5738	.344 .000	−.735 .000	−.521 .000	−.243 .000	−.107 .000	−.026 .000
1.5290	−.930 .000	−.351 .000	−.099 .000	−.039 .000	−.009 .000	.000 .000

Transition probabilities

I, J	D(GC)	PSX	PSY	PSZ	PSXSX	PSYSY	PSZSZ	PSYSZ	PSXSZ	PSXSY
1–2	17.07	.020	2.051	.612	.498	.159	1.219	1.108	2.263	4.329
1–3	32.97	.256	.054	.009	1.584	3.944	.529	1.540	.000	.261
1–4	42.63	.012	.009	.000	.070	.154	.016	.031	.191	.573
1–5	56.15	.005	.008	.001	.472	.669	.017	.110	.154	.640
1–6	84.81	.000	.000	.001	.021	.044	.005	.006	.003	.030
2–3	15.90	.071	2.305	1.143	.579	.695	2.544	1.224	.945	.014
2–4	25.56	.310	.020	.001	.018	1.675	1.342	1.968	.045	.008
2–5	39.08	.163	.139	.006	.617	1.663	.254	.809	.667	1.211
2–6	67.74	.000	.002	.000	.306	.395	.006	.046	.043	.356
3–4	9.65	.007	1.370	1.196	.742	1.144	3.728	1.097	.038	1.775
3–5	23.18	.799	.775	.160	.300	.113	.782	1.426	.561	.018
3–6	51.84	.016	.020	.000	.733	1.090	.035	.359	.350	.949
4–5	13.53	.732	.843	.323	2.783	1.580	.169	.060	.027	2.427
4–6	42.18	.024	.024	.000	.321	.642	.055	.416	.384	.499
5–6	28.65	1.138	1.129	.155	2.849	.082	1.964	3.799	2.595	.910

TABLE 1. *Energy levels, wave functions, and transition probabilities for angles and field strengths indicated*—Continued

THETA = 60.00 PHI = .00 B = 1000.0

Energy levels and wave functions

E(CM−1)	(5/2)		(3/2)		(1/2)		(−1/2)		(−3/2)		(−5/2)	
−.6309	.028	.000	−.117	.000	.612	.000	−.760	.000	.181	.000	.004	.000
−.4016	−.001	.000	.217	.000	−.743	.000	−.565	.000	.279	.000	−.060	.000
−.1260	−.003	.000	−.093	.000	.097	.000	.312	.000	.930	.000	−.142	.000
.0072	−.132	.000	.956	.000	.251	.000	.062	.000	.050	.000	.009	.000
.4597	−.001	.000	.009	.000	.036	.000	−.013	.000	−.149	.000	−.988	.000
.6915	.991	.000	.131	.000	.016	.000	.030	.000	.004	.000	−.001	.000

Transition probabilities

I, J	D(GC)	PSX	PSY	PSZ	PSXSX	PSYSY	PSZSZ	PSYSZ	PSXSZ	PSXSY
1–2	6.88	.036	2.542	.309	.015	.005	.002	.017	.626	1.398
1–3	15.15	.752	.428	.007	1.730	2.785	.125	1.449	.751	1.248
1–4	19.14	.322	.338	.008	1.986	2.679	.052	.604	.836	2.633
1–5	32.72	.009	.000	.003	1.078	.916	.007	.049	.060	1.001
1–6	39.67	.000	.003	.004	.470	.677	.019	.027	.021	.571
2–3	8.27	1.059	1.397	.151	1.734	.619	.281	.582	.922	1.787
2–4	12.27	1.580	1.434	.047	1.271	.472	.194	1.430	.951	.623
2–5	25.84	.040	.017	.010	.976	1.600	.077	.285	.235	1.205
2–6	32.80	.005	.018	.002	1.776	1.630	.003	.105	.117	1.747
3–4	4.00	.116	.109	.039	1.300	1.101	.008	.030	.000	1.192
3–5	17.57	1.155	1.264	.019	.513	.024	.315	4.596	4.354	.355
3–6	24.53	.001	.002	.001	.074	.058	.001	.050	.053	.072
4–5	13.57	.001	.001	.003	.032	.054	.003	.028	.030	.046
4–6	20.53	1.260	1.198	.019	.547	.042	.286	4.746	4.598	.124
5–6	6.96	.000	.000	.000	.000	.000	.000	.002	.002	.000

THETA = 60.00 PHI = .00 B = 2000.0

Energy levels and wave functions

E(CM−1)	(5/2)		(3/2)		(1/2)		(−1/2)		(−3/2)		(−5/2)	
−.8096	.034	.000	−.159	.000	.576	.000	−.743	.000	.298	.000	−.030	.000
−.4246	−.039	.000	.328	.000	−.662	.000	−.358	.000	.546	.000	−.162	.000
−.1198	.042	.000	−.311	.000	.211	.000	.528	.000	.711	.000	−.271	.000
.1249	−.238	.000	.845	.000	.428	.000	.185	.000	.109	.000	−.025	.000
.3877	−.001	.000	.015	.000	.023	.000	−.071	.000	−.309	.000	−.948	.000
.8413	.969	.000	.239	.000	.049	.000	.034	.000	.007	.000	−.001	.000

Transition probabilities

I, J	D(GC)	PSX	PSY	PSZ	PSXSX	PSYSY	PSZSZ	PSYSZ	PSXSZ	PSXSY
1–2	11.55	.004	2.619	.438	.018	.012	.059	.150	1.752	3.593
1–3	20.69	.544	.021	.000	1.867	3.790	.337	1.690	.172	.147
1–4	28.04	.090	.126	.006	1.080	1.652	.061	.362	.641	1.988
1–5	35.92	.008	.001	.002	.583	.557	.000	.079	.106	.592
1–6	49.53	.000	.001	.002	.224	.357	.016	.032	.022	.285
2–3	9.14	.218	1.992	.679	.362	.050	.683	.417	.974	.628
2–4	16.49	1.161	.795	.053	.128	.156	.566	1.639	.734	.008
2–5	24.37	.135	.100	.020	.433	1.561	.350	1.171	.882	.786
2–6	37.98	.011	.024	.000	1.226	1.360	.003	.207	.220	1.343
3–4	7.34	.635	.730	.309	2.434	1.374	.150	.200	.022	2.245
3–5	15.23	.942	1.125	.090	1.813	.063	1.198	3.383	2.618	.926
3–6	28.83	.036	.040	.000	.337	.471	.011	.395	.404	.445
4–5	7.88	.043	.054	.000	.537	.395	.011	.109	.111	.501
4–6	21.49	1.206	1.122	.071	1.681	.103	.952	4.162	3.613	.505
5–6	13.61	.000	.000	.000	.007	.007	.000	.005	.005	.008

TABLE 1. *Energy levels, wave functions, and transition probabilities for angles and field strengths indicated*—Continued

THETA = 60.00 PHI = .00 B = 3000.0

Energy levels and wave functions

E(CM-1)	(5/2)		(3/2)		(1/2)		(−1/2)		(−3/2)		(−5/2)	
−1.0038	.037	.000	−.174	.000	.543	.000	−.726	.000	.376	.000	−.069	.000
−.5105	.063	.000	−.353	.000	.608	.000	.192	.000	−.628	.000	.265	.000
−.1069	.100	.000	−.449	.000	.230	.000	.578	.000	.494	.000	−.397	.000
.2553	.313	.000	−.727	.000	−.513	.000	−.229	.000	−.026	.000	.238	.000
.3576	.058	.000	−.091	.000	−.106	.000	−.217	.000	−.468	.000	−.843	.000
1.0082	.940	.000	.326	.000	.090	.000	.044	.000	.012	.000	.000	.000

Transition probabilities

I, J	D(GC)	PSX	PSY	PSZ	PSXSX	PSYSY	PSZSZ	PSYSZ	PSXSZ	PSXSY
1–2	14.80	.002	2.384	.537	.049	.050	.199	.306	2.375	4.515
1–3	26.91	.389	.005	.003	1.868	4.328	.509	1.855	.017	.005
1–4	37.77	.021	.047	.003	.427	.737	.042	.160	.524	1.573
1–5	40.84	.005	.000	.002	.373	.424	.002	.087	.039	.139
1–6	60.36	.000	.001	.001	.104	.183	.011	.024	.014	.137
2–3	12.11	.004	2.310	.993	.164	.243	.806	.391	1.240	.066
2–4	22.97	.773	.272	.014	0.53	1.621	1.088	2.423	.319	.186
2–5	26.04	.056	.153	.027	.093	.944	.445	.955	1.116	.603
2–6	45.56	.006	.015	.000	.758	.960	.012	.182	.186	.889
3–4	10.87	.506	1.594	.691	.907	.497	.061	.111	.243	2.292
3–5	13.94	.923	.594	.132	2.909	.002	2.763	2.932	1.017	.552
3–6	33.45	.066	.071	.000	.416	.863	.081	.746	.726	.690
4–5	3.07	.129	.233	.399	2.217	.301	.884	.135	.003	1.385
4–6	22.59	1.097	1.027	.131	2.527	.090	1.661	3.644	2.661	.761
5–6	19.52	.047	.046	.010	.346	.110	.066	.050	.024	.206

THETA = 60.00 PHI = .00 B = 4000.0

Energy levels and wave functions

E(CM-1)	(5/2)		(3/2)		(1/2)		(−1/2)		(−3/2)		(−5/2)	
−1.2072	.040	.000	−.178	.000	.516	.000	−.710	.000	.430	.000	−.106	.000
−.6209	.077	.000	−.359	.000	.582	.000	.083	.000	−.631	.000	.348	.000
−.1147	.142	.000	−.501	.000	.232	.000	.567	.000	.313	.000	−.505	.000
.3181	.238	.000	−.471	.000	−.309	.000	.043	.000	.394	.000	.685	.000
.4361	.304	.000	−.460	.000	−.477	.000	−.402	.000	−.404	.000	−.380	.000
1.1887	.907	.000	.394	.000	.133	.000	.059	.000	.018	.000	.002	.000

Transition probabilities

I, J	D(GC)	PSX	PSY	PSZ	PSXSX	PSYSY	PSZSZ	PSYSZ	PSXSZ	PSXSY
1–2	17.59	.005	2.175	.613	.124	.071	.382	.427	2.689	4.826
1–3	32.78	.283	.018	.005	1.677	4.402	.645	1.931	.000	.077
1–4	45.76	.003	.011	.000	.032	.093	.016	.021	.357	.974
1–5	49.30	.005	.009	.002	.377	.555	.017	.121	.072	.218
1–6	71.88	.000	.000	.001	.047	.094	.008	.015	.008	.065
2–3	15.19	.010	2.412	1.158	.222	.305	1.047	.478	1.480	.016
2–4	28.17	.476	.015	.000	.153	3.130	1.900	3.395	.022	.005
2–5	31.71	.082	.185	.017	.049	.168	.035	.117	.987	.841
2–6	54.29	.002	.008	.000	.482	.659	.014	.134	.133	.586
3–4	12.98	.002	2.161	1.144	.303	.363	1.329	.533	.519	1.996
3–5	16.52	1.018	.120	.049	2.147	.023	2.615	2.407	.000	.048
3–6	39.10	.061	.065	.000	.403	1.035	.146	.826	.771	.758
4–5	3.54	.111	.508	2.180	.003	1.143	1.023	.084	1.335	2.208
4–6	26.12	.365	.344	.051	.528	.048	.893	1.707	1.144	.045
5–6	22.58	.737	.719	.168	3.308	.297	1.623	1.804	.916	1.337

TABLE 1. *Energy levels, wave functions, and transition probabilities for angles and field strengths indicated*—Continued

THETA = 60.00 PHI = .00 B = 5000.0

Energy levels and wave functions

E(CM−1)	(5/2)		(3/2)		(1/2)		(−1/2)		(−3/2)		(−5/2)	
−1.4170	.041	.000	−.178	.000	.494	.000	−.695	.000	.468	.000	−.140	.000
−.7431	.086	.000	−.360	.000	.568	.000	.008	.000	−.610	.000	.410	.000
−.1413	−.167	.000	.514	.000	−.238	.000	−.540	.000	−.168	.000	.575	.000
.3401	−.232	.000	.425	.000	.235	.000	−.165	.000	−.506	.000	−.653	.000
.5813	.380	.000	−.441	.000	−.540	.000	−.438	.000	−.352	.000	−.233	.000
1.3799	.875	.000	.446	.000	.173	.000	.075	.000	.025	.000	.004	.000

Transition probabilities

I, J	D(GC)	PSX	PSY	PSZ	PSXSX	PSYSY	PSZSZ	PSYSZ	PSXSZ	PSXSY
1–2	20.22	.010	2.020	.672	.237	.078	.587	.524	2.846	4.916
1–3	38.27	.211	.025	.007	1.424	4.237	.748	1.938	.005	.149
1–4	52.71	.004	.006	.000	.042	.115	.018	.031	.257	.646
1–5	59.95	.002	.005	.001	.219	.342	.014	.075	.081	.239
1–6	83.91	.000	.000	.001	.022	.049	.006	.009	.004	.031
2–3	18.05	.033	2.403	1.261	.340	.340	1.359	.593	1.544	.135
2–4	32.50	.323	.016	.000	.133	3.173	2.008	3.145	.005	.023
2–5	39.73	.080	.097	.007	.158	.586	.135	.348	.705	.836
2–6	63.69	.001	.004	.000	.313	.449	.012	.093	.090	.388
3–4	14.44	.009	1.998	1.355	.415	.593	2.002	.674	.175	1.453
3–5	21.68	.707	.274	.094	.916	.316	2.310	2.306	.121	.013
3–6	45.63	.043	.046	.000	.368	1.036	.169	.744	.676	.730
4–5	7.23	.345	.790	1.560	.692	1.436	.134	.029	1.112	2.688
4–6	31.19	.208	.196	.029	.131	.267	.770	1.411	.908	.012
5–6	23.96	.855	.870	.271	4.426	.277	2.489	2.079	.745	1.741

THETA = 75.00 PHI = .00 B = 1000.0

Energy levels and wave functions

E(CM−1)	(5/2)		(3/2)		(1/2)		(−1/2)		(−3/2)		(−5/2)	
−.6476	.031	.000	−.143	.000	.652	.000	−.723	.000	.173	.000	.004	.000
−.3999	−.005	.000	.250	.000	−.694	.000	−.605	.000	.294	.000	−.059	.000
−.0902	.013	.000	−.194	.000	.060	.000	.311	.000	.916	.000	−.153	.000
−.0197	−.152	.000	.926	.000	.297	.000	.112	.000	.139	.000	−.007	.000
.5187	.002	.000	−.007	.000	−.033	.000	.016	.000	.160	.000	.986	.000
.6387	−.988	.000	−.150	.000	−.021	.000	−.033	.000	−.005	.000	.001	.000

Transition probabilities

I, J	D(GC)	PSX	PSY	PSZ	PSXSX	PSYSY	PSZSZ	PSYSZ	PSXSZ	PSXSY
1–2	7.43	.007	2.536	.331	.001	.000	.001	.011	.739	1.620
1–3	16.72	.714	.266	.004	2.246	3.496	.138	1.532	.494	1.033
1–4	18.84	.271	.418	.012	1.351	1.981	.060	.526	1.045	2.715
1–5	34.99	.007	.000	.003	.909	.758	.007	.040	.051	.835
1–6	38.59	.000	.004	.004	.527	.752	.020	.039	.030	.634
2–3	9.29	.861	1.805	.182	1.084	.297	.246	.517	1.202	1.636
2–4	11.41	1.743	1.094	.047	1.597	.506	305	1.538	.642	.499
2–5	27.56	.037	.016	.008	1.113	1.732	.068	.298	.251	1.336
2–6	31.16	.008	.024	.002	1.640	1.512	.003	.145	.163	1.629
3–4	2.12	.134	.141	.226	1.382	1.140	.012	.022	.003	1.377
3–5	18.27	1.139	1.241	.024	.534	.015	.371	4.470	4.196	.326
3–6	21.87	.022	.022	.001	.040	.051	.001	.206	.209	.057
4–5	16.15	.019	.022	.001	.096	.088	.000	.139	.139	.105
4–6	19.75	1.239	1.161	.027	.770	.067	.383	4.515	4.318	.197
5–6	3.60	.000	.000	.000	.000	.000	.000	.002	.002	.000

TABLE 1. *Energy levels, wave functions, and transition probabilities for angles and field strengths indicated*—Continued

THETA = 75.00 PHI = .00 B = 2000.0

Energy levels and wave functions

E(CM−1)	(5/2)		(3/2)		(1/2)		(−1/2)		(−3/2)		(−5/2)	
−.8443	.043	.000	−.201	.000	.623	.000	−.705	.000	.268	.000	−.026	.000
−.4304	−.057	.000	.391	.000	−.601	.000	−.445	.000	.514	.000	−.143	.000
−.0714	−.103	.000	.460	.000	−.033	.000	−.446	.000	−.708	.000	.277	.000
.0934	.265	.000	−.719	.000	−.494	.000	−.314	.000	−.247	.000	.095	.000
.5091	.005	.000	.009	.000	.015	.000	−.076	.000	−.317	.000	−.945	.000
.7436	.956	.000	.281	.000	.070	.000	.044	.000	.013	.000	.001	.000

Transition probabilities

I, J	D(GC)	PSX	PSY	PSZ	PSXSX	PSYSY	PSZSZ	PSYSZ	PSXSZ	PSXSY
1–2	12.42	.001	2.534	.467	.002	.008	.016	.056	1.888	3.812
1–3	23.19	.516	.008	.000	2.345	4.684	.400	1.957	.057	.072
1–4	28.13	.038	.137	.007	.397	.703	.044	.173	.773	1.961
1–5	40.60	.005	.000	.002	.467	.430	.001	.053	.069	.441
1–6	47.63	.000	.002	.002	.244	.399	.019	.047	.032	.312
2–3	10.77	.112	2.508	.706	.126	.047	.326	.210	1.499	.377
2–4	15.72	1.287	.361	.024	.237	.252	.977	2.067	.297	.005
2–5	28.18	.083	.061	.012	.611	1.614	.239	.890	.712	.971
2–6	35.22	.018	.036	.000	1.094	1.304	.009	.312	.335	1.257
3–4	4.94	.354	.776	.911	1.328	.700	.100	.093	.000	2.392
3–5	17.41	.866	.981	.093	1.223	.000	1.245	3.291	2.447	.456
3–6	24.45	.156	.152	.001	.038	.296	.122	1.035	.992	.185
4–5	12.47	.179	.221	.007	1.188	.491	.151	.491	.417	.907
4–6	19.50	1.077	.971	.105	2.465	.213	1.229	3.319	2.621	.832
5–6	7.03	.001	.001	.001	.021	.015	.000	.004	.006	.019

THETA = 75.00 PHI = .00 B = 3000.0

Energy levels and wave functions

E(CM−1)	(5/2)		(3/2)		(1/2)		(−1/2)		(−3/2)		(−5/2)	
−1.0540	.051	.000	−.227	.000	.600	.000	−.690	.000	.325	.000	−.054	.000
−.5181	−.096	.000	.436	.000	−.546	.000	−.331	.000	.588	.000	−.219	.000
−.0665	−.184	.000	.546	.000	.010	.000	−.473	.000	−.551	.000	.375	.000
.2260	.353	.000	−.558	.000	−.567	.000	−.389	.000	−.185	.000	.238	.000
.5382	.046	.000	−.010	.000	−.050	.000	−.184	.000	−.458	.000	−.867	.000
.8744	.910	.000	.386	.000	.133	.000	.069	.000	.027	.000	.007	.000

Transition probabilities

I, J	D(GC)	PSX	PSY	PSZ	PSXSX	PSYSY	PSZSZ	PSYSZ	PSXSZ	PSXSY
1–2	16.08	.000	2.320	.570	.008	.019	.051	.100	2.562	4.752
1–3	29.63	.350	.002	.002	2.006	4.846	.616	2.128	.002	.002
1–4	38.40	.006	.045	.003	.129	.273	.027	.068	.537	1.323
1–5	47.77	.002	.000	.001	.236	.240	.000	.040	.038	.166
1–6	57.85	.000	.001	.001	.108	.201	.014	.034	.019	.144
2–3	13.55	.004	2.605	1.022	.056	.105	.313	.147	1.791	.003
2–4	22.32	.772	.112	.004	.003	1.635	1.489	2.680	.143	.090
2–5	31.69	.049	.062	.011	.258	1.153	.320	.838	.771	.727
2–6	41.77	.011	.023	.000	.678	.975	.027	.294	.299	.851
3–4	8.78	.234	1.408	1.190	.436	.161	.067	.097	.056	2.150
3–5	18.14	.667	.619	.130	1.331	.124	2.270	2.910	1.240	.230
3–6	28.23	.181	.178	.005	.023	.563	.357	1.383	1.248	.274
4–5	9.37	.312	.474	.174	2.797	.506	.924	.528	.187	1.840
4–6	19.45	.987	.881	.210	3.809	.208	2.235	2.753	1.500	1.247
5–6	10.09	.020	.022	.018	.284	.124	.033	.000	.010	.202

TABLE 1. *Energy levels, wave functions, and transition probabilities for angles and field strengths indicated*—Continued

THETA = 75.00 PHI = .00 B = 4000.0

Energy levels and wave functions

E(CM-1)	(5/2)		(3/2)		(1/2)		(−1/2)		(−3/2)		(−5/2)	
−1.2706	.058	.000	−.241	.000	.583	.000	−.679	.000	.363	.000	−.080	.000
−.6278	−.122	.000	.453	.000	−.518	.000	−.258	.000	.607	.000	−.277	.000
−.0791	−.238	.000	.561	.000	.030	.000	−.481	.000	−.441	.000	.449	.000
.3369	−.417	.000	.451	.000	.570	.000	.358	.000	.031	.000	−.410	.000
.6128	−.147	.000	.042	.000	.162	.000	.318	.000	.550	.000	.739	.000
1.0278	.854	.000	.465	.000	.201	.000	.105	.000	.048	.000	.018	.000

Transition probabilities

I, J	D(GC)	PSX	PSY	PSZ	PSXSX	PSYSY	PSZSZ	PSYSZ	PSXSZ	PSXSY
1–2	19.29	.001	2.139	.648	.024	.025	.098	.132	2.966	5.121
1–3	35.75	.249	.006	.004	1.636	4.692	.787	2.202	.001	.028
1–4	48.23	.001	.017	.001	.049	.133	.021	.036	.416	.978
1–5	56.50	.000	.001	.001	.130	.149	.001	.029	.005	.022
1–6	68.95	.000	.000	.001	.046	.099	.010	.021	.009	.064
2–3	16.46	.001	2.567	1.202	.073	.109	.359	.153	2.005	.093
2–4	28.94	.531	.040	.000	.104	3.083	2.055	3.428	.053	.091
2–5	37.22	.007	.047	.007	.066	.455	.174	.359	.676	.635
2–6	49.67	.005	.012	.000	.427	.683	.030	.220	.212	.551
3–4	12.48	.110	1.936	1.449	.048	.061	.001	.020	.233	1.652
3–5	20.76	.542	.228	.070	1.137	.486	3.111	3.044	.452	.055
3–6	33.21	.136	.138	.006	.026	.732	.481	1.314	1.148	.343
4–5	8.28	.219	.724	.817	2.810	.088	1.906	.413	.012	2.491
4–6	20.73	.851	.757	.271	3.936	.051	3.091	2.585	.895	1.065
5–6	12.45	.128	.137	.128	1.363	.345	.337	.044	.025	.811

THETA = 75.00 PHI = .00 B = 5000.0

Energy levels and wave functions

E(CM-1)	(5/2)		(3/2)		(1/2)		(−1/2)		(−3/2)		(−5/2)	
−1.4914	.063	.000	−.248	.000	.569	.000	−.670	.000	.390	.000	−.101	.000
−.7481	−.140	.000	.461	.000	−.502	.000	−.208	.000	.607	.000	−.322	.000
−.1038	−.274	.000	.559	.000	.038	.000	−.484	.000	−.357	.000	.500	.000
.4150	−.446	.000	.377	.000	.538	.000	.281	.000	−.125	.000	−.524	.000
.7281	−.265	.000	.043	.000	.252	.000	.416	.000	.575	.000	.601	.000
1.2002	.795	.000	.519	.000	.265	.000	.146	.000	.074	.000	.030	.000

Transition probabilities

I, J	D(GC)	PSX	PSY	PSZ	PSXSX	PSYSY	PSZSZ	PSYSZ	PSXSZ	PSXSY
1–2	22.30	.002	2.004	.710	.050	.027	.150	.157	3.231	5.272
1–3	41.63	.186	.008	.004	1.329	4.475	.927	2.237	.006	.053
1–4	57.19	.001	.008	.001	.026	.088	.018	.027	.324	.717
1–5	66.59	.000	.001	.001	.076	.099	.001	.021	.000	.000
1–6	80.75	.000	.000	.000	.019	.049	.007	.012	.004	.027
2–3	19.33	.008	2.506	1.322	.107	.107	.427	.171	2.117	.282
2–4	34.90	.382	.020	.000	.167	3.961	2.500	3.868	.023	.076
2–5	44.29	.000	.031	.004	.003	.065	.039	.062	.553	.581
2–6	58.45	.001	.006	.000	.270	.458	.025	.150	.137	.346
3–4	15.57	.058	2.193	1.658	.003	.074	.107	.003	.319	1.187
3–5	24.96	.433	.036	.014	.790	.974	3.518	3.262	.081	.012
3–6	39.12	.087	.092	.005	.034	.767	.477	1.094	.955	.374
4–5	9.39	.044	.953	1.497	1.241	.032	1.668	.277	.345	2.857
4–6	23.56	.638	.559	.239	3.053	.010	3.417	2.485	.610	.589
5–6	14.16	.289	.333	.358	2.927	.471	1.050	.174	.109	1.626

TABLE 1. *Energy levels, wave functions, and transition probabilities for angles and field strengths indicated*—Continued

THETA = 90.00 PHI = .00 B = 1000.0

Energy levels and wave functions

E(CM−1)	(5/2)	(3/2)	(1/2)	(−1/2)	(−3/2)	(−5/2)
−.6535	.034 .000	−.165 .000	.688 .000	−.688 .000	.158 .000	.006 .000
−.3991	−.006 .000	.271 .000	−.648 .000	−.649 .000	.287 .000	−.054 .000
−.0664	.109 .000	−.708 .000	−.161 .000	.161 .000	.649 .000	−.117 .000
−.0406	−.122 .000	.610 .000	.280 .000	.280 .000	.668 .000	−.100 .000
.5796	.230 .000	.032 .000	−.024 .000	.024 .000	.157 .000	.959 .000
.5800	−.959 .000	−.158 .000	−.031 .000	−.031 .000	.030 .000	.231 .000

Transition probabilities

I, J	D(GC)	PSX	PSY	PSZ	PSXSX	PSYSY	PSZSZ	PSYSZ	PSXSZ	PSXSY
1–2	7.63	.000	2.522	.337	.002	.002	.000	.004	.769	1.680
1–3	17.61	.954	.001	.001	3.536	5.460	.208	2.047	.013	.008
1–4	18.39	.001	.664	.016	.007	.004	.000	.010	1.520	3.714
1–5	36.99	.005	.001	.002	.473	.323	.014	.014	.057	1.043
1–6	37.01	.001	.005	.005	.919	1.171	.015	.069	.022	.391
2–3	9.98	.000	2.931	.231	.004	.007	.001	.012	1.815	2.041
2–4	10.75	2.591	.000	.003	2.565	.722	.565	2.078	.012	.008
2–5	29.36	.038	.005	.008	1.890	2.524	.046	.362	.131	.789
2–6	29.37	.004	.038	.001	.886	.697	.011	.084	.303	2.190
3–4	.77	.000	.151	1.976	.002	.003	.000	.012	.028	1.441
3–5	19.38	.314	.899	.024	.061	.013	.132	1.090	3.062	.056
3–6	19.39	.899	.314	.003	.256	.000	.276	3.758	1.539	.004
4–5	18.61	.861	.358	.001	.783	.151	.246	3.471	1.401	.221
4–6	18.62	.357	.862	.031	.458	.071	.168	.989	2.805	.414
5–6	.01	.000	.000	1.253	.001	.001	.000	.002	.082	.001

THETA = 90.00 PHI = .00 B = 2000.0

Energy levels and wave functions

E(CM−1)	(5/2)	(3/2)	(1/2)	(−1/2)	(−3/2)	(−5/2)
−.8565	.051 .000	−.241 .000	.665 .000	−.665 .000	.232 .000	−.018 .000
−.4306	−.076 .000	.445 .000	−.530 .000	−.530 .000	.470 .000	−.117 .000
−.0530	−.211 .000	.658 .000	.235 .000	−.235 .000	−.603 .000	.218 .000
.0784	.233 .000	−.463 .000	−.462 .000	−.462 .000	−.518 .000	.191 .000
.6289	.346 .000	.118 .000	.044 .000	−.044 .000	−.278 .000	−.886 .000
.6328	.879 .000	.286 .000	.077 .000	.077 .000	.129 .000	.341 .000

Transition probabilities

I, J	D(GC)	PSX	PSY	PSZ	PSXSX	PSYSY	PSZSZ	PSYSZ	PSXSZ	PSXSY
1–2	12.78	.000	2.498	.478	.004	.003	.000	.007	1.924	3.872
1–3	24.11	.524	.001	.002	2.650	5.350	.470	2.163	.010	.008
1–4	28.05	.001	.147	.006	.004	.001	.001	.003	.833	2.010
1–5	44.56	.003	.000	.003	.605	.632	.000	.072	.016	.120
1–6	44.68	.000	.003	.001	.072	.180	.024	.031	.074	.588
2–3	11.33	.000	2.918	.713	.000	.004	.001	.004	1.821	.280
2–4	15.27	1.426	.000	.005	.313	.336	1.298	2.408	.003	.008
2–5	31.79	.022	.068	.005	.231	.628	.097	.270	.891	1.897
2–6	31.90	.059	.023	.001	1.515	2.232	.069	.821	.145	.396
3–4	3.94	.000	.791	1.591	.003	.007	.001	.030	.006	2.465
3–5	20.46	.876	.193	.028	.443	.195	1.225	3.795	.430	.014
3–6	20.57	.193	.852	.054	.125	.008	.197	.909	3.357	.009
4–5	16.52	.170	1.083	.094	.528	.137	.127	.681	2.321	1.989
4–6	16.63	1.071	.171	.062	4.072	.633	1.494	2.801	.268	.316
5–6	.11	.000	.002	2.638	.005	.004	.000	.007	.980	.028

TABLE 1. *Energy levels, wave functions, and transition probabilities for angles and field strengths indicated*—Continued

THETA = 90.00 PHI = .00 B = 3000.00

Energy levels and wave functions

E(CM−1)	(5/2)		(3/2)		(1/2)		(−1/2)		(−3/2)		(−5/2)	
−1.0718	.068	.000	−.281	.000	.649	.000	−.649	.000	.272	.000	−.039	.000
−.5172	−.133	.000	.508	.000	−.453	.000	−.453	.000	.534	.000	−.170	.000
−.0545	−.294	.000	.607	.000	.272	.000	−.272	.000	−.556	.000	.298	.000
.2121	.347	.000	−.330	.000	−.517	.000	−.517	.000	−.385	.000	.295	.000
.7055	.490	.000	.233	.000	.074	.000	−.074	.000	−.341	.000	−.761	.000
.7259	.729	.000	.364	.000	.163	.000	.163	.000	.261	.000	.464	.000

Transition probabilities

I, J	D(GC)	PSX	PSY	PSZ	PSXSX	PSYSY	PSZSZ	PSYSZ	PSXSZ	PSXSY
1–2	16.64	.000	2.294	.584	.004	.003	.000	.006	2.620	4.832
1–3	30.52	.333	.001	.002	2.034	5.094	.690	2.264	.008	.007
1–4	38.52	.001	.044	.002	.004	.000	.002	.000	.535	1.259
1–5	53.32	.001	.001	.003	.317	.387	.003	.063	.004	.018
1–6	53.93	.000	.001	.000	.005	.039	.016	.012	.047	.279
2–3	13.88	.000	2.771	1.015	.000	.002	.002	.001	2.031	.001
2–4	21.88	.802	.000	.004	.000	1.766	1.751	2.964	.001	.008
2–5	36.68	.006	.065	.005	.032	.187	.065	.115	1.012	1.564
2–6	37.30	.042	.007	.000	.941	1.895	.165	.897	.037	.083
3–4	8.00	.000	1.391	1.529	.002	.009	.003	.041	.034	2.192
3–5	22.80	.804	.050	.018	.545	.681	2.442	4.367	.059	.002
3–6	23.41	.050	.685	.083	.050	.006	.092	.254	2.760	.009
4–5	14.80	.044	1.370	.404	.199	.052	.047	.169	1.223	3.383
4–6	15.41	1.249	.045	.067	7.245	.633	3.596	2.834	.008	.131
5–6	.61	.001	.025	4.195	.010	.007	.000	.011	3.144	.231

THETA = 90.00 PHI = .00 B = 4000.0

Energy levels and wave functions

E(CM−1)	(5/2)		(3/2)		(1/2)		(−1/2)		(−3/2)		(−5/2)	
−1.2932	.081	.000	−.305	.000	.636	.000	−.636	.000	.296	.000	−.055	.000
−.6254	−.176	.000	.531	.000	−.409	.000	−.409	.000	.556	.000	−.208	.000
−.0697	.355	.000	−.560	.000	−.292	.000	.292	.000	.514	.000	−.356	.000
.3238	−.446	.000	.212	.000	.515	.000	.515	.000	.266	.000	−.394	.000
.8019	.520	.000	.307	.000	.101	.000	−.100	.000	−.385	.000	−.684	.000
.8627	.606	.000	.415	.000	.261	.000	.261	.000	.347	.000	.452	.000

Transition probabilities

I, J	D(GC)	PSX	PSY	PSZ	PSXSX	PSYSY	PSZSZ	PSYSZ	PSXSZ	PSXSY
1–2	20.03	.000	2.124	.664	.004	.003	.000	.005	3.057	5.231
1–3	36.70	.232	.001	.002	1.588	4.823	.876	2.333	.007	.006
1–4	48.51	.001	.018	.001	.003	.000	.003	.000	.396	.891
1–5	62.85	.000	.001	.002	.157	.211	.004	.041	.001	.004
1–6	64.68	.000	.000	.000	.000	.014	.009	.007	.017	.098
2–3	16.67	.000	2.658	1.201	.000	.001	.002	.000	2.233	.144
2–4	28.47	.532	.000	.004	.069	3.046	2.198	3.540	.000	.007
2–5	42.82	.002	.042	.003	.007	.082	.041	.059	.854	1.177
2–6	44.64	.014	.002	.000	.509	1.185	.141	.585	.012	.025
3–4	11.80	.000	1.823	1.637	.001	.010	.005	.042	.170	1.631
3–5	26.15	.629	.019	.012	.490	1.274	3.345	4.487	.010	.000
3–6	27.97	.019	.399	.062	.027	.003	.047	.092	1.911	.081
4–5	14.34	.017	1.537	.903	.084	.020	.022	.059	.336	3.881
4–6	16.17	1.106	.018	.057	7.708	.199	5.433	2.736	.004	.063
5–6	1.83	.001	.108	3.910	.013	.008	.001	.013	4.753	.761

TABLE 1. *Energy levels, wave functions, and transition probabilities for angles and field strengths indicated*—Continued

THETA = 90.00 PHI = .00 B = 5000.0

Energy levels and wave functions

E(CM-1)	(5/2)		(3/2)		(1/2)		(−1/2)		(−3/2)		(−5/2)	
−1.5180	.091	.000	−.322	.000	.627	.000	−.627	.000	.313	.000	−.069	.000
−.7439	−.207	.000	.542	.000	−.380	.000	−.380	.000	.565	.000	−.236	.000
−.0948	−.398	.000	.520	.000	.303	.000	−.304	.000	−.479	.000	.397	.000
.4096	.511	.000	−.117	.000	−.491	.000	−.491	.000	−.167	.000	.464	.000
.9114	.520	.000	.356	.000	.123	.000	−.123	.000	−.415	.000	−.633	.000
1.0357	.508	.000	.439	.000	.339	.000	.339	.000	.391	.000	.407	.000

Transition probabilities

I, J	D(GC)	PSX	PSY	PSZ	PSXSX	PSYSY	PSZSZ	PSYSZ	PSXSZ	PSXSY
1–2	23.22	.000	1.997	.726	.003	.002	.000	.004	3.359	5.411
1–3	42.70	.171	.001	.002	1.262	4.571	1.030	2.380	.005	.005
1–4	57.83	.001	.008	.001	.003	.000	.003	.000	.306	.651
1–5	72.88	.000	.000	.001	.082	.116	.003	.025	.001	.002
1–6	76.61	.000	.000	.000	.000	.006	.005	.004	.005	.030
2–3	19.47	.000	2.570	1.330	.000	.001	.002	.000	2.368	.357
2–4	34.61	.382	.000	.003	.131	3.878	2.584	3.936	.000	.005
2–5	49.66	.001	.026	.002	.002	.045	.028	.035	.677	.885
2–6	53.39	.003	.001	.000	.267	.652	.085	.318	.005	.009
3–4	15.13	.000	2.068	1.767	.000	.008	.006	.037	.279	1.153
3–5	30.19	.478	.009	.008	.402	1.816	3.927	4.517	.002	.000
3–6	33.91	.009	.205	.034	.016	.001	.027	.039	1.264	.150
4–5	15.05	.008	1.616	1.375	.041	.008	.012	.025	.014	3.841
4–6	18.78	.809	.009	.039	6.186	.001	6.058	2.668	.011	.036
5–6	3.73	.001	.241	3.332	.012	.007	.001	.011	5.572	1.464

6. Appendix 1. Some Remarks on the Program

The matrix to be diagonalized is a 6 by 6 hermitian matrix. This matrix is equivalent to a 12 by 12 real symmetric matrix replacing each element:

$$a_{ij}+ib_{ij} \quad \text{by} \quad \begin{pmatrix} a_{ij} & -b_{ij} \\ b_{ij} & a_{ij} \end{pmatrix}.$$

The wave functions are treated similarly. The functions in the 12 column vector represent the real part of the wave functions at the odd positions, the imaginary part at the even positions. The diagonalization is performed using the Jacobi's method [29]. This method consists of the following steps:

The first subroutine will select the largest off-diagonal element a_{ij}; it will diagonalize the 2 by 2 matrix consisting of a_{ii}, a_{jj}, and a_{ji}. A second subroutine will rotate the wave functions $|i\rangle$ and $|j\rangle$ to accomplish this diagonalization. As a result of this transformation all elements will be modified. The procedure is then repeated by looking again for the largest matrix element (which may be larger than the first matrix element). Beyond a certain iteration, the largest element will decrease.

The convergence of the method is based on the relation:

$$\sum_{ij} (a_{ij}^2+b_{ij}^2)=\sum_i \lambda_i^2,$$

where λ_i are the eigenvalues of the matrix. One can estimate the number of steps necessary to obtain elements of a certain magnitude; it is proportional to (n^2-n) where n is the dimensionality of the matrix [29]. The matrix is considered diagonalized if the off diagonal elements are less than a predetermined value. Actually, a weighted criterion was used based on the second order correction of the perturbation theory:

$$\sum_j \left| \frac{a_{ij}^2}{a_{ii}-a_{jj}} \right| < \epsilon \quad \text{for all } i$$

and ϵ was chosen to be 10^{-5}. Smaller values led to "accidental" divergences. The machine was prevented from using this criterion if a_{ii} was equal to a_{jj}. The number of iterations range from 4 (the minimum) to about 150.

Finally two more subroutines were used, one to order the levels, and one to calculate the dipolar and quadrupolar transition probabilities as indicated in eqs (2) and (3).

7. References

[1] Kagan, M. R., Lally, J. F., Meister, R., and Meijer, P. H. E., Phys. Rev. **166,** 234 (1968).
[2] Mattuck, R. D., and Strandberg, M. W. P., Phys. Rev. Letters **3,** 369, (1959).
[3] Mattuck, R. D., and Strandberg, M. W. P., Phys. Rev. **119,** 1204 (1960).
[4] Dobrov, W. I., Phys. Rev. **134,** 734 (1964).
[5] Howarth, D. J., Royal Radar Establishment (1960).
[6] Cross, C. S., and Kikuchi, R., Technical Report, University of Michigan Z 1238. (24 June 1959).
[7] Unpublished figures obtained from the Bell Tel. Lab.
[8] Lessin, I., U.S.A.F. Cambridge Report AFCRL 66–692 (1966).
[9] Moore, C. E., NBS (US) Circ. No. 467.
[10] Moorjani, K., and Mc Avoy, N., Phys. Rev. **132,** 504 (1963).
[11] Geschwind, S., and Remeika, J. P., Phys. Rev. **122,** 751 (1961).
[12] Borgnis, F. E., Phys. Rev. **98,** 1000 (1955).
[13] Desilets, E. H., and Meister, R., J. Appl. Phys. **36,** 261 (1965).
[14] Kornienko, L. S., and Prokhorov, A. M., JETP **33,** 805, 1955 (Trans. JETP **6,** 620, 1958).
[15] Bogle, G. S., and Symmons, J. F., Proc. Phys. Soc. (London) **73,** 531, (1959).
[16] Symmons, H. F., and Bogle, G. S., Proc. Phys. Soc. (London) **79,** 468, (1962).
[17] Abragam, A., and Pryce, M. H. L., Proc. Roy. Soc. **A205,** 135, (1951).
[18] Bleaney, B., and Trenam, R. S., Proc. Roy. Soc. (London) **223,** 1 (1954).
[19] Bleaney, B., and Ingram, D. J. E., Proc. Roy. Soc. **A205,** 336, (1951).
[20] de L. Kronig, R., and Bouwkamp, C. J., Physica **6,** 290, (1939).
[21] Stevens, K. W. H., Proc. Phys. Soc. (London) **A65,** 209 (1952).
[22] Hutchings, M. T., Solid State Physics **16,** 227 (1964).
[23] Shiren, N. S., and Tucker, E. B., Phys. Rev. Letters **6,** 105, (1961).
[24] Shiren, N. S., Bull. Am. Phys. Soc. **7,** 29 (1962).
[25] Tucker, E. B., Phys. Rev. Letters **6,** 183 (1962).
[26] Dobrov, W. I., Phys. Rev. **134,** 734 (1964).
[27] Guermeur, R., Joffrin, J., Levelut, A., and Penne, J., Compt. Rend. Acad. Sc. (Paris) **260,** 108 (1965).
[28] Nye, J. F., Physical Properties of Crystals (Oxford University Press, 1957) and Birss, R. R., Symmetry and Magnetism (North Holland Publishing Company, Amsterdam, 1964).
[29] Wilkinson, J. H., Algebraic Eigenvalue Problems (Oxford, Oxford University Press 1965).

(Paper 73A2–550)

JOURNAL OF RESEARCH of the National Bureau of Standards—A. Physics and Chemistry
Vol. 73A, No. 2, March–April 1969

Publications of the National Bureau of Standards*

Selected Abstracts

Cassidy, E. C., Abramowitz, S., Beckett, C. W., **Investigations of the exploding wire process as a source for high temperature studies,** *Mono. 109 (Nov. 1968), 55 cents.*
Numerous experiments with electrically exploded wires are described. The results include time-resolved measurements of electrical energy, power, voltage, and current during the discharge; periodic still and high-speed photographs of the entire explosion process; integrated and time-resolved measurements of the intensity and spectral distribution of the radiation emitted; and time-resolved absorption spectra from the products of the discharge, with emphasis on observations of the spectrum of the AlO molecule. The apparatus, instrumentation, and fast-measurement techniques developed in order to permit these direct experimental observations and measurements, under the extreme and transient conditions of the explosive discharge, are also described. Results from calculations of the composition, entropy, enthalpy, and density of the explosion mixture are given.

Key words: Electrical discharges; exploding wire; high current; high speed; high speed photography; high temperature; high voltage; light sources; time-resolved electrical measurements; time-resolved spectroscopy.

Cord, M. S., Petersen, J. D., Lojko, M. S., Haas, R. H., **Microwave spectral tables, Polyatomic molecules without internal rotation,** *Mono. 70, Vol.* **IV** *(Oct. 1968), $5.50.*
Measured frequencies, assigned molecular species, and assigned quantum numbers are given for about 14,000 spectral lines of polyatomic molecules without internal rotation observed by coherent radiation techniques. Molecular data, such as rotational constants, dipole moments, and various coupling constants, determined by such techniques, are also tabulated. References are given for all included data.

Key words: Centrifugal distortion constant; coherent radiation technique; dipole moment; l-doubling; microwave spectra; molecular spectra; polyatomic molecules; quadrupole coupling constants; rotational constant; spectral lines.

Flynn, D. R., Peavy, B. A., Jr., Ed., **Thermal Conductivity, Proceedings of Seventh Conference, National Bureau of Standards, Gaithersburg, Md., Nov. 13–16, 1967,** *Spec. Publ. 302 (Sept. 1968), $6.25.*
The Seventh Conference on Thermal Conductivity was held at the National Bureau of Standards on November 13–16, 1967. This volume contains the texts of the papers presented. Topics covered include surveys of the present state of knowledge regarding the thermal conductivity of different materials, descriptions of different apparatuses for measuring thermal conductivity, new experimental data on the thermal conductivity or diffusivity of a variety of materials, and correlations between experimental results and theoretical predictions.

Key words: Conductance; conductivity; contact conductance; contact resistance; electrical conductivity; electrical resistivity; heat transfer; Lorenz function; resistivity; temperature; thermal conductivity; thermal diffusivity; thermal resistivity; thermophysical properties.

Janz, G. J., Dampier, F. W., Lakshminarayanan, G. R., Lorenz, P. K., Tomkins, R. P. T., **Molten salts: Volume 1, Electrical conductance, density, and viscosity data,** *NSRDS–NBS 15 (Oct. 1968), $3.00.*

Data on the electrical conductance, density and viscosity of single-salt melts were compiled from a comprehensive search of the literature up to December 1966 and a critical assessment made of the compiled data. Recommended values were determined and are presented as functions of temperature in the form of equations and tables.
The results for some 174 compounds as single-salt melts are reported; no attempt was made in the present effort to embrace the results for molten salt mixtures. Data are presented for fluorides, chlorides, bromides, iodides, carbonates, nitrites, nitrates, oxides, sulfides, sulfates, and a miscellaneous group.

Key words: Data compilation; density; electrical conductance; molten salts; standard reference data; viscosity.

Kropschot, R. H., Birmingham, B. W., Mann, D. B., Ed., **Technology of liquid helium,** *Mono. 111 (Oct. 1968), $2.00.*
The discovery of the element helium was made just 100 years ago in 1868. Today helium is produced in large quantities and used in many technological applications. This treatise is a source document containing information on helium resources, production, conservation, thermodynamic properties, liquefaction and refrigeration techniques, transportation and storage of liquid and safety requirements. It also contains a discussion of uses for liquid and cold gas in cryoelectronics, superconductivity, bubble chambers, cryopumping and missile and space systems. The book brings together articles by noted authorities in cryogenic technology in which they discuss their specialized field in great depth.

Key words: Conservation; cryoelectronics; cryogenics; cryopumping; helium; liquefaction; magnets; purification; refrigeration; safety; storage; thermodynamic properties; transportation.

Lutz, G. J., Boreni, R. J., Maddock, R. S., Meinke, W. W., Ed., **Activation analysis: A bibliography,** *Tech. Note 467, Parts 1 and 2 (Sept. 1968), $6.50 set.*
References to activation analysis in the open literature are published from a computer readout. The first part of the two-part series contains references numbered according to their accession to the system. The second part contains an author index and three additional indices for "element determined," "matrix analyzed," and "technique used." The two parts, when used together, permit a literature search defined by the three indices. Part 1 will be updated periodically by addenda containing new references while Part 2 will be periodically revised and replaced by new pages which include cross references to the new accessions.

Key words: Activation analysis; bibliography; element determined; literature file; matrix analyzed; technique used.

McClenon, R. C., Hilsenrath, J., **Reform: A general-purpose program for manipulating formatted data files,** *Tech. Note 444 (Aug. 1968), 40 cents.*

A program listing and description is given of REFORM, an independent program with which it is possible to manipulate and edit

files containing as many as nine different fixed-field card formats. It can select or abridge information from any of the cards and print that information, or reformat new cards in any desired order or arrangement. Provision is made for introducing as many as twenty-six arbitrary strings of characters, each of which may be up to seventy-nine characters in length, thereby permitting the insertion of labels, headings, or comments into the file. The program, which operates on the 1108 computer at NBS, is written in ASA FORTRAN, and care has been taken to reduce to a minimum the program changes required to make the program run on other computers.

Key words: File editor; fixed-field file editor; Fortran program; insert program; packing program; reformatting; report generator; unpacking program.

Moiseiwitsch, B. L., Smith, S. J., **Electron impact excitation of atoms,** *NSRDS–NBS 25 (Aug. 1968), $2.00.*
The experimental and theoretical literature about the electron impact excitation of atoms is reviewed. Theoretical methods ranging from the Bethe and Born approximations to the close coupling approximations are discussed and intercompared. Where possible, on theoretical grounds or through intercomparison, the reliability of the various methods is discussed.
A general critique of the optical method of measuring excitation functions is given, with the objective of promoting higher quality future experimental work. A critical study of existing experimental work leads to the conclusion that most workers have ignored important physical and instrumental effects, and it may be presumed that the data in the literature is subject to many unrecognized systematic errors. The literature on hydrogen and helium is discussed critically. The literature on the alkalis, heavy rare gases, mercury, cadmium and zinc is surveyed but the quality of the literature does not support critical review beyond some general comments about the physics of these atoms.

Key words: Atom; electron; excitation; experimental; helium; hydrogen; impact; review; theoretical.

Bennett, L. H., Mebs, R. W., Watson, R. E., **Solute Knight shifts in noble metals,** *Phys. Rev. 171, No. 3, 611–626 (July 15, 1968).*
Knight shifts of Cu, Cd, Al, In, Sn and Ga as dilute solutes in Au; Hg and Al as dilute solutes in Ag; In as a dilute solute in Cu; and Sn as a dilute solute in Ag-Au alloys, are reported. These data are considered together with all other Knight shift data on dilute solutes in the 3 noble metals. Assuming the solute atom to be situated most nearly in a free conduction electron state when dissolved in Ag, the changes in Knight shift when dissolved in Cu or Au indicate a valence effect which is opposite in sense for these latter 2 noble metals. The Cd resonance linewidths for Au-Cd alloys show appreciable broadening with increase in alloy content or test frequency. Values of hyperfine fields for the free atom are presented together with alternative values of the paramagnetic spin susceptibility of the host. The problem of exchange enhancement of the spin susceptibility is discussed. Values for Knight's parameter ξ usually considered as a measure of the amount of s-character in the metal are tabulated and discussed. The valence effects found in the Knight shifts, are also evident in the ξ values. The requirement of orthogonalization of the conduction electron states to the metallic ion cores leads to a reconsideration of the origin of the solvent Knight shifts in noble metal alloys.

Key words: Alloys; Au; Ag; Cu; In; Ga; Sn; Cd; P; Zn; Hg; Al; hyperfine fields; Knight shift; noble metals; susceptibility.

Cassidy, E. C., Abramowitz, S., **Time-resolved emission and absorption studies of exploding wire spectra** *(Proc. 4th Conf. Exploding Wires, Boston, Mass., Oct. 18–21, 1967), Book, Exploding Wires, 4, 109–124 (Plenum Press Inc., New York, N. Y., 1968).*
Emission and absorption studies of the spectra produced by exploding wires in oxygen, nitrogen, hydrogen, or argon atmospheres are described. A drum camera and a rotating shutter are used for continuous and time-resolved recording of the explosion spectra. A high-intensity light source (a second exploding wire or Lyman flashtube), synchronized with the rotating shutter, is flashed through the explosion vapor for the absorption studies. Results from experiments performed under a variety of controlled conditions are presented. Effects of environment, pressure, and electrical energy on the spectrum are discussed, and conditions found conducive to production of selected features are indicated. The exploding wire is shown to be a rich source for study of the AlO molecule, and observation of a number of new bands (believed to be part of the $B\,^2\Pi_i - X\,^2\Sigma^+$ transition) is reported. Preliminary experiments with titanium wires exploded in oxygen suggest that the exploding wire may also be a desirable source for spectral studies of the TiO molecule. Some results from this work are included.

Key words: Exploding wire; time-resolved spectrosopy; electrical discharges; AlO, TiO.

Christ, B. W., Giles, P. M., **On the detection of retained austenite in high-carbon steels by Fe^{57} Mössbauer spectroscopy, with appendix,** *Trans. Met. Soc. AIME* **242,** *1915–1925 (Sept. 1968).*
Mössbauer effect measurements have been made on 1-mil thick foils of commercial 1 w/o carbon steel and Iron 2 w/o carbon alloy. The experimental method requires about 3–5 volume percent of a phase in the multiphase steel sample for detection. Room temperature Mössbauer patterns obtained on austenitized and quenched samples exhibit 15, and possibly 21, lines. A sharp, paramagnetic singlet and a quadrupole doublet, poorly-resolved from the singlet, are attributed to austenite. Remaining lines are due to martensite. Accurate evaluation of austenite line parameters is not feasible if significant amounts of other phases such as carbides or martensite occur simultaneously with austenite. This is demonstrated by comparison of hyperfine interactions determined for austenite in multiphase high carbon samples with those reported for iron-carbon austenite in a nearly 100% austenitic sample. Lines from carbides are incompletely resolved from austenite lines, as demonstrated by comparison of austenite line positions with carbide line positions calculated from published values of hyperfine interactions. One martensite line overlaps an austenite line in the pattern for commercial 1 w/o carbon steel. Results of this study suggest that the usefulness of Fe^{57} Mössbauer spectroscopy for quantitative analysis of austenite in quenched and tempered steels may be restricted by poor resolution.

Key words: Retained austenite; Fe^{57} Mössbauer effect; high carbon steel; carbides; resolution; hyperfine; martensite.

Christ, B. W., Smith, G. V., **Effects of impurities on yield and flow strength of zone refined iron,** *Mem. Sci. Rev. Met.* **LXV,** *208–223 (June 15, 1968).*
Effects of impurities on yield and flow strength of hydrogen-purified, zone-refined iron and of dilute, binary alloys made from it in the temperature range 77–300° K have been examined. Data from the literature are compared with new data obtained on hydrogen-purified iron and iron-0.01 and 0.026 wt.% nitrogen alloys. In 300 °K tensile tests, hydrogen purification causes substantial changes in the shape of the upper yield, the magnitude of yield stress, the grain-size dependence of yield stress and the response to strain aging treatments. However, hydrogen purification decreases total interstitial impurity by only 0.0008 wt.%.
Dilute iron alloys are found to exhibit unusual, but widely documented solution strengthening behavior. The room temperature strength is proportional to impurity concentration. However, low-temperature strength is inversely proportional to impurity concentration. This phenomenon, termed "alloy softening", is more pronounced in poly-than in monocrystals, and for interstitial than substitutional impurities.
It is concluded that hydrogen-purification of zone-refined iron affects mechanical behavior by modifying interstitial impurity distribution, rather than by total removal of interstitial impurity. Alloy softening may be due to an increase in mobile dislocation density related to solute rearrangements during thermal treatments.

Key words: Upper yield point; lower yield stress; friction stress; strain aging; hydrogen-purified iron; iron-nickel; ironnitrogen monocrystals; polycrystals; alloy softening; grain boundary ledge density; Peierl's stress.

Dickson, R. W., Spinner, S., **An improved method for the determination of torsional and flexural resonance frequencies of cylindrical specimens,** *J. Mater.* **3,** *No. 3, 716–724 (1968).*
A suspension method is described for obtaining torsional as well as flexural mechanical resonance frequencies of cylindrical specimens which overcomes many of the difficulties previously encountered in determining the torsional modes for such specimens. The method is readily adaptable for such measurements as a function of temperature. Also internal friction measurements using this method yield responses having less suspension losses than other suspension systems, resulting in more reliable values of internal friction from the specimen.

Key words: Cylinders; loop; suspension; torsional mechanical resonance frequency.

Edmiston, C., Krauss, M., **Pseudonatural orbitals as a basis for the superposition of configurations. II. Energy surface for linear H_3,** *J. Chem. Phys.* **49,** *No. 1, 192–205 (July 1, 1968).*
A superposition of configurations (SOC) trial function is applied to the H_3 energy surface. The convergence of the SOC trial function is improved by constructing the configurations with approximate or pseudonatural orbitals (PNO). For a given atomic function basis the PNO exhaust the accuracy of that basis in relatively few configurations compared to the total of all possible configurations. Gaussian-type functions (GTF) are then practicable as a basis for a SOC trial function.
Results are presented for the linear H_3 energy surface. The error when one hydrogen is removed to infinity is 0.1 eV and an extrapolation of this error yields a "probable" activation energy of 0.53 eV or 12 kcal.

Key words: Electronic energy surface; H_3; superposition of configurations; Gaussian-type functions; correlation energy; Hartree-Fock.

Fano, U., Cooper, J. W., **Spectral distribution of atomic oscillator strengths,** *Rev. Mod. Phys.* **40,** *No. 3, 441–507 (July 1968).*
Information on the spectrum of oscillator strength for neutral atoms in their ground states is surveyed with particular regard to recent progress in the far uv–soft X-ray range and to the theoretical interpretation of data from experiments and from numerical calculations. The analysis brings out numerous aspects of atomic mechanics and problems that remain unsolved. An effort is made to interconnect different theoretical approaches within the framework of the theory of atomic spectra.

Key words: Absorption; light; oscillator strength; spectra distribution; X-ray.

Fatiadi, A. J., **Bromine oxidation of inositols for preparation of inosose phenylhydrazones and phenylosazones,** *Carbohydrate Res.* **8,** *135–147 (1968).*
The application of bromine oxidation of inositols to give inososes, followed by conversion of the latter into phenylhydrazones or phenylosazones, is described. The diketone from *myo*-inositol gives a phenylosazone in 22–30% yield, and L-inositol gives a monoketone phenylhydrazone (12% yield) and a diketone phenylosazone (28% yield); the corresponding enantiomorphs were obtained in 8% and 29% yield, respectively. The diketone from quebrachitol yields a new phenylosazone (29% yield) and no monoketone was isolated. Pinitol gave a new diketone phenylosazone (10–15% yield) which showed rapid mutarotation in 1:1 (v/v) ethanol–*p*-dioxane. In addition, a new phenylosazone has been obtained from DL-*epi*-inosose-2 phenylhydrazone. (+)-*proto*-Quebrachitol (from acorns) has been converted into a phenylosazone (20% yield). *myo*-Inositol has been converted by bromine oxidation into DL-*xylo*-pentahydroxy-2-cyclohexen-1-one in low yield.

Key Words: Bromine; inositol; inosose phenylhydrazone; inosose phenylosazone; mutarotation; oxidation.

Florin, R. E., Sicilio, F., Wall, L. A., **The paramagnetic species from titanous salts and hydrogen peroxide,** *J. Phys. Chem.* **72,** *No. 9, 3154–3161 (Sept. 1968).*
The radical species giving ESR spectra on mixing titanous salts and hydrogen peroxide cannot be hydroxyl as formerly supposed. Observed kinetics are inconsistent with simple generation and disappearance schemes. In organic substrate mixtures the species increases with time while organic radicals decrease. The two "hydroxyl" species are probably forms of HO_2 complexed with Ti^{4+}. The rate constant k_1 of the initial reaction $Ti^{3+} + H_2O_2 \rightarrow OH + OH^- + Ti^{4+}$ is estimated as equal to or greater than 200 M^{-1} sec^{-1} from appearance rate of $Ti^{4+} \cdot H_2O_2$, and 800–1800 $M^{-1}sec^{-1}$ from indirect analysis of radical concentration-time curves.

Key words: Electron spin resonance; free radicals; hydroperoxyl radical; hydroxyl radical; titanic complexes; and titanium trichloride.

Krause, R. F., Jr., Douglas, T. B., **The heats of formation of $AlClF_2$ and $AlCl_2F$ from subliming AlF_3 in the presence of $AlCl_3$ vapor,** *J. Phys. Chem.* **72,** *No. 10, 3444–3451 (Oct. 1968).*
The volatility of AlF_3, which was measured between 1196 and 1256 °K by an entrainment method, was enhanced by the presence of $AlCl_3$ vapor. When the $AlCl_3$ vapor was generated at 373 or 394 °K, the amount of sublimed AlF_3 was observed to be from 1.7 to 7.4 times that expected in an inert medium. The vapor mixture saturated with AlF_3 was considered to include the two mixed-halide monomers formed according to:

$$(m/3)\,AlCl_3 + (1 - 3/m)\,AlF_3 = AlCl_mF_{(3-m)},$$

where m is 1 or 2. After correcting for the formation of Al_2F_6, Al_2Cl_6, and the 22 possible mixed-halide dimers, a least-square fit to the entrainment data yielded $\Delta H^\circ_{1225} = 0.5$ kcal with an estimated uncertainty of ± 1 kcal for both the above all-monomer reactions.

Key words: $AlCl_3$; AlF_3; entrainment method; dimerization correction; heat of reaction; mixed halides; sublimation.

Folman, M., Klein, R., **Second layer migration with trapping on first layer sites: hydrogen, nitrogen, and carbon monoxide on tungsten,** *Surface Sci.* **11,** *430–442 (1968).*
Second layer migration of hydrogen, nitrogen, and carbon monoxide on tungsten is observed with a field emission microscope. The initial deposition on the tungsten surface at 4.2 °K is made with molecular beams with the tungsten emitter axis perpendicular to the beam direction. The migration of the deposit is effected at temperatures far below those for which the chemisorbed layer is mobile. The shapes of the sharp line boundaries as the second layer migrates over the chemisorbed layer and onto the clean tungsten substrate are quite different for the three gases observed. It is proposed that, in addition to the barrier effects of certain planes of the tungsten, the density of trap sites on the clean surface dictates the boundary configuration. The trap site densities differ for the different gases.

Key words: Field emission; second layer migration; nitrogen; hydrogen; carbon monoxide; tungsten.

Gebbie, K. B., Thomas, R. N., **Non-LTE diagnostic stellar spectroscopy. II. On the Schuster mechanism for the production of emission lines,** *Astrophys. J.* **154,** *285–296 (Oct. 1968).*
We investigate the conditions under which the Schuster mechanism can produce emission lines. We consider Schuster's original formulation, together with Milne's modification and a general non-LTE formulation. We conclude that while emission lines may result in particular circumstances, it is unlikely that observations of bright lines can be interpreted by this mechanism.

Key words: Diagnostic stellar spectroscopy; emission line; non-LTE formulation; Schuster mechanism; spectroscopy.

Gebbie, K. B., Thomas, R. N., **Non-LTE diagnostic stellar spectroscopy. I. Conceptual and analytical background,** *Astrophys. J.* **154,** *271–283 (Oct. 1968).*
Seeking a nonrestrictive determination of the state of a stellar atmosphere, defined as the occupation numbers describing the energy states of the directly-observable parts of the star, we delineate those regions where thermodynamic equilibrium state parameters can be adopted for internal energy states either because collisional processes predominate or because the radiation field satisfies certain homogeneity conditions. The boundary values for the state parameters of the LTE stellar interior must generally be determined in a

lower atmospheric region satisfying these homogeneity conditions on the radiation field; spectroscopic diagnostics generally refer to an upper atmospheric region not satisfying the homogeneity conditions. We summarize an approach to specifying the state parameters describing these latter regions, and the analytical basis for determining their values. This paper then provides the background for the specific applications in the following papers.

Key words: Stellar atmosphere; LTE; thermodynamic equilibrium; state parameters; radiation field; collisional processes.

Green, M. S., **Generalized Ornstein-Zernike approach to critical phenomena,** *J. Math. Phys.* **9,** *No. 6, 875–890 (June 1968).*
A generalization of the Ornstein-Zernike integral equation is derived and suggestions are made about a possible application to an improved theory of critical phenomena. A fundamental maximum principle of statistical mechanics is used to place the generalized equation in the context of phase transitions and critical points. The equation is a relationship between a generalized correlation matrix by means of which the average fluctuation product of any two sum functions may be expressed and a generalized direct correlation matrix which is the second functional derivative of the functional in the maximum principle. The existence of a critical eigenvector of the direct correlation matrix is proposed and three physical meanings of this vector are given. An explicit formula for the direct correlation matrix is given and is used to derive two asymptotic properties. This formula exhibits an unexpected relationship between the generalized Ornstein-Zernike equation and the Percus-Yevick equation.

Key words: Ornstein-Zernike theory; fundamental maximum principle; generalized Ornstein-Zernike equation; entropy-energy-volume; molecular distribution functions; potentials of average force; Percus-Yevick equation; critical phenomena; fluctuations, phase transitions.

Jacox, M. E., Milligan, D. E., **Matrix-isolation study of the infrared spectrum of the free radical F_2CN,** *J. Chem. Phys.* **48,** *No. 9, 4040–4046 (May 1, 1968).*
In studies of the reaction of photolytically produced F atoms with FCN in Ar and N_2 matrices at 14 °K, the free radical F_2CN is stabilized in sufficient concentration for observation of its electronic spectrum and of six infrared absorptions, double bond character. Products of further F atom attack on F_2CN, including CF_2HF and CF_3NF_2, are observed in these experiments. Evidence is presented suggesting that the species FC=NF may also be stabilized.

Key words: CF_2NF; CF_3NF_2; F atom reaction; FCN; F_2CN; FC-NF; free radical; infrared spectrum; matrix isolation; photolysis; ultraviolet spectrum.

Johannesen, R. B., Gordon, C. L., **Titanium(IV) bromide (titanium tetrabromide),** *Book, Inorganic Syntheses IX, Chapt. IV, 46–50 (McGraw-Hill Book Co., New York, N.Y., 1967).*
Directions are given for the preparation of titanium tetrabromide. Distilled titanium tetrachloride is treated with an excess of gaseous hydrogen bromide and the product distilled under dry nitrogen into a container which can be sealed. Titanium tetrabromide prepared in this manner was found to contain 0.03% of chloride. The yield was 85%.

Key words: Titanium(IV) bromide; titanium tetrabromide; titanium tetrachloride.

Ku, H. H., **Expressions of imprecision, systematic error, and uncertainty associated with a reported value,** *Meas. Data* **2,** *No. 4, 72–77 (July–Aug. 1968).*
The work of a calibration laboratory is described in terms of a sequence of operations that results in the collection, storage and transmittal of information. Since the information content of the statements of uncertainty determines the worth of a reported value, these statements deserve to be well formulated. An annotated guide to such commonly used expressions of uncertainties is given in table form for convenient reference.

Key words: Accuracy; calibrations; expression of uncertainty; measurements; precision; standard error; systematic error; uncertainty.

Kuriyama, M., **Theory of x-ray diffraction by a distorted crystal. II. Scattering amplitude for a wave packet of finite size,** *J. Phys. Soc. Japan* **25,** *No. 3, 846–856 (Sept. 1968).*
The X-ray scattering amplitude for a finite wave packet diffracted by a distorted crystal has been calculated by the use of a previously formulated theory (M. Kuriyama, J. Phys. Soc. Japan **23,** 1369 (1967)). An approximation used for deriving the final expression of the scattering amplitude is that the lateral sizes of an incident beam of ordinary X-ray energy are greater than several hundred microns. When the beam is finite in its lateral size, only a limited portion of the crystal is responsible for scattering. The geometrical arrangement of the limited region has been discussed in terms of an observation point on the crystal exit surface, an incident (glancing) angle and an observation (detector) angle. The internal wave fields and paths of classical energy flow are also discussed from the viewpoint of the present formulation.

Key words: Atom; displacement; distorted crystal; energy flow; finite beam; theory; wave field; wave packet; X-ray diffraction.

Kuyatt, C. E., **Measurement of electron scattering from a static gas target, Book, Methods of Experimental Physics,** *Vol. 7. Atomic and Electron Physics, Chapt. 1, Electron-Atom Interactions,* Ed. B. Pederson and W. L. Fite, *pp. 1–43 (Academic Press Inc., New York, N.Y., 1968).*
The quantitative aspects of the measurement of elastic and inelastic scattering of electrons from static gas targets is discussed. Basic arrangements for the measurement of total and differential cross sections are reviewed, followed by a critical discussion of the calculation of scattering geometries, of the transmission of energy analyzers, of Faraday cup electron collectors, and of electron multiplier detectors. Other topics treated are scattering chambers, use of generalized oscillator strengths to express corss-section data, Doppler broadening of energy distributions, pressure variation of scattered signals, and calibration methods for cross section and absolute electron energy.

Key words: Elastic electron scattering cross section; inelastic electron scattering cross section; differential electron scattering cross section; calculation of scattering geometries; transmission of energy analyzers; Faraday cup; electron multiplier; scattering chambers; generalized oscillator strength; Doppler broadening; absolute electron energy.

Madey, T. E., Yates, J. T., Jr., **Desorption by electron impact: oxygen adsorbed on tungsten,** *Surface Sci.* **11,** *327–351 (1968).*
The interaction of oxygen with a polycrystalline tungsten ribbon has been examined using electron stimulated desorption. At least three binding states of adsorbed oxygen have been identified: a physically adsorbed state which forms at 20 °K, and two chemisorbed states designated β_1 and β_2. Both the physisorbed state and the β_1 state liberate positive ions when bombarded by 100 eV electrons; no positive ions were observed on electron bombardment of the β_2 state. The results indicate that the physisorbed state and the β_1 state are molecular. There is an enhanced adsorption of oxygen above 500 °K which is primarily due to the creation of binding sites by thermal rearrangement of the oxygen covered surface. The maximum in the ion energy distribution is at 6.5 volts for β_1 oxygen and at 0.5 volt for physisorbed oxygen. The total cross section Q_{B_1} for electronic desorption from the β_1 state is 7×10^{-19} cm²; the ionic cross section $Q^+_{B_1}$ is $\gtrsim 3.4 \times 10^{-20}$ cm². The maximum ion yields g^+ (ions/electron) are $g^+ = 1.5 \times 10^{-6}$ for 300 °K adsorption, $g^+ = 3.3 \times 10^{-6}$ for adsorption at 730 °K, and $g^+ = 5 \times 10^{-5}$ for adsorption at 20 °K.

Key words: Oxygen; tungsten; chemisorption; physisorption; desorption; electron impact; electronic desorption; cross section; binding state.

Moore, G. A., **Application of computers to quantitative analysis of microstructures** *(Proc. Third Intern. Materials Symp., Berkeley, Calif., June 13, 1966), Book, Ceramic Microstructures,* Ed. R. M. Fulrath and J. A. Pask, *Chapt. 3, pp. 71–120 (John Wiley & Sons, Inc., New York, N. Y., 1968).*
The problems and methods of quantitative microscopy are basicly identical in all microscopic sciences. Results are limited by the finite resolution of real micrographs and real observations and by the statistical necessity of processing a very large number of observations, thus dictating automatic scanning and computer processing methods.

The presence or absence of a specific phase can be represented by a two-dimensional binary array which can be rapidly processed to yield the required measurements. Logical modification by the computer is frequently necessary to substitute for some of the logical discriminations normally made by the human analyst and to facilitate the desired measurements.
Using high precision scanning equipment, the inaccuracies of measurement remain comparable to the limits imposed by statistics. Presently attainable precision is, however, an order of magnitude better than can normally be obtained by manual methods.

Key words: Analysis of microstructures; quantitative microscopy; automatic scanning (of micrographs); precision scanning (of micrographs); computer processing (of micrographs); logical modification of pictures.

Moore, G. A., **Automatic scanning and computer processes for the quantitative analysis of micrographs and equivalent subjects** (*Proc. Symp. on Automatic Photo Interpretation, Washington, D.C., June 1967*), *Book, Pictorial Pattern Recognition, pp. 275–326* (*Thompson Book Co., Washington, D.C., 1968*).
Basically identical measurement problems are treated in the microscopic branches of all material sciences and in microbiology and medical diagnosis. Visual-manual methods, in use over a century, permit determination of the relative volume of a material phase, and of the average size and spacing of particles of this phase. Redefining a phase as the set of all areas having similar nature and a distinctive tone or color in a photograph, these established methods can be extended to several varieties of non-micrographic pictures.
Statistical considerations require the order of one million observations per picture to attain reasonable precision, dictating automatic scanning and computer processing. Treatment of phase images in binary format permits feasible memory capacities and processing time. Production of a valid binary image requires both high precision scanning and a battery of logical processes which can substitute for darkroom operations and logical discriminating normally made by a human analyst. Other logical processes permit dissection and description of individual phase areas. Attainable measurement precision is an order of magnitude greater than is normally attained by manual methods.

Key words: Analysis of microstructures; automatic scanning (of micrographs); computer processing (of micrographs); logical modification of pictures; precision scanning (of micrographs); quantitative microscopy.

Pechukas, P., **Generalized Langevin equation of Mori and Kubo,** *Phys. Rev.* **164,** *No. 1, 164–175 (Dec. 5, 1967).*
We derive and discuss the generalized Langevin equation of Mori and Kubo for an arbitrary stationary stochastic process with continuously differentiable correlation function.

Key words: Langevin equation; stationary stochastic process; fluctuation-dissipation theorem.

Peiser, H. S., **The relative magnitude of jump rates for point-defect paths between equivalent sites around a trap,** *J. Korean Phys. Soc.* **1,** *No. 1, 5–8 (Mar. 1968).*
To a limited but significant extent, the relative magnitude of jump rates for point-defect paths between equivalent sites around a trap of noncubic symmetry in crystals is governed by cross-over points of equivalent paths on the stereographic representation of the trap environment and by true intersections of paths caused by mirror planes of symmetry. The chief consequence is that in simple experiments the number of defect path types that cause observable internal-friction effects is greatly limited. Moreover, a closer estimate than is otherwise possible can be made of the number of distinct paths needed for complete or partial relaxations, associated with an external influence.

Key words: Crystal relaxation; crystal symmetry; crystal trap; defect mobility crystal; point-defect; point group.

Santoro, A., Weir, C. E., Block, S., Piermarini, G. J., **Absorption corrections in complex cases. Application to single crystal diffraction studies at high pressure,** *J. Appl. Cryst.* **1,** *Part 2, 101–107 (June 1968).*
A method is described for evaluating the absorption corrections in complex cases in which objects other than the crystal itself take part in the absorption. The method has been applied to the high-pressure cell developed in this laboratory; and it has been tested on a set of intensities obtained from a single crystal of bromine grown and maintained under 10 kbar pressure.

Key words: Absorption correction; high-pressure; X-ray diffraction; bromine; crystal structure.

Scharf, K., **Steady-state response of silicon radiation detectors to X and gamma rays,** *Proc. Symp. Physics and Nondestructive Testing, ITT Research Institute, Chicago, Ill., Sept. 27–30, 1966, 1, 235–298 (Air Force Materials Laboratory, Wright-Patterson Air Force Base, Ohio, 1968).*
A review is given of investigations of the steady-state response of silicon radiation detectors to x and gamma rays which were carried out in the Radiation Physics Division of the National Bureau of Standards. Theoretical relations between photocurrents generated in such detectors by x and gamma rays and exposure rate and quality of radiation are explained. Measurements of the dependence of the generated photocurrent on exposure rate, quality of radiation, voltage applied, and detector temperature carried out on different types of detectors are presented, and different modes of operation of silicon radiation detectors are discussed. By using a special electrical compensation method, exposure rates were measured ranging from 100 mR/hr of ^{137}Cs gamma rays to 10^6 R/hr of 30-kV x rays.

Key words: Radiation detection; radiation detectors; silicon; semiconducting devices; dosimetry; X rays: gamma rays; photovoltaic effects; photodiodes.

Steiner, B., **The cross section for the photodetachment of electrons from I^-**, *Phys. Rev.* **173,** *No. 1, 136–142 (Sept. 5, 1968).*
The cross section for photodetachment of I^- at 347 nm, 0.5 eV above threshold, has been determined to be $2.9 \pm 0.5 \times 10^{-17}$ cm^2. This value has been obtained in a crossed beam experiment by comparison with photodetachment from H^- at 993 nm 0.5 eV above *its* threshold. The present determination permits placement of the previously determined relative cross section curve for the first electron volt above threshold on an absolute scale. The entire experimental curve is compared with the recent calculation of Robinson and Geltman. Although the shapes of the two curves are very similar, the new experimental cross section exceeds the calculation by a factor of two.

Key words: Absolute cross section; iodine; negative ions; photodetachment.

Other NBS Publications

Bullis, W. M., Measurement of carrier lifetime in semiconductors, An annotated bibliography covering the period 1949–1967, Tech. Note 465 (Nov. 1968), 60 cents.
Lederer, P. S., NBS interagency transducer project, Tech. Note 469 (Oct. 1968), 30 cents.
Schaffer, R., Ed., Organic Chemistry Section: Summary of activities July 1967 to June 1968, Tech. Note 457 (Sept. 1968), $1.25.
Stevens, M. E., Nonnumeric data processing in Europe, A field trip report, August–October 1966, Tech. Note 462 (Nov. 1968), 65 cents.
Taylor, J. K., Ed., Microchemical Analysis Section: Summary of activities July 1967 to June 1968, Tech. Note 455 (Oct. 1968), $1.25.
Technical highlights of the National Bureau of Standards, Annual Report, Fiscal Year 1968, Spec. Publ. 308 (Nov. 1968), $1.00.

Altschuler, H. M., Comments on "An improved method for measuring scattering parameters of nonreciprocal two-ports," IEEE Trans. Microwave Theory Tech. **MTT-16,** No. 4, 261–262 (Apr. 1968).
Arenhovel, H., General formulas for describing the absorption of polarized photons by oriented nuclei, Phys. Rev. **171,** No. 4, 1212–1216 (July 20, 1968).

Bach, R. L., Caswell, R. S., Energy transfer to matter by neutrons, Radiation Res. **35**, No. 1, 1–25 (July 1968).

Birmingham, B. W., Ed., A Report on the 1967 Applied Superconductivity Conference, Cryogenics **8**, No. 3, 176–179 (June 1968).

Bowen, R. L., Paffenbarger, G. C., Mullineaux, A. L., A laboratory and clinical comparison of silicate cements and a direct-filling resin: A progress report, J. Prosthetic Dentistry **20**, No. 5, 426–437 (Nov. 1968).

Branscomb, L. M., Physics and the nation in a crystal ball, Phys. Today **21**, No. 8, 23–28 (Aug. 1968).

Brauer, G. M., McLaughlin, R., Huget, E. F., Aluminum oxide as a reinforcing agent for zinc oxide-eugenol-*o*-ethoxybenzoic acid cements, J. Dental Res. **47**, No. 4, 622–628 (July–Aug. 1968).

Brooks, R., Horton, A. T., Torgesen, J. L., Occlusion of mother liquor in solution-growth crystals, J. Crystal Growth **2**, 279–283 (1968).

Bullis, W. M., Measurement problems in microcircuit processing, (Proc. Government Microcircuit Applications Conf., Gaithersburg, Md., Oct. 1–3, 1968) GOMAC Digest **1**, 215–217 (Office of Naval Research, Washington, D.C., Oct. 1968).

Corruccini, R. J., Principles of thermometry (measurement of temperature), Book, Treatise on Analytical Chemistry, Ed. I. M. Kolthoff, P. J. Elving, and E. B. Sandell, Part I, Theory and Practice **8**, Ch. 87, 4937–4990 (Interscience Publishers, New York, N.Y., 1968).

Clark, A. F., Powell, R. L., Longitudinal magnetoresistance of pure single-crystal copper, Phys. Rev. Letters **21**, No. 12, 802–804 (Sept. 16, 1968).

Danielson, B. L., An optical Faraday rotation technique for the determination of magnetic relaxation times, IEEE Trans. Mag., **MAG-4**, No. 2, 176–178 (June 1968).

Dibeler, V. H., Liston, S. K., Mass-spectrometric study of photoionization. IX. Hydrogen cyanide and acetonitrile, J. Chem. Phys. **48**, No. 10, 4765–4768 (May 15, 1968).

Dibeler, V. H., Liston, S. K., Mass spectrometric study of photoionization. XII. Boron trifluoride and diboron tetrafluoride, Inorg. Chem. **7**, No. 9, 1742–1746 (Sept. 1968).

Dick, C. E., Motz, J. W., Inelastic scattering cross sections for 200- and 400-keV electrons, Phys. Rev. **171**, No. 1, 75–80 (July 5, 1968).

Drechsel, D., On the model-independent evaluation of inelastic electron scattering data at low momentum transfer, Nucl. Phys. **A113**, No. 3, 665–675 (June 7, 1968).

Fatiadi, A. J., Acylation of tetrahydroxy-p-benzoquinone, J. Chem. Eng. Data **13**, No. 4, 591–593 (Oct. 1968).

Hardy, S. C., Coreill, S. R., Morphological stability of a growing cylindrical crystal of ice, J. Appl. Phys. **39**, No. 7, 3505–3507 (June 1968).

Hiza, M. J., Heck, C. K., Kidnay, A. J., Liquid-vapor and solid-vapor equilibrium in the system hydrogen-ethylene, Proc. Symp. Cryogenic Advance in the Space Program, Tampa, Florida, May 19-22, 1968, **64**, No. 88, 57–65 (American Institute of Chemical Engineering, New York, N.Y., 1968).

Huget, E. F., Brauer, G. M., Reactivity of the components of tooth structure, J. Colloid Interface Sci. **27**, No. 4, 714–721 (Aug. 1968).

Hummer, D. G., Rybicki, G. B., Redshifted line profiles from differentially expanding atmospheres, Astrophys. J. **153**, L107–L110 (Aug. 1968).

Hyde, K. E., Gordon, G., Kokoszka, G. F., Magnetic properties of some binuclear copper(II) complexes, J. Inorg. Nucl. Chem. **30**, 2155–2161 (1968).

Iverson, W. P., Microbiological corrosion, Proc. Conf. Corrosion and Protection of Pipes and Pipelines, London, England, June 13, 1968 (Technical Exhibited Ltd., London, England, 1968).

Jespersen, J. L., Kamas, G., Gatterer, L. E., MacDoran, P. F., Satellite VHF transponder time synchronization, Proc. **IEEE 56**, No. 7, 1202–1206 (July 1968).

Joiner, B. L., Rosenblatt, J. R., The mean deviation and range for $n=3$, Am. Stat. **22**, No. 4, 37–38 (Oct. 1968).

Judd, D. B., Color science and the paint industry, J. Paint Technol. **40**, No. 525, 470–477 (Oct. 1968).

Kirby, R. K., Rothrock, B. D., Thermal expansion of vitreous selenium from −190° to +30°C, J. Am. Ceram. Soc. **51**, No. 9, 535 (Sept. 1968).

Kokoszka, G. F., Linzer, M., Gordon, G., Electron paramagnetic resonance spectra of polycrystalline dimeric complexes. Copper propionate monohydrate and zonc-doped copper propionate monohydrate, Inorg. Chem. **7**, No. 9, 1730–1735 (1968).

Kushner, L. M., The National Bureau of Standards and the Fire Research and Safety Act of 1968, Fire J. **62**, No. 5, 32 (Sept. 1968).

McCaa, W. D., Jr., Nahman, N. S., Phenomena and devices, frequency and time-domain analysis of a superconductive coaxial line using the two-fluid model, J. Appl. Phys. **39**, No. 6, 2592–2596 (May 1968).

McClintock, M., Jennings, D. A., Mizushima, M., Contribution to the Raman line profile in liquids from molecular reorientation, Phys. Rev. Letters **21**, No. 5, 276–278 (July 29, 1968).

Macedo, P. B., Napolitano, A., Inadequacies of viscosity theories for B_2O_3, J. Chem. Phys. **49**, No. 4, 1887–1895 (Aug. 15, 1968).

Mazur, J., McCrackin, F. L., Monte Carlo studies of configurational and thermodynamic properties of self-interacting linear polymer chains, J. Chem. Phys. **49**, No. 2, 648–665 (July 15, 1968).

Mears, T. W., Young, D. S., Measurement and Standard Reference Materials in clinical chemistry, Am. J. Clin. Pathol. **50**, No. 4, 411–421 (Oct. 1968).

Milligan, D. E., Jacox, M. E., Matrix-isolation study of the reaction of F_2 and of F atoms with NCN. The infrared spectra of the species NF_2CN and FNCN, J. Chem. Phys. **48**, No. 11, 4811–4816 (June 1, 1968).

Munis, R. H., Finkel, M. W., Goniometric measurements ofinfrared transmitting materials, Appl. Opt. **7**, No. 10, 2001–2004 (Oct. 1968).

Omar, A., Peterson, R. L., On the validity of the Boltzmann relazation equation, Physica **39**, No. 1, 156–160 (July 1, 1968).

Pecker, J-C., Thomas, R. N., Saturation in Fraunhofer lines, Observatory Letter **88**, No. 964, 115–117 (June 1968).

Peterson, R. L., Short-range magnetic order in a modified Weiss molecular-field theory, Phys. Rev. **171**, No. 2, 586–590 (July 10, 1968).

Potzick, J., ac-dc Regulator-modulator, Rev. Sci. Instr. **39**, No. 8, 1219–1220 (Aug. 1968).

Ray, C. D., Tsukishima, T., Hyland, R. N., McLane, C. K., Carpenter, R. J., Analysis of a frequency-swept one-bit digital correlator, J. Appl. Phys. **39**, No. 8, 3534–3542 (July 1968).

Romanoff, M., Performance of ductile-iron pipe in soils, J. Am. Water Works Assoc. **60**, No. 6, 645–655 (June 1968).

Saunders, J. B., Bruening, R. J., A new interferometric test and its application to the 84-in. reflecting telescope at Kitt Peak National Observatory, Astron. J. **73**, No. 6, 415–531 (Aug. 1968).

Schmidt, L. B., Case, W. E., Harrington, R. D., Surface dependence of ferrimagnetic resonance fields in polycrystalline NiAl ferrite, Proc. **IEEE 56**, No. 7, 1236–1237 (July 1968).

Shumaker, J. B., Jr., Popenoe, C. H., Experimental test of H_β Stark-broadening theory at high electron densities, Phys. Rev. Letters **21**, No. 15, 1046–1048 (Oct. 7, 1968).

Sieck, L. W., Continuum emission from zenon in the vapor phase induced by absorption of 1470-Å radiation, J. Phys. Chem. **72**, No. 9, 3129–3133 (Sept. 1968).

Simmons, J. A., Coriell, S. R., Solution of the Stefan problem for whisker evaporation, J. Appl. Phys. **39**, No. 7, 3459–3463 (June 1968).

Stevens, M. E., Progress and prospects in mechanized indexing, (Proc. Symp. on Mechanized Abstracting and Indexing, Moscow, U.S.S.R., Sept. 28–Oct. 1, 1966), UNESCO/NS/209 (United Nations Educational Scientific and Cultural Organization, Paris, France, Apr. 1967).

Steward, W. G., Smith, R. V., Brennan, J. A., Cooldown time for simple cryogenic pipelines (Proc. Tenth Midwestern Mechanics Conf., Colorado State University, Fort Collins, Colo., Aug. 21–23, 1967), Book, Developments in Mechanics **4**, 1513–1525 (Johnson Publ. Co., Boulder, Colo., 1968).

Swanson, N., Codling, K., Excitation of K-shell electrons in Be by soft x-rays and 20-keV electrons, J. Opt. Soc. Am. **58**, No. 9, 1192–1194 (Sept. 1968).

Tanttila, W. H., Mahler, R. J., James, L. W., Magnetic parametric nuclear spin saturation, Appl. Phys. Letters **13**, No. 1, 27–29 (July 1, 1968).

Tauber, S. J., Imprecision-problems for information processing, Am. Doc. **19**, No. 4, 413–414 (Oct. 1968).

Thomas, R. N., Symposium on Wolf-Rayet stars: A summary, Astrophysical Letters **2**, 147–148 (1968).

Toots, J., Fowler, H. A., Marton, L., Reflectance and $1/\epsilon$ resonance

of beryllium in the far ultraviolet, Phys. Rev. **172,** No. 3, 670–676 (Aug. 15, 1968).
Turgel, R. S., A comparator for thermal ac-dc transfer standards, ISA Trans. **6,** No. 4, 286–292 (1967).
Van Blerkom, D., Hummer, D. G., A non-LTE theory of overlapping lines near the series limit, Astrophys. J. **154,** 741–750 (Nov. 1968).
West, E. D., Churney, K. L., A two-body model for the calorimeters with constant-temperature environment, J. Appl. Phys. **39,** No. 9, 4206–4215 (Aug. 1968).
Wiederhorn, S. M., Moisture assisted crack growth in ceramics, Intern. J. Fracture Mech. **4,** No. 2, 171–177 (June 1968).
Wildhack, W. A., Improving measurement accuracy for high systems reliability, Electronics **41,** No. 5, 280 (Mar. 4, 1968).
Wildhack, W. A., Mason, H. L., Powers, R. S., Jr., Accuracy charts for RF measurements, Proc. **IEEE 55,** No. 6, 1056–1063 (June 1967).
Wolcott, N. M., Falge, R. L., Jr., Ferromagnetism of $CrBe_{12}$, Phys. Rev. **171,** No. 2, 591–595 (July 10, 1968).
Wolcott, N. M., Falge, R. L., Jr., Bennett, L. H., NMR studies in paramagnetic and ferromagnetic $CrBe_{12}$, Phys. Rev. Letters **21,** No. 8, 546–549 (Aug. 19, 1968).
Zalubas, R., Present state of analysis of the first spectrum of thorium (Th I), J. Opt. Soc. Am. **58,** No. 9, 1195–1199 (Sept. 1968).

**Publications for which a price is indicated are available by purchase from the Superintendent of Documents, U.S. Government Printing Office, Washington, D.C. 20402 (foreign postage, one-fourth additional). The NBS non-periodical series are also available from the Clearinghouse for Federal Scientific and Technical Information, Springfield, Va. 22151. Reprints from outside journals and the NBS Journal of Research may often be obtained directly from the authors.*

U.S. GOVERNMENT PRINTING OFFICE : 1969 OL—331–607

Gov

SUBMA OCT 46129
UNIVERSITY MICROFILMS INC
ATTN SERIALS SECTION
300 NORTH ZEEB RD
ANN ARBOR MICH 48106

POSTAGE AND FEES PAID
U.S. GOVERNMENT PRINTING OFFICE

JOURNAL OF RESEARCH of the National Bureau of Standards
A. Physics and Chemistry

Vol. 73A, No. 2 March–April 1969

Contents

Page

Color representation of electron microprobe area-scan images by a color separation process. Harvey Yakowitz and Kurt F. J. Heinrich. 113

Configurations $3d^n4p$ in singly ionized atoms of the iron group. C. Roth. 125

Configurations $3d^n4p + 3d^{n-1}4s4p$ in Sc II, Ti II, and V II. C. Roth. 159

Effective interactions in the even configurations of the third spectra of the iron group. Y. Shadmi, E. Caspi, and J. Oreg. 173

Test of a kinetics scheme: Emission in $H(^2S)+NO(^2\Pi)$. M. Krauss. 191

A nuclear magnetic resonance and relaxation study of dimethoxyborane. T. C. Farrar and T. Tsang. 195

The effects of low energy irradiation on organometallics. Organometal halides of group IVA. F. E. Brinckman, Gerald F. Kokoszka, and Norman K. Adams, Jr. 201

Measurements of gaseous diffusion coefficients by a gas chromatographic technique. S. P. Wasik and K. E. McCulloh. 207

Phase relations in the Ru-Ir-O_2 system in air. C. L. McDaniel and S. J. Schneider. 213

Heats of reaction of natural rubber with sulfur. Norman Bekkedahl and James J. Weeks. 221

A table of rotational constants of symmetric top molecules giving rise to microwave spectra. Matthew S. Lojko and Yardley Beers. 233

Energy levels, wave functions, dipole and quadrupole transitions of Fe^{+++} ions in sapphire. Jacques Lewiner and Paul H. E. Meijer. 241

Publications of the National Bureau of Standards. 269

Library of Congress Catalog Card Number: 62-37059

For sale by the Superintendent of Documents, U.S. Government Printing Office, Washington, D.C. 20402.
Single copies vary in price. This issue $2. Subscription price: $9.50 a year; $2.25 additional for foreign mailing.
UNITED STATES GOVERNMENT PRINTING OFFICE, WASHINGTON : 1969